Identification of glaucomatous optic nerve progression by scanning laser tomography

James Chee-Hian Tan
MBBS, FRCOphth.

Moorfields Eye Hospital and the Institute of Ophthalmology
University College London

A thesis submitted for the degree of
Doctor of Philosophy at the University of London

December, 2002

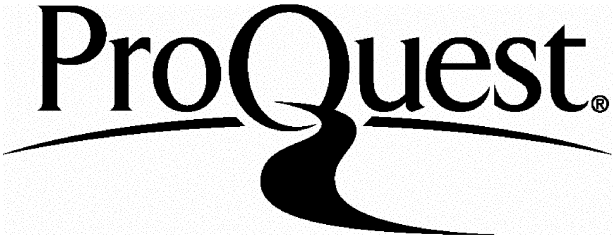

To Mum and Dad

Abstract

Analysis of sequential scanning laser tomography of the optic nerve head must be able to tell disease-induced change from measurement variability if it is to be useful for identifying glaucoma progression. Variability in neuroretinal rim area measurement was found to differ between optic nerves and between regions within each nerve, and was influenced by glaucomatous morphology, varying test conditions and different reference planes. Up to 95% of this variability could be explained by fluctuation in the height between the nerve surface and reference plane, and of the nerve head's centre of gravity along the z-axis. Such fluctuation, whether due to image variability or progressive disease, affects the position of conventional reference planes and limits their usefulness as absolute measures of change.

A novel reference plane was designed that is customised to each optic nerve head, lies at a depth compatible with least variability, and stays in position despite glaucomatous damage. Its position in any nerve is calculated from surface height at the nerve margin in multiple topography images, and kept constant throughout each image series. It was found that the reference plane's description of neuroretinal rim was more reproducible and corresponded more closely with actual rim appearance compared with conventional reference planes.

An analytical approach was devised to identify change based on this new reference plane. Variability in each 30° sector of rim area in each nerve was estimated by modelling variability within images from all time-points of any nerve's image series. Confidence limits of variability represented variability in each sector, and only change repeatedly exceeding these limits in two of three tests was attributed to disease. Assessed by 90% and 95% limits of variability, progression was identified with a sensitivity and false positive rate of 90% and 6%, and 83% and 3% respectively in ocular hypertension converter eyes with unambiguous glaucomatous visual field change and unchanging eyes of normal controls. When tested in various presentations of suspected and manifest normal-pressure and high-pressure glaucoma, progression was detected in glaucoma suspect eyes without visual field defects, eyes that progressed to develop field defects, and eyes with established and more severe glaucoma.

Preface

The progressive damage of glaucoma may be identified by longitudinally evaluating the optic nerve for change. If the identification of glaucomatous progression is to be reliable and clinically useful, every step of the chain of evaluation – data collection, processing and analysis – must be reproducible. But current testing and analysis by the widely used methods of perimetry and disc photography is mostly subjective, qualitative and not very reproducible, limiting the extent to which these tests are useful for identifying progression.

Confocal scanning laser tomography is used to measure the topography of the optic nerve head. Imaging by the technique is reportedly accurate and reproducible, but it is unclear if its sequential measurements are reproducible enough to be useful for identifying progression. What is the best way to analyse sequential topographical data to detect change is also unclear. Given the present difficulty in identifying progression, it seemed worthwhile to study scanning laser tomography as an alternative to conventional methods. This thesis examines what is known of glaucoma progression then describes the devising and testing of an analytical approach for identifying optic nerve progression by scanning laser tomography.

Studies in scanning laser tomography aimed to:

- Characterise measurement variability and its sources, and devise ways to optimise reproducibility in topographical measurements of the optic nerve head
- Design a reference plane that would reproducibly and accurately define topographic parameters of the optic nerve head
- Devise a method for estimating and accounting for measurement variability in a way that is specific to each nerve and its longitudinal measurements
- Develop a reliable and clinically accurate and meaningful analytical approach for identifying glaucomatous optic nerve change
- Test the accuracy and clinical usefulness of the analytical approach for identifying change in a rigorously defined reference dataset, and apply the approach in various clinical presentations of glaucoma.

Chapter 1 describes the disease of glaucoma, its mitigating factors, and its natural history. Chapter 2 is a review of the functional anatomy of the optic nerve head and the physical signs of glaucomatous deterioration. Chapter 3 examines why research is needed into alternative methods for detecting progression. Chapter 4 fully introduces the technique of confocal scanning laser tomography of the optic nerve head. Chapter 5 describes methods and materials used in this investigation. Chapters 6 to 8 are studies on magnification and reproducibility that formed the basis for the devising of a novel reference plane, as described in Chapter 9. Chapter 10 introduces an analytical approach for identifying glaucomatous optic nerve progression and describes its testing. Chapter 11 contains studies on the application of the approach in various presentations of glaucoma. Chapter 12 synthesises key findings from this investigation and identifies directions for future work.

Contents

List of figures

List of tables

Symbols used in equations

Symbol	*Description*

CHAPTER 8: REASONS FOR RIM AREA VARIABILITY

MHC	Mean height of the contour line above the mean height of the reference ring measured along the topographical z-axis
diff	Variability calculated as the difference of measurements
sd	Variability calculated as the standard deviation of measurements
RIMVAR	Rim area variability
REF	Variability in the distance between MHC and the reference plane along the topographical z-axis
HTILT	Variability in horizontal tilt compensation
VTILT	Variability in vertical tilt compensation
X, Y, Z	Variability in the distance between the centers of gravity of the optic nerve head and its contour line as measured on the x-, y- and z-axis respectively
HRef	Z-axis distance (height) between the reference plane and the mean topographical height of the reference ring
REFht	Distance between MHC and HRef on the topograpaphical z-axis
R^2	Coefficient of determination

CHAPTER 9: A NOVEL REFERENCE PLANE

MHC	Mean height of the contour line above the mean height of the reference ring measured along the topographical z-axis
$LOW_{5\%}$	Lowest region of the contour line in a mean topography image; calculated from the means of the 5% lowest heights on the contour line in each of the single topography images used to derive the mean topography image
R	Z-axis distance of the experimental reference plane beneath $LOW_{5\%}$ where rim area variability is least

REFdis	Distance of the experimental reference plane below *MHC*; this can be calculated once $LOW_{5\%}$ and R are known
REFpos	Position of the experimental reference plane as measured on the topographical z-axis

CHAPTER 10: ANALYTICAL APPROACH FOR IDENTIFYING GLAUCOMATOUS OPTIC NERVE CHANGE

L	Sector rim area difference between pairs of intra-visit single topography images
C	Number of combinations of pairs of images from a single visit to give the number of L values for that visit
m	Number of images acquired in a single visit
r	Number of images in each combination (r=2)
n_i	n=number of single topography images per session; i=ith value of n.
$VARLIM_a$	Limit of variability for a single rim area sector
a	Sector number corresponding to its location on the circumference of the optic nerve head
Y	Value of the t-statistic for degrees of freedom for L corresponding to a chosen two-tailed probability value
X	Mean of observations of L

Acknowledgements

I am deeply grateful to Professor Roger Hitchings and Professor Fred Fitzke, my supervisors, for their guidance and mentoring, and for much that I have learnt about glaucoma and its research. Dr Shatish Kundaiker (King's College London), Professor Geoffery Arden (City University) and Professor Peng Khaw (Moorfields and Institute of Ophthalmology) wittingly or unwittingly stimulated me to broaden my enquiry. Dr 'Samy' Poinoosawmy, now retired from Moorfields, was a limitless source of enthusiasm throughout; we also worked together to study magnification changes in HRT imaging (chapter 6), validate the experimental reference plane (chapter 9) and identify progression in normal pressure glaucoma (chapter 11). Miss Wendy Franks patiently verified converter fields and contributed much to the discussion on visual field progression in chapter 3. Mr Ted Garway-Heath made helpful suggestions on analysing reproducibility in chapter 7 and aspects of HRT imaging. I thank Ted and Debbie Kamal, my predecessors in the ocular hypertension clinic, for their part in the early collecting of longitudinal data. Normal longitudinal data, especially, was crucial to this investigation and provided by a band of faithful normal subjects who are too many to name here, whose visits were made possible by the Friends of Moorfields. Ed White, Ian Thresher and the technicians of Moorfields Glaucoma Research Unit gave me invaluable technical support; Ed also worked on validating the experimental reference plane (chapter 9). A number of organisations generously supported various aspects of this work and I would like to thank and acknowledge them here: The Frances and Renee Hock Trust, International Glaucoma Association, University College London Graduate School, Committee of Vice Chancellors and Principals of United Kingdom Universities (now Universities UK), Glaucoma Society of UK and Eire, US Glaucoma Research Foundation and Alcon UK. Not least, I am thankful to my wife Chiew Lin for all her encouragement, and our son Joseph for endless diversions during the writing of this thesis.

Chapter 1
GLAUCOMA

1.1 DESCRIPTION

Glaucoma is an optic neuropathy that is recognised clinically by the appearance of characteristic cupping of the optic nerve head in association with deficit in visual function (Hitchings, 2000). It has as its basis slowly progressive loss of retinal ganglion cells and their axons, and as a major risk factor, intraocular pressure (IOP). Worldwide, at least 67 million people are estimated to have glaucoma (Quigley, 1996). The cupping and visual impairment of glaucoma increases as the disease progresses, and left unchecked glaucoma may blind.

The importance of IOP as a risk factor is supported by epidemiological, clinical, histopathological and experimental studies, as reviewed by Sommer (1989, 1996), Wilson and Martone (1996), and Quigley (1995, 1999). But it is clear by population surveys that many people have glaucoma – roughly a third – without their IOP exceeding the standard cut-off of 21 mmHg on isolated measurements (Hollows and Graham, 1966; Sommer et al, 1991a; Dielemans et al, 1994; Leske et al, 1995; Coffey et al, 1993; Mitchell et al, 1996; Bengtsson, 1981). Conversely, many individuals with apparently raised IOP do not appear to be harmed. This means that the level of IOP is only loosely associated with the diagnosis of glaucoma, and by inference, its progression.

Factors other than IOP must then be implicated in the pathogenesis of glaucoma, and well accepted as important are age (Dielemans et al, 1994; Leske et al, 1995; Mitchell et al, 1996), genetic predisposition (Polansky et al, 1997; Stone et al, 1997) and having a positive family history (Tielsch et al, 1994; Wolfs et al, 1998; Leske et al, 2001a), and race (Sommer et al, 1991a, 1991b; Leske et al, 1995; Tielsch et al, 1991). Myopia (Mitchell et al, 1999), diabetes (Tielsch et al, 1995; Klein et al,

1994; Mitchell et al, 1997), systemic hypertension (Tielsch et al, 1995; Dielemans et al, 1995) and vascular conditions, such as migraine (Klein et al, 1993; Wang et al, 1997) and vasospasm, have also been suggested as relevant.

Glaucoma is classified according to its clinical presentation, which reflects a mixture of current concepts and older definitions not requiring an optic neuropathy. Glaucoma may be primary or secondary, and evolves acutely or chronically. Chronic glaucoma with raised IOP of undetermined cause is termed primary. Primary chronic glaucoma is categorised according to whether the anterior chamber drainage angle of the eye is open or closed, called primary open angle glaucoma (POAG) or primary angle closure glaucoma (PACG) respectively. The term PACG relates primarily to the angle closure leading to elevated IOP and does not necessarily imply an optic neuropathy. At diagnosis, however, up to 75% of people with PACG already have visual field defects or optic discs that look glaucomatous (Congdon et al, 1996; Foster et al, 1996). The term normal pressure glaucoma (NPG), otherwise known as normal tension glaucoma (NTG), is reserved for primary chronic glaucoma with open angles but IOP within normal statistical limits (less than 22 mmHg). Glaucoma, where the cause of raised IOP is known, is termed secondary. Chronically elevated IOP may be secondary to many causes, for example, intraocular inflammation and pigment dispersion. Acute glaucoma describes a rapid rise in IOP associated with symptoms such as visual disturbance and pain. A narrow anterior chamber angle closing to become apposed is usually the cause. Like PACG, the term acute glaucoma is a misnomer because it does not specifically describe an optic neuropathy but it remains used for historical reasons. In this thesis, the term glaucoma refers to POAG or NPG unless otherwise stated.

The term ocular hypertension is usually kept separate from the definition of glaucoma. People with ocular hypertension have idiopathically elevated IOP above 21 mmHg that has apparently not caused damage. Ocular hypertension is not rare, with its prevalence estimated at over 90 million people worldwide (The World Bank, 1993) and higher than that of POAG (Sommer et al, 1991a; Mitchell et al, 1996). Eyes with ocular hypertension are considered at risk of developing glaucoma.

In diagnosing glaucoma, the optic disc and visual field are evaluated to tell if the disease is present; in practice, evidence of white-on-white visual field abnormality is usually needed to corroborate the finding of a glaucomatous-appearing optic disc. This is because the normal morphology of the optic disc varies widely between individuals (Jonas et al, 1988a; 1999) and can be indistinguishable from the appearance of nerves already affected by glaucoma, especially when disease is early. Although visual field testing helps with this ambiguity, it is known that visual field defects are not the earliest sign of glaucoma; other parameters of visual function may already be abnormal (Falcao-Reis et al, 1990; Johnson et al, 1995; Silverman et al, 1990), and physical signs of glaucoma may be present, such as retinal nerve fibre layer defects (Sommer et al, 1991c) and progressive disc cupping (Sommer et al, 1980; Pederson and Anderson, 1980). Hence, whether the optic nerve is considered glaucomatous, or even changing, depends a lot on how the nerve and its function is assessed. Indeed, historically, the concept of glaucoma has evolved with its own methods of testing (Kronfield, 1974).

Currently, glaucoma is treated by lowering IOP to a level that is judged by the clinician to be compatible with slowed or stopped progression. Once this lower level is reached, IOP needs to be maintained at its new level indefinitely as the disease is chronic. Telling whether initial IOP reduction is enough to stop further deterioration, however, is largely guesswork and only testing over the longer term will disclose if the neuropathy remains progressive.

1.2 NATURAL HISTORY OF VISUAL LOSS

Observing how visual fields change over time can tell us about how glaucoma progresses, which may be considered in four phases: occult, threshold, critical (Hart and Becker, 1982) and compatible with blindness.

1.2.1 Occult period

Initially, subclinical disease is present during a prolonged occult period in which white-on-white visual fields remain normal. Non-specific perimetric signs are blind spot change, isopter shrinkage and increased localised scatter (Aulhorn and Harms, 1967; Aulhorn and Karmeyer, 1977; Drance, 1969; Werner and Drance, 1977; Hart and Becker, 1982). Other measures of visual function may be abnormal such as sensitivity to contrast (Falcao-Reis et al, 1990), colour (Johnson et al, 1995), motion (Silverman et al, 1990) and the spatial frequency doubling illusion (Maddess and Henry, 1992). Frequency doubling perimetry (FDP) and short wavelength automated perimetry (SWAP) are tests suggested as useful for glaucoma diagnosis. SWAP examines colour sensitivity which reportedly becomes abnormal before conventional visual fields in glaucoma, and can predict future white-on-white perimetric abnormalities in eyes with ocular hypertension (Johnson et al, 1993). The wider application of SWAP has been limited, however, because lens opacities absorb spectrally similar light and may confound results (Moss et al, 1995). While tests such as FDP and SWAP can show differences between groups of normal, susceptible and glaucoma subjects, their diagnostic significance in individuals is not proved. It also remains to be determined whether these tests are useful for assessing glaucoma progression. Despite visual fields being well-preserved, anatomical change correlating with retinal ganglion cell loss (Quigley et al, 1982; Kerrigan-Baumrind et al, 2000) may already be seen at the optic nerve head (Pederson and Anderson, 1980) and retinal nerve fibre layer (Sommer et al, 1991).

1.2.2 Threshold of detection and conversion

Visual field defects at the threshold of detection can be intermittent (Hart and Becker, 1982; Werner and Drance, 1977). Such defects may even disappear after treatment, only to reappear later; where intermittent abnormalities can take up to five years to become consistently present (Hart and Becker, 1982). Visual field defects that appear abruptly may simply represent those at threshold arriving at the end of their transient phase.

'Conversion' refers to persistent visual field defects developing in eyes without previous field defects and the term is usually used in ocular hypertension. Normal

fields 'convert' when visual sensitivity in one or more field locations decreases to cross threshold and comes to lie outside normal limits; this can be considered the earliest detectable form of visual field progression (Hart and Becker, 1982). Conversion does not imply that glaucoma has suddenly appeared; more likely, previously undetectable, subclinical disease has worsened to finally become detectable.

Aulhorn and Harms (1966) reported that the earliest visual field defects at conversion were spot-like scotomata in the arcuate and central 30° of the visual field. Inferior arcuate defects were predominantly nasal, but superior arcuate defects were more central and more likely to be near fixation. Contrary to Bjerrum's findings from 1889, they found that early scotomata were only uncommonly connected to the blind spot. Drance (1969) added that early nasal steps were as common as early arcuate defects and that early absolute scotomata were surrounded by relative defect. Heijl and Lvnquist (1983) later confirmed on automated static perimetry what Aulhorn and Harms (1966) and Drance (1969) had earlier found on manual kinetic perimetry. According to Hart and Becker (1982), the onset of early defects in ocular hypertension eyes converting on visual fields is gradual in 76%, abrupt in 7%, but transient in 17%.

Eyes with ocular hypertension are at increased risk of conversion to glaucoma. In the population based Barbados Eye Study (Leske et al, 2001b), the risk of conversion in ocular hypertension was six times higher than in people without any risk factors for glaucoma. Prospective studies in people with untreated ocular hypertension by the Collaborative Glaucoma Study (Armaly et al, 1980) (13 year study) and Kitazawa et al (1977) (9.5 year study) showed a conversion rate of 1.0-2.0%/year. Quigley et al (1994) (12 year study) found conversion in 10.5% of 647 prospectively followed treated and untreated subjects with ocular hypertension, giving a conversion rate of 0.9%/year. The risk of conversion in ocular hypertension is suggested to rise with IOP. Wilson and Martone (1996) estimated from pooled incidence data that the relative risk of developing glaucoma for baseline IOP below 24 mmHg was under 5.0, but for baseline IOP above 30 mmHg was greater than 15, at least three times more. Studies generally support a trend toward higher rates of conversion in groups with starting IOP over 26-30 mmHg (Armaly et al, 1980; David et al, 1977; Hovding and Aasved, 1986). However, randomised control trials

have failed to conclusively show that lowering IOP affects the rate of conversion in ocular hypertension (Kass et al, 1989; Epstein et al, 1989; Schulzer et al, 1991a; Kamal et al, 1999a).

Conversion also occurs in people with risk factors for glaucoma other than elevated IOP. In the Collaborative Glaucoma Study (Armaly et al, 1980), increased risk of conversion was seen not just in ocular hypertension but also in eyes with baseline IOP below 22 mmHg. In fact, age was the strongest risk factor for conversion, with subjects aged over 60 years seven times more likely to convert than those aged less than 40 years. Quigley et al (1994) reported that increasing age was an independent risk factor for conversion in a 12-year prospective study of ocular hypertension. In the Barbados Eye Study (Leske et al, 2001b), almost equal numbers of people with and without raised IOP were found to convert to glaucoma in the population, indicating that factors other than elevated IOP also influenced the risk of progression to conversion.

1.2.3 Critical phase

Once past threshold, glaucoma enters a critical phase carrying significant risk of blindness. Disease is no longer early and despite treatment up to two thirds of eyes will show visual deterioration (O'Brien and Schwartz, 1990; Chen and Bhandari, 2000; Hart and Becker, 1982; Jay and Murdoch, 1993; Katz et al, 1997; Poinoosawmy et al, 1999; Rasker et al, 2000; Kwon et al, 2001). Individuals with unilateral glaucoma have a 26% risk of developing contralateral field abnormality within five years (Susanna et al, 1978). Significant visual impairment may be present within a decade (Hattenhauer et al, 1998; Molteno et al, 1999; Hart and Becker, 1982) and absolute visual field loss within thirty years (Jay and Murdoch, 1993; Rasker et al, 2000). Scotomata frequently evolve by deepening, but enlargement, commonly in Bjerrum's area, and the development of new defects are also common (Mikelberg and Drance, 1984). Change over time usually follows a linear or curvilinear course but it may be episodic, having a step-wise pattern. More extensive and dense scotomata have been suggested to decay faster and more linearly (Mikelberg et al, 1986). Susceptibility to developing abnormality between upper and lower visual field hemispheres appears to be disparate. Over a decade, however, 22-43% of eyes with only one hemisphere affected initially will proceed

to develop bi-hemispheric defects (Hart and Becker, 1982; Mikelberg and Drance, 1984). Because superior defects tend to be more central (Aulhorn and Karmeyer, 1977; Heijl and Lundqvist, 1983), the visual impact of upper hemispheric involvement is expected to be greater. Ultimate visual prognosis is worse when both hemispheres are affected simultaneously: Hart and Becker (1982) found that despite treatment, 54% of eyes with initial bi-hemispheric involvement suffered absolute visual field loss over a decade.

1.2.4 Blindness

Blindness may occur despite treatment. The Olmsted County community study found that despite treatment, the risk of developing unilateral blindness was 27% and bilateral blindness was 9% over 20 years. Molteno et al (1999) found that despite IOP being controlled below 22 mmHg after filtration surgery, the probability of retaining useful vision declined by 31% over 15 years, with half of visual disability attributable to glaucoma. Kwon et al (2001) found a cumulative rate of glaucoma blindness over 22 years of 19% despite treatment.

Glaucoma is the third most important cause of worldwide blindness (The World Bank, 1993) and the commonest form of irreversible blindness (Thylefors et al, 1995). The extent of blindness from glaucoma is known mainly from blindness registries, in which diagnostic criteria and the completeness of information may vary. In England and Wales, glaucoma is estimated to be at least partly responsible for 13% of blindness. About a million people are registered blind or partially sighted in the United Kingdom. A survey of low vision clinic registers in Stockholm found that glaucoma was at least partly responsible for 55% of bilateral blindness. Prevalence of glaucoma-related blindness in persons aged over 50 years was seven times higher when compared with all age groups combined (Blomdahl et al, 1997). In the United States, the Model Reporting Area study pooled data from blindness registries in 16 states and found that the prevalence of glaucoma blindness in people aged 45-64 years was 8.8/100 000 in whites and 131.4/100 000 in non-whites (98% of whom were black) (Kahn and Moorhead, 1973, Wilson and Martone, 1996). Prevalence rose with age: in people aged over 85 years, prevalence was 261.4/100 000 and 746.9/100 000 for whites and non-whites respectively, representing a 30-fold increase in whites and six fold increase in non-whites. The Baltimore Eye

Survey also found more glaucoma blindness with increasing age and in blacks than whites, with blacks going blind on average ten years earlier (Tielsch, 1990). The number of bilaterally blind people in the US was estimated in 1990 as 890 000 (Tielsch, 1990; 1993); 12 000 new cases every year are expected to be due to glaucoma (Wilson and Martone, 1996). Sometimes there is already severe visual impairment at diagnosis: in Taiwan, a population survey found that about 20% of people just diagnosed with PACG were already visually impaired and seeing worse than 6/15 in the better eye (Congdon et al, 1996). Over 10% were already bilaterally blind, with visual acuities worse than 6/60. In the Olmstead County community study, at least one eye of 5% of persons with open angle glaucoma was already blind at diagnosis (Hattenhauer et al, 1998). Rigorous treatment can help those with uncontrolled disease (Migdal et al, 1994; Jay and Murray, 1988; Collaborative Normal Tension Study Group, 1998a; 1998b; The AGIS investigators, 2000), and it would seem that timely diagnosis and identification of progression is crucial to preventing visual disability and blindness from glaucoma.

Chapter 2
THE OPTIC NERVE IN GLAUCOMA AND PROGRESSION

2.1 FUNCTIONAL ANATOMY OF THE OPTIC NERVE

2.1.1 Ganglion cells

The optic nerve is a conduit for ganglion cell axons carrying partially processed visual information from the eye to the brain. The optic nerve is really a tract of white matter of the central nervous system (CNS) that retains many CNS features such as being myelinated by oligodendrocytes, covered by meninges, and having astrocytes and microglia. Anatomically the optic nerve can be subdivided into four parts: intraocular (*papilla, optic disc or optic nerve head*), intraorbital, intracanalicular and intracranial. The optic nerve ends in the optic chiasm but ganglion cell axons continue as the optic tract to synapse in the lateral geniculate body. The intraocular portion of the optic nerve – the optic nerve head – is taken to be the site of end-organ damage in glaucoma and many of the signs of the disease are seen here.

The bodies of ganglion cells are in the ganglion cell layer of the retina. Here, visual information is received from rod and cone photoreceptors through synapses with bipolar cells, the second order neurones of the visual pathway, and intervening amacrine and horizontal cells. Ganglion cells are morphologically diverse and have been classified by their common histological and physiological features as seen in the retinae of primates, cats and rabbits.

Classification. Polyak (1941) classified ganglion cells as two functionally significant classes. Midget cells had small soma and single apical processes that gave off dendrites in the inner plexiform layer, and are now thought to correspond to a physiological class of cells called P-cells (Rodieck et al 1985; Shapley and

Perry, 1986; Kaplan et al, 1990). P-cells process visual information by receptive fields having a small concentric centre-surround organisation (order of magnitude of a single cone) and respond optimally to colour stimuli in the red-green spectrum, but have low contrast sensitivity. Speed of axonal conduction in P-cell fibres is considered slow to medium, and their axons project to the parvocellular layer of the lateral geniculate nucleus.

Polyak described parasol cells as having larger bodies with several apical processes, giving off dendrites with more extensive arborisation than midget cells. Two physiological classes of cells are associated with parasol cells. The first has concentric centre-surround receptive fields and responds optimally to blue stimuli. The second has receptive fields that are sensitive to luminous contrast, motion, respond to a broad band of spectral sensitivity, and have high scotopic sensitivity. These cells are termed M-cells, have fast axonal conduction velocities and project to the magnocellular layer of the lateral geniculate nucleus (Rodieck et al 1985; Shapley and Perry 1981; Kaplan et al, 1990). Additionally, existence of a third retinogeniculate pathway, called the koniocellular or K-cell pathway, which is anatomically distinct from M- and P-cells and mediates blue-yellow opponent information, has recently been reported (Martin et al, 1997).

About 90% of our million or so ganglion cells are classified as P-cells, with M-cells making up most of the remaining 10%. P- and M-cell physiological systems are called the 'parallel pathways' of visual processing. Separate studies report the mean diameters of ganglion cell axons in the optic nerve as 0.72μm and 0.96μm (Repka and Quigley, 1989; Mikelberg et al, 1989). Ganglion cell axons transmit electrical nerve impulses, but they also transport essential neurotrophins and subcellular constituents to and from the brain.

Functional significance to glaucoma and its testing. Ganglion cell loss underlies the reduced visual sensitivity seen in glaucoma, and this can be replicated in experimental primate glaucoma (Harweth et al, 1999). In 'early' glaucoma, visual deficits that are not detectable by white-on-white perimetry may be detected by selectively testing visual sensitivity to short spectral wavelengths (Johnson et al, 1995), motion (Silverman et al, 1990), phase reversal/flicker (Anderson and

O'Brien, 1997), contrast (Falcao-Reis et al, 1990) and the spatial frequency doubling illusion (Maddess and Henry, 1992), all of which probe functions conventionally attributed to the M-cell pathway. Whether abnormality on such testing reflects a preferentially reduced M-cell population is not clear. M-cells are suggested to correspond to large-bodied retinal ganglion cells, which in turn are reported to be selectively lost in glaucoma (Dandona et al, 1991; Glovinsky et al, 1991; Quigley et al, 1987). But some have not found any selectivity in cell loss (Kalloniatis et al, 1993; Vickers et al, 1997). Some studies of the lateral geniculate nucleus in human and primate glaucomatous eyes have reported more loss in its magnocellular than parvocellular layers (Dandona et al, 1991; Chatuverdi et al, 1993; Weber et al, 2000) but others (Yucel et al, 2000; 2001) found in primate experimental glaucoma that while lateral geniculate nucleus cells were lost both in its parvo- and magnocellular layers, parvocellular loss was greater. It may also be that the apparently selective loss of large ganglion cells simply reflects cell body shrinkage (Morgan et al, 2000; Weber et al, 1998). Alternatively, it could be that while both M- and P-cell populations are similarly reduced in glaucoma, visual abnormalities from M-pathway dysfunction become manifest first because M-cells are fewer, more sparse and have less 'redundancy' than do P-cells (by a factor of nine) (Johnson, 1994).

Ganglion cell death. Because of embryological attrition by apoptosis, adult eyes have half as many ganglion cells as fetal eyes (Rakic and Riley, 1983; Provis et al, 1985). In adults, ganglion cells are still lost, but more slowly, at an estimated rate of 500-2000 per year (Repka and Quigley, 1989; Mikelberg et al, 1989; Balaszi et al 1984). By what process the physiological loss of adult ganglion cells occurs is not well described.

In glaucoma, the primary site of ganglion cell axonal damage leading to cell death is believed to be at the level of the optic nerve head's lamina cribrosa which lies in line with the sclera (Anderson and Hendrickson, 1974; Minckler et al, 1977; Quigley et al, 1981). Here, mechanical distortion, diminished blood supply or secondary neurotoxicity could lead to cell damage. At least some ganglion cell death in glaucoma occurs by apoptosis (Quigley et al, 1995; Kerrigan et al, 1997; Okisaka et al, 1997), postulated as due either to primary injury or secondary degeneration (Schwartz and Yoles, 2000). Apoptosis may be a pathway by which

putative pathological mechanisms such as elevated hydrostatic pressure (Agar et al, 2000; 2001), glutamate neurotoxicity (Dreyer et al, 1996; Vorwerk et al, 2000), neurotrophic deprivation (Pease et al, 2000; Yuan and Yanker, 2000) and autoimmunity (Tezel and Wax, 2000) cause ganglion cell death. Nitric oxide (Neufeld, 1999) and intracellular calcium toxicity and ischaemia have also been reported to lead to ganglion cell death, probably by affecting the mitochondria.

2.1.2 The retinal nerve fibre layer

The retinal nerve fibre layer (RNFL) contains the axons of ganglion cells travelling from the ganglion cell layer of the retina to the optic nerve head, and is visible ophthalmoscopically as fine, bright striations. Processes of Muller cells bundle axons together into fascicles surrounded by astroglia and a rich capillary bed. Axons tend not to deviate from their own bundles and course radially toward the optic nerve head where they turn perpendicularly to form the neuroretinal rim. They then traverse the lamina cribrosa, beyond which they become myelinated to speedily and efficiently conduct electrical impulses by saltatory conduction.

Axons from the upper and lower halfs of the retina do not intermingle and are separated by the median raphe passing through the fovea. Nasal axons travel straight to the optic nerve head. Axons originating in the foveal and macular region travel in the papillomacular bundle and enter the optic nerve head temporally. Axons from superior, inferior and temporal to the macular region arch around the papillomacular bundle to form the arcuate bundles and enter the optic nerve head superiorly and inferiorly. The arcuate bundles are thicker than the papillomacular bundle, where the RNFL is thinnest. The RNFL is thickest at the edge of the optic nerve head where it becomes heaped up, hence the term papilla (Quigley and Addicks, 1982; Radius, 1980; Varma et al, 1996).

2.1.3 The optic nerve head

The optic nerve head has a superficial nerve fibre layer, and pre-laminar, laminar and post-laminar portions. The ***superficial nerve fibre layer*** of the optic nerve head is covered by the inner limiting membrane of Elschnig, a continuation of the inner

limiting membrane of the retina which is derived from astrocytes. Astroglia between bundles of axons in this region is sparse but increases progressively towards the retro-laminar region; it makes up 5% of the volume of the superficial nerve fibre layer, 15% of the pre-laminar region, and 23% of the laminar region (Minckler et al, 1976a). Wang et al (2002) report that astroglia in the retina and optic nerve head are morphologically and functionally changed in glaucoma.

The ***pre-laminar*** optic nerve head comprises the neuroretinal rim, optic cup and central retinal vessels. The neuroretinal rim contains bundles of unmyelinated axons lying within channels made from astrocytes. Astrocytes and capillaries are interspersed between axons. Apart from structural support, astrocytes have a role in repair, glycogen storage, electrolyte homeostasis, inactivating neurotransmitters and participating in immune responses. The lamina cribrosa can be seen in the floor of the cup with its sieve-like pores. The central retinal vessels are surrounded by connective tissue and lie centrally in this region.

The ***lamina cribrosa*** in the laminar portion of the optic nerve head is a dense strip of connective tissue bridging the scleral foramen where the strong wall of the eye is deficient. The remarkably engineered cribriform plates of the lamina have two roles to balance: they provide structural and nutritional support to axon bundles traversing its pores, while maintaining the structural integrity of the eye. The development of laminar trabeculae is accompanied by ingrowth of branches of the short ciliary arteries and circle of Zinn, and scleral connective tissue and glia (Anderson et al, 1967). It is thus not surprising that each trabeculum has its own collagen-surrounded capillary. About ten stacked cribriform plates alternate with sheets of glia and blend peripherally with sclera (Anderson, 1969; Radius and Gonzales, 1981).

The cribriform plates have pores arranged almost but not exactly in anterior-posterior register to form tunnels for traversing axons. The course of axons does not strictly adhere to the tunnel arrangement, however, as a few axons deviate from one tunnel to another (Morgan et al, 1998). Deviant axons may be particularly susceptible to injury were the cribriform plates to collapse into each other as is reported to happen in glaucoma (Quigley et al, 1983). Astrocytes make up 40% of the axonal bundle tissue mass (Minckler et al, 1976a). The several hundred pores in

each plate (Ogden et al, 1988; Dandona et al, 1990) are bounded by strong trabeculae and vary in size by region. Quigley and Addicks (1981) showed that pores in the superior and inferior laminar quadrants are bigger than pores in the nasal and temporal quadrants so that the lamina cribrosa is not uniform in structure, being denser temporally and nasally than superiorly and inferiorly. The nature of pore size variation differs between individuals (Radius and Gonzales, 1981). It is postulated that structural variation within the lamina cribrosa and between people influences axon susceptibility to mechanical damage from IOP and predisposition to glaucoma.

The cribriform plates have a core of longitudinally orientated elastin fibres (Hernandez et al, 1987; 1989; 1991; 1992; 1994). The plates insert into a specialised concentric region of sclera that is rich in circumferentially orientated elastin. By contrast, the sclera outside this insertion region has short, sparse and randomly orientated elastin fibres. The cribriform plates are more elastin-dense than surrounding sclera and expected to be more flexible. With age, elastic fibres thicken, lengthen and look more tubular, and collagen fibres change in composition and become more densely packed so that the lamina cribrosa probably becomes more rigid.

In the ***post-laminar*** region, axons are myelinated posterior to the lamina cribrosa; this is the intra-orbital portion of the optic nerve. The nerve increases in calibre because of myelination, is bathed in cerebrospinal fluid, and invested in thick meninges. Myelination is by oligodendrocytes, and immunologically competent microglia here participate in phagocytosis.

2.2 OPHTHALMOSCOPIC APPEARANCE OF THE OPTIC DISC

Ophthalmoscopically, the optic disc is usually vertically oval with a central pale region called the cup, and outer concentric pink region called the neuroretinal rim. The optic cup has no nerve fibres but the pink neuroretinal rim carries ganglion cell axons converging on the nerve.

Size of the optic disc. The optic disc's size varies widely and is associated with factors such as race (Chi et al, 1989; Varma et al, 1994) and refractive error (Jonas et al, 1988c; Varma et al, 1994; Ramrattan, 1999). The inner scleral ring of Elschnig represents the disc margin while the outer scleral ring marks the edge of the scleral canal. Disc size tends to vary with the size of the scleral canal (Jonas et al, 1988d). Jonas et al (1988a) reported in a clinic sample that disc area ranged from 0.86-5.54 mm^2 with a mean of 2.69 mm^2. Disc area data pooled from studies of white clinic populations ranges from 0.80-6.00 mm^2, with a seven-fold difference seen between the largest and smallest discs (Jonas et al, 1999). This reflects the large anatomical variation between people, but also likely differences in image magnification between ocular imaging systems. In fact, disc size has a narrower range when measured histologically: mean area of 2.48-2.75 mm^2 and mean diameter of 1.78-1.87 mm (Ogden et al, 1988, Jonas et al, 1988d, Quigley et al, 1990). Two histological studies, one in primates (Quigley et al, 1991a) and the other in humans (Jonas et al, 1992a), have shown that the number of optic nerve axons increases with disc area. Axon density varies inversely with disc size (Jonas et al, 1992a). Although large discs may have more neural reserve than small discs, it is postulated that the lamina cribrosa of larger discs is displaced more by variation in IOP (Chi et al, 1989). There is no consensus on whether disc size influences susceptibility to glaucoma.

Size of the normal neuroretinal rim is inversely proportional to optic cup size. Mean normal rim area is reported to range from 1.13-1.97 mm^2 (Britton et al, 1987, Caprioli, 1987, Jonas et al, 1988a, Chi et al, 1989, Funk et al, 1989, Tsai et al, 1992, Varma et al, 1994). Normal rim area is significantly correlated with the area of the optic disc and hence large optic discs tend to have more neuroretinal rim and axons than small discs (Quigley et al, 1991a; Jonas et al, 1992a). The cup tends to be large in big optic discs and small or even non-existent in small discs (Jonas et al (1988a). The normal rim is broadest inferiorly, then superiorly, then nasally, and thinnest temporally, so that the cup normally looks horizontally oval; change in this pattern suggests glaucomatous damage (Kirsch and Anderson, 1973a; 1973b). The normal rim configuration correlates with the RNFL being thicker and more visible inferiorly and superiorly in the arcuate bundles than over the temporal papillomacular bundle.

2.3 PHYSICAL SIGNS OF PROGRESSION

Various signs may be seen in and around the optic nerve that betray progression or a risk of progression. This section reviews what is known of the nature of physical change at the optic nerve head as seen in eyes with suspected and manifest glaucoma.

2.3.1 Decreased rim, increased cupping

The optic nerve head becomes increasingly cupped with disease progression.

Pattern of progressive cupping over the period of conversion in longitudinal studies. Progressive cupping may be seen before visual field defects appear in eyes with ocular hypertension and ocular hypertension eyes converting to glaucoma (Pederson and Anderson, 1980; Sommer et al, 1980; Tuulonen and Airaksinen, 1991; Airaksinen et al, 1992; Zeyen and Caprioli, 1993; Odberg and Riise, 1985; Funk, 1991a; 1991b; Motolko and Drance, 1981; Yablonski et al, 1980). Pederson and Anderson (1980) found that 79% of 29 ocular hypertension eyes with conversion and progressive cupping showed generalised cup expansion, whereas 17% had cupping mainly in the vertical axis. Tuulonen and Airaksinen (1991) noted that of 23 converters, as many had concentric cupping as vertical cupping (44% each). Sommer et al (1980) reported that the cup became vertically oval in 67% of eyes. Because the normal cup tends to be horizontally oval, vertical rim loss would have to exceed horizontal rim loss for the cup to initially appear concentrically enlarged then vertically oval. Such vertical change may be missed in subjective assessment, however, so that progressive cupping is perceived to be symmetrical (Airaksinen et al, 1996). Cross-sectional studies agree that change in the inferior and superior rim poles tends to exceed nasal and temporal change, at least initially, making the cup vertically oval with time (Kirsch and Anderson, 1973a; 1973b; Read and Spaeth, 1974).

Rate of neuroretinal rim loss in longitudinal studies. Airaksinen et al (1992) studied 123 eyes by planimetry and found progressive rim area loss in 57% of eyes with ocular hypertension and 79% of glaucomatous eyes. The more initial rim there was, the greater the percentage rim loss. Pattern of change was linear in 49%, curvilinear in 29% and episodic in 22%. The rate of rim area loss in normal eyes was 0.23%/year by linear regression, and 2.75%/year in ocular hypertension and 3.47%/year in glaucoma, 12 and 15 times the rate in normal eyes respectively. Zeyen and Caprioli (1993) found that the average rate of rim area progression before conversion was 1.7%/year but after conversion was 2.1%/year, a rate not dissimilar to that calculated by Airaksinen et al (1992).

Patterns of neuroretinal rim loss at different stages of disease in cross-sectional studies. Jonas et al (1993a) compared disc photographs of 801 glaucoma eyes (POAG) with 495 normal control eyes for regional differences in rim area at various stages of visual field damage. Overall, they found that the largest differences between early glaucoma and normal eyes were in the inferior and superior poles.

1. Eyes with early disease (average mean deviation (MD)=-3.3dB) differed most from normal eyes in the inferior (rim area was 15% less than normal), and superior poles (12%); differences elsewhere were less (temporal 3%, nasal 4%).
2. In moderate disease (MD=-4.4dB), differences were most inferiorly (38%) and superiorly (34%), followed by in the horizontal temporal region (31%). Rim difference was least nasally (28%).
3. In moderate-advanced disease (MD=-7.3dB), differences were greatest inferiorly (60%), and similar superiorly (58%) and temporally (57%). The difference was 46% nasally.
4. In advanced disease (MD=-13.4db), differences temporally (83%) exceeded those inferiorly (74%) and superiorly (77%). The difference was least nasally (61%).
5. In severe disease (MD=-18.1dB), rim difference was greatest temporally (97%) followed by superiorly (88%) and inferiorly (84%). The largest remaining rim was seen nasally (83%).

They suggested that rim loss at a given stage of glaucoma may involve any region of the optic nerve head, but the location of most pronounced loss varies with severity of disease.

Small optic nerve heads with small and shallow cupping or no cup may undergo:

1. *Overpass cupping.* This change is very early and does not reach the lamina cribrosa. The optic nerve head seems to have a hollow underneath its surface, appearing as subtle central pallor. Many eyes do not have visual field defects (Spaeth et al, 1976; Read and Spaeth, 1974; Hitchings and Spaeth, 1976).
2. *Saucerisation.* The surface looks like having collapsed, leaving a gradually sloping saucer-like region. Saucerisation is often focal, inferotemporal, and associated with a paracentral field defect (Spaeth et al, 1976).

Larger optic nerve heads with larger cups may have:

1. *Concentric enlargement of the cup.* The rim appears to thin uniformly so that the cup enlarges symmetrically and cup/disc ratio remains constant in all axes. It may seem to lack instantly recognisable features of glaucoma (Pederson and Anderson, 1980; Spaeth et al, 1976).
2. *Vertical extension.* The cup extends superiorly and inferiorly to exceed change in its horizontal axis, giving the impression of a vertically elongating centrally placed cup (Spaeth et al, 1976).
3. *Temporal unfolding.* The rim thins primarily in the temporal half of the disc and does not seem to affect the nasal rim and blood vessels. The cup looks vertically elongated because change is more vertically than horizontally, and the cup appears to be located in the temporal optic nerve head (Spaeth et al, 1976; Read and Spaeth, 1974).
4. *Notching or focal extension.* The cup appears to extend into the rim to produce a cresenteric-shaped notch in the internal edge of the neuroretinal rim (Kirsch and Anderson, 1973a; Read and Spaeth, 1974; Spaeth et al, 1976; Hitchings and Spaeth, 1976). The edge of the notch is usually steeper than the surrounding rim, and it may deepen as well as expand sideways. A large notch that has grown sideways may blend with the contour of the rim edge and appear less obvious. Notches are less apparent in small cups and are seen more commonly inferiorly than superiorly (Kirsch and Anderson, 1973a; Spaeth et al, 1976). An *acquired pit* is a subtype of notching representing very localised tissue loss. It occurs in regions of extensive rim loss and is characterised by focal deepening into optic nerve tissue at the edge of the disc. Continued localised depression eliminates more surrounding neural tissue and affects the adjacent peripapillary region to cause atrophy, mottling and change in pigmentation.

5. *Nasal cupping.* Ongoing damage appears localised to the nasal portion of the disc (Spaeth, 1993). It may, however, represent mild asymmetry in concentric cup enlargement.
6. *Senile sclerotic cupping.* Diffuse rim loss occurs, the cup's slope is gradual, and the optic nerve head looks pale. There is usually associated marked peripapillary atrophy (Broadway et al, 1999; Geijssen and Greve, 1987).
7. *Bean pot cupping.* Cupping is very advanced and bulges laterally beyond the scleral lip (Spaeth et al, 1976; Hitchings and Spaeth, 1976).

2.3.2 Increased visibility of the lamina cribrosa

More of the lamina cribrosa becomes visible and its pores appear more elongated with increased cupping (Miller and Quigley, 1988; Susanna, 1983; Bhandari et al, 1997). The bigger cup makes the optic nerve head look paler.

Histopathological correlate. Quigley et al (1983) showed in post-mortem human glaucoma eyes that the cribriform plates become compressed then collapse and bow posteriorly. The lamina cribrosa rotates at its scleral insertion, and extent of posterior bowing increases with increasing glaucoma severity. Similar changes are seen in primate models of glaucoma (Pederson and Gaasterland, 1984). Posterior bowing of the lamina cribrosa with elevated IOP has been replicated in *in vivo* and *in vitro* studies (Coleman et al, 1991; Burgoyne et al, 1995a; 1995b; Zeimer and Ogura, 1989). Experimental studies show that slow and rapid axonal transport can get blocked at the lamina cribrosa with raised IOP (Anderson and Hendrickson 1974, Minckler et al 1976b; 1977; Quigley and Anderson, 1977). Larger inferior and superior lamina pores are thought to correlate with axons being more prone to damage in this region (Quigley and Addicks, 1981; Quigley and Green, 1979; Quigley et al, 1983). Lamina cribrosa changes seen with elevated IOP are postulated to cause injury, loss of structural and nutritional support for nerve fibres, and ultimately ganglion cell death.

Ultrastructural changes. Collagen and elastin help the lamina cribrosa to withstand mechanical stress and strain. In POAG, the extracellular matrix of the lamina is loose and disorganised, basement membrane thickened, laminar beams broken, and elastic fibres fragmented (Hernandez et al, 1990; 1992). The lamina cribrosa in

primate glaucoma resembles that of human glaucoma (Morrison et al, 1990). With progression, elastin fibres become more disorganised, granular and reduced in number (Hernandez, 1992). Ultrastructurally, elastic fibres are fragmented and associated with non-fibrillar elastic-like material and bundles of microfibrils (Hernandez, 1992), possibly reflecting a cycle of abnormal degradation and biosynthesis. The density of collagen in cribriform plates decreases (Hernandez, 1992; Quigley, et al, 1991b). Together, these changes could weaken cribriform plates leading to collapse and further tissue remodelling.

2.3.3 Increased disc pallor

Increased cupping lays bare more of the pale lamina cribrosa so that the optic nerve head looks more pale. Pallor of the neuroretinal rim has also been reported. Quigley et al (1982b, 1984) found that capillary volume was decreased along with thinned neuroretinal rim and suggested that this made rim tissue more transparent to allow underlying collagenous connective tissue to reflect more light, causing pallor. This correlates with the clinical association between increased translucency and diminished pinkness of the glaucomatous rim (Hitchings and Spaeth, 1976). Increased pallor is associated with capillary filling defects in the rim and cup and leakage on fluorescein angiography which increases in size and number with progression (Nanba and Schwartz, 1988). This is even seen in ocular hypertension (Tuulonen et al, 1987, Nanba and Schwartz, 1988) and has been associated with RNFL atrophy (Nanba and Schwartz, 1988) and visual field loss (Fishbein and Schwartz, 1977; Tuulonen et al, 1987). However, assessing pallor is highly subjective and expected to be poorly reproducible. Ocular media opacities and uncertainty in telling the neuroretinal rim from the central optic cup and surrounding peripapillary atrophy makes assessing pallor difficult. Colour variation may also arise in photographic processing.

2.3.4 Shifted blood vessels

The course, pattern of branching and diameter of blood vessels may change with increased cupping. Branches of the major vascular trunk adjacent to the nasal neuroretinal rim may be displaced nasally as the cup enlarges (Varma et al, 1987).

"Bayonetting" describes blood vessels that appear kinked as they cross the cup edge. A blood vessel that has lost underlying rim but which remains suspended without support is called an "overpass" vessel. A circumlinear vessel that has lost adjacent rim tissue and appears to have receded from the rim edge is termed "bared". Blood vessels may narrow with progressive glaucoma and be associated with regions of greatest rim and RNFL loss (Jonas and Schiro, 1993b).

2.3.5 Disc haemorrhages

Characteristics. Disc haemorrhages are regarded as a marker of progressive glaucoma. They have a predilection for the temporal half of the optic nerve head, especially infero-temporally, followed by supero-temporally then horizontal-temporally (Hendrickx et al, 1994; Jonas and Xu, 1994; Diehl et al, 1990). This corresponds regionally to the early preferential infero-temporal and supero-temporal neuroretinal rim loss and Bjerrum scotomata reported in early glaucoma. They resolve within two and 35 weeks after appearing, with most lasting more than four weeks (Kitazawa et al, 1986; Heijl, 1986; Sonnsjo, 1988). Between 12-64% of disc haemorrhages recur, often in the same disc quadrant (Kitazawa et al, 1986; Hendrickx et al, 1994; Shihab et al, 1982; Bengtsson et al, 1981). Disc haemorrhages are postulated to be caused by microinfarctions (Begg et al, 1971; Lichter and Henderson, 1978), venous occlusion or mechanically ruptured small blood vessels (Quigley et al, 1981).

The overall prevalence of disc haemorrhages in population surveys ranges from 0.8-1.4% (Klein et al, 1992; Healey et al, 1998; Bengtsson et al, 1981). In the Blue Mountains Eye Study, the prevalence of disc haemorrhages in glaucoma was 13.8%. This was higher in NPG (25%) than POAG (8%)(Healey et al, 1998). The clinic-based prevalence of disc haemorrhages in glaucoma ranges from 2.4-58.3% (Kitazawa et al, 1986; Jonas and Xu, 1994; Diehl et al, 1990). Prospective clinic-based studies agree that the incidence of disc haemorrhages is higher in NPG than POAG (Hendrickx et al, 1994; Gloster, 1981, Krakau et al, 1983; Kitazawa et al, 1986). After follow up over 6-32 months, Kitazawa et al (1986) reported disc haemorrhages in 20.5% of NPG eyes but only 4.2% of POAG eyes. In a prospective study of up to 15 years, Rasker et al (1997) found disc haemorrhages in 2.9% of NPG eyes but 1.6% of POAG eyes.

Marker of progression. In *POAG*, between 33-89% of eyes with disc haemorrhages eventually show visual field progression, 1.4-4.3 times more than eyes without disc haemorrhages (Diehl et al, 1990, Rasker et al, 1997; Siegner and Netland, 1996; Drance et al, 1977; Shihab et al, 1982; Airaksinen and Tuulonen, 1984). Disc haemorrhages are more common in POAG than ocular hypertension. In the Blue Mountains Eye Study, the prevalence of disc haemorrhages in POAG was 8%, five-fold more than in ocular hypertension (1.5%) (Healey et al, 1998). According to Kitazawa et al (1986), Gloster (1981), and Diehl et al (1990), the prevalence of disc haemorrhages in ocular hypertension is 4.4-8.4 times less than in POAG, although a study by Rasker et al (1997) found prevalence was similar between groups.

Disc haemorrhages in eyes with *ocular hypertension* may portend progression to glaucoma. In ocular hypertension, between 22-53% of eyes with disc haemorrhages eventually develop visual field defects, 2.2-11.3 times higher than eyes without disc haemorrhages (Airaksinen et al, 1981b; Diehl et al, 1990; Siegner and Netland, 1996; Drance et al, 1977). Between 32-83% of eyes with disc haemorrhages already have signs of optic disc abnormality, 3.8-4.3 times more than eyes without disc haemorrhages (Siegner and Netland, 1996; Airaksinen et al, 1981a). Airaksinen et al (1981b) reported that 24% of ocular hypertension eyes with disc haemorrhages eventually developed RNFL defects. In ocular hypertension, Diehl et al (1990) observed progressive RNFL atrophy in 42% of eyes within one year of disc haemorrhages being observed, 14 times more often than in eyes without disc haemorrhages. Neuroretinal rim and RNFL abnormalities are 3.5-3.8 times more common in eyes with than without disc haemorrhages (Airaksinen et al, 1981a; Airaksinen and Tuulonen, 1984 Diehl et al, 1990; Siegner and Netland, 1996).

In *NPG*, between 80-100% of eyes with disc haemorrhages show later visual field progression, a rate 2.5 times higher than NPG eyes without disc haemorrhages (Chumbley and Brubaker, 1976; Siegner and Netland, 1996; Kitazawa et al, 1986).

Normal eyes. Disc haemorrhages may not always represent progression, however, as they are also seen in people not diagnosed with glaucoma or ocular hypertension. In clinic-based studies, Jonas and Xu (1994)(595 normal eyes) and Diehl et al (1990)(661 normal eyes) found no disc haemorrhages in normal eyes but Kitazawa

et al (1986) found disc haemorrhages in two of 473 normal eyes, giving a prevalence of 0.4%. Bengtsson et al (1981) found disc haemorrhages in 5 of 1496 normal persons in a Swedish population, giving a prevalence of 0.3%. The Blue Mountains Eye Study found a higher prevalence of 1.0% (Healey et al, 1998). Although disc haemorrhages were more prevalent in glaucoma, the relatively small number of glaucoma subjects in this study (108 of 3654) meant that most disc haemorrhages (70%) were actually seen in people without a diagnosis of glaucoma. In people not diagnosed with glaucoma or ocular hypertension, cup-disc ratios were higher in eyes with disc haemorrhages than eyes without haemorrhages, and it could be that the former were at risk of manifest glaucoma. However, they found that disc haemorrhages were also independently associated with diabetes, systemic hypertension and migraine.

2.3.6 Increased peripapillary chorioretinal atrophy

Description. Peripapillary chorioretinal atrophy is categorised as two zones called alpha and beta (Jonas et al, 1989a, 1989b, 1992b). Both can increase as glaucoma progresses. The beta zone is adjacent to the optic nerve head, between the optic nerve head and edge of normal retina. Large choroidal vessels, sclera and irregular pigmentation are usually visible in the beta zone. The alpha zone is peripheral to the optic nerve head and beta zone; it has a variegated hypo-hyperpigmented appearance due to the underlying retinal pigment epithelium and choroid being thinned. The beta zone is present in 12-20% of normal eyes but the alpha zone is reportedly universal (Jonas et al, 1989a; 1989b; 1992b). In glaucoma, peripapillary atrophy is correlated with rim loss, narrow retinal vessels, poorly visible RNFL and the field location of most marked abnormality (Jonas et al, 1989a; 1989b; 1992b). The alpha and beta zones are larger, and the beta zone more frequent in eyes with glaucoma compared with normal eyes. Increased peripapillary atrophy represents a more deficient blood-retinal barrier (Tso et al, 1975).

Progressive change in glaucoma. Airaksinen et al (1987) found in a group of eyes with POAG that the area of peripapillary atrophy increased linearly over five years and was correlated with concurrent rim area loss. Rockwood and Anderson (1988) observed progressive peripapillary changes in 21% of eyes with POAG having visual field progression. Tezel et al (1997a; 1997b) retrospectively studied 98 eyes

of ocular hypertension converters and found in 49% that peripapillary atrophy increased before visual field or optic disc change was detected. Over at least ten years, peripapillary enlargement was five times more common in ocular hypertension converters than 252 control ocular hypertension eyes without conversion. Multivariate analysis suggested that area of the beta zone relative to optic disc size at baseline was a significant risk factor for conversion (relative risk of 1.32). Motolko and Drance (1981) found that peripapillary atrophy was larger in ocular hypertension converter eyes than in control ocular hypertension eyes. Jonas and Königsreuther (1994) found that peripapillary atrophy and rim area were inversely correlated in 104 subjects with ocular hypertension, but not in 216 normal control subjects. Kasner et al (1989) found that having peripapillary crescents in ocular hypertension increased the risk of glaucoma by two to three fold. These studies suggest that peripapillary atrophy, especially beta zone atrophy, is an early sign of glaucoma in ocular hypertension, and that progressively enlarged atrophy reflects deterioration.

Histopathological correlate. Hayreh et al (1998, 1999) found that peripapillary atrophy progressively enlarged in 36 primate eyes with experimental ocular hypertension. This was more marked temporally than nasally. Histologically, the choroid was thinned with pigment reduced, choriocapillaris fragmented, retinal pigment epithelium damaged, but Bruch's membrane relatively preserved. The beta zone was bigger and more common at the end of the study. There was associated progressive glaucoma-like cupping, seen histologically as septal thickening in the laminar and retrolaminar optic nerve head, backward bowing of the lamina cribrosa, axonal loss and increased glial density. The area of the beta zone was negatively correlated with rim area and always larger in the eye with raised IOP.

2.3.7 Development and enlargement of retinal nerve fibre layer defects

Description. Retinal nerve fibre layer defects are regions where the RNFL is thinned and the normal striate pattern of the RNFL lost, as can be seen by red-free photography. Green light is brilliantly backscattered by the RNFL but absorbed by melanin in the retinal pigment epithelium and choroid, which appear dark.

Experimental studies suggest that RNFL defects become discernable when normal RNFL thickness halves (Quigley and Addicks, 1982). Thickness of RNFL lying between second order retinal blood vessels and the inner limiting membrane is about 50μm. Thinning of the portion of RNFL overlying blood vessels results in these vessels standing out in relief against the surrounding retinal surface. Experimental studies show RNFL defects are associated with reduced numbers of nerve fibres (Radius and Pederson, 1984).

Significance. Hoyt and Newman (1972) were the first to associate RNFL defects with glaucoma and suggested the defects were an early sign of disease. Sommer et al (1991c) corroborated this in a longitudinal study of eyes with ocular hypertension which showed that RNFL defects could precede visual field conversion by as much as six years. Quigley et al (1992), Tuulonen and Airaksinen (1991) and Diehl et al (1990) confirmed this finding, showing that between 78-100% of converter eyes already had RNFL defects before visual field defects appeared. The number of ganglion cells in eyes with ocular hypertension may already be significantly reduced despite their white-on-white kinetic visual fields remaining normal (Quigley et al, 1982a). Although this finding has been disputed (Mikelberg et al 1995b), it has since been replicated in post mortem ocular hypertension eyes that had received static perimetry (Kerrigan-Baumrind et al, 2000) and monkeys with experimental ocular hypertension and able to perform automated perimetry (Harweth, 1999).

Characteristics of change. RNFL defects tend to be seen earliest in the inferior and superior arcuate bundles corresponding to the inferior and superior poles of the optic nerve head respectively. RNFL defects in glaucoma may appear localised or diffuse, and can progress. Localised defects are often preceded by small splinter haemorrhages, look wedge-shaped, and fan out from the optic nerve head margin to the periphery (Airaksinen et al, 1981b; Jonas and Schiro, 1994). Tuulonen and Airaksinen (1991) in a longitudinal study of 23 eyes with ocular hypertension reported diffuse RNFL loss in 52%, localised loss in 31% and combined localised and diffuse loss in 17%. All the RNFL defects progressed with follow up. Quigley et al (1992) found in a longitudinal study of 37 converter eyes with RNFL defects that 49% of RNFL defects progressed after five years. Jonas and Schiro (1994) saw localised RNFL defects in 20% of 421 glaucoma eyes but only 0.5% of 193 normal

eyes. Localised defects were mainly in the arcuate bundles and increased over time to become more diffuse. It has been suggested that localized RNFL defects are more common in NPG than POAG (Yamazaki et al, 1991). Tuulonen and Airaksinen (1991) noted that localized and diffuse atrophy could be seen simultaneously in the same eye and that fresh defects appeared over time. Arcuate bundle striations were lost with further progression to leave only subtle striations in the papillomacular bundle. Remaining RNFL striations may be lost completely in advanced glaucoma.

RNFL defects have been seen adjacent to disc haemorrhages, which the defects follow by six to eight weeks (Airaksinen et al, 1981b). Diehl et al (1990) noted RNFL defects appearing after disc haemorrhages in 42% of eyes with ocular hypertension and 50% of eyes with POAG. This correlates with findings after experimental optic nerve transection where RNFL striations become less visible after a month to be lost completely after a further month (Quigley et al, 1977a). RNFL defects may lie next to rim notches or marked peripapillary atrophy (Airaksinen et al 1981b; Jonas and Schiro 1994; Jonas and Xu, 1994). Airaksinen and Heijl (1983) found that RNFL defects preceded new perimetric abnormality in eyes already having visual field defects.

Chapter 3
CONVENTIONAL TESTING FOR PROGRESSION

3.1 INTRAOCULAR PRESSURE: IMMEDIATE ESTIMATE OF LONGER TERM COURSE

It can be inferred from population studies that the absolute level of IOP below which ganglion cell loss from glaucoma ceases varies widely between people. We are still ignorant of how other risk factors influence the disease and IOP is the only risk factor that can be manipulated to stop or slow progression. However, random IOP is only loosely correlated with optic nerve damage and there are limits to which IOP can be reduced, dictated by treatment side effects and the possibility of hypotony, especially from filtration surgery.

IOP is commonly measured by applanation tonometry, which itself has inaccuracies (Foster et al, 2000). In measuring IOP, clinicians should be aware of extremes of corneal thickness (Shah et al, 1999), observer bias (Hollows and Graham, 1966), and the diurnal rhythm of IOP (Liu et al, 1999), which varies between individuals and with disease.

The course of glaucoma varies between individuals so that individualising therapy is necessary. But telling whether treatment goals are achieved depends a lot on subjective clinical judgment, aided by reliable clinical measurements where available. Clinicians are forced initially to guess a level of IOP – known as 'target pressure' – which will stop or slow further damage and visual impairment (Singh et al, 2000; Hitchings and Tan, 2001). Once target pressure is achieved, the level of IOP still needs to be monitored over time. Peak IOP over many readings has been suggested as more predictive of visual field progression than random IOP readings (Bergea et al, 1999; Zeimer et al, 1991; Asrani et al, 2000). However, the real guide

for long-term clinical management is not IOP itself but the apparent course taken by the optic neuropathy; it is standard practice to evaluate this by sequentially examining the visual field and optic disc.

3.2 VISUAL FIELD TESTING

White-on-white perimetry is the cornerstone of clinical visual testing in glaucoma and the test most widely used to assess progression. Perimetry has evolved from manual kinetic methods, such as Bjerrum tangent and Goldmann testing, to automated static perimetry. The latter is more standardised and widely used today, and includes the Humphrey and Octopus systems. Apart from being used to detect and monitor glaucoma, visual field testing, especially binocularly, also reflects vision in daily life (Esterman, 1982; Johnson and Keltner, 1983; Mills and Drance, 1986) and quality of life (Viswanathan et al, 1999; Wilson et al, 1998). Still, automated static perimetry is a subjective test. Its results are prone to variability and affected by factors such as cataract, which can confound the interpretation of true glaucomatous change. It is useful and relevant in seeking to identify progression by scanning laser tomography to examine methods used to detect visual field progression, the difficulties experienced, and solutions advocated.

3.2.1 Visual field fluctuation

Repeat testing over a period during which measurable change is unlikely will not yield identical results. This difference in results on repeat tests is called *variability* and indicates the method's intrinsic reproducibility; it reflects how consistently change can be detected. *Sensitivity to change*, on the other hand, reflects the ability of perimetry to detect small amounts of progression. In general, disease-induced change greatly exceeding measurement variability is more likely to consistently be detected than relatively small change. An ideal test should be sensitive to change and reproducible.

The constituents of variability in automated static perimetry (Humphrey and Octopus) are *short-term fluctuation* and *long-term fluctuation*. The psychophysical *differential light threshold* in these systems is defined as the luminance value of a

light stimulus over its background that has a probability of being seen 50% of the time. Hence, there is scatter in determining this threshold (Bebie et al 1976; Flammer et al 1984a; 1984b; 1984c).

Short-term fluctuation is the amount of variability in measuring threshold within a single test session, and is influenced by the perimeter's thresholding algorithm. The subject's ability to understand and do the test, and one's criteria for deciding if a light stimulus is present is also important. Short-term fluctuation is affected by test point location, sensitivity, and general visual field status. Variability is incrementally greater with test point eccentricity: higher nasally than temporally, and superiorly compared with inferiorly (Flammer et al, 1984a; 1984b; Heijl et al, 1987); so, the reliable detection of regional change can be expected to vary by location. Fluctuation is also more in regions of relative defect than normal areas, and increases with the depth of defect (Flammer et al, 1984a; 1984b; Heijl et al, 1989). This occurs to the point where visual threshold in relatively deep scotomata may vary across the entire range of normal to absolute defects. It follows that fluctuation is more in advanced than mildly damaged visual fields.

Long-term fluctuation (Bebie et al, 1976; Flammer et al, 1984a; 1984c) is defined as the physiological fluctuation in retinal sensitivity, and is the net variability not explained by short-term fluctuation (Flammer et al, 1984a; 1984c). Like short-term fluctuation, long-term fluctuation is also influenced by severity of disease (Flammer et al, 1984a; 1984c; Heijl et al, 1989a). Such variability underscores the complex issue of longitudinal visual field assessment and highlights the difficulty of detecting perimetric change with advancing disease.

3.2.2 Methods for detecting progression

3.2.2.1 Subjective evaluation

The method in widest use for detecting visual field progression is subjective evaluation—simply looking through charts. Subjectively assessing the results of serial automated perimetry is not easy. It requires the analysis of complex three-dimensional numerical information (visual sensitivity presented spatially) in time. There are no well-accepted standards for subjective evaluation (Anderson et al,

2000) and because criteria for deciding if perimetric deterioration is present are likely to differ between observers, the interpretation of longitudinal visual field data can be inconsistent.

Subjective vs statistical analysis. Werner et al (1988) compared agreement between six glaucoma experts and six statistical analytical methods. Statistical methods included Students t-tests, ANOVA with trend analysis, and linear regression that were applied globally and to regions of glaucoma visual field series. Agreement in at least five of six was present in 73% by statistical methods, 50% by clinicians, and in only 40% when clinician and statistical groups were combined. Results were independent of disease severity or number of tests. This suggests that for detecting progression, better agreement is seen with statistical methods than subjective evaluation. Favourable agreement between statistical methods has also been reported in other studies (McNaught et al, 1996; Viswanathan et al, 1997a; Westcott et al, 2001).

3.2.2.2 Objective criteria

An alternative to subjective assessment is the use of objective methods of analysis. Analytical methods that have been used to detect visual field progression are 1) clinical trial criteria, 2) event analysis and 3) trend analysis.

Clinical trial criteria. A number of multicentre trials have adopted objective criteria for evaluating visual field deterioration, which are helpful for standardising interpretation of results within studies. The Collaborative Normal Tension Glaucoma study (Collaborative NTG study) (Collaborative Normal Tension Study Group, 1998a; 1998b), Early Manifest Glaucoma Treatment Study (EMGT) (Leske et al, 1999a, Katz, 2000), Advanced Glaucoma Intervention Study (AGIS) (The AGIS Investigators, 1994a; 1994b; Katz, 1999, Katz et al, 1999), Collaborative Initial Glaucoma Treatment Study (CIGTS) (Katz, 2000, Katz et al, 1999), and Ocular Hypertension Treatment study (OHTS) (Gordon and Kass, 1999) have all used visual field criteria requiring specified minimum change, often within a cluster of test locations, before apparent progression is attributed to disease.

There are several issues of note with using clinical trial criteria. Firstly, although the analytical criteria are objective, perimetry is still a subjective test. Secondly, test clusters and definitions of statistical change are not uniform between studies: for instance, the Collaborative NTG study required a cluster of at least two locations within an existing localized defect to change by 5dB or more; while AGIS used minimum threshold change, eccentrically-weighted in predefined clusters, to score disease severity between 0 and 20. Criteria adopted by CIGTS and EMGT are different too. Thirdly, while plausible and clinically reasonable, the empirical bases of these analytical methods are not well described. Fourthly, there is no evidence that the scales of scoring systems necessarily reflect uniform increments of disease severity; consequently, each study probably interprets progression differently (Katz et al, 1999, Katz, 1999).

Event analysis defines progression to have occurred if threshold sensitivity at a particular field test location changes more than the expected variability of a baseline pair of visual fields. Glaucoma Change Probability (Heijl et al, 1991) (Humphrey Statpac 2, San Leandro, California, USA) and Delta (Bebie and Frankhauser, 1982) (Octopus, Interzeag, Switzerland) analytical programs are examples. The advantage of this approach lies in its theoretical ability to detect an event of change with as few as three tests. Efforts have also been made to compensate for the variability in glaucoma, hill of vision characteristics and media opacities in determining true change (Bengtsson et al, 1997a; Heijl et al, 1991; Katz, 2000). Statistically accounting for changing fluctuation with increasing visual field damage, however, is very complex, requiring confirmatory repeat testing to preserve specificity (Schulzer, 1994; Schulzer et al, 1991b; Chauhan et al, 1999).

Trend analysis. With trend analysis, the pattern of change in sequential visual fields is modelled over time. Rates of change are assessed relative to the rate of physiological age-related loss estimated in cross-sectional studies (Holmin and Krakau, 1982), and can reveal subtle progression otherwise obscured by test fluctuation (Fitzke et al, 1996; Hitchings, 1994). Underlying test variability, nature and rate of disease progression, test frequency, and position of fields within a particular time series can influence results (Katz et al, 1997; Smith et al, 1996; Spry et al, 2000; Wild et al, 1997). Linear regression analysis has been studied for modelling change in individual test locations, hemifield zones and global indices.

While analysing single test locations may have the greatest sensitivity (Katz et al, 1997; McNaught et al, 1995), adjacent locations are not independent and outcomes should be interpreted with this in mind (Lachenmayr et al, 1995). Sensitivity in single locations can also be expected to be more fluctuant than sensitivity averaged over clusters of single locations. PROGRESSOR (Institute of Ophthalmology, London, UK), an analytical computer program that interprets progression at single locations, can be used to highlight regions showing change and describe individual patterns of disease (Fitzke et al, 1996; Hitchings, 1994). It has also been found to agree reasonably with event analysis for identifying progression (Birch et al, 1995; McNaught et al, 1996; Viswanathan et al, 1997a), and AGIS scores in identifying and predicting progression (Westcott et al, 2001).

3.2.3 Concurrent disease

Cataract. Cataract is an important confounder when evaluating whether change in visual sensitivity is caused by glaucoma. Although the effect of age on visual sensitivity can to some extent be accounted for, that of cataract advancement is less predictable and more difficult to eliminate. While both cataracts and glaucoma may diffusely reduce differential light sensitivity, the nature of their reduction differs: reduced sensitivity tends to be homogenous with cataracts, but not with glaucoma (Guthauser and Flammer, 1988; Heuer et al, 1988; Lam et al, 1991; Wood et al, 1989). Hence, studying the pattern of visual field loss, instead of the overall volume of loss, is better for following disease when cataract is present. As such, indices that presume to selectively reflect the glaucomatous process, such as "pattern standard deviation" or "loss variance", are presented by computer analytical systems.

Glaucoma progression may still be obscured despite this type of analysis. Smith et al (1997) found that while the index of mean deviation, which reflects global field depression, improved following cataract surgery in glaucoma patients, corrected pattern standard deviation (reflecting shape) worsened. Increased field uniformity with cataract may therefore confound the interpretation of changes in shape from glaucoma progression, which is only unmasked following cataract surgery.

Age and perimetric learning. Increasing age, while associated with increased cataract and pupillary miosis, has itself been suggested to affect visual field tests

(Katz and Sommer, 1986). Perimetric learning is prolonged in patients with glaucoma in whom up to five sequential tests may be necessary to achieve sufficient baseline reliability (Heijl and Bengtsson, 1996; Heijl et al, 1989b).

3.2.4 Experience of clinical trials

Several multicentre clinical trials have shown that detecting progression by static perimetry is difficult and uncertain. To a large part, this is because there is no accepted gold standard against which the different methods and outcomes may be compared.

AGIS was a trial that adopted visual field change as an outcome measure for evaluating different treatments in advanced POAG (The AGIS Investigators, 1994a). It used a grading algorithm based on clustered point thresholds that were weighted by age and eccentricity, and checked for reproducibility. Nevertheless, a mock trial showed that the test algorithm was prone to significant inaccuracies and long-term fluctuation (The AGIS Investigators, 1994b).

OHTS. The OHTS (Gordon and Kass, 1999) is a longitudinal trial that has adopted Humphrey's glaucoma hemifield test and corrected pattern standard deviation analysis to detect initial visual field changes in ocular hypertension. Normal-appearing visual fields in ocular hypertension may be expected to demonstrate less variability than fields showing glaucoma (Flammer et al, 1984a; Werner et al, 1982). At interim analysis, however, a high false positive rate necessitated stricter criteria for confirming field defects. Despite this, visual field abnormalities could not be confirmed in 86% of eyes on retesting (Keltner et al, 2000). Although transiently altered sensitivities may arise from increased variability in early dysfunction (Hart and Becker 1982; Werner and Drance, 1977) distinguishing this from long-term fluctuation is difficult, requiring repeat testing and longitudinal monitoring (Hart and Becker, 1982; Keltner et al, 2000; Schulzer, 1994; Werner, 1994).

CIGTS, EMGT, AGIS. Katz et al (1999) compared the detection of progression in the same visual field series by CIGTS, EMGT and AGIS objective criteria with the subjective judgment of two glaucoma specialists. The incidence of progression

using AGIS (11%) was half that of CIGTS (22%) and EMGT (23%), while EMGT tended to diagnose progression a year before AGIS and CIGTS. Clinicians and all methods agreed on progression in 8.9% of patients, while only 50% of fields identified as progressing in each group were from the same patients. When subjective assessment was used as the gold standard, the sensitivity and specificity for ascertaining progression was 36% and 96% for AGIS, 50% and 91% for EMGT and 57% and 87% for CIGTS respectively. There was poor agreement between different objective criteria, and between objective criteria and subjective evaluation. Thus, each study criterion carries a different concept of glaucomatous change, which in turn differs from the subjective interpretation of visual field progression.

The Collaborative NTG study sought to determine whether reducing intraocular pressure in NPG would slow progression of visual field loss (Collaborative Normal Tension Glaucoma Study Group, 1998a; 1998b). The detection of field progression was used both as entry criteria for randomisation and as the primary outcome measure. During interim analysis, an astounding false positive rate of 57% was found despite confirmatory retesting being required (Schulzer et al, 1991b; Schulzer, 1994). Consequently, stricter criteria were introduced, requiring greater threshold change and up to six repeat tests to confirm change. Other experts also agree that such extensive repeat testing is necessary just to confirm change (Werner, 1994). The revised criteria were estimated to reduce false positives from 57% to 2%, while maintaining good sensitivity. As in AGIS, visual field fluctuation had confused the interpretation of disease progression.

At completion of the Collaborative NTG study, a further confounding variable was recognized: cataract had developed in 26% of the treatment group compared to 11% of the non-treated group (Collaborative Normal Tension Glaucoma Study Group, 1998a). The duration to cataract formation was 822 days in the former and 1200 days in the latter. Both these differences were statistically significant and necessitated *post hoc* analysis to statistically adjust for the effect of cataract in evaluating field progression (Collaborative Normal Tension Glaucoma Study Group, 1998a, 1998b; Leske et al, 1999b).

3.2.5 Recent developments

Various techniques have been described to improve the detection of visual field progression. These include neural networks (Brigatti et al, 1996) and the image analysis of perimetric grids using filtering techniques (Fitzke et al, 1995). Known methods of testing and analysis have undergone further development mainly to improve reproducibility and remove the influence of cataract.

Swedish Interactive Threshold Algorithm (SITA) has recently been introduced to replace conventional full threshold testing in the Humphrey Field Analyzer (Humphrey, San Leandro, California, USA) (Bengtsson et al, 1997b). The advantage of this newer strategy is that it requires half the test time and up to 30% fewer test presentations than full threshold testing, with no measurable compromise in test result quality (Bengtsson and Heijl, 1998a; 1998b; Bengtsson et al, 1998; Wild et al, 1999a; 1999b). Perimetric input data is modelled according to known patterns of normal and glaucoma visual fields to produce threshold and certainty estimates at each test location (Bengtsson et al, 1997b). With SITA, average and point-wise sensitivities have been shown to be higher than in full threshold testing, while visual field defects tend to be defined as statistically deeper (Bengtsson and Heijl, 1998). Potentially less patient test fatigue, more robust results, and improved use of visual field testing resources should enable better targeted and more frequent testing in patients particularly at risk of deterioration. Studies also suggest that the family of SITA strategies is more reproducible than conventional full threshold testing (Bengtsson and Heijl, 1998a; Bengtsson et al, 1998). How sensitive SITA is to change, however, is unknown.

Glaucoma Change Probability (GCP). A method that seeks to better distinguish between glaucoma-related sensitivity loss and the diffuse effect of media opacity is the GCP program based on pattern deviation (Katz, 2000; Leske et al, 1999a) rather than total deviation probability maps. Because pattern deviation maps have been observed to change less than total deviation maps following cataract surgery (Bengtsson et al, 1997a), progression analysis with the former is postulated as less susceptible to advancing media opacities. A study of alternative GCP methods in longitudinal visual fields found that progression was detected 54% more frequently with total deviation compared with pattern deviation maps, with kappa agreement

between the two only moderate (Katz, 2000). This difference was attributed to the influence of media opacities being subtracted through pattern deviation analysis. Such an approach has been adopted for assessing visual field change in the EMGT study (Leske et al, 1999a), which in due course should provide insights into its usefulness for monitoring glaucoma.

PROGRESSOR (Fitzke et al, 1996) includes a modification of point-wise linear regression to adjust for the effect of developing cataract. Membrey et al, (2001), Unoki et al (2000) and Viswanathan et al (2001) studied regression slopes of unadjusted visual sensitivity, total deviation and pattern deviation values, and trends in the pattern deviation to try to separate out the localised component of sensitivity loss from diffuse change to help account for the influence of media opacities.

3.2.6 A clinical perspective

Identifying glaucoma progression by demonstrating change in visual fields is not straightforward. Clinical studies agree that reliably detecting glaucoma progression by perimetry is difficult, confirming the likely experience of clinicians. Confidently detecting progression requires that measured change should be more than test variability and the age-related loss of visual sensitivity.

Agreed and standardised criteria for assessing visual field progression are needed but difficult to formulate (Anderson et al, 2000). Results are influenced by the variability of the test and person's performance. True glaucomatous change should be repeatable but to confirm or refute apparent progression may require many tests, and other confounders such as cataract need to be considered. Any confirmed change should be interpreted in the context of disease severity, its expected course, and the likelihood that a patient will experience visual disability. This requires an estimation of the rate of visual deterioration and knowledge of where in the visual field progression has occurred. How well the pattern of disease can be estimated, however, depends on the frequency of testing and number of fields in a series (Viswanathan et al, 1997b), especially in very gradual progression. Simultaneously considering all these issues when interpreting sequential visual fields, even when helped by objective analysis, is not easy for the clinician.

3.3 OPTIC DISC PHOTOGRAPHY

3.3.1 Description

Optic disc photography is the standard method for documenting the optic disc clinically (Hitchings et al, 1993; Airaksinen et al, 1996). Disc photography is either monoscopic or stereoscopic, with the latter done in true stereo or pseudostereo. Simultaneous stereoscopic disc photography from fixed but disparate angles gives true stereo photographs, achieved by using beam-splitting prisms or simultaneous stereo cameras. Sequential disc imaging, where an Allen separator or moved camera is used to change the angle of photography, produces pseudostereo photographs.

3.3.2 Analysis of disc photographs

Sequential disc photographs of a patient are records of optic disc appearance at different points in time that can be examined for change. Sophisticated methods, though still subjective, may be used for analysis. Flicker chronoscopy is used to qualitatively evaluate morphological differences in disc photographs taken at different times (Heijl, 1993). By stereophotogrammetry, three-dimensional aspects of the optic disc, such as depth, volume and contour, can be measured, although the technique needs true stereoscopic photography and special expertise (Takamoto and Schwartz, 1993). Planimetry is used to measure the dimensions and area of the optic disc based on depth cues (Douglas, 1993), meaning that measurement is made with respect to surface contour rather than solely by monoscopic cues such as colour. The RNFL can be imaged using red-free light photography, but this technique requires expert operation, and special interference filters, and photographic film and processing (Airaksinen and Tuulonen, 1993). As with disc photographs, analysing RNFL photographs is qualitative and subjective.

3.3.3 Reproducibility

Intraobserver agreement. Armaly and Sayegh (1969) introduced the concept of cup/disc ratio. Assessing cup-disc ratios in photographs tends to be consistent when conducted by a single observer. Klein et al (1985) reported concordances of 92.1% and 97.4% in same-observer estimates of horizontal and vertical cup-disc ratios

respectively. Lichter (1977) found good intraobserver agreement in estimating cup-disc ratios. Cooper et al (1982) found only small mean differences in cup width estimations in five repeat intraobserver measurements of 24 photographs. Sommer et al (1980) reported small intraobserver differences in estimating cup width between two repeat measurements in 40 photographs. Reported weighted kappa values for intraobserver agreement are 0.70 (Tielsch et al, 1988) and 0.90 (Varma et al, 1992).

Intraobserver v interobserver agreement. Studies are unanimous in finding that interobserver agreement in estimating cup-disc ratio in photographs is less than intraobserver agreement. Lichter (1977) found in 16 expert observers that interobserver agreement was worse than intraobserver agreement. Varma et al (1992) and Tielsch et al (1988) found that median weighted kappa for estimating vertical cup-disc ratios was higher for intraobserver than interobserver agreement between expert observers; 0.79 and 0.57-0.69 respectively in the former study, and 0.86 and 0.74 respectively in the latter study. Klein et al (1985) reported that the concordance in estimating vertical cup-disc ratios was 97.4% for the same observer but 72.7% between different observers. Kappa agreement between observers in estimating vertical cup-disc ratio has been reported to be as low as 0.33 (Kahn et al, 1975; Tielsch et al, 1988). Varma et al (1992) found only moderate agreement between six expert observers in identifying optic discs as glaucomatous, with median weighted kappa between 0.50-0.55.

Sources of variability. Various factors affect the assessment of disc photographs. Identifying the margins of the optic disc and cup in disc photographs is highly operator dependent. Peripapillary atrophy and haloes, pale-looking optic discs and thick RNFL influences interpretation of the disc edge. The cup edge is even more difficult to interpret: ease in distinguishing between the cup and rim is influenced by the cup's contour and slope, image contrast between the cup and rim, quality of stereo disparity in stereophotographs and stereopsis of observers. The obliquity of nerve insertion also affects the appearance of the optic disc. The cup edge should be defined by surface contour (Jonas et al, 1988a; 1998b; Tuulonen and Airaksinen, 1991). Colour cues are helpful too (Tuulonen et al, 1992), although contour is more reliable than colour (Assad and Caprioli, 1992) and should be used as the main guide. There is also no consensus on whether blood vessels straddling the cup edge

should be included as part of rim measurements (Jonas et al, 1988a; 1988b; Tuulonen and Airaksinen, 1991; Airaksinen et al, 1985). Lichter (1977) and Varma et al (1992) reported that interobserver agreement in evaluating vertical cup-disc ratio was better in stereoscopic than monoscopic photographs.

Studies indicate that evaluating disc photographs can be very inconsistent, even when by expert observers, and that longitudinal evaluation should be by the same observer. Although disc photography is objective and seems cheap and easy, its analysis is subjective and does not have agreed and validated standards. Consequently, observers vary in their own subjective criteria of what constitutes the extent of the disc and cup in photos so that reliably detecting morphological change by disc photography remains difficult.

Chapter 4
CONFOCAL SCANNING LASER TOMOGRAPHY OF THE OPTIC NERVE HEAD

4.1 DESCRIPTION OF SCANNING LASER TOMOGRAPHY

4.1.1 Background

The introduction of confocal scanning laser tomography marked a significant advance in ocular imaging. The technique described by Zinser et al (1989) allowed detailed analysis of the optic nerve head's surface topography over 65,536 locations, based on 2,097,152 separate measurements in 32 depth planes, all achieved in a matter of seconds. Early research quickly showed that these measurements were accurate and reproducible (Weinreb and Dreher, 1990; Dreher and Weinreb, 1991; Dreher et al, 1991). This vast amount of data could also be expressed as highly resolved colour images of the optic nerve head. Scanning laser tomography was thus attractive on two fronts: it offered objective and reproducible three-dimensional measurement with good image resolution, and bridged the gap between qualitative and quantitative evaluation. With advances in computer technology in the 1990's, image acquisition, data retrieval, processing and analysis became speedier and the technique more user friendly.

4.1.2 Principle of scanning laser tomography

The scanning laser tomograph (Zinser et al, 1989; 1990) is a type of confocal microscope that images structures in the fundus of the eye in optical sections *in vivo* and reconstructs their anatomy three-dimensionally using software. The imaging has two crucial features: sequential point-by-point laser imaging and a confocal optical system.

Point-by-point laser imaging. A HeNe laser with a wavelength in the red spectrum, usually 632.8 nm or 670 nm, is focused at a given point in a particular plane of an object of interest. The light reflected from this point is separated from the incident beam of light and deflected by a beam splitter to a light detection unit where it is registered. This registered information is digitised and stored in computer memory. Adjacent point locations are imaged in sequence so that a total of, say, 256 points are measured in a horizontal and vertical grid to give a resolution of 65,536 pixels per image. More points imaged per unit distance give a higher resolution. In point-by-point imaging, filters and polarisers can be placed in the path of the light reflected from each point. This allows the properties of the imaging system to be easily and specifically manipulated to improve the quality of the system and extract desired information. For example, the combination of a polarising beam splitter and quarter-wave retarder ensures that it is mainly specularly reflected light which is detected and registered (Bartsch and Freeman, 1994). In commercial systems, this principle is used to detect the internal limiting membrane, the principal specular reflector in the normal human retina (Knighton, 1995).

Confocal optics. In the confocal system, a pinhole aperture is positioned like a diaphragm in front of the light detector at a location that is optically conjugate with the focal point and focal plane of the laser beam, as shown in **Figure 4.1**. Light reflected at the focal plane is focused in the plane of the aperture and passes to the detector without being diminished in intensity. Light reflected from outside the focal plane is not focused at the aperture so that only a fraction of its light reaches the detector where it is registered at a lower intensity. The intensity of the registered signal is maximal precisely where the focal plane is confocal with the pinhole aperture as illustrated in **Figure 4.2**. In tomography, point-by-point scanning is conducted in sequential optical planes through the depths of a structure. The confocal arrangement ensures that spatial resolution remains high both perpendicular to and along the optical axis.

Axial intensity distribution. Each point in a topography image has its own axial intensity distribution based on the registered intensity at the same point in each of

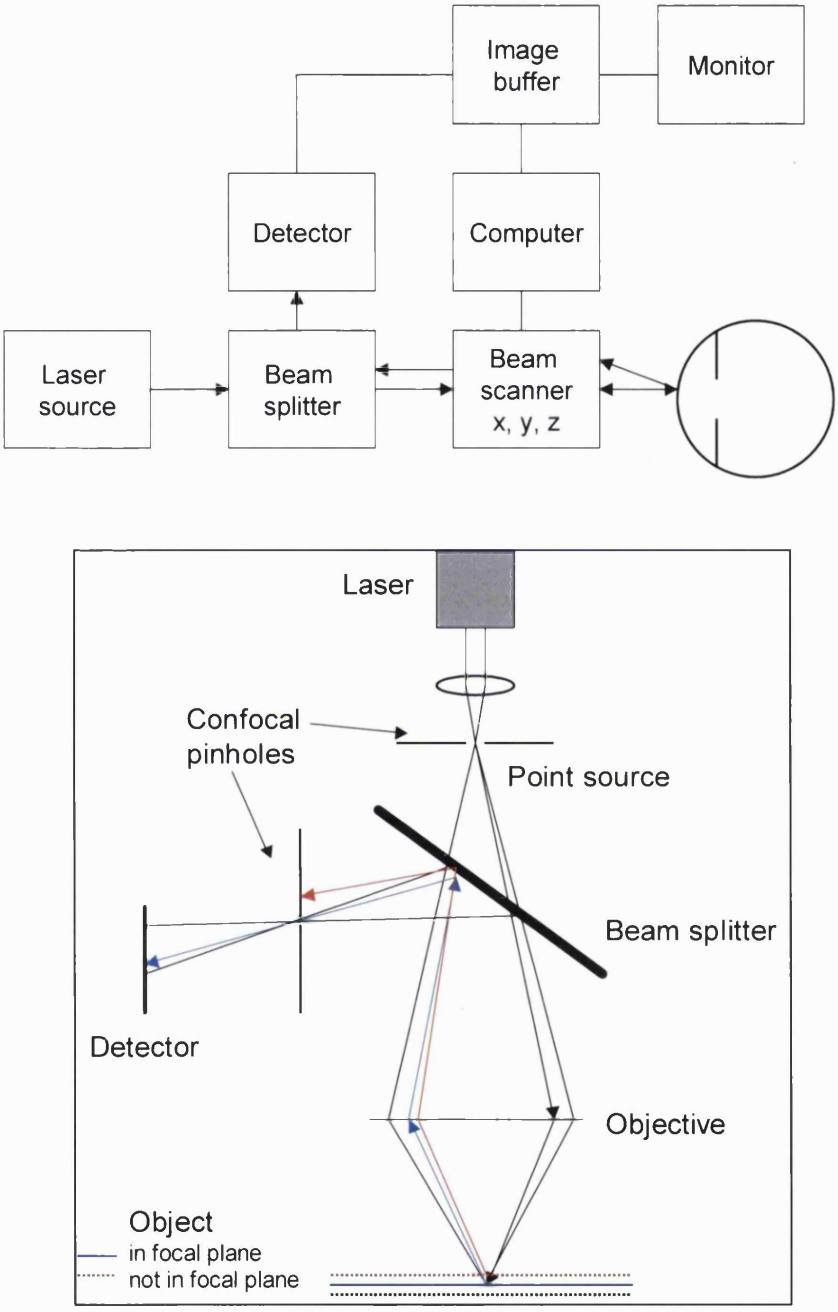

FIGURE 4.1. Set up for scanning laser tomography. *Top*: standard wiring; *bottom:* confocal optics.

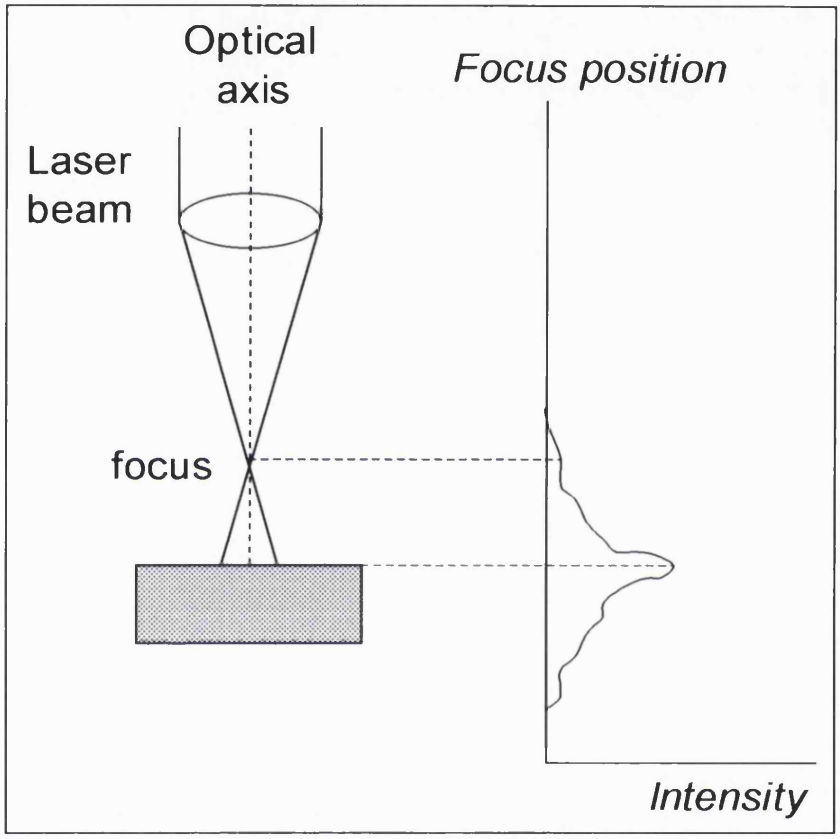

FIGURE 4.2. Axial intensity profile of an object with a single reflecting surface. In a confocal system, intensity of the detected light depends on where the focal point is on the optical axis. The profile shows that intensity is maximal when the focal point is on the object's surface.

the 32 tomographic sections. The peak of the axial intensity distribution profile represents registered light of greatest intensity, corresponding to the principal reflecting surface; in **Figures 4.2, 4.3 and 4.4** the y-axis value at the peak represents light intensity at the principal reflecting surface, and the x-axis value indicates its location on the optical axis (z-axis). The distribution of axial intensity is gaussian at the foveola but tends to vary with retinal location (Bartsch and Freeman, 1993); knowing this helps in choosing a method to locate the distribution's peak. Reflections from deeper layers of the retina at different fundus locations contribute differently to the axial intensity distribution (Bartsch and Freeman, 1994). The HRT assumes that the peak of the axial intensity distribution corresponds to the inner limiting membrane and locates this peak by calculating the centre of gravity of the distribution profile (Zinser et al, 1990).

Commercial systems. The Heidelberg Retina Tomograph (HRT; Heidelberg Engineering, Germany) images in 32 evenly spaced serial sections through an object of interest with 256x256 points imaged per section, as shown in **Figure 4.5** (Zinser et al, 1989). A *tomographic image series* is thus generated. A newer version of the Heidelberg Retina Tomograph has been introduced, called the HRT II, which uses the same principles of imaging as its predecessor. Main differences relate to the HRT II's fixed imaging distance and fixation target, higher image resolution, and better user-friendliness in the acquiring and processing of images. The TopSS (Laser Diagnostics Technologies, San Diego, CA) has a similar optical and imaging design to the HRT but different image analysis software. The Zeiss scanning laser ophthalmoscope scans a matrix of 500 x 600 points in eight optical planes (Cioffi et al, 1993). Reference to scanning laser tomography in the rest of this thesis relates to the Heidelberg Retina Tomograph ('HRT I') unless otherwise stated.

Topographic image series and single topography images. Cartesian coordinates representing horizontal, vertical and optical axes (x, y, z) identify the location of each image point in each optical plane. Sequential images at each optical plane within tomographic image series are stacked in register by the software and errors of shifting, tilting and rotation corrected to reconstruct a new image called a *single topography image* and is described more in Section 4.1.5.

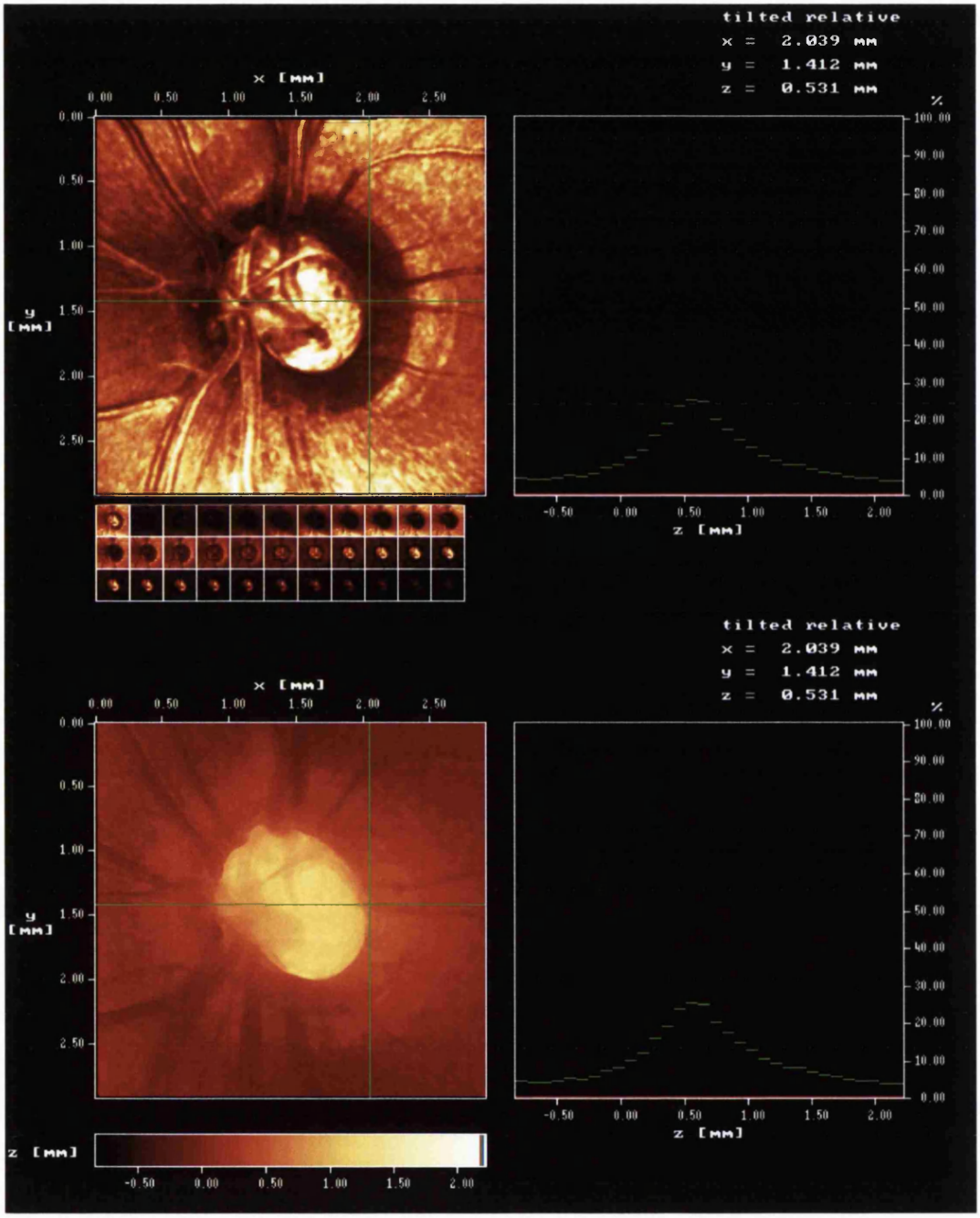

FIGURE 4.3. Gaussian axial intensity distribution. *Left column*=Intensity (*top*) and topography *(bottom*) images of the same optic nerve head. *Right column*= axial intensity (*top*) and topographical height (*bottom*) have gaussian distributions at the optic nerve head location indicated by the cross-hair.

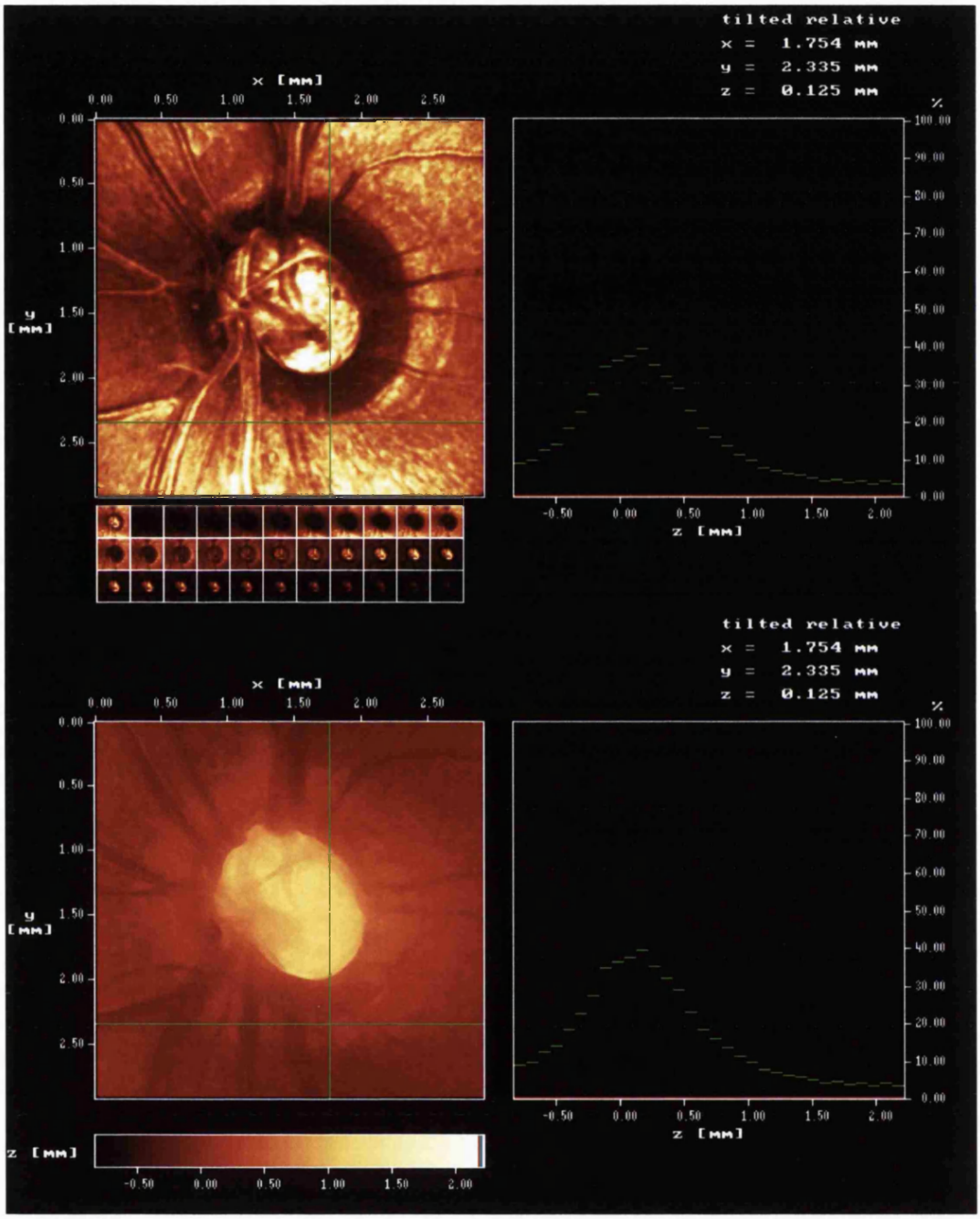

FIGURE 4.4. Non-gaussian axial intensity distribution. *Left column*: Intensity (*top*) and topography (*bottom*) images of the same optic nerve head. *Right column*=Topographical height (*top*) and axial intensity (*bottom*) at the cross-hair have distributions that are skewed to the right.

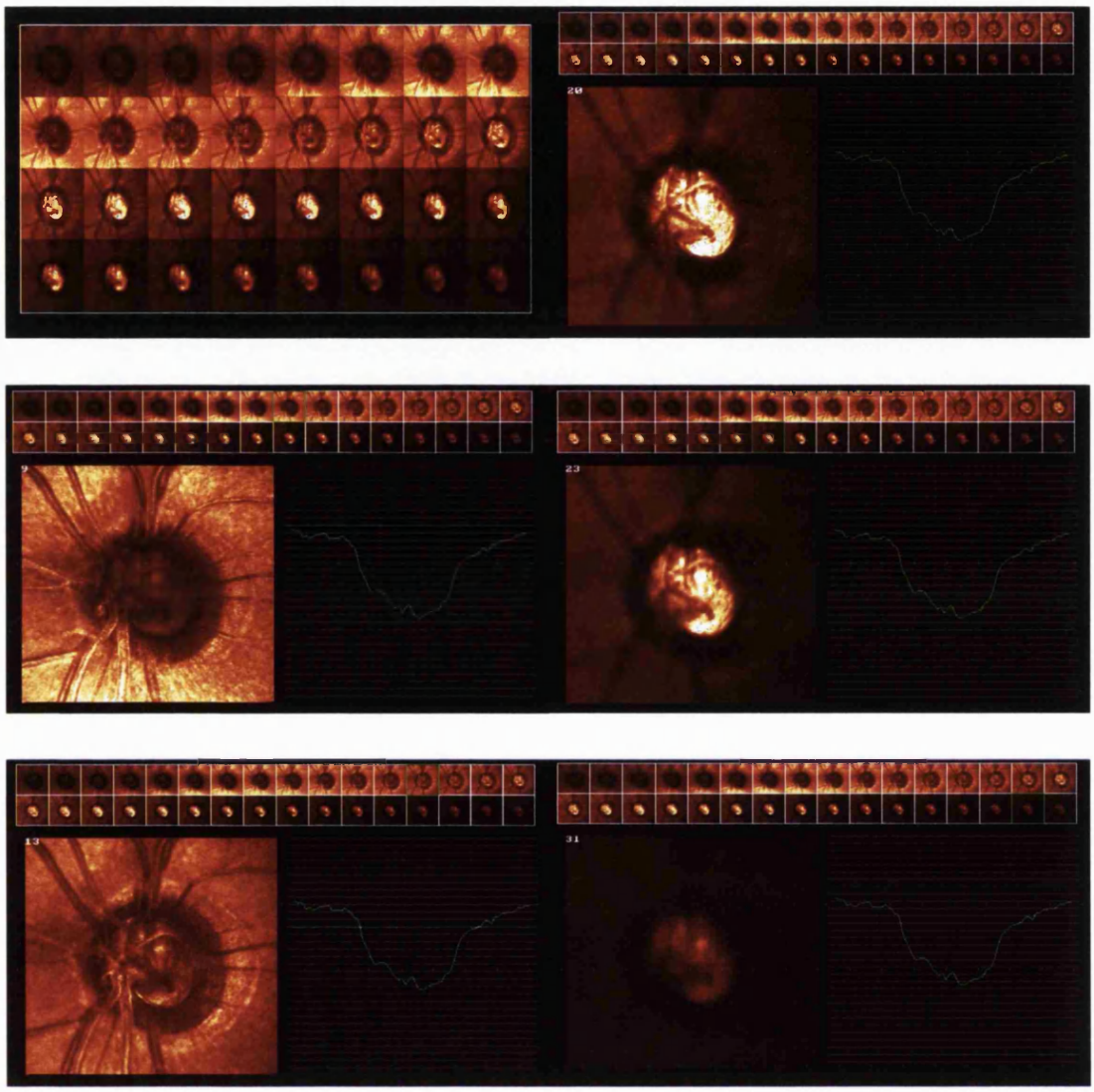

FIGURE 4.5. Tomography of the optic nerve head to produce a tomographic image series. *Top left*=series of images through the optic nerve head in 32 sequential planes lying 50μm apart along the visual axis. *Other panels*: images at different levels starting vitread. The tomographic level of each image is indicated by the green box in its accompanying image series (inset) and white horizontal line in the profile plot adjacent to each image; *middle left*=section 9, *bottom left*=section 13, *top right*=section 20, *middle right*=section 23, *bottom right*=section 31.

4.1.3 Resolution

The axial resolution of the scanning laser tomograph represents its ability to distinguish between two optical interfaces on the optical axis. An optical interface is a region between two media where there is a change in refractive index. Experimentally, axial resolution has been shown to be in the region of 300-450μm (Zinser et al, 1990). Axial resolution in the eye is not improved by increasing the size of the aperture or pupil because of the limitation of spherical abberation. The HRT has a transverse resolution of 10μm.

4.1.4 Ametropia, magnification and accuracy

Ametropia. In the HRT, each topography image consists of 65,536 pixels, with each pixel carrying a measurement representing absolute height between the retinal surface and focal plane at a single point; that is, the location of the focal plane in each eye serves as the absolute zero level of all pixel height values. Location of the focal plane varies between eyes and is estimated from an eye's focal length as modelled from corneal curvature. The focal plane of an emmetropic eye should coincide with the surface of the optic nerve head. In ametropia, divergence of the laser beam is adjusted to bring the focal plane to the surface of the optic nerve head (Heidelberg Engineering, 1993).

Magnification. The HRT corrects for ocular magnification using data on anterior corneal surface curvature and refraction. The optics of the crystalline lens are worked out from a gradient index model, and standard assumptions are made for the posterior corneal surface curvature, focal length of the lens, anterior chamber depth and refractive indices of the cornea and vitreous (Zinser et al, 1990).

Different versions of HRT software have corrected for variations in magnification differently. Bartz-Schmidt et al (1994) found that HRT measurement of the diameter of the optic nerve head based on HRT software version 1.08 matched direct measurements obtained during intraocular surgery (mean error=3%; SD=0.9%). However, while measurement error in HRT software version 1.08 did not vary with ametropia, error in version 1.07 varied by 3% per dioptre; this is

because software version 1.08 used refraction data to correct for image size whereas version 1.07 did not. Hosking and Flanagan (1996) used HRT software version 1.11 and found that image size was affected if the focus setting was altered in eyes having stable refraction, and recommended that each subject's focus settings should be kept constant. Junescu-Cuypers et al (1998) used software version 2.0 and found that image size variability was markedly reduced when the contour line was exported to other images in a series. They concluded that software version 2.0, which scales image size to the baseline image from which the contour line is exported, helped stabilise magnification within image series. Garway-Heath et al (1998) compared different formulae, including that of the HRT, for correcting ocular magnification with a method they adopted as a gold standard (Bennett et al, 1994). They found that the HRT method agreed best with their adopted gold standard and concluded that it was accurate.

Dreher and Weinreb (1991) found that scanning laser tomograph measurements of holes in a phakic model eye had an average error of 2.0% for transverse diameter and 11.7% for depth. The shape of the holes in images approximated that of the actual holes. In a model eye, Janknecht and Funk (1994) found that holes of various shapes could be accurately described. The pooled relative error for various volume measurements ranged from 3.8-11.3% based on analysis by a 'curved' reference surface (prior to HRT software v1.09). The shape of this reference surface varied with the contour line's height profile, however, and it is possible that variation in the shape of the curved surface might itself have introduced measurement error (see Section 4.1.7.2). Schematic and model eyes used to calculate corrections for magnification in imaging systems simulate 'average' human eyes, and the accuracy with which image magnification is corrected in any eye depends on how closely the eye's characteristics approximate average values used in calculations (Arnold et al, 1993; Garway-Heath et al, 1998; Rudnicka et al, 1998).

4.1.5 Processing of Heidelberg Retina Tomograph images

Two or more (usually three) *sets of tomographic image series* are acquired of the same eye in the same imaging session. Each tomographic image series is reconstructed by software as a *single topography image* as described in Section 4.1.2. Single topography images from the same test session are then aligned in

register and corrected for shift, tilt and rotation to calculate a *mean topography image*. **Figure 4.6** is an example. *Pixel height variability* in a mean topography image is given by HRT software as the mean standard deviation (SD) of pixel heights across constituent single topography images. Theoretically, the accuracy of pixel heights in mean topography images should be $\sqrt{3}$ times higher than in single topography images (Heidelberg Engineering, 1993). Weinreb et al (1993) confirmed this empirically, showing that reproducibility improved by increasing the number of single topography images for analysis, and concluded that deriving a mean topography image from three single topography images optimised reproducibility and was practical clinically.

4.1.6 Characteristics of height data in pixels

Pixel coordinate systems. Pixel height values from any of three coordinate systems can be used in analysis: 1) absolute, 2) relative and 3) tilted (Heidelberg Engineering, 1993). The *absolute coordinate system* measures retinal height from the focal plane. However, inaccuracies in determining the eye's refractive status can mislocate the focal plane by about 350μm per dioptre. An alternative to using the focal plane of the eye as a zero-reference is to adopt a relatively stable part of topography as a zero-referencing region. For this, the HRT defines an annulus centred on the image frame and located in the image periphery called the *reference ring,* shown in **Figure 4.7**. The reference ring has an outer diameter 94% and width 3% of the image size. The position of the reference ring corresponds anatomically to the far peripapillary retina of the image, which is taken to be relatively unchanged in glaucoma. In the *relative coordinate system,* pixel heights are measured relative to mean retinal height in the reference ring. The *tilted coordinate system* is the product of software compensation for varying horizontal and vertical tilting of the imaged retinal surface that makes horizontal the imaged plane of the retina. This is achieved with reference to an imaginary plane fitted to the retinal surface height along the reference ring. The degree of compensatory tilting needed is calculated directly by a tangent function (personal communication, M Reutter, Heidelberg Engineering). All analysis decribed in this thesis was based on topographical measurements by the relative coordinate system combined with the tilted coordinate system.

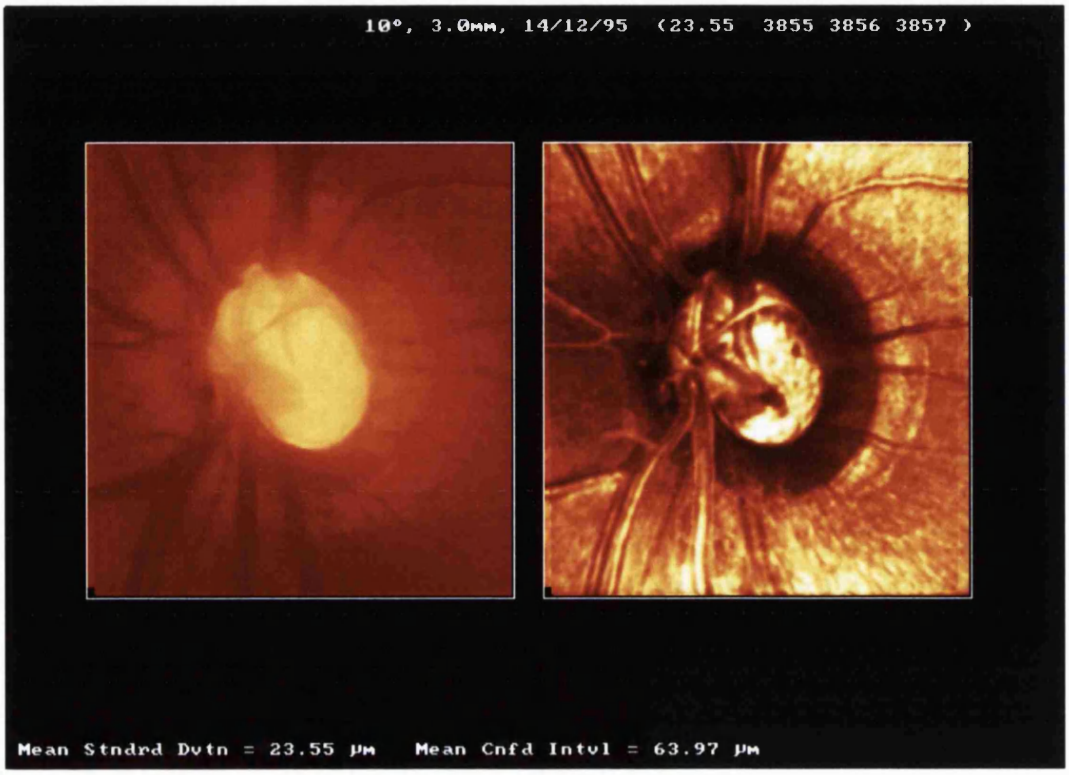

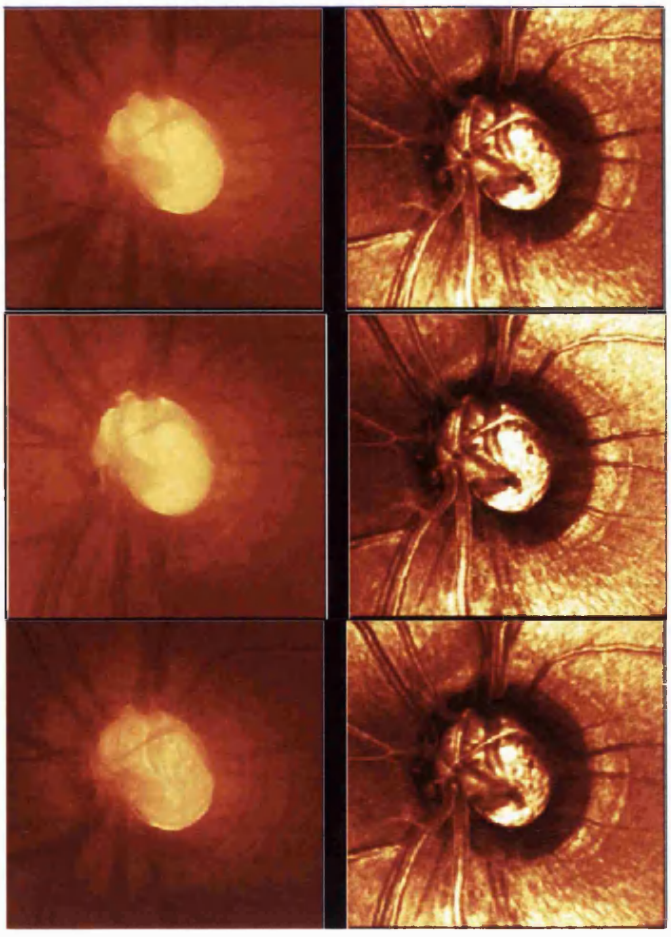

FIGURE 4.6. Mean topography and intensity images of the same optic nerve head (*top, large*) derived from three single topography images acquired in the same test session.

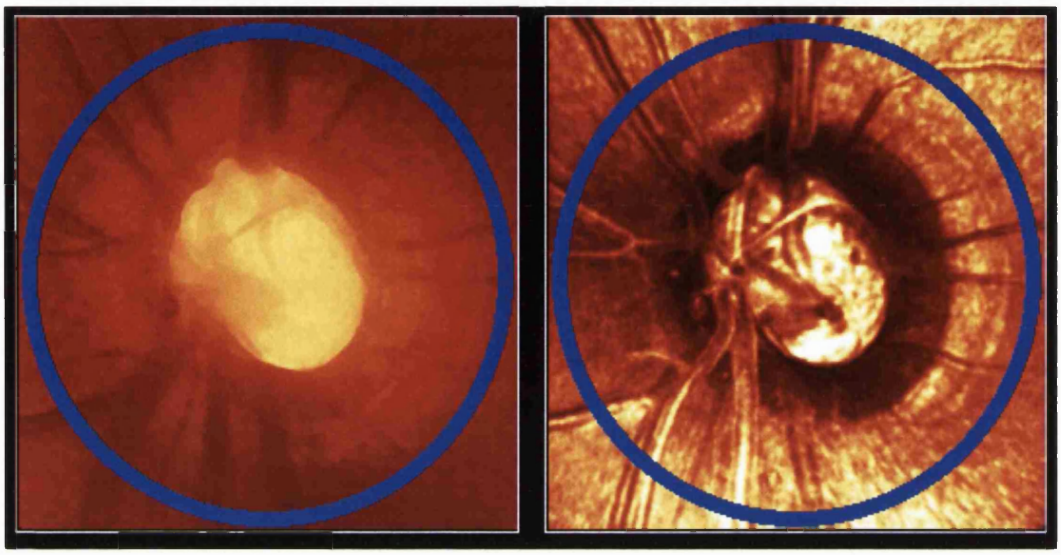

FIGURE 4.7. Location of the reference ring in topography (*left*) and intensity (*right*) images of the same eye.

4.1.7 Topographic parameters

4.1.7.1 Description

Topographic parameters are determined with respect to a reference plane and represent familiar anatomical features of the optic nerve head. Any tissue lying above the reference plane (rim tissue or vessels) and within the contour line marking the optic nerve head margin represents neuroretinal rim, while the space below the reference plane is the optic cup. HRT software calculates the following topographic parameters: 1) disc area, 2) cup area, 3) cup disc area ratio, 4) rim area, 5) height variation contour, 6) cup volume, 6) rim volume, 7) mean cup depth, 8) maximum cup depth, 9) cup shape measure, 10) mean retinal thickness and 11) retinal cross-sectional area.

4.1.7.2 Reference plane for deriving parameters

A reference plane establishes a level in topography that defines the inner extent of topographic parameters in the optic nerve's three-dimensional architecture (the *contour line* (see Section 4.1.7.3) defines their outer extent), as illustrated in **Figure 4.8**. It is vital that the reference plane's position relative to the optic nerve head is appropriate to the nerve's morphology and remains unchanged in images of the same nerve. Alteration from image to image of this positional relationship may cause apparent changes that reflect artifact rather than disease, limiting the reference plane's usefulness as an absolute measure for change. Topographic parameters, if ascertained reliably, could be useful as markers of progression.

The problem of how best to position the reference plane. Various approaches have been proposed for positioning reference surfaces but it is not clear which is most useful for analysis to identify glaucoma or its change at the optic nerve head. Different anatomical landmarks presumed as either unchanged or relatively unaffected by glaucoma have been proposed for positioning the reference plane. Initial HRT software used a "curved" reference surface whose shape relied on the height profile of the contour line that marks the margin of the optic nerve head (Burk et al, 1990; HRT software before v1.09). Subsequently, flat reference

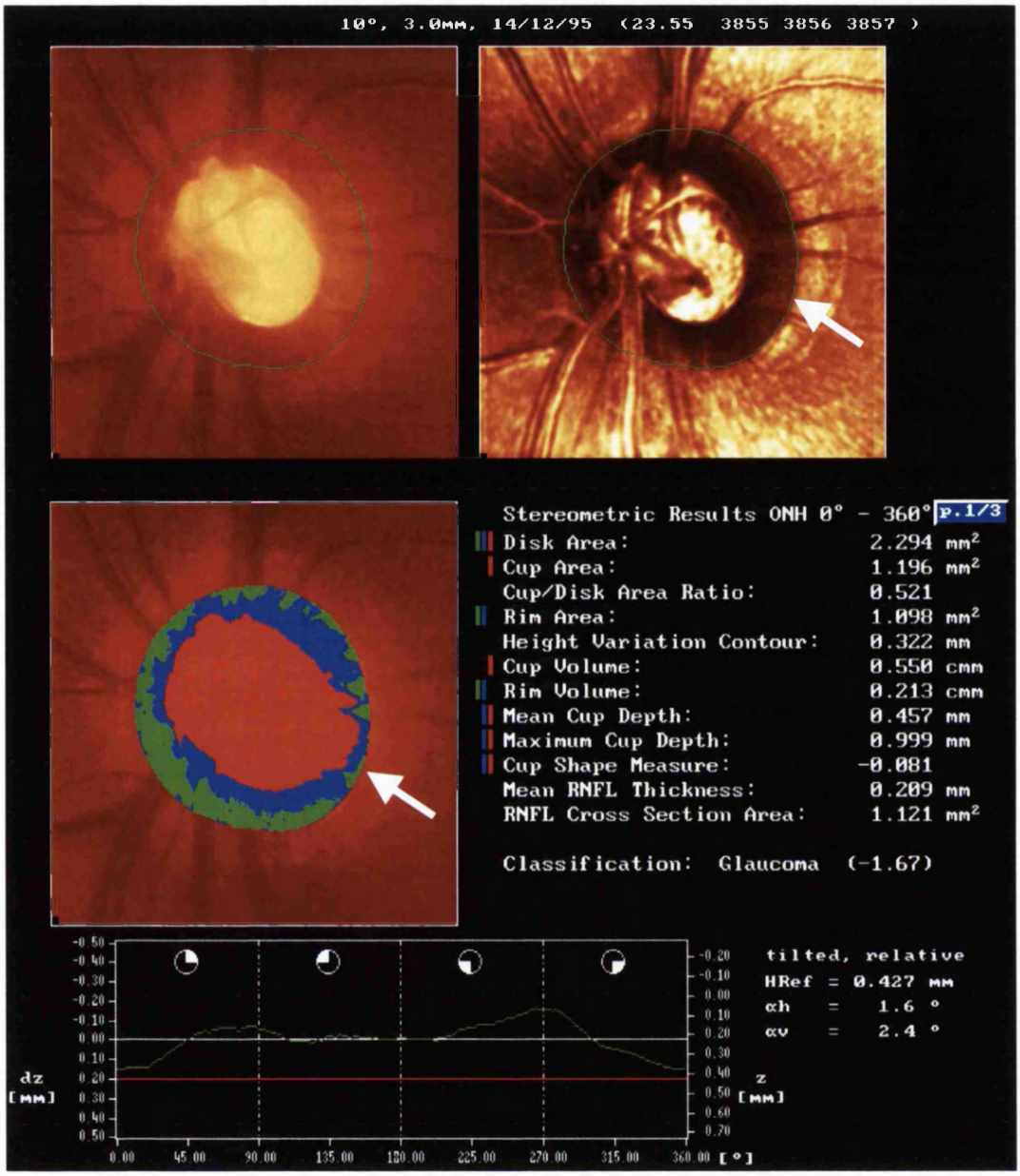

FIGURE 4.8. Left optic nerve head analysed by the contour line and HRT software's default standard reference plane. The *green line* marking the optic nerve head margin (*top, left and right*) is the contour line. *Bottom (plot)*, the contour line's height profile is plotted in green; beneath it lies the standard reference plane (*red horizontal line*). *Middle:* optic nerve head tissue lying above the reference plane and within the contour line represents neuroretinal rim (*blue & green*); the space below the reference plane is the optic cup (*red*). To the right of the image are the measurements of topographic parameters. Description of neuroretinal rim by the standard reference plane (*middle*) is different from that seen in the topography (*top left*) and intensity (*top right*) images, especially just inferotemporally (*white arrow*). Description of rim tissue by a reference plane does not necessarily correspond to rim tissue as seen ophthalmoscopically; instead it relies very much on the reference plane's position in the optic nerve head.

surfaces known as reference planes were adopted. Burk *et al* (5th International Scanning Laser Conference, Heidelberg, 1993, HRT software v1.09-2.01) described a reference plane positioned 320μm posterior to peripapillary retinal height in the reference ring, which is thought to be stable in glaucoma. However, it was later reported that this position did not cater for morphological variations as the reference plane in some eyes lay above parts of the optic nerve head margin to underestimate rim tissue (Burk et al, 2000). Later, Burk et al (2000) described a reference plane positioned 50μm below a small 6° section of the inferotemporal optic nerve head margin as they considered this region of the nerve relatively unchanged in glaucoma, although Chen et al (2001) have disputed this. This reference plane, called the *standard reference plane,* is chosen as default in current HRT software (HRT software v1.11-2.01 and HRTII).

Various other landmarks have been proposed by which reference planes may be positioned. These include features of peripapillary sclera and Elschnig's ring (Maier et al, 1990, Frohn et al, 1990), retinal pigment epithelium (Tuulonen et al, 1993), retinal height at the optic nerve head margin (Burk et al, 2000; Tuulonen et al, 1993) and peripapillary retina (Miller and Caprioli, 1992; Burk et al, 1990). Studies by Ang et al (2000) and Menezes et al (1995) indicate that HRT measurements of macular volume and height are more reproducible if the distance between the reference plane and contour line is kept constant. At present, there is insufficient evidence to support the use of one particular reference plane over another either for diagnosis or for monitoring.

4.1.7.3 Contour line

A *contour line* defines the optic nerve head as the region of interest in HRT software and is drawn on the inner margin of the scleral ring of Elschnig to mark the edge of the nerve, as shown in Figure 4.8. Its height profile represents the height profile of the optic nerve head margin. The influence of blood vessels on the contour line profile is removed by software interpolation (Heidelberg Engineering, 1993).

Variability in drawing the contour line. Frohn et al (1990) reported considerable variability in identifying the inner margin of the scleral ring of Elschnig in

topography images. Iester et al (2001) found that interobserver variability in determining HRT disc area, cup area and cup volume by experts was significantly less if stereoscopic disc photographs aided the drawing of contour lines. Garway-Heath et al (1999) found that for drawing the contour line, interobserver variability was higher than intraobserver variability by 82% for rim area and 62% for cup volume. Their findings also differed between reference planes: interobserver CV for rim area and rim volume was 4.5% and 8.5% respectively for the standard reference plane, and 3.6% and 4.7% respectively for the 320μm reference plane.

Exporting the contour line: variability and scaling. HRT software allows a contour line to be exported to other images of the same eye. Orgul et al (1997), using an older version of HRT software (version 1.11), reported that variability in exporting the contour line caused topographic parameter variability of between 0.4-3.1% for exporting to the same image, and 7.4-24.1% for exporting between different images. By exporting a common contour line from a baseline image to other images of the same eye, Junescu-Cuypers et al (1998) showed that images could be scaled by HRT software to help standardise magnification within longitudinal image series of the same eye.

4.1.7.4 Comparison with stereoscopic disc photography

Three-dimensional information: conceptual differences. Both scanning laser tomography images and stereoscopic photographs of the optic disc contain three-dimensional information but express this information differently. Topography images are colour-coded digital surface elevation maps. Stereoscopic photographs, by offering disparate views, allow the perceiving of three-dimensional features of the optic nerve head by stereopsis. For the analysis of parameters such as rim area, both methods require the outer disc margin to be outlined. Subsequent to this step, however, rim analysis in scanning laser tomography is by a reference plane and objective, but analysing stereoscopic disc photographs by planimetry requires stereopsis and subjective interpretation of the cup edge.

Discrepancy in measuring the size of the disc, cup and rim. Zangwill et al (1995) and Hatch et al (1999) reported that agreement between stereo-photographs and HRT analysis was closer for vertical cup/disc ratio than horizontal cup/disc ratio.

Dichtl et al (1996) found that rim/disc ratios in HRT analysis were higher than in planimetry, with differences greatest nasally, least temporally, and increasing with disease severity. They suggested that inclusion of the usually nasal-lying main vessel trunk and its primary branches as rim tissue by planimetry contributed to the differences seen nasally. Jonas et al (1998c) confirmed these findings in 432 eyes. They also found that HRT estimates of rim area by the standard reference plane tended to be smaller, and estimates of disc area tended to be larger, compared with planimetry, despite HRT contour lines being drawn with the help of stereoscopic disc photographs. Any discrepancy in disc area estimates did not vary with planimetric disc size and was possibly due to differences in image magnification between the systems. However, differences in the techniques' estimates of rim area varied with planimetric rim size: HRT measurements tended to be less than planimetry when rim area was small, but more than planimetry when rim area was larger. Similarly, Sung et al (2002) reported that vertical cup-disc ratio measurements by standard reference plane analysis tended to be higher compared with Discam digital planimetry. Ikram et al (2002) and Hatch et al (1999) found that HRT vertical cup-disc ratio was higher than when cup-disc ratio analysed in stereoscopic disc slides and ophthalmoscopy. Position of the reference plane, drawing of the contour line, and HRT inclusion of vessels lying above the reference plane as part of the rim were highlighted as possible reasons for this discrepancy.

Variability in marking the disc margin. Garway-Heath et al (1999) found that reproducibility in planimetry and scanning laser tomography was similar when the same observer drew the disc margin, but differed when the drawing was by different observers: in planimetry, interobserver variability was about four times higher than intraobserver variability for disc area (CV= 8.1% and 1.5% respectively) and rim area (CV=17.1% and 4.0% respectively). In scanning laser tomography, interobserver variability was roughly 80% more than intraobserver variability for both disc area and rim area. Tielsch et al (1988) agree that interobserver variability can be considerable when marking the disc margin in stereoscopic photographs.

4.2 REPRODUCIBILITY

Understanding the nature and sources of variability in HRT imaging and analysis is relevant to trying to develop reliable methods to identify progression.

4.2.1 Pixel reproducibility

Description. The HRT calculates the centre of gravity of the axial intensity distribution to estimate the distribution's peak; scatter in estimating the peak can be taken to reflect variability in locating surface height at a particular point. Accuracy in determining the peak of the axial intensity distribution in HRT images is estimated as within 20μm (Zinser et al, 1990), approximating pixel variability estimated empirically in human eyes. Using the Laser Tomographic Scanner (predecessor to the HRT), Dreher et al (1991) manually aligned images of normal optic discs (five each) and found that the pooled SD of pixel heights over the optic nerve head was 42.6μm but over flatter peripapillary retina was 38.7μm. Weinreb et al (1993) used an early version of HRT software with an automated alignment algorithm that averaged single topography images to generate mean topography images. They found in five eyes of five normal subjects that pixel SD ranged from 16.2μm to 27.2μm. Rohrschneider et al (1994) reported mean SD was 22μm in normal eyes. Lusky et al (1993) reported that the mean pixel SD in ten normal eyes was 30.1μm. Chauhan et al (1994) reported that the SD of pixel heights in clusters was 25.9μm. Cioffi et al (1993) used a Zeiss prototype scanning laser tomograph and found that the pooled confidence interval for pixel variability over 30 images in 19 normal eyes was 102μm (equivalent SD about 50μm).

4.2.1.1 Sources of variability in pixel measurements

Variation in topography. Many investigators have found higher pixel height variability over the optic nerve head, especially in the region of the cup edge, compared with over flatter peripapillary retina. High variability has been associated with steep contours in topography such as at the cup edge and over blood vessels (Dreher et al, 1991; Chauhan et al, 1994; Cioffi et al, 1993; Brigatti et al, 1995).

There are possible explanations for this. Firstly, light is unpredictably reflected off unevenly sloped or undulating surfaces, making its detection variable and affecting the way in which the principal reflecting surface is located. Secondly, Bartsch and Freeman (1994) showed that the variable contribution to the axial intensity distribution of different retinal layers at different depths in different fundus locations influenced the distribution's shape and therefore variability. Thirdly, inadequately corrected errors in image alignment are likely to affect steeply sloping contours more than flat regions in topography. Fourthly, Bartsch and Freeman (1994) found that the apparent elevation of retinal blood vessels in images represents artifact. The axial intensity distribution over blood vessels is the sum of light reflected from blood vessels (light here is mostly absorbed) and the overlying inner limiting membrane. Reflection properties of vessel walls, which slope steeply, are different from the blood column within vessels. Differences in the reflectance properties of vessel walls, the blood column and internal limiting membrane relative to each other could thus have a combined effect on the axial intensity distribution profile. Fifthly, Chauhan and McCormick (1995) found that variability decreased by a mean of 13.6% in the whole image, 12.3% in the optic nerve head and 18.5% over the peripapillary retina when imaging was synchronised electrocardiographically to the cardiac pulse. This suggests that image variability is influenced by the cardiac cycle and pulsations of blood vessels.

Glaucoma vs normal eyes. Studies report that pixel height variability tends to be higher in glaucoma than in normal eyes, although most have not found differences to be statistically significant (Dreher et al, 1991; Cioffi et al, 1993; Brigatti et al, 1995). Only Chauhan et al (1994) found that glaucoma eyes had significantly more variability than normal eyes ($p=0.01$). They pooled pixels into clusters of 'superpixels' and found that variability was significantly more in glaucoma than normal eyes over the optic nerve head but not peripapillary retina, possibly because glaucomatous cups are steeper.

Interval between tests. Chauhan and McDonald (1995) concluded that the interval between test visits did not affect pixel variability as no statistically significant changes were seen when intervals were lengthened (although there was a trend toward increase). However, their analysis of variability was based on averaged

estimations across the optic nerve head, flatter peripapillary retina, and across the group of subjects, which may have obscured any small differences.

Pupil size and cataract. Tomita et al (1994) reported that mean image pixel SD worsened by about 8μm in 10 young healthy eyes following miosis by pilocarpine. Dreher et al (1991) dilated the pupils of glaucoma eyes to at least 6 mm but did not dilate normal control eyes that were sized between 2.5-3.5 mm. They found that pixel variability was not correlated with pupil size and did not differ significantly between glaucoma and normal eyes. Zangwill et al (1997) qualitatively and quantitatively graded image quality in eyes with cataracts and found that image quality improved by 64% and 27% respectively with pupil dilation. Multiple regression analysis indicated that lens opacity accounted for about 50% of image variability. It was difficult, however, to predict which subjects would benefit from mydriasis. The extent to which mydriasis helps image quality is probably limited by the angle of scanning being allowed to vary more to cause parallax errors (Orgul et al, 1995a).

4.2.2 Reproducibility of topographic parameters

Global variability of parameters. Rohrschneider et al (1994) analysed single topography images by a curved reference surface and reported a coefficient of variation (CV) for rim area of 8.5%, for cup area of 5.5% and for cup volume of 7.7%. Repeat imaging was conducted in the same visit but it is not known if different operators were involved. Mikelberg et al (1993) analysed single topography images by a curved reference surface and reported that CV for cup area was 3.4-4.1% for testing by different operators in the same visit. Results were not compared with data from single operator testing in the same study, however.

Variability in regions of parameters. While it cannot be assumed that variability in parameters is uniform across the imaged optic nerve head, most studies have concentrated only on the global and not regional variability of topographic parameters (Mikelberg et al, 1993; Rohrscheneider et al, 1994; Garway-Heath et al, 1999). The amount of measurement variability in different parts of the optic nerve head will affect the identification and characterisation of localised glaucomatous

change, as described photographically by Pederson and Anderson (1980), Sommer et al (1980), Tuulonen and Airaksinen (1991) and Jonas et al (1993).

4.2.2.1 Sources of variability in topographic parameters

Changing eye-scanner alignment. Orgül *et al* (1995a) found that changing eye-scanner alignment between images was a significant source of variability, affecting cup volume more than cup area. Scanning misalignment, which affects depth estimation, was suggested to influence area estimates by less as it is measured perpendicular to the optical axis. Orgul et al (1995b) replicated this finding in rabbit eyes.

Cataract and pupil size. Janknecht and Funk (1995) found that variability in cup volume in a model eye tended to increase as the opacity of simulated cataract increased, although differences were not significant. Zangwill et al (1997, 1999) found that pupil dilation in eyes with cataracts affected pixel variability but not the variability of topographic parameters, and that the degree of cataract was not predictive of parameter variability. Orgul et al (1995a) suggest, however, that pupil dilation makes imaging more prone to eye-scanner misalignment.

Variation in topography. Surface contour of the optic nerve head is not uniform and variability in its description by a reference plane can be expected to differ from region to region, being influenced by features such as slope, blood vessels (Dreher et al, 1991; Cioffi et al, 1993; Chauhan et al, 1994; Brigatti et al, 1995) and the cardiac cycle (Chauhan and McCormick, 1995).

Variability in drawing and exporting the contour line can result in parameter variability as reviewed in Section 4.1.7.3.

Different test operators, visits and reference planes. Jonescu-Cuypers (1998) found that rim area variability was generally more in imaging over different days which were separated by one day to one year (median SD=0.040 mm^2 (30% more); range: 0.022 to 0.054 mm^2) compared with repeat imaging on the same day (SD=0.03 mm^2). It is unclear if or how exactly reproducibility is affected by scanning involving different operators, or analysis by different reference surfaces

(Weinreb, 1998). Garway-Heath et al (1999) reported some differences in rim area variability between standard and 320μm reference plane analysis.

4.3. CLINICAL APPLICATION

4.3.1 Cross-sectional analysis

Correlation with visual fields. Studies across groups comprising normal, glaucoma suspect and glaucoma eyes have found that topographic parameters are correlated with the global and pattern indices of white-on-white visual fields (Iester et al, 1997a; 1997b) and short wavelength automated perimetry (Teesalu et al, 1997; 1998).

Identifying eyes with glaucoma. Various methods of analysing HRT images have been proposed to help distinguish glaucoma eyes from normal eyes. Methods such as ranked segment distributions of rim sectors (Asawaphureekorn et al 1996), normalised rim/disc area ratios (Bartz-Schmidt et al, 1996), multivariate discriminant analysis (Mikelberg et al, 1995a; Bathija et al, 1998), linear regression analysis of rim area (Wollstein et al, 1998), linear regression of peripapillary slope (Caprioli et al 1998), neural networks (Uchida et al 1996) and curve fitting to the shape of the optic nerve head (Swindale et al, 2000) have been proposed. However, it is hard to know how well these methods compare because their validation has not been standardised: case samples from clinic populations have varied in their size (range: 91-228 eyes), definition and severity of glaucoma, number of subjects used to calculate normal reference intervals (usually small), and reference plane definition. Also, common normal datasets have been used to derive normal reference intervals and for validation, potentially introducing bias. Among parameters, cup shape, which measures the skew of cup pixel heights and does not rely on a reference plane, has been suggested by several studies as useful for distinguishing glaucoma from normal optic discs (Brigatti et al 1995, Iester et al, 1997a, Uchida et al, 1996).

Miglior et al (2001) compared some of the above analytical methods for diagnosis – multivariate analysis, ranked segment distribution analysis and normalised rim/disc area ratios – in the same dataset of 359 images of normal and glaucoma subjects,

classified by visual field status. They found that kappa agreement between these analytical methods and visual field status ranged from fair to poor. Ally et al (2001) found that area beneath the receiver operating characteristic (ROC) curves for linear regression analysis (Wollstein et al, 1998) and discriminant analysis (Mikelberg et al, 1995a; Bathija et al, 1998) was similar. Mardin et al (1999) found that for a specificity of 95%, sensitivity of multivariate discriminant analysis was 83.6% in established glaucoma eyes but 42.2% in ocular hypertension eyes with 'pre-perimetric glaucoma'.

4.3.2 Glaucoma progression

Mardin et al (2000) sought to identify glaucomatous disc change by subjectively examining the HRT image series of 61 eyes of 36 patients with glaucoma, and 74 eyes of 39 normal controls. Over an average of three years, progressive rim area loss was identified in 55.7% of glaucoma eyes. Other signs suggestive of progression were disc haemorrhages (27.9%), reduced RNFL visibility (0.5%), blood vessel narrowing (0.7%), and increased peripapillary atrophy (0.4%). No change was seen in normal control eyes over an average two years of follow up. Measured by the standard reference plane, rim area, cup area and cup volume were significantly decreased over follow up in the glaucoma group ($p<0.01$) but not in normal controls ($p>0.05$).

Kamal et al (1999b) compared pairs of optic nerve head HRT images from 13 ocular hypertension converters acquired 12 months apart and prior to the development of confirmed visual field abnormality. Control data matched for age and duration of follow up was also analysed. Using the standard reference plane for analysis and Wilcoxon significance testing, rim area, cup area and cup/disc area ratio were found to have changed by 7-10% in the group of converters, significantly more than in controls. By region, statistically significant changes were seen in superonasal cup area (11.0%), superonasal rim area (6.6%), superonasal cup/disc area ratio (11.7%), inferonasal cup volume (28.4%), temporal rim volume (15.6%), inferotemporal rim volume (23.6%), and superotemporal rim area (6.9%). The largest rim changes were seen inferotemporally, then temporally and superotemporally. Why changes in the rim did not always correspond to adjacent cup changes is not clear, however. Nevertheless, these results suggest that scanning

laser tomography is useful for detecting glaucomatous optic nerve change, and that such change may even be detected before confirmed changes in the visual field.

Kamal et al (2000) subsequently analysed pairs of HRT images of individual ocular hypertension eyes for change by comparing changes in their measurements against normal limits of variability. Normal limits of variability were defined as 95% confidence limits of measurement variability in 21 normal controls. Pairs of images separated by 16-21 months in 164 ocular hypertension eyes and 21 converter eyes were analysed. 13/21 (62%) converters and 47/164 (29%) of ocular hypertension eyes had deteriorating disc exceeding normal variability. Both groups showed similar patterns of change: this was most commonly in inferotemporal (8.5%) and inferonasal cup volume (11%), and superotemporal cup area (7.3%). However, 15/164 (9%) of eyes with ocular hypertension showed 'improvement' while change was not detected in 8/21 (38%) of converters, prompting the authors to suggest that variability had not been adequately accounted for by their method. Still, these early findings suggest that scanning laser tomography may be able to detect change in eyes at risk of developing future glaucoma and before their fields become abnormal.

Burgoyne et al (2002) proposed a method based on statistical analysis by analysis of variance to detect changes in single parameters (univariate) or groups of parameters (multivariate) when comparing images of baseline and follow up pairs of visits. They used TopSS scanning laser tomography (software version 3.0.20B; Laser Diagnostic Technology (LDT), San Diego, CA), in which the average of all pixel elevation values outside the disc margin was used as a zero-reference for topographical height measurements, and the reference plane fixed 150μm below zero of the z-axis. They then studied 12 monkeys that had experimental glaucoma in one eye with the fellow eye serving as a control, and six single topography images per eye per visit. By combining the parameters 'mean position of the disc', 'maximum depth' and 'superior peripapillary retina' they reported a low false positive rate for detecting change. Using a criterion requiring two positive tests in a row to confirm change, multivariate analysis detected change in 11/12 monkey eyes with experimental glaucoma (sensitivity=92%) and one to two of 12 contralateral normal eyes. The method was later reported by the same group to be at least as good as expert subjective assessment of stereoscopic disc photographs for change (Ervin et al, 2002).

Chauhan et al (2000) described a technique for detecting statistical change in clusters of HRT image pixels (16 pixels made up a 'superpixel') so that triplets of images from baseline and follow up pairs of visits could be compared. The probability that change in superpixels exceeded variability was evaluated by analysis of variance and expressed as probability maps. Probability maps were generated to indicate whether change in superpixel locations across the optic nerve head and peripapillary retina were significantly greater than variability, in a way analogous to that proposed by Quigley and Pease (1996) and Yamada et al (1997; 1998) for Glaucoma-scope digital stereography. Based on computerised simulation and data from one normal eye, Chauhan et al (2000) reported that their technique had a false positive rate of less than 5%.

Chauhan et al (2001) subsequently tested their analytical technique using probability maps in longitudinal image series of 77 glaucoma patients, and compared findings with Statpac-2 visual field progression analysis and subjectively assessed stereoscopic disc photographs of the same patients' eyes. Criteria for verifying change were introduced, requiring repeatable significant change in clusters of at least 20 superpixels on at least three consecutive tests. A criterion for minimum size of change, as determined in 37 normal controls, was also introduced. Analysis by probability maps and Statpac-2 agreed on either the presence or absence of progression in 56% of eyes. Of eyes identified as progressing by both techniques, about half were detected by scanning laser tomography before confirmed visual field change. There was 81% concordance between assessment by probability maps and disc photographs. The method's empirical false positive rate is not known.

4.3.3 Reversal of cupping

Detection. Optic nerve head 'reversal of cupping' may be seen when IOP is lowered, being most pronounced in infants' eyes but also evident in adult eyes (Katz et al, 1989; Shin et al, 1989; Greenidge et al, 1985; Quigley, 1977). Several investigators have studied 'reversal of cupping' with the HRT. Irak et al (1996) analysed by the standard reference plane the images of 49 patients in whom IOP had been reduced by a mean of 43.8% by filtration surgery (SD=29.9%). They

found that percentage IOP decrease was correlated with percentage decreases in cup area, cup volume and cup-disc area ratio, and percentage increases in rim area, rim volume, retinal cross-sectional area and mean height of the contour line. Up to a third of change was attributed to IOP reduction. Lesk et al (1999) found, using standard reference plane analysis, that 11/13 eyes had larger cup measurements after IOP was reduced by about 40% after filtration surgery. Change in cup area, rim area, cup-disc area ratio and mean cup depth was significantly correlated with proportionate IOP reduction. Bowd et al (2000) used the standard reference plane and found that cup area, cup volume and cup-disc area ratio increased significantly after IOP was reduced by topical medication by a mean of 10.8 mmHg (36%, SD=4.3 mmHg). At least 12% of change was attributed to IOP reduction. Conversely, Azuara-Blanco et al (1998) raised IOP by 20-25 mmHg over baseline using ophthalmodynamometry in 20 healthy eyes for two to three minutes. When analysed by the standard reference plane, cup area, cup volume and maximum cup depth were found to increase with IOP, although interestingly, they did not find that rim area and rim volume changed. They postulated that IOP had posteriorly displaced the lamina cribrosa.

Duration of reversal. Reports vary on how long the HRT-measured reversal of cupping persists after IOP reduction. Irak et al (1996), using the standard reference plane, found that the reversal of parameters persisted till at least three months after surgery. Kotecha et al (2001) used the standard reference plane and reported that rim area and rim volume were significantly higher than at baseline at two years post-operatively, though interestingly not at three and 12 months; reasons for this finding were not given. At two years, superotemporal, superonasal, nasal and inferonasal rim volume were significantly higher than at baseline, but temporal and inferotemporal rim volume were not, possibly reflecting the standard reference plane being fixed to the contour line inferotemporally. Kotecha et al (2001) reported that reversal of cupping tended to persist in regions with least damage when compared with normative data, as published by Wollstein et al (1998). Topouzis et al (1999) found that the reversal of cup volume, height variation of the contour, and mean cup depth initially observed after filtration surgery was not detectable at four and eight months postoperatively. Cup shape measure, more negative after surgery, was significantly different from baseline four months after surgery but not at eight months post-operatively.

Chapter 5
METHODS AND MATERIALS

THE PRESENT INVESTIGATION

5.1 Study subjects

Subjects in this investigation were recruited from two research clinics at the Glaucoma Research Unit at Moorfields Eye Hospital: 1) the *ocular hypertension and early glaucoma clinic*, attended by subjects with ocular hypertension, POAG and normal controls, and 2) the *normal pressure glaucoma clinic* attended by patients with NPG. Subjects attended the clinics two to three times per year (4-6 monthly) and underwent scanning laser tomography and Humphrey 24-2 perimetry at each visit. The length of HRT longitudinal image series data for subjects ranged from two to eight years (mean 6.2 years). All subjects had stereoscopic disc photographs. Optic nerve head appearance was not taken into account for entry into the study. This study adhered to the tenets of the Declaration of Helsinki having appropriate institutional review board approval and subjects' informed consent. Criteria for selecting subjects was as follows:

Eyes of ***normal controls*** were taken to be unchanging. Normal subjects were volunteers comprising spouses or friends of hospital patients, hospital staff, or members of external non-medical social organisations. They had 1) IOP on Goldmann tonometry repeatedly below 22 mmHg, 2) serially normal and reliable Humphrey 24-2 visual fields with AGIS visual field scores of zero (The AGIS investigators, 1994a), 3) no concurrent ocular disease, 4) no family history of glaucoma, 5) refractive errors less than ±6D, and were 6) aged over 40 years.

Subjects with ***ocular hypertension*** had 1) a history of IOP greater or equal to 22 mmHg in one or both eyes without IOP lowering treatment, 2) open angles on gonioscopy, 3) initially normal Humphrey 24-2 visual fields with AGIS scores of

zero determined following a learning period of three consecutive tests, 4) refractive errors less than ±6D, 5) no concurrent ocular disease or previous intraocular surgery, 6) were aged over 40 years. Some subjects had previously participated in a randomised control trial of betaxolol treatment in ocular hypertension (Kamal et al, 1999a). Participants in this trial had continued to receive optic nerve head imaging despite the trial ending in 1998. Optic nerve head appearance was not part of the criteria for initial recruitment to the clinic or randomized control trial.

Ocular hypertension converters were taken to have glaucoma progression in the period leading up to conversion. They initially had a diagnosis of ocular hypertension but over follow up had developed visual field defects, as defined by AGIS criteria (score>0; The AGIS Investigators, 1994a), in the same locations on three consecutive tests. An independent glaucoma expert (Miss W.A. Franks) confirmed this. Other possible causes of visual field defects were excluded.

Patients with ***primary open angle glaucoma (POAG)*** had 1) pre-treatment IOP exceeding 21 mmHg on at least two separate occasions, 2) reproducible and reliable Humphrey 24-2 visual field defects with AGIS scores exceeding zero, 3) open anterior chamber angles, 4) no known ocular disease other than glaucoma and 5) concurrent glaucomatous cupping compatible with the visual field abnormality. Most patients were treated medically and had IOP under 22 mmHg at the time of testing. A few had undergone or went on to undergo glaucoma filtration surgery during the period of follow up. Severity of visual field abnormality was not used to restrict entry into the study.

Subjects with ***established normal pressure glaucoma (established NPG)*** who were recruited from the NPG clinic had: 1) untreated mean IOP on phasing of less than 21 mmHg with no single reading exceeding 23 mmHg, 2) open drainage angles on gonioscopy, 3) no concurrent ocular disease, previous intraocular surgery or any secondary cause for raised IOP such as previous ocular trauma or steroid use, and 4) reproducible visual field abnormality according to AGIS criteria and 5) concurrent glaucomatous cupping compatible with the visual field abnormality. Severity of visual field abnormality was not used to restrict entry into the study.

Subjects with established NPG had ***asymmetric NPG*** if their contralateral eye had no visual field defect. The contralateral eye with no field abnormality was considered to have ***suspected NPG***. Over the course of monitoring, some eyes with suspected NPG went on to develop reproducible visual field defects and 'converted' according to the criteria used for ocular hypertesion converters; these eyes were called ***NPG converters***.

5.2 Scanning laser tomography

Acquiring images. Scanning laser tomography was conducted with the Heidelberg Retina Tomograph (HRT; Heidelberg Engineering, Heidelberg, Germany) and standard image analysis was by HRT software version 2.01 (1998). Research technicians dedicated to the Moorfields Glaucoma Research Unit conducted imaging. At least three sets of tomographic image series were acquired of both eyes of each subject at each sitting. More than three sets of tomographic image series were acquired per eye at each sitting if one or more of the acquired sets were considered to be of poor quality by the operator. Each subject contributed images from only one eye for analysis.

Image processing. Single topography images were reconstructed from sets of tomographic image series by HRT software, as described in Section 4.1.2 and 4.1.5. Mean topography images were derived from triplets of single topography topography images from each imaging session. Both mean and single topography images were studied in this investigation. All images were in 10° frames. Height in pixels was measured from the mean height of the reference ring, the zero referencing region in topography images, as described in Section 4.1.6. Only mean topography images with mean pixel SD<50μm were accepted as reliable for subsequent analysis as recommended by the manufacturers; examples of excluded images are shown in **Figure 5.1**. Images that were grainy and having a 'honeycombed' appearance were also excluded; examples are shown in **Figure 5.2**.

Drawing and exporting contour lines. The contour line was drawn to mark the inner margin of the scleral ring of Elschnig, as described in Section 4.1.7.3. All contour lines were drawn by the same observer (JT). All subjects had stereoscopic

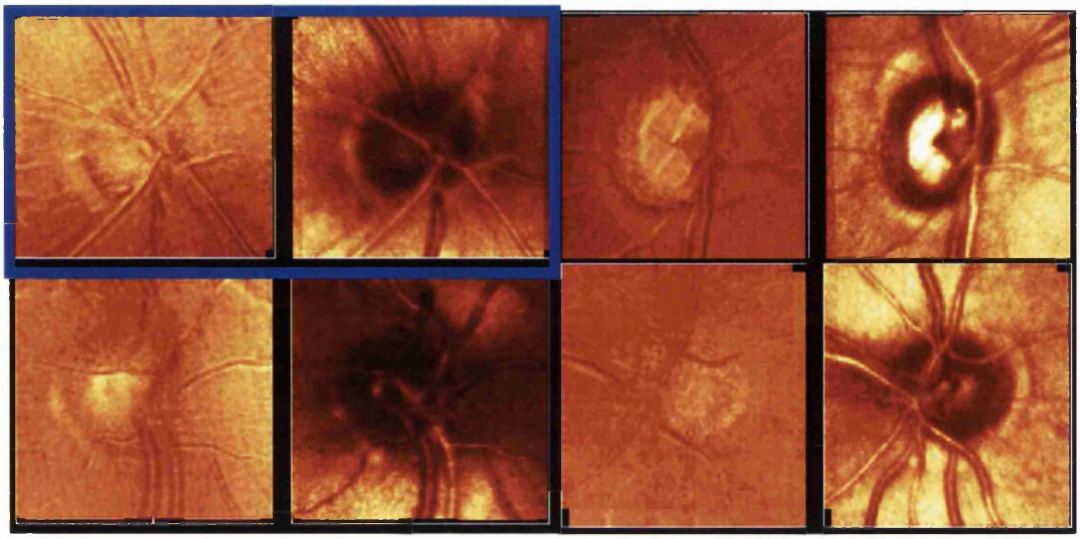

FIGURE 5.1. Examples of pairs of mean topography images with mean SD>50μm. One pair is highlighted (*top left*). For each pair, *left*=topography image, *right*=intensity image. SD of pairs: *top left*=101.98μm, *top right*=63.56μm, *bottom left*=SD=58.63μm, *bottom right*=65.76μm.

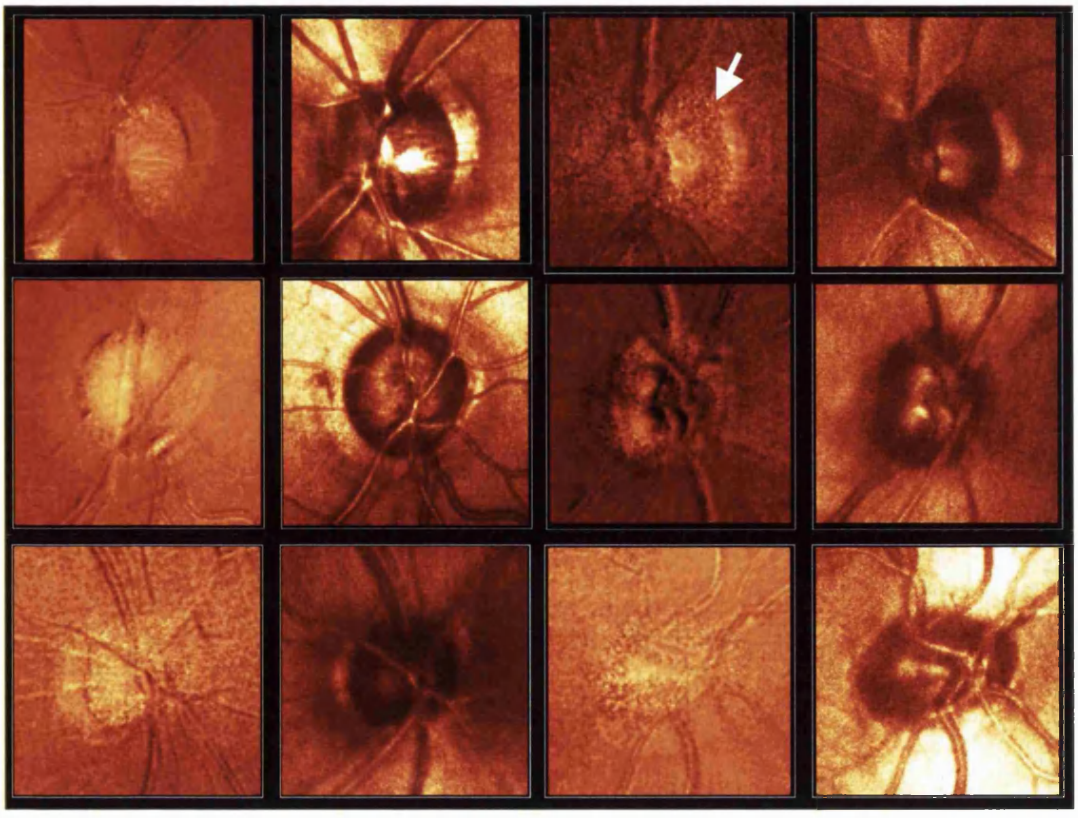

FIGURE 5.2. Examples of pairs of grainy images that were excluded from analysis, shown as topography and intensity images for each eye. 'Honeycombed' appearance is best seen in topography images (*left* in each pair). The *arrow* indicates a particularly marked example.

disc photographs that could be used to guide the drawing of the contour line. Contour lines were needed in all images for analysis. When more than one image of the same eye was analysed, a contour line was only drawn in one selected image and that image designated as 'baseline'. The contour line from the baseline image was then exported to other images of the same eye, designated as 'follow up' images, using the HRT software 'export' facility.

Conventional HRT reference planes. Images were analysed by two conventional HRT reference planes that have been used in various published studies:

1) The *standard reference plane* is set 50μm posterior to the mean of height values between 350-356° on the contour line (HRT software v1.11 to 2.01, Heidelberg Engineering, 1993; Burk et al, 2000), as illustrated in **Figure 5.3**.
2) The *320μm reference plane* is set at a fixed offset 320μm posterior to the mean height of the reference ring (HRT software v1.09 to 1.10). This is illustrated in **Figure 5.4.** The reference ring is centred on the image frame, located in its periphery, and has an outer diameter 94% (2.7mm) and width 3% (0.15mm) of the image size (Heidelberg Engineering, 1993) as shown in **Figure 4.7.**

Additionally, a new experimental reference plane was devised and tested; this is described in Chapter 9.

5.3 Perimetry

Subjects underwent Humphrey Field Analyser 24-2 automated static perimetry (Humphrey Instruments Inc, Palo Alto, CA, USA) in both eyes at each visit. All testing was by research technicians dedicated to the Glaucoma Research Unit.

Global indices. Mean deviation (MD) and corrected pattern standard deviation (CPSD) indices given by Humphrey software were used as general measures of visual field status.

Visual field conversion. Subjects' visual fields were evaluated for change at each visit, but only field progression in the form of conversion in glaucoma suspects was

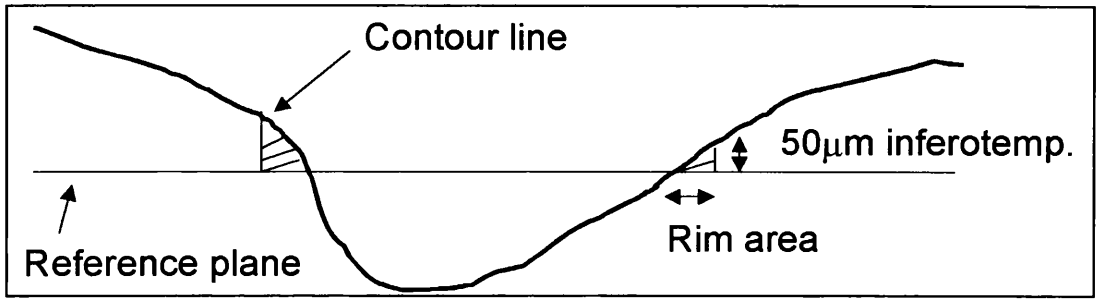

FIGURE 5.3. Diagram illustrating the position of the standard reference plane 50μm below the average of height values between 350-356°on the contour line. The shaded region represents the neuroretinal rim.

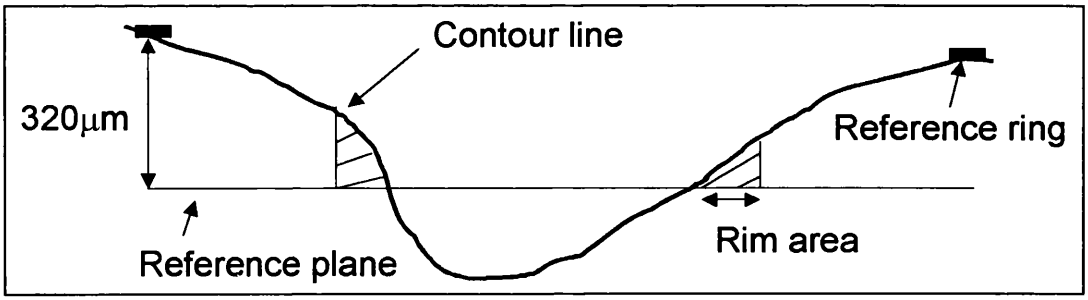

FIGURE 5.4. Diagram illustrating the position of the 320μm reference plane 320μm below the mean topographical height of the reference ring. The shaded region represents the neuroretinal rim

specifically noted for further analysis in this investigation (see also Section 5.4). Conversion was defined as reproducible glaucomatous field defects developing in previously normal fields. AGIS criteria (The AGIS investigators, 1994a) were used to score visual fields, wherein a score of greater or equal to one indicated abnormality. Field abnormality had to be repeatable in the same field locations on at least three consecutive reliable tests and independently verified by a glaucoma expert before conversion was accepted. Possible causes of field defects other than glaucoma were excluded.

AGIS visual field scoring criteria. Scoring by AGIS visual field criteria is based on the number of test locations with total sensitivity deviations exceeding specified levels in Humphrey 24-2 grid clusters, as shown in **Figure 5.5.** The grid is divided into upper and lower hemifields, each with nasal and temporal regions. Deviation of sensitivity from normal is relative to the standard age-matched normal database in the Humphrey perimeter. Fifty-two test locations are analysed after excluding points above and below the physiological blind spot.

A *nasal defect* comprises a cluster of three or more depressed nasal locations that may cross the horizontal midline. A *nasal step* comprises at least one depressed nasal location either above or below the horizontal midline. A *hemifield defect* requires a cluster of three or more depressed locations in a hemifield.

The scoring system is as follows:

- For nasal defects or steps, a score of 1 is given. If at least 4/6 nasal locations are depressed by 12 dB or more, a further score of 1 is added.
- In hemifields, clusters of 3-5 depressed locations are scored 1, 6-12 with a 2, 13-20 with a 3, more than 20 with a 4.
- If half or more of depressed locations are depressed by at least 28 dB, a score of 5 is added; for at least: 24 dB, 4 is added; 20 dB, 3 is added; 16dB, 2 is added; 12dB, 1 is added.
- For hemifields without clusters of three depressed locations, a score of 1 is added if there is a pair of depressed locations in which one location is depressed by 12 dB or more.

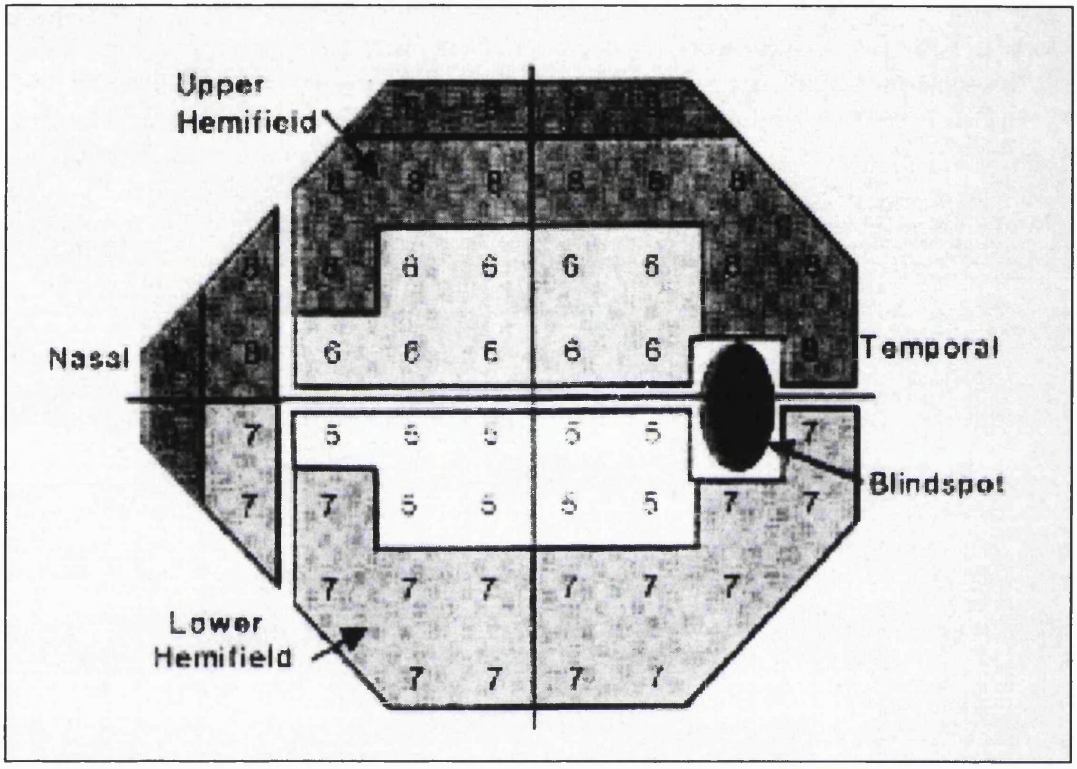

Figure 5.5. AGIS visual field scoring template

Scores are added over the whole field and have a range of 0-20. A score of 0 represents no significant defect, 1-5 early glaucoma, and 20 represents end-stage glaucoma in which all test locations are deeply depressed.

For a visual field to be reliable, it should have:

1. No more than 20% fixation losses
2. No more than 33% false-positive or false-negative responses

A subject initially meeting the criterion of having developed a field defect score of one or more from a baseline score of zero (no defect) was invited back for repeat perimetry within one month. If the field defect was reproduced, a third confirmatory test was needed within four months of the initial visual field with defect. If the defect was reproduced on two consecutive tests (three in a row), the subject's entire field series was given to a glaucoma expert to be independently assessed to confirm or refute conversion (Miss WA Franks). IOP-lowering treatment was started in all subjects with confirmed conversion. Subjects in whom conversion was not confirmed or visual fields were unreliable were invited back for retesting within one month. If defects were still unconfirmed on the second or third attempt, a routine follow up visit was organised for four months time.

5.4 Reference dataset for evaluating change and validating methods for identifying progression

Longitudinal image series of *ocular hypertension converter* and *normal control* eyes were combined as a single reference dataset to test, refine and validate the analytical methods we devised for identifying progression. Ocular hypertension converter eyes were assumed to have unambiguous glaucoma progression in the period leading to the development of reproducible visual field defects (conversion). Normal control eyes were taken to be unchanged over the period of monitoring. Ocular hypertension converters and normal controls were matched for age and duration of follow up by HRT imaging. Each subject contributed one eye for analysis.

The testing of image series of converter eyes was considered appropriate and rigorous enough for validating glaucomatous change because of the following. 1)

Identifying and confirming progression in conversion fields is simple and unambiguous compared with trying to detect progression in glaucomatous fields. In conversion, it is clear that change has occurred once reproducible perimetric abnormality develops where there previously had been no abnormality. In glaucomatous fields, however, interpreting progression on a background of considerable variability can make the identification of true glaucomatous change difficult. 2) Visual field abnormality was defined objectively by the National Institutes of Health-devised AGIS criteria (The AGIS Investigators, 1994a; 1994b). Abnormality had to meet strict requirements for being reproducible, needing to be repeated in the same test locations on three consecutive tests, then be independently confirmed by a glaucoma expert who was well-versed with AGIS criteria. 3) All subjects had extensive experience with visual field testing. 4) It was then reasonable to assume that eyes undergoing visual field conversion by these criteria had underlying glaucomatous progression with concurrent optic nerve change (Pederson and Anderson, 1980; Sommer et al, 1980; Tuulonen and Airaksinen, 1991; Airaksinen et al, 1992; Zeyen and Caprioli, 1993; Odberg and Riise, 1985; Funk, 1991, 1991b; Motolko and Drance, 1981; Yablonski et al, 1980).

5.5 Statistical analysis

Statistical analysis was done in the statistical software packages SPSS v9 for Windows (SPSS Inc; Chicago, IL, 1998) and Minitab v9.2 for Windows (Minitab Inc; State College, PA, 1993). Graphical analysis and presentation was conducted in the graphical software package, Origin v4.1 (Microcal Software Inc; Northampton, MA, 1996).

Chapter 6
MAGNIFICATION CHANGES IN SCANNING LASER TOMOGRAPHY

Evaluation of the optic disc for glaucoma progression should be in image series in which magnification is unchanged over time. Ametropia-related magnification is usually corrected by applying measurements of the eye such as refraction, keratometry, axial length and anterior chamber depth to equations modelling human ocular dioptrics (Littmann, 1982; Bengtsson and Krakau, 1977; Garway-Heath et al, 1998; Bennett et al, 1994). While refractive errors are assumed to be mostly axial in origin and reasonably estimated from corneal curvature (Littmann, 1982; 1988; Bengtsson and Krakau, 1977), lens power is also an important determinant of refraction and its variation can affect magnification (Bengtsson and Krakau, 1977, 1992; Mansour, 1990). Effective lens power cannot be measured *in vivo*, however, and so 'average' values are usually assumed when correcting for magnification.

In what way magnification is affected by a change in lens power is not well-characterised. While studying progression at the optic disc, the author has seen the size of the disc change over time within series of scanning laser tomography images, even in eyes not receiving treatment to lower intraocular pressure. Axial length is not expected to have altered in these eyes but the power of the crystalline lens may have. To study this possibility, scanning laser tomography was conducted in a model eye in which lens power, axial length and the eye-scanner distance were varied in different combinations.

6.1 Investigations

6.1.1 Model eye

A simulated optic disc in a model eye (Rudnicka et al, 1992) was imaged using the Heidelberg Retina Tomograph. Lens power in this model eye was alterable by exchanging intraocular lenses (IOL) to mimic refractive changes caused by the lens. The model eye had a cornea, lens and spherical fundus housed in a matt black Perspex box as shown in **Figure 6.1.** The cornea and crystalline lens of gas-permeable contact lens material had a refractive index of 1.435 (Boston RXD; Polymer Technology Corp, MA). The original crystalline lens mount was substituted with a custom-made IOL mount of exactly the same dimensions (Institute of Ophthalmology, London, UK) as illustrated in **Figure 6.2**. The IOL mount had an aperture on its anterior surface with a diameter of 5.00 mm. On the posterior surface of the mount was an opening into which an IOL could be placed flush against the back surface of the aperture with its haptics sprung into a circumferential groove at the same level. A disc with a concave hemispheric surface represented the fundus; in the middle of this was a drilled round hole with a rectangular profile and diameter of 1.65 mm. The hole represented the optic cup as shown in **Figure 6.3**. The distance of the concave disc to the IOL mount could be varied using a micrometer and read off a vernier externally (Figure 6.2). Anterior and posterior chambers of the model eye were filled with distilled water. For emmetropia in the unmodified model eye, equivalent corneal and crystalline lens powers were +43.9 and +20.8 respectively, corresponding to an axial length of 24.4 mm (Rudnicka et al, 1992).

6.1.2 Lens power

The IOL mount at the lens plane of the eye could be replaced with lenses of different power. All IOLs were of the same make (Model CR3BUO; Alcon Laboratories, Hamel Hampstead, UK), made of polymethylmethacrylate (PMMA) and rigid, had an optic diameter of 7.0 mm, haptic length of 13.5 mm and A-constant of 119.0. They were mounted with their front surfaces facing forwards.

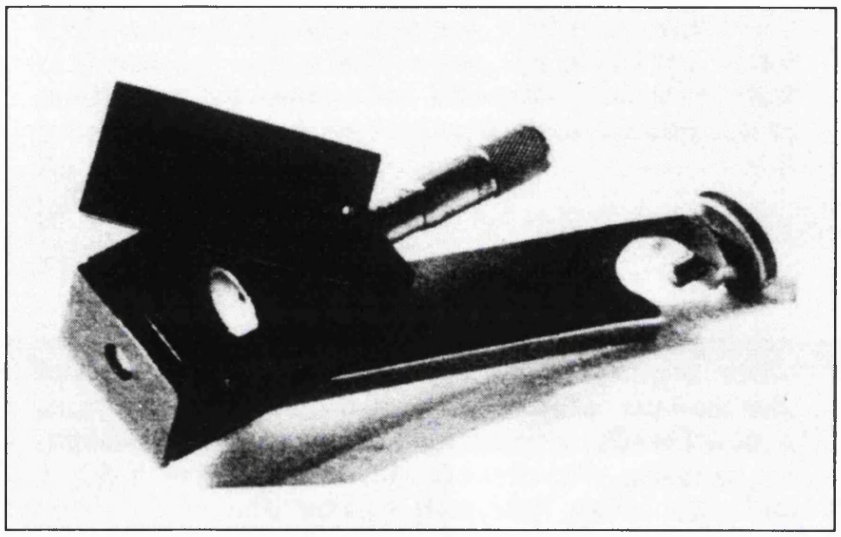

FIGURE 6.1 Photograph of the model eye with its interior exposed.

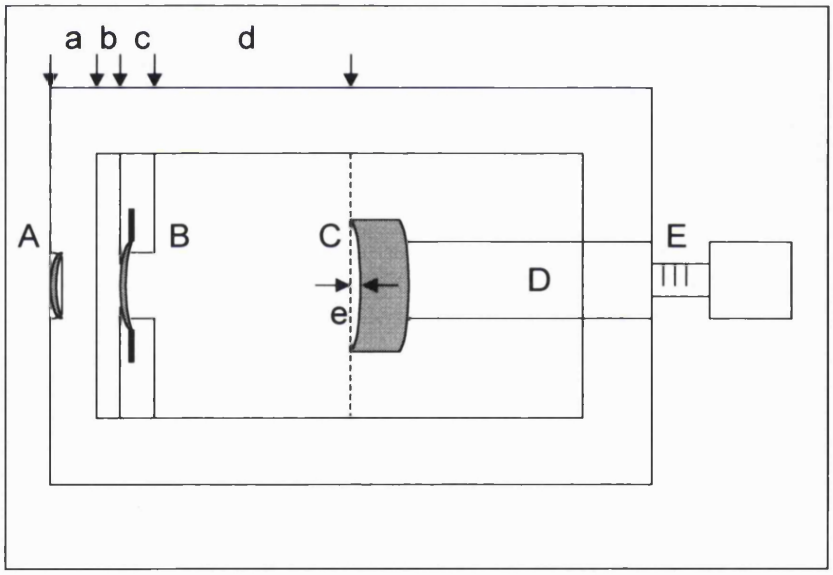

FIGURE 6.2 Cross-sectional schematic of the model eye's optical set up. A=cornea, B=IOL mount and IOL, C=concave disc (fundus) with drilled hole to simulate optic disc (cup), linked to a micrometer (D), E=vernier. *Dimensions*: a=3.04mm, b=2.30mm, c=3.05mm, d=17.96mm, e=2.81mm. Adapted from Rudnicka AR, Edgar DF, Bennett AG 1998 Construction of a model eye and its applications. *Ophthal Physiol Opt* 1992;12:485-490.

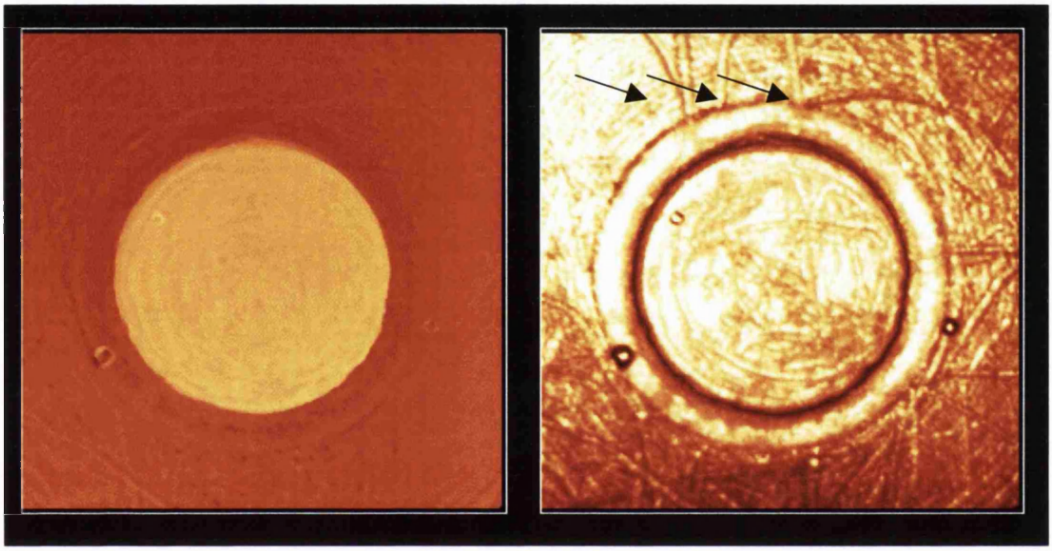

FIGURE 6.3 Topography (*left*) and intensity (*right*) images of the model eye's optic disc. *Arrows* point to examples of grooves intersecting the disc edge that were used as landmarks for measuring distances within each image.

The simulated optic disc was positioned centrally in ten-degree images during scanning. Distance between the scanner head and corneal vertex of the model eye was measured (eye-scanner distance), and the two were locked in place during imaging. Ametropia at each setting was read off HRT software directly. In this setup, IOL power of +20.0D and axial length of 21.5 mm were consistent with emmetropia. HRT software gave the model eye's refraction at this setting as 0.0D, indicating that the focal plane of imaging was at the optic disc surface. This was confirmed by objective retinoscopy.

6.1.3 Testing and measurement

Testing was along four lines. To study the: 1) *effect of changing lens power*, the model eye's optic disc was imaged through IOLs of different powers (+16D to +25D) with axial length held constant; 2) *effect of changed axial length*, the disc was imaged with IOL power kept constant at +20.0D but axial length changed in steps of 1.0 mm between 17.5-23.5 mm, 3) *effect of different eye-scanner distance*, (1) and (2) were repeated as the distance between the scanner and model eye was altered in 1 cm steps between 1.5-4.5 cm, and 4) *usefulness of scaling* the size of HRT images by exporting the contour line, (1), (2) and (3) were done before and after exporting the contour line. All imaging and analysis was by the same operator.

Linear distances between fixed landmarks in each topography image (intersection of grooves with the optic disc edge as shown in Figure 6.3) from each test setting were measured using a mouse-guided cursor in the software's 'interactive measures' function. Each measurement in each image was repeated seven times and the median value used for analysis. Because the scan angle was small (10° frame), it was assumed that magnification did not change with eccentricity in the field of the image (Holden and Fitzke, 1988).

6.2 Results

6.2.1 Ametropia, IOL power, axial length and eye-scanner distance

Figure 6.4 A shows that a myopic shift with respect to emmetropia occurred in the model eye with increasing lens power (A1) and increasing axial length (A2) (all r>-

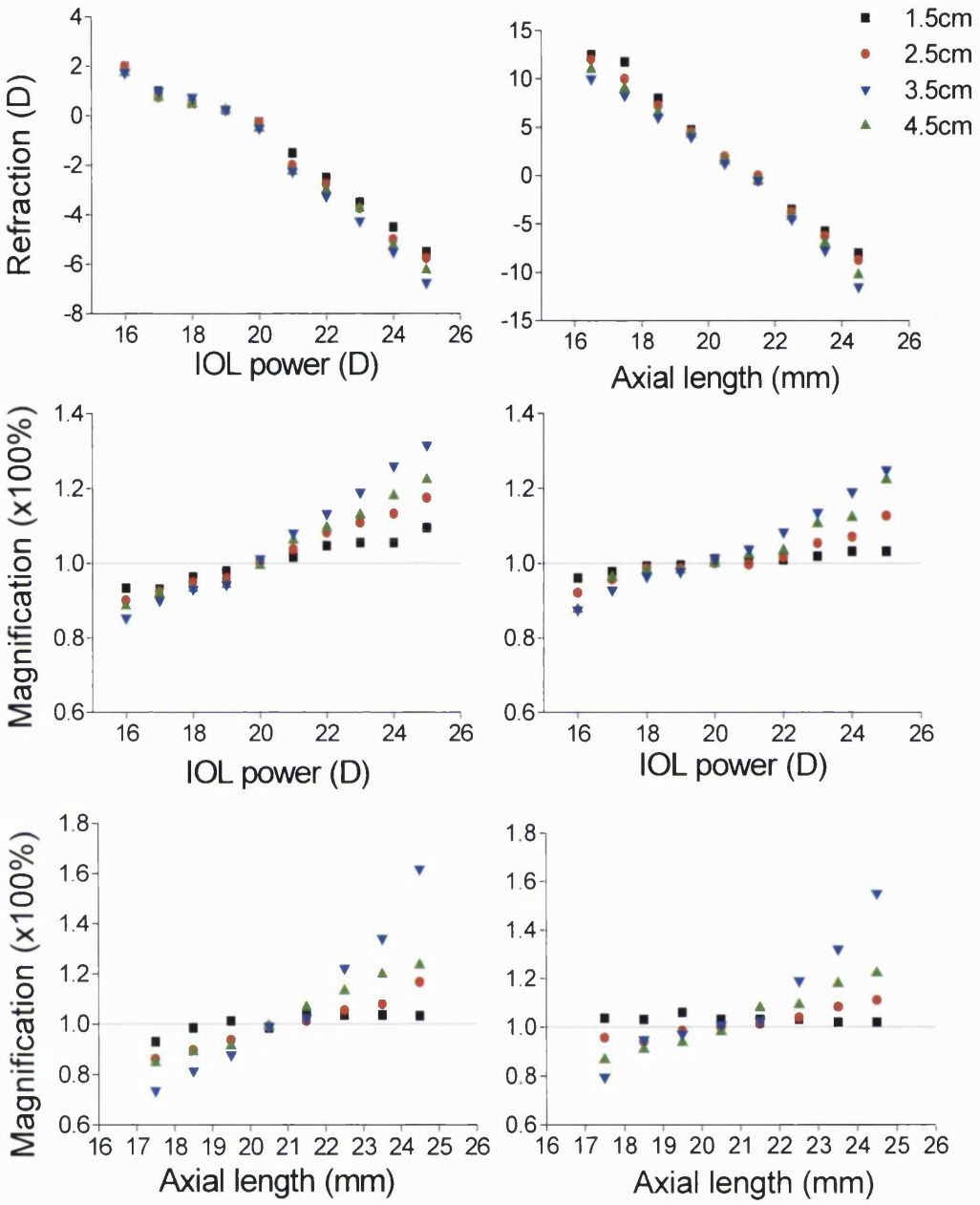

FIGURE 6.4. A. Relationship between ametropia and IOL power (*top left*) and axial length (*top right*) at different eye-scanner distances. The model eye is emmetropic when lens power=+20.0D and axial length=21.5 mm. Data points for different eye-scanner distances: *squares*=1.5 cm, *circles*=2.5 cm, *upright triangles*=3.5 cm, *inverted triangles*=4.5 cm.

B. Relationship between lens power and magnification at different eye-scanner distances before (*middle left*) and after (*middle right*) the contour line was exported. Axial length was kept constant at 21.5 mm throughout. *y=1.0* is the line of equivalence: data points lying here represent images having the same magnification as the eye at emmetropia.

C. Relationship between axial length and lens power at different scan distances before (*bottom left*) and after (*bottom right*) the contour line was exported. Lens power was kept constant at +20.0D throughout.

0.980, $p<0.0001$). For unscaled images: in A1, the regression slope for scanning at 2.5 cm ($y= -0.82x+16.3$) indicated that ametropia changed by –0.82D for each +1D increase in lens power. In A2, the regression slope for scanning at 2.5 cm ($y= -2.65x+57$) indicated a -2.65D change in refraction for every 1.0 mm increase in axial length. Thus, change in ametropia due to a 1.0 mm increase in axial length was equivalent to a +3.2D increase in lens power.

6.2.2 IOL power, image scaling and magnification

In **Figure 6.4 B1**, unscaled image size varied with changing lens power. Magnification increased for lens powers greater than +20.0D but images were minified for lens powers of less than +20.0D and hyperopia. Magnification (or minification) tended to be more marked with longer eye-scanner distances, especially at higher degrees of ametropia. Regression slopes were steeper for longer eye-scanner distances; in B1 slopes were: for 1.5 cm=0.013, 2.5 cm=0.020, 3.5 cm=0.026, 4.5 cm=0.034.

Figure 6.4 B2 shows that magnification plots for changing lens power became less steep after contour lines were exported, indicating that magnification due to lens change was less after image scaling. For a given eye-scanner distance of 2.5 cm, relative flattening of plots with scaling was most noticeable for lens powers ranging from +19 to +21D, roughly within ±2D of emmetropia. Post-scaling plots also became less steep as the eye-scanner distance shortened; slope was least for scanning at 1.5 cm, where magnification varied only minimally despite lens changes. For an eye-scanner distance of 2.5 cm, a +2D increase in lens power resulted in the unscaled image being magnified by 8.2% relative to emmetropia but scaling virtually eliminated magnification (1.7%; B1 to B2). However, for a +4D increase in lens power, scaling only reduced magnification from 13% to 7.0%. Image-to-image scaling appeared most effective over a wide range of lens powers when the eye-scanner distance was 1.5 cm.

6.2.3 Axial length, image scaling and magnification

Figure 6.4 C1 shows that variation of the unscaled image size varied with axial length, being more pronounced at longer eye-scanner distances. Regression slopes were steeper for longer eye-scanner distances; in C1, slopes were: for 1.5 cm=0.013, 2.5 cm=0.041, 3.5 cm=0.060, 4.5 cm=0.12.

Figure 6.4 C2 shows that the effect of changed axial length on magnification was less pronounced in scaled images, especially at shorter eye-scanner distances. For scaled images, the plot for an eye-scanner distance of 2.5 cm was relatively flat for axial lengths between 19.5-22.5 mm, equivalent to ametropia varying between roughly ±3-5D. For an eye-scanner distance of 2.5 cm, an increase in axial length of 1.0mm resulted in 5.5% image magnification in unscaled images (relative to emmetropia), but scaling reduced magnification to 1.2% (C1 to C2). However, for increased axial length of 2.0mm, scaling only reduced magnification from 8.3% to 7.9%. Image-to-image scaling appeared most effective over a wide range of axial lengths when the eye-scanner distance was 1.5 cm.

Figure 6.5 shows images of the model eye's optic disc increasing in size as IOL power is progressively increased. **Figures 6.6, 6.7 and 6.8** are examples of real optic discs with changed magnification over time.

6.3 Discussion

Magnification corrections by standard formulae are expected to be most accurate in eyes approximating the assumptions made of 'average eyes' in each formula. Littmann (1982) assumed that ametropia is mostly axial in origin and based his formulae on emmetropic eyes of varying length. Bengtsson and Krakau (1992) took the thickness of the crystalline lens to be constant. The HRT assumes that the focal length of the crystalline lens and anterior chamber depth is constant according to a gradient index model (Garway-Heath et al, 1988; Zinser et al, 1989). Such formulae are not designed to empirically account for changes in lens power.

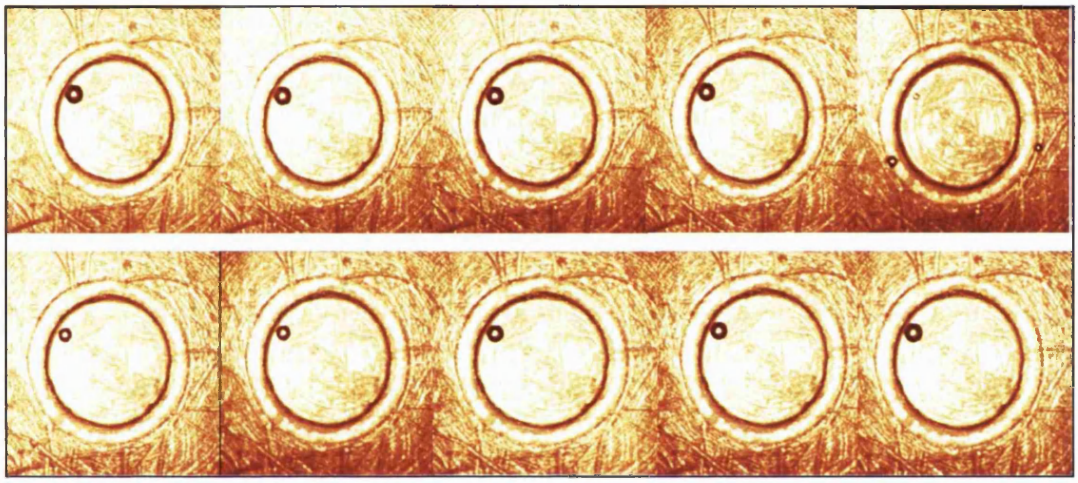

FIGURE 6.5. Change in image size with increased IOL power. *IOL power left to right: top row*=+16 to +20D, *bottom row*=+21 to +25D. Eye-scanner distance (2.5 cm) and axial length (21.5 mm) are constant throughout.

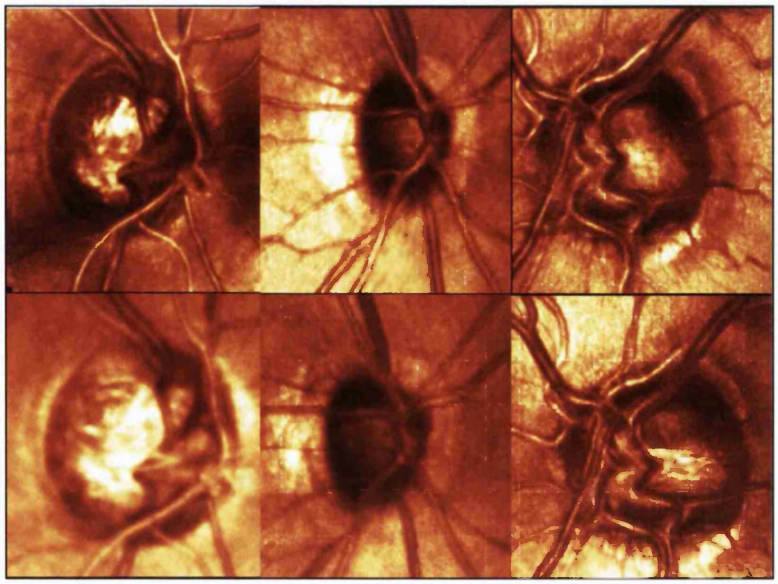

FIGURE 6.6. Examples of images with changed magnification; blurred follow up images suggest cataract formation. Altered eye-scanner distance could have have been an additional mitigating factor in these examples. *LEFT column: top*=baseline (t=0; -0.85D), *bottom*=follow up (t=3 years; -1.50D). *CENTRE column: top*=baseline (t=0; -1.00D), *bottom*=follow up (t=6 years; -3.00D). *RIGHT column: top*=baseline (t=0; -0.75D), *bottom*=follow up (t=6 years; -2.50D). Values for ametropia are as given by HRT software. Images are unscaled; exporting the contour line did not rectify the changed magnification.

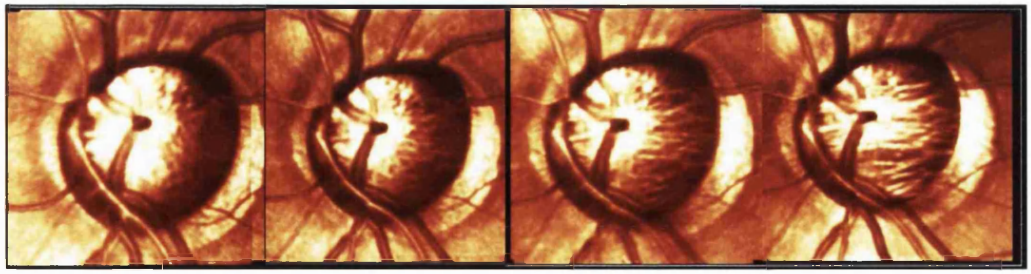

FIGURE 6.7. Changed magnification in this highly myopic eye with unchanged refraction over time is consistent with eye-scanner distance changing from one image to the next. *From left to right*: t=0, 2, 4 and 6 years. All had ametropia of -12.00D. Images are unscaled; exporting the contour line did not rectify the changed magnification.

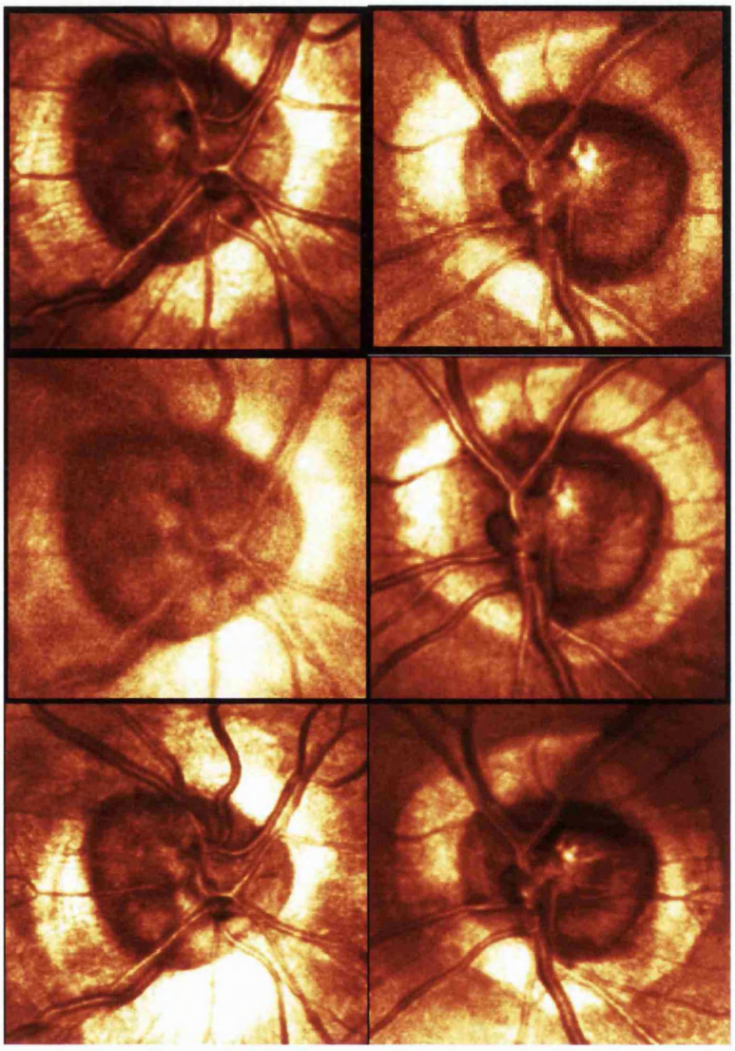

FIGURE 6.8. Images with changed magnification in both eyes of a high myope. Myopia is more pronounced in the right eye. *Left column*=right eye; *right column*=left eye. *Top*=baseline (t=0): *right eye*=-11.25D, *left eye*=-8.75D. *Middle*=follow up (t=6 years): refraction is unchanged but images are grainy and blurred because of cataract. *Bottom*=following cataract surgery and implanted IOL, images are sharp but minified. Myopia is reduced compared with pre-operatively; *right eye*=-4.00D and *left eye*=-3.50D. Values for ametropia are as given by HRT software. Images are unscaled; exporting the contour line did not rectify the changed magnification.

Increased lens power caused a myopic shift and increased magnification in the model eye. Glaucoma is chronic, its follow up is over years, and changes in the ageing lens can be expected during this time; indeed the treatment of glaucoma itself may accelerate cataract formation (Collaborative Normal-Tension Glaucoma Study Group, 1998a). Age-related lens changes are well known to cause myopic shifts and the present study shows that this is compatible with increased magnification. Other studies agree that variation in lens power (Bennett et al, 1994; Bengtsson and Krakau, 1992) and lens radius (Lottmar, 1984) is important. We found that lens power increasing by +1D induced a third the myopia and magnification expected of an increase in axial length of 1 mm. Axial length itself is reported to decrease by a mean of roughly half a millimeter (range to 2.8 mm) following trabeculectomy (Cashwell and Martin, 1999; Nemeth and Horoczi, 1992), especially with antimetabolite use (Cashwell and Martin, 1999; Kook et al, 2001), and should be noted.

The effect of eye-scanner distance on magnification varied with ametropia, whether caused by changed axial length or lens power. Magnification increased with longer eye-scanner distances, especially for high refractive errors, as has been observed elsewhere (Lotmar, 1984; Arnold et al, 1993; Pach, 1989). Image size was most stable when the eye-scanner distance was shortest: magnification remained virtually unchanged across a wide range of lens powers and axial lengths for an eye-scanner distance of 1.5 cm. This was particularly so after image-to-image scaling. Keeping the eye-scanner distance unchanged between images should help stabilise magnification in longitudinal image series too. The HRT-II, unlike the HRT, has a fixed eye-scanner distance which is recommended by the manufacturers as 15mm.

HRT software uses spectacle refraction and keratometry but not axial length to correct for magnification. Without spectacle refraction and keratometry data, however, the HRT can still determine ametropia from the divergence of its laser beam (Garway-Heath et al, 1998); we used this to determine ametropia in the model eye. It is suggested that magnification over a cross-section of eyes could be better corrected if variation in axial length were accounted for (Garway-Heath et al, 1998; Bennett et al, 1994). We found, however, that image size varied with lens power despite axial length being constant. Thus, even if axial lengths were measured accurately, magnification would still not be sufficiently corrected in eyes that

deviate from standard assumptions, such as those already with cataract or that develop cataract over time.

It was found that the image-to-image scaling in HRT software helped compensate, at least partly, for changed magnification due to changes in lens power and axial length. This indicates, as has another report (Junescu-Cuypers et al, 1998), that it is useful to export the contour line to images of the same eye. The extent to which magnification was corrected by scaling depended on the eye-scanner distance and degree of induced ametropia. Given the difficulty in accounting for changes in lens power, it may be useful if the image-to-image scaling procedures in HRT software were further refined as a means of correcting lens-induced magnification. In the meantime it would be advisable to re-establish baseline images following intraocular surgery, note significant changes in patients' refraction over time, try to maintain a standard and short eye-scanner distance, and check image series during analysis to exclude possible changes in magnification.

Chapter 7

TOPOGRAPHICAL VARIABILITY ACROSS THE OPTIC NERVE HEAD

A detailed description of measurement variability is needed to provide a framework for interpreting longitudinal data. It is unclear whether variability is uniform across the optic nerve head or if it varies regionally. It cannot be assumed that reproducibility is unaffected by scanning involving different operators and test visits. What is the influence of different reference planes on the topographical parameters they define also requires study. An ideal approach for identifying change should be suited to variations in optic nerve head morphology and be able to identify patterns of diffuse and localised progression.

The following was studied: 1) test-retest variability of different topographic parameters, from which 2) a single reliable parameter was selected for its pattern of variability to be evaluated across regions of the optic nerve head. 3) The effect on variability of scanning involving different operators and visits was assessed 4) in normal and glaucoma eyes. 5) The possibility that different reference planes vary in their influence on reproducibility was also investigated.

7.1 Investigations

7.1.1 Subjects

42 subjects—21 normal controls and 21 with glaucoma (POAG)—underwent testing. Their criteria for selection is described in Section 5.1 and **Table 7.1** shows the age-matched groups' demographics. Visual field indices and rim area were significantly different between groups ($p<0.05$).

Mean±SD	Normal	Glaucoma	p-value
N=	21	21	-
Age (years)	66.5±9.2	68.8±11.5	0.70
Male gender	12	10	-
Right eyes	13	10	-
Visual field MD (dB)	+0.11±1.2	-4.6±1.9	0.0000
Visual field CPSD(dB)	0.89±0.75	3.3±1.8	0.0000
Rim area by 320μm reference plane: median (range) in mm^2	1.40 (1.03-1.98)	1.02 (0.39-1.95)	0.001
Rim area by standard reference plane: median (range) in mm^2	1.31 (0.86-1.77)	1.00 (0.03-1.40)	0.001
Mean SD (μm) of mean images*	22.6±8.1	25.9±9.65	0.17
Mean SD (μm) of mean images†	22.9±10.2	27.2±10.5	

TABLE 7.1. Subjects' demographics. Glaucoma eyes had POAG. Image reliability data from the first sessions of the first test visit* and second visit† are shown.

7.1.2 Test-retest imaging

Test-retest HRT imaging of both eyes of normal and glaucoma subjects was by experienced operators. Three sets of well-centred HRT image series in 10° image frames were acquired at each session. Corneal curvature, scan depth and focus settings were kept constant and pupils were not dilated.

Subjects attended *two test visits* separated by six to eight months. Each visit comprised *two imaging sessions* separated by at least an hour. The same operator conducted scanning in both imaging sessions on the first visit, and one session of the second visit. A separate operator conducted scanning in the second imaging session of the second visit. Imaging sessions were conducted in random order and measurement variability was appraised along four lines: (1) *intraoperator-intravisit*, 2) *intraoperator-intervisit*, 3) *interoperator-intravisit* and 4) *interoperator-intervisit*. Longitudinal imaging requires repeat testing over many visits, likely by different operators, and what effect these factors have on reproducibility was evaluated.

7.1.3 Image analysis

Mean topography images derived from each session's triplets of single topography images were used for analysis. Images were randomly selected from one eye of each normal control or the eye with perimetric abnormality in those with unilateral glaucoma.

Global measurements of topographic parameters were read off HRT software and transferred to spreadsheets. Parameters analysed were: 1) disc area, 2) cup area, 3) cup disc area ratio, 4) rim area, 5) cup volume, 6) rim volume, 7) mean cup depth, 8) maximum cup depth, 9) cup shape, 10) retinal thickness and 11) retinal cross-sectional area. In this chapter, *rim* will be used to denote the HRT parameter representing anatomical *neuroretinal rim*, while HRT *cup* represents the anatomical *optic cup.*

To study ***regional variability***, the most reliable parameter was chosen to be analysed further in 30° sectors round the optic nerve head (located by angle between 0-360°). Two sets of test-retest data for global and regional measurements of topographic parameters were analysed, with each derived by different reference planes: 1) standard reference plane and 2) 320μm reference plane, as described in Sections 4.1.7.2 and 5.2.

7.1.4 Statistical analysis

The variability of parameters having different units, and the influence of different visits and operators was analysed by the coefficient of variation (CV). CV is the ratio of standard deviation (SD) to the mean of observations expressed as a percentage. Based on the analysis by CV, a single reproducible parameter was selected to study regional and global variability. For this analysis, agreement between repeat measurements was evaluated as described by Bland and Altman (1986). Reproducibility is represented by the agreement between measurements, reflected in graphs as the width of *agreement intervals* (95% confidence intervals of differences). Regional variability was studied in 30° sectors around the optic nerve head. Variability in sectors (width of agreement intervals) was plotted by angular location (0-360°) in bar graphs and in polar plots. Significance testing to determine if sector variability (differences) changed with different operators and visits was by the Wilcoxon signed-rank test for unpaired non-parametric data (Mann-Whitney test).

7.2 Results

7.2.1 Variability of topographic parameters

Figure 7.1 shows that CV for parameters (except disc area) tended to be more in interoperator-intervisit than intraoperator-intravisit testing regardless of the reference plane used.

Apart from disc area, rim area had the overall lowest CV, which was also reasonably proportioned to its point estimates. Rim area CV was not appreciably

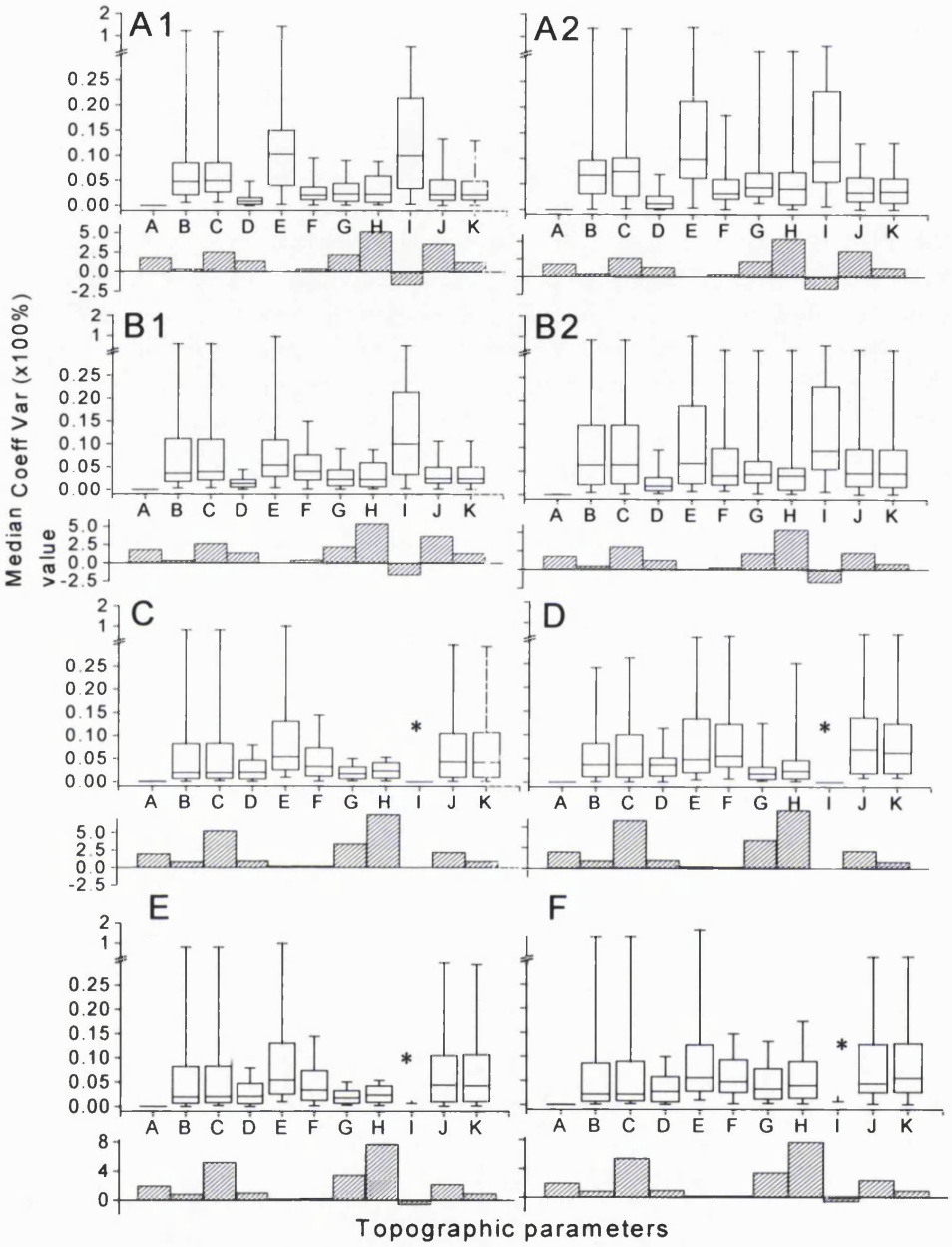

FIGURE 7.1. Variability of topographic parameters as measured by the coefficient of variation. *Graphs for normal eyes: graph A*=standard reference plane, *graph B*=320μm reference plane; (1)=intraoperator-intravisit variability, (2)=interoperator-intervisit variability. *Box plots*=median, first and third quartiles, *error bars*=95% percentiles. *Bar graphs*=corresponding point-estimates. *X-axis*: A=disc area, B=cup area, C=cup-disc area ratio, D=rim area, E=cup volume, F=rim volume, G=mean cup depth, H=maximum cup depth, I=cup shape measure (*data not analysed in glaucoma), J=retinal thickness, K=retinal cross-sectional area. *Graphs for glaucoma eyes: graph C*=intraoperator-intravisit variability, *graph D*=interoperator-intervisit variability; both by the standard reference plane. *Graph E*=intraoperator-intravisit variability, *graph F*=interoperator-intervisit variability; both by the 320μm reference plane.

influenced by different operators and visits: in normal eyes, median rim area CV for intraoperator-intravisit and interoperator-intervisit testing was 1.1% and 1.6% respectively for the 320μm reference plane; and 1.5% and 2.3% respectively for the standard reference plane (Figure 7.1 A and B). A comparable pattern was seen in glaucoma for the standard reference plane (Figure 7.1 C and D) and 320μm reference plane (Figure 7.1 E and F). In interoperator-intervisit testing, 95% percentiles for rim area CV by either reference plane did not exceed 9% in normal and 12% in glaucoma. Subsequent study of variability was thus confined to a single parameter, rim area.

7.2.2 Rim area variability

Global rim area variability. Agreement intervals for global rim area in **Figure 7.2** tended to widen with different operators, different visits or both, suggesting that each influenced variability independently. This trend was more marked with the standard reference plane. Agreement intervals were wider in glaucoma than normal eyes with either reference plane, and testing involving different operators and visits affected glaucoma eyes more than normal eyes (C & D compared with A & B). Bias reflecting glaucomatous rim change in the period between visits was not evident in glaucoma eyes (Figure 7.2 C1-2, D1-2: no downward and leftward shift, mean of differences almost zero). Overall, agreement intervals were wider in standard reference plane than 320μm reference plane data and different operators and visits tended to influence the former more. Magnitude of increased variability with intervisit-interoperator testing was similar in normal and glaucoma eyes (about 50% in both).

Regional rim area variability. In **Figure 7.3**, agreement intervals for regional rim area in normal eyes were not uniformly wide around the disc but tended to peak temporally (A and B: 0-90°, 270-360°). This was a stereotyped pattern in normal eyes irrespective of the reference plane. Variability tended to increase with different operators and visits; this was more pronounced temporally, especially with the standard reference plane. A similar increase was seen in glaucoma, but its pattern varied between reference planes (C and D): very high nasal variability was seen in glaucoma eyes with the standard but not 320μm reference plane.

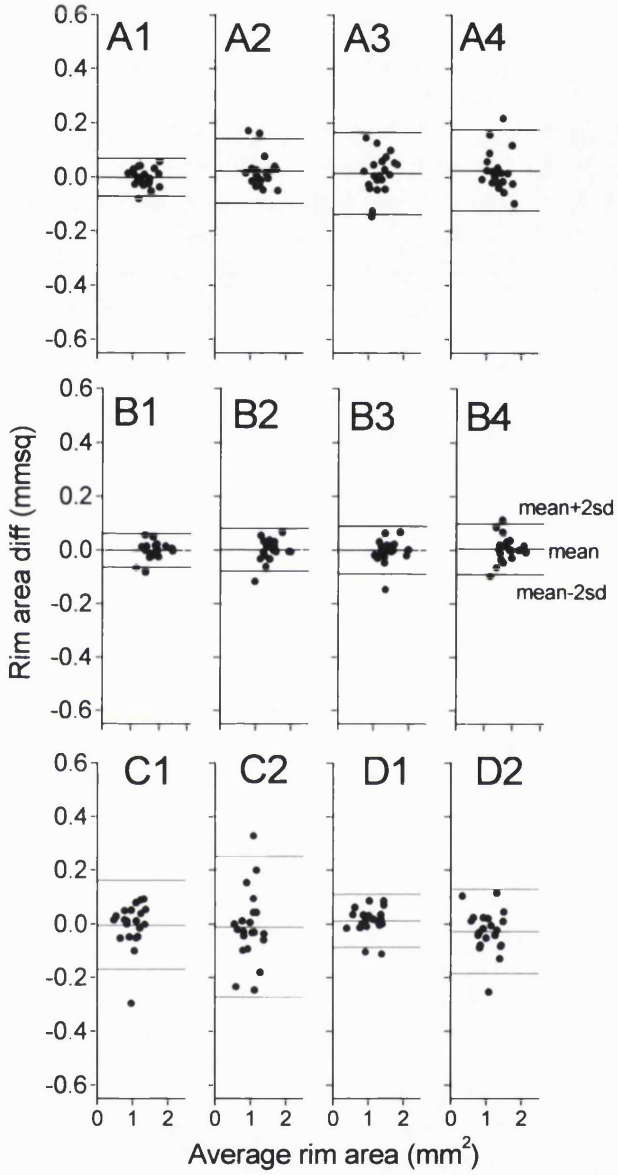

FIGURE 7.2. Agreement plots for global rim area. *Graphs for normal eyes: Graph A*= standard reference plane, *Graph B*=320μm reference plane; variability: (1)=intraoperator-intravisit; (2)=interoperator-intravisit; (3)=intraoperator-intervisit; (4)=interoperator-intervisit. *Graphs for glaucoma eyes: Graph C*= standard reference plane, *Graph D*=320μm reference plane; variability: (1)=intraoperator-intravisit, (2)= interoperator-intervisit.

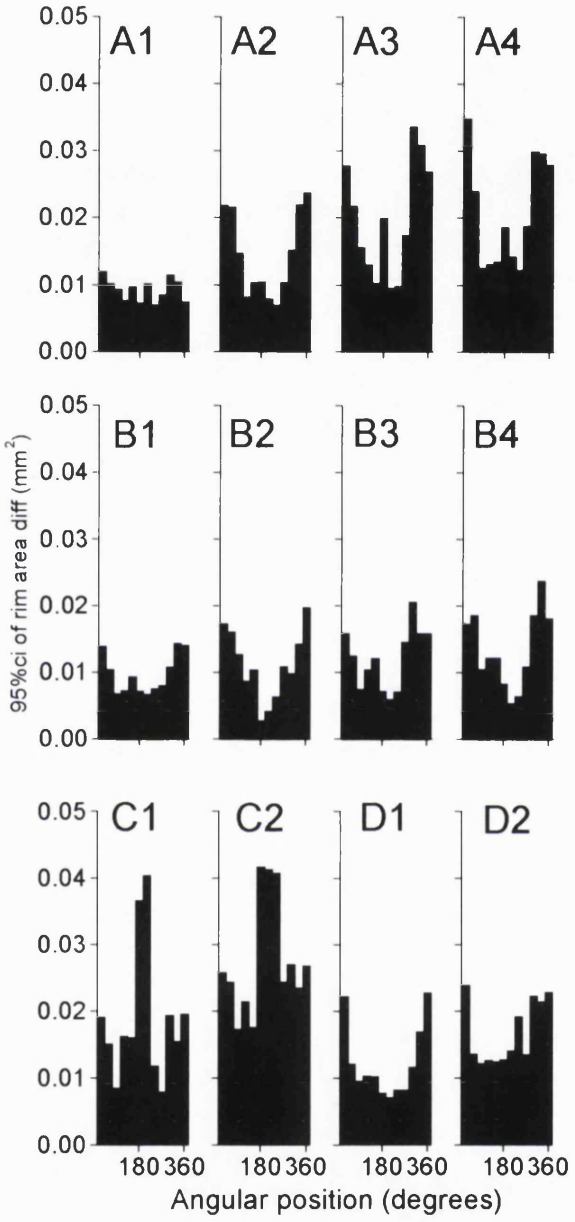

FIGURE 7.3. Regional rim area variability. *Graphs for normal eyes:* (A)=standard reference plane, (B)=320μm reference plane; variability: (1)=intraoperator-intravisit, (2)=interoperator-intravisit, (3)=intraoperator-intervisit, (4)=interoperator-intervisit. *Graphs for glaucoma eyes:* (C)=standard reference plane, (D)= 320μm reference plane; variability: (1)=intraoperator-intravisit, (2)=interoperator-intervisit. *Each bar*=95% agreement interval for a 30° sector of rim area located on the optic nerve head circumference between 0-360°, with 0°=temporal, 90°=superior, 180°=nasal, 270°=inferior.

Figure 7.4 shows the same information as Figure 7.3, but as polar plots. Variability was not correlated with rim area ($p>0.05$).

Figure 7.5 depicts the sectors in normal optic nerves in which variability was significantly less ($p<0.05$) in intraoperator-intravisit testing than testing involving different visits, operators or both (intraoperator-intervisit, interoperator-intravisit or interoperator-intervisit testing). The number and location of sectors having significantly increased variability due to these factors differed between reference planes.

7.3 Discussion

Variability in topographic parameters tended to increase because of different operators, separate visits or both. Amongst parameters, CV for rim area was lowest and least affected by different operators and visits. Rim area variability tended to be higher in glaucoma than normal eyes, and temporally in the optic nerve head. Rim area variability that is selectively higher in certain regions of the nerve may affect the detection of localised progression, as has been described photographically (Tuulonen and Airaksinen, 1991; Jonas et al, 1993a). Patterns of regional variability were influenced by reference plane definition and by glaucoma. In normal eyes, increased variability due to different operators, visits or both was significant in certain regions of the optic nerve head ($p<0.05$), with its pattern of increase differing between reference planes.

Previous studies comparing parameter variability have used the older 'curved' reference surface, evaluated single topography images, and not studied the effect of different operators and visits (Mikelberg et al, 1993; Rohrschneider et al, 1994). In the present study, flat reference planes were used to analyse mean topography images that were acquired by different operators over different visits. CV for rim area was lower than that of other parameters, reasonably proportioned to its point-estimates, and affected least by different operators and visits. Orgül et al (1995a) also found that area measurements were more reproducible than volume measurements (they studied SD of the cup) and suggested that the former, being derived perpendicular to the optical axis, was less influenced by inaccuracies in estimating depth.

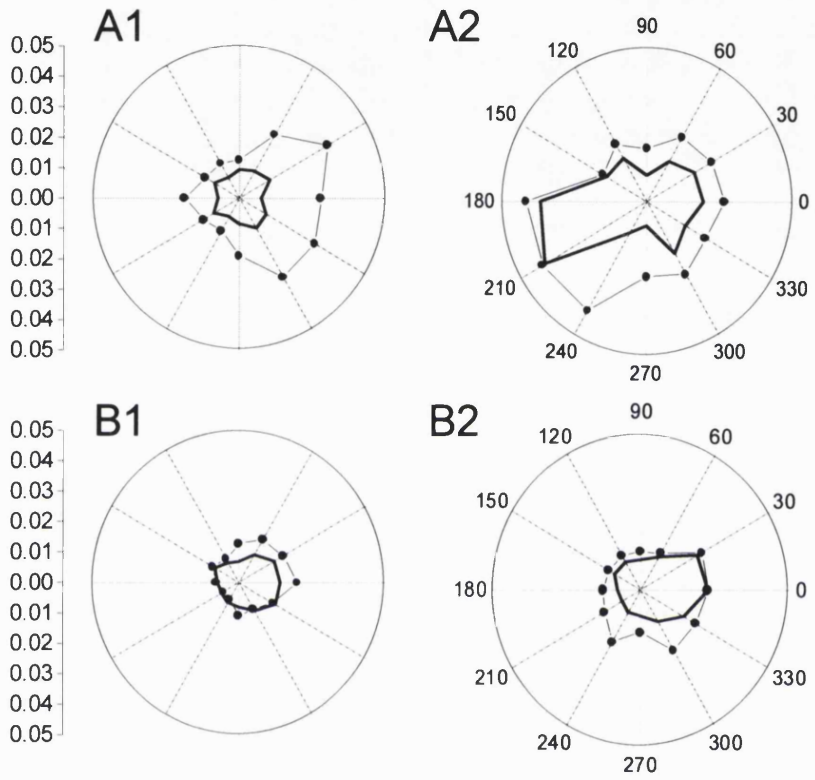

FIGURE 7.4. Polar plots of the 95% confidence intervals of differences for sector rim area in normal (1) and glaucoma (2) eyes for the standard reference plane (A) and 320μm reference plane (B). *Each plot:* n=21; *bold*=intravisit/intraoperator variability, *circles*=intervisit/interoperator variability. 0°=temporal, 90°=superior, 180°=nasal, 270°=inferior.

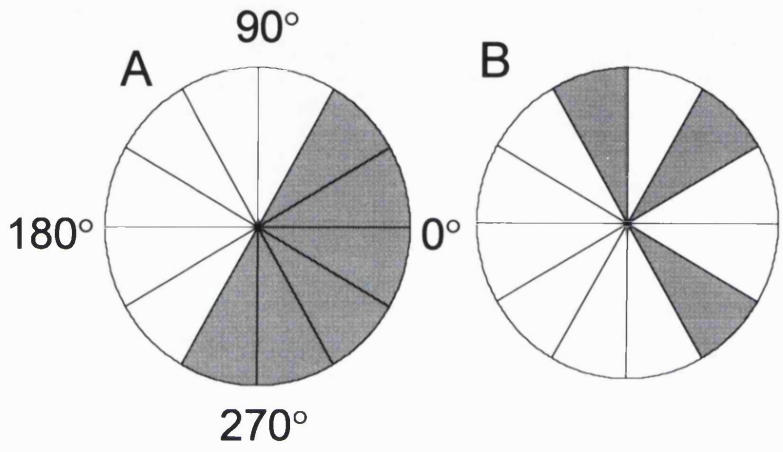

FIGURE 7.5. Schematic diagrams showing normal optic nerve head sectors where variability increased significantly ($p<0.05$) with testing by different operators, visits or both. *A*=standard reference plane, *B*=320μm reference plane, both shown as left eye aspect. *Shaded regions*=sectors with significantly greater variability ($p<0.05$) in testing involving different operators, visits or both compared with same operator-same visit testing.

Variability in topographic parameters tended to be higher with different scan operators, test visits or both, suggesting that each influenced reproducibility independently. This has implications for longitudinal analysis where testing is in many visits and likely by different operators. Increased variability due to these factors was not uniform across the optic nerve head but was significantly higher in certain regions of the optic nerve head ($p<0.05$), with its regional pattern of increase differing between reference planes. These results agree with Junescu-Cuypers et al (1998) who found that rim area variability was generally less in repeat imaging on the same day (SD=0.03 mm^2) than over different days separated by one day to one year (median SD=0.040 mm^2 (30% more); range: 0.022 to 0.054 mm^2). Chauhan and MacDonald (1995) found a trend toward increased pixel variability in testing over different visits but did not find this increase statistically significant. However, their analysis of variability was based on averaged estimations of variability across the optic nerve head and flatter peripapillary retina, and across groups, which could have obscured small differences. By contrast, the present study focused on variability in discrete regions within the optic nerve head. These findings and those of Junescu-Cuypers et al (1998) indicate that it is important to account for variability due to different operators and visits when evaluating progression.

A few points should be noted in the analysis presented here. Firstly, CV for cup area was higher than for rim area, when the variability of both should have been the same. This was due to the point-estimates for cup area being small relative to variability (CV=SD/mean) rather than cup area being more variable *per se*. In fact, SD for cup area and rim area was actually similar ($p>0.05$). Rim volume and cup volume also had small point-estimates relative to variability. Hence, analysis by CV was presented with plots of point-estimates so that parameters with different units could be compared meaningfully (Figure 7.1). Secondly, cup shape was uniformly negative in normal eyes but ranged from negative to positive in glaucoma eyes (negative and positive values represent a skew in cup height distributions toward low or high values respectively), making CV difficult to analyse meaningfully in glaucoma. Nevertheless, a reasonable feel of cup shape variability could be gained from the analysis of normal eyes. Thirdly, the possibility that progression occurred between visits in glaucoma cannot be excluded. However, such change, if present, should have manifested as bias in the agreement plots but was not evident. Also, the proportionate increase in variability from interoperator/intervisit testing was similar

in normal and glaucoma eyes (1.5x and 1.6x for the 320μm and standard reference planes respectively). It is possible that change, if present, was imperceptibly small relative to variability; which if true may well reflect a low signal-to-noise ratio in standard HRT analysis with decreased sensitivity to subtle progression.

While seemingly different, the data and variability in pixels and parameters are not actually independent of each other. Firstly, pixel variability, which reflects variability in the shape of topography, affects parameter variability because parameters are derived from the very same pixels. However, unlike pixels, parameter variability is subject to possible additional variability caused by a reference plane. Secondly, at least some of the variability seen in 320μm reference plane data should reflect the variability in pixels as both the zero-referencing of pixel height and positioning of the reference plane are by a common reference ring (Heidelberg Engineering, 1993). Thirdly, pixel height is variable where contour is steep, such as at the cup edge (Dreher et al, 1991; Cioffi et al, 1993; Chauhan et al, 1994; Brigatti et al, 1995). The reference plane's intersecting of the optic nerve head in this region is crucial to defining topographic parameters and so increased pixel variability here can have an important influence on the measurement of parameters.

There are possible reasons for the patterns of regional variability seen. Firstly, the optic nerve head normally tilts slightly inferotemporally and so a reference plane will tend to be more superficial temporally than nasally. Slight shifts could thus lift the reference plane above the temporal but not nasal rim surface, causing rim area to be selectively reduced temporally. Secondly, because the slope of the temporal cup tends to be more gradual, slight shifts of the reference plane can be expected to affect rim area more temporally than nasally. Thirdly, the standard reference plane is fixed to a small 6° section of the inferotemporal contour line where it "pivots", hence any image tilting or shifts in the position of the reference plane may cause more variation opposite the pivot nasally. This, together with the possibility that the nasal rim is depressed in disease, may explain the finding in this study of higher nasal variability in the analysis of glaucoma data by the standard reference plane, as **Figure 7.6** illustrates. It appears therefore that a reference plane which is appropriately positioned and stable relative to the optic nerve head is vital to ensuring reproducibility.

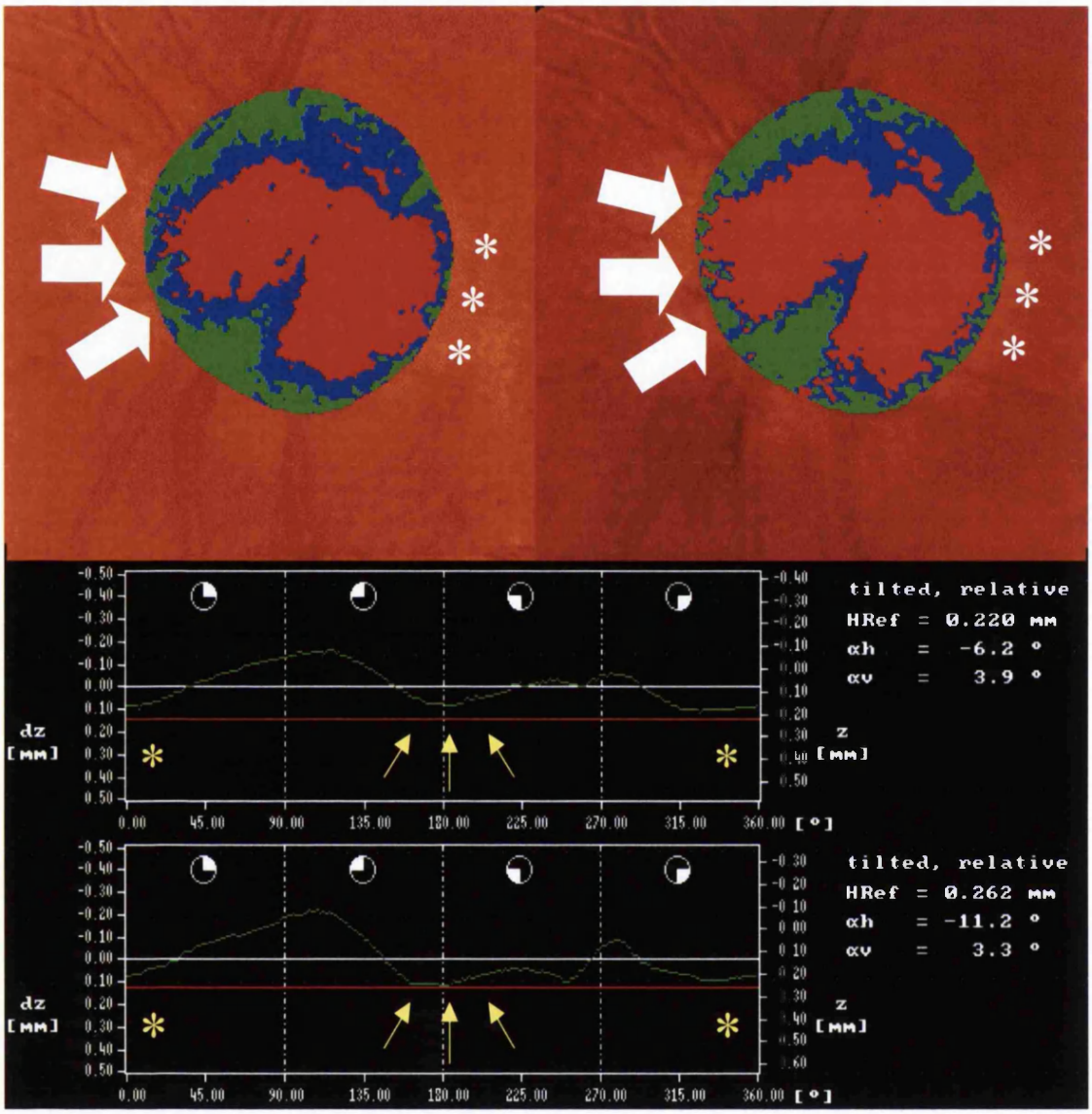

FIGURE 7.6. Rim area variability as analysed by the standard reference plane. *Top*: optic nerve head images are from the same glaucomatous eye and visit (*left & right*); *Bottom*: corresponding contour height profiles (upper profile for left image and lower profile for right image). Profiles are less variable temporally than nasally, and temporal rim (*stars*) is less variable than nasal rim (*fat arrows*). Greatly elevated regions, such as between 90-135° in the profiles, are least variable in the images. Horizontal tilt compensation differed by 5° between images (*αh in profile diagrams*) suggesting that images were scanned at different angles.

The nasal region here is relatively low lying (*nasal=slim arrows* in profiles, *fat arrows* in images). *Top to bottom profile*: nasal region is depressed relative to the reference plane (red horizontal line) so that it comes to lie at an equivalent level to the temporal region (*temporal*=0-45°, 315-360° in profiles, *stars* in images) and is associated with decreased rim area nasally (*fat arrows* from *left* to *right*).

Chapter 8
REASONS FOR RIM AREA VARIABILITY

Possible sources of rim area variability were studied to help direct strategies to optimise reproducibility in image analysis. The relationship between rim area variability and variability in three-dimensional features of topography was assessed in two parts: 1) in a *cross-section* of normal and glaucoma test-retest images using different reference planes, and 2) *longitudinally*, in image series by different reference planes.

8.1 Investigations

8.1.1 Subjects

Seventy-two age-matched subjects—30 normal and 42 with glaucoma (POAG) — underwent test-retest imaging by the same operator in the same visit (intravisit/intraoperator), giving a sample size of 72. Their criteria for selection are described in Section 5.1 and their demographics are shown in **Table 8.1**. Variability in longitudinal data was assessed in the single topography image series of 20 normal subjects.

8.1.2 Test-retest imaging

Intravisit/intraoperator test-retest variability was investigated in the first part of the study. Each subject underwent optic nerve head imaging in two sessions on the same day with sessions separated by at least an hour. Three well-centred topography images were acquired at each session. Corneal curvature, scan depth and focus settings kept constant and pupils were not dilated. One experienced operator performed both tests.

Mean ± SD	Normal	Glaucoma
N=	30	42
Age (years)	66.5±9.2	69.2±10.2
Male gender	17	21
Right eyes	14	16
Visual field MD (dB)	+0.11±1.2	-3.9±1.7
Visual field CPSD(dB)	0.89±0.75	3.1±1.8

TABLE 8.1. Subjects' demographics. Eyes with glaucoma had POAG.

8.1.3 Image analysis

First part of the study: test-retest variability. Test-retest images from one randomly selected eye of glaucoma and normal subjects were analysed. Each subject had two separate sets of mean topography images with corresponding single topography image triplets. Rim area in both single and mean topography images was evaluated by the 1) standard reference plane and 2) 320μm reference plane, as described in Section 5.2.

Second part of the study: variability in longitudinal data. Variability in longitudinal data was investigated in single topography image series of normal subjects. Only subjects with more than 20 single topography images from over at least three years were studied (three per visit over at least seven test visits). Each subject contributed an image series from one eye. Each series was analysed separately. All single topography images had contour lines imported from corresponding baseline images in the first part of the study. Rim area was analysed by the: 1) standard reference plane, and 2) 320μm reference plane. Images in each series had been acquired by 3-6 different experienced or less experienced operators due to the turnover of technical staff in the research clinic; this reflected the realities of longitudinal testing.

Identifying sources of rim area variability. Factors potentially influencing rim area variability (*RIMVAR*) were studied: variability in the: a) position of the reference plane relative to the optic nerve head margin (*REF*), b) orientation of the scanned optic nerve head (*HTILT, VTILT*), and c) optic nerve head's surface geometry (*X, Y, Z*). Both (b) and (c) are independent of reference planes. Analysis in pairs of mean topography images was as differences (*diff*), and in series of single topography images was as standard deviations (*sd*).

1. ***RIMVAR*:** rim area variability; analysed as *RIMVARdiff* and *RIMVARsd.*

2. ***REF:*** variability in the z-axis distance between the reference plane and surface height of the optic nerve head margin. This distance was calculated as [HRef – MHC], where HRef=distance between the reference plane and mean reference

ring height, and MHC=mean height of the contour line measured from the reference ring. MHC represented the optic nerve head's position on the z-axis as shown in **Figure 8.1**. Analysis was for *REFdiff* and *REFsd*.

3. ***HTILT and VTILT.*** HRT software tilts each image horizontally and vertically to compensate for the inclination of the imaged peripapillary retinal plane. Variation in tilt-compensation *(HTILT and VTILT)* was taken to represent the variable orientation of the optic nerve head and peripapillary retina between images. Analysis was for *HTILTdiff* and *VTILTdiff*, and *HTILTsd* and *VTILTsd*.

4. ***X, Y, Z:*** variability in the distance between the centres of gravity of the 1) optic nerve head and 2) contour line along each of the topographical axes (x, y and z). The centre of gravity is the weighted geometrical centre of pixel heights (personal communication with G. Zinser). Their geometrical relationship, reflected in the distance between centres of gravity, was studied. Analysed images were tilt-corrected and pixel heights measured by the reference ring. Analysis was for *Xdiff, Ydiff, Zdiff*, and *Xsd, Ysd, Zsd*.

8.1.4 Statistical analysis

How well *RIMVAR* was explained by six independent variables, *REF, HTILT, VTILT, X, Y* and *Z*, was investigated by multiple regression analysis. Variables were considered explanatory if statistically significant ($p \leq 0.05$). Non-contributory variables ($p > 0.05$) were excluded by backward elimination. Multicollinearity indicated that independent variables were interrelated. Adjusted coefficients of determination (adjusted R^2) reflected how well each model explained *RIMVAR*.

First part of the study. Normal and glaucoma eyes were grouped together (taken to represent a continuum of morphology) and studied to identify sources of rim area variability. Positive or negative signs indicated the direction of change on repeat testing. Positive: *RIMVARdiff*=initial test value exceeded the retest; *REFdiff*=decreased distance in the retest image; *HTILTdiff* and *VTILTdiff*=net

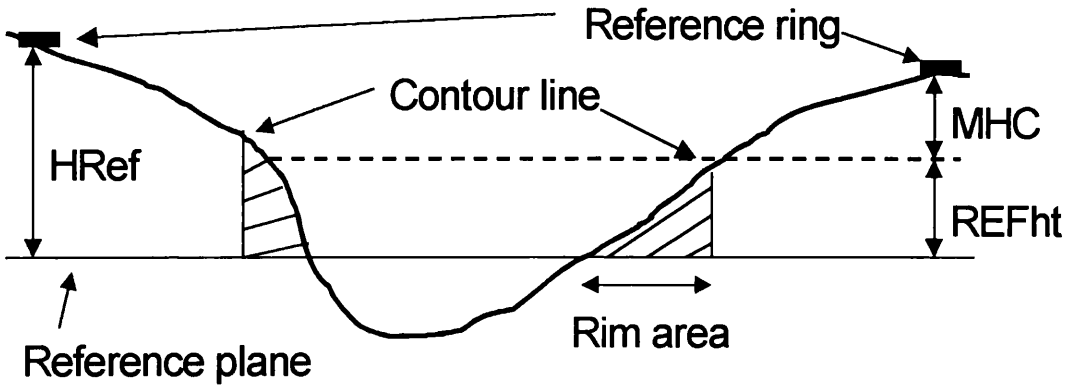

FIGURE 8.1. Features of optic nerve head topography. Cross-sectional profile of the surface of the optic nerve head illustrating the concepts of 1) contour line, 2) reference plane, 3) reference ring, 4) HRef, 5) MHC, 6) REFht/REF and 7) rim area. *HRef*=distance between the reference plane and mean height of the reference ring, *MHC*=mean height of the contour line above/below the mean height of the reference ring, *REFht*=distance between mean contour line height and HRef (variability in *REFht* is referred to as *REF* in the text). All distances are measured on the topographical z-axis.

downward angular displacement in the image top left-hand corner; *Xdiff, Ydiff* and *Zdiff*=net nasal shift, inferior displacement and depression respectively.

Second part of the study. The relationship between *RIMVARsd* and independent variables was studied in each image series to try to explain variability in sequential imaging. The range of differences for explanatory variables was calculated to give an idea of the size of variation.

To characterise regional variability, agreement intervals (95% confidence intervals of differences and SD)(Bland and Altman, 1986) for 30° sectors were graphed in bar charts and polar plots. The Wilcoxon signed ranks test was used to test for significance in non-parametric data.

8.2 Results

8.2.1 First part: test-retest variability in the same visit

Table 8.2 shows adjusted R^2 values for single and mean topography images. In single topography images, 40% and 43% of *RIMVAR* was explained in standard and 320μm reference plane data respectively. In mean topography images, even more *RIMVAR* was explained: 60% and 58% in standard and 320μm reference plane data respectively.

REF and *Z* were most frequently significant as determinants of *RIMVAR* for either reference plane in both mean and single topography images ($p<0.05$, Table 8.2). Standardised regression coefficients for *REF* and *Z* were also generally larger than other variables, indicating that they contributed more to *RIMVAR*. Models describing *RIMVAR* differed between reference planes, suggesting that each reference plane had a different influence on rim area variability. Multicollinearity was only found between *Xsd* and *Ysd* in single topography images analysed by the standard reference plane ($r^2=0.46$, $p=0.000$), but neither variable contributed to the model. *REF* was significantly higher in standard than 320μm reference plane data in mean topography images ($p=0.027$; median *REFdiff*: standard reference plane=16μm, 320μm reference plane=12μm) and single topography images

Image type and reference plane	*R^2	Independent variables of statistical significance ($p<0.05$)		
		Variable	Standard. Coeff.	p-value
Mean topo. 320um ref. plane	0.58	Zdiff	-0.43	0.000
		REFdiff	-0.35	0.000
		HTILTdiff	0.24	0.005
		Xdiff	-0.21	0.012
Single topo. 320um ref. plane	0.43	REFsd	0.57	0.000
		Zsd	0.32	0.001
Mean topo. Standard ref. plane	0.60	REFdiff	0.62	0.000
		Zdiff	-0.34	0.000
Single topo. Standard ref. plane	0.40	REFsd	0.47	0.000
		HTILTsd	0.22	0.016

TABLE 8.2. Summary of multiple regression models of significant sources of test-retest rim area variability in a cross-section of 72 normal and glaucoma eyes. *Adjusted R^2; *Topo*=topography; *Ref. plane*=reference plane; *Standard. coeff.*=standardised coefficient.

(p=0.000; median *REFsd*: standard reference plane=30μm, 320μm reference plane=20μm). *Zdiff* and *Zsd* did not differ between reference planes (p>0.05).

8.2.2 Second part: variability in longitudinal image data

Table 8.3 shows that adjusted R^2 values had a range of 0.62-0.95 for the standard reference plane (median= 0.84), and a range of 0.61-0.97 (median= 0.86) for the 320μm reference plane. Thus, a substantial proportion of *RIMVARsd* was explained: a median of 84% in standard reference plane data and 86% in 320μm reference plane data.

As in test-retest data, *RIMVARsd* within image series was most frequently explained by *REFsd* and *Zsd* (p<0.05). With the 320μm reference plane, *REFsd* was significant in 19/20 (95%) of eyes and *Zsd* significant in 16/20 (80%) of eyes. With the standard reference plane, *REFsd* was significant in 20/20 (100%) of eyes and *Zsd* in 19/20 (95%) of eyes. The distance between MHC and HRef (HRef-MHC) varied by as much as 726μm in analysis by the standard reference plane (median=150μm, Q1,Q3=110,332μm), significantly more than in analysis by the 320μm reference plane (p=0.000, Wilcoxon test); in the latter, the [HRef-MHC] distance varied by only as much as 166μm (median=116μm, Q1,Q3=74,140μm). Within series, *Zdiff* varied by as much as 285μm (median=78μm, Q1,Q2=59,125μm; not affected by reference plane definition). Other variables that were repeatedly significant were *Xsd* (8/20 (40%) of eyes with either reference plane) and *Ysd* (7/20 (35%) of eyes with the standard reference plane). Explanatory models for *RIMVAR* differed between reference planes as seen in Table 8.3. No multicollinearity was found.

Legend for TABLE 8.3 (next page) Summary of multiple regression models for individuals' image series in the second part of the study. *N*=subject number, *=Adjusted R^2

N	320μm reference plane		Standard reference plane	
	*R^2	Significant variable (standardised coefficient, p value)	*R^2	Significant variable (standardised coefficient, p value)
1	0.61	REF (-0.54, 0.000), X (-0.57, 0.001), Z (-0.38, 0.015)	0.95	REF (0.82, 0.000), X (-0.40, 0.000) Z (-0.60, 0.000)
2	0.94	REF (-0.49, 0.000), Y (-0.17, 0.003), Z (-0.89, 0.000)	0.84	Z (-1.03, 0.000), REF (-0.39, 0.000)
3	0.97	REF (-0.23, 0.000), Z (-0.85, 0.000), VTILT (0.11, 0.000)	0.83	Z (-1.25, 0.000), REF (-0.88, 0.000)
4	0.82	REF (-0.86, 0.000), X (-0.39, 0.000)	0.91	X (-0.30, 0.009), Z (-0.34, 0.002), REF (-0.86, 0.000)
5	0.71	REF (-0.55, 0.000), Z (-0.67, 0.000)	0.70	REF (-1.11, 0.000), VTILT (0.28, 0.019), Z (-1.20, 0.000)
6	0.92	REF (-0.56, 0.000), Z (-0.41, 0.000), V (0.18, 0.047)	0.62	Z (-0.94, 0.000), REF (-0.36, 0.022)
7	0.70	REF (-0.33, 0.018), Z (-0.80, 0.000), X (0.36, 0.018)	0.89	X (0.61, 0.000), Z (-0.81, 0.000), REF (-0.76, 0.000)
8	0.86	REF (-0.68, 0.000), Z (-0.40, 0.000)	0.90	Z (-0.50, 0.000), REF (-0.92, 0.000)
9	0.90	REF (-0.48, 0.000), X (0.17, 0.029), Y (0.18, 0.037), Z (0.96, 0.000)	0.90	X (0.15, 0.025), Z (-0.69, 0.000), REF (-0.93, 0.000)
10	0.68	REF (-0.50, 0.000), X (0.43, 0.001), Y (-0.40, 0.002), Z (-0.34, 0.007)	0.82	X (0.26, 0.019), Z (-0.18, 0.040), REF (-0.69, 0.000)
11	0.94	REF (-1.01, 0.000), Z (-0.41, 0.000)	0.86	X (-0.48, 0.000), Z (-0.27, 0.000) REF (-0.96, 0.000)
12	0.69	REF (-0.58, 0.000), X (-0.48, 0.000), Z (-0.31, 0.031), HTILT (-0.28, 0.019)	0.62	HTILT (-0.24, 0.045), REF (-0.79, 0.000)
13	0.93	REF (-0.72, 0.000), X (0.18, 0.037), Z (-0.23, 0.007), HTILT (-0.16, 0.039)	0.66	Z (-0.65, 0.001), HTILT (-0.36, 0.022), REF (-0.53, 0.003)
14	0.80	REF (-0.442, 0.000), X (-0.21, 0.032), Z (-0.77, 0.000)	0.77	Z (-0.68, 0.000), REF (-0.58, 0.000)
15	0.49	Z (-0.67, 0.000)	0.76	Z (-0.72, 0.000), REF (-0.63, 0.000)
16	0.76	REF (-0.75, 0.000), Y (0.27, 0.015), VTILT (-0.26, 0.026)	0.88	Y (0.15, 0.050), Z (-0.16, 0.019), HTILT (-0.19, 0.010), VTILT (-0.18, 0.019), REF (-0.76, 0.000)
17	0.70	REF (-0.35, 0.043), Y (0.73, 0.000)	0.77	X (-0.32, 0.007), Y (0.48, 0.003), Z (-0.28, 0.036), REF (-0.62, 0.000)
18	0.94	REF (-0.52, 0.000), Z (-0.51, 0.000), VTILT (0.15, 0.04)	0.89	X (0.33, 0.001), Z (-0.55, 0.000), REF (-0.42, 0.000)
19	0.82	REF (-0.87, 0.000), Z (-0.72, 0.000)	0.85	Z (-0.77, 0.000), REF (-0.83, 0.000)
20	0.89	REF (-0.47, 0.000), Y (-0.43, 0.000), Z (-0.81, 0.000)	0.92	Y (-0.29, 0.000), Z (-0.52, 0.000), REF (-0.75, 0.000)

8.3 Discussion

Between 40-60% of rim area variability in test-retest images could be explained by the factors studied. In image series, even more variability—a median of about 85%—was explained. *REF* and *Z* almost always contributed to the models and can be considered important causes of rim area variability. The nature of variability differed between the standard and 320μm reference planes. Influence of the factors studied may well underlie what was previously reported in Chapter 7: 1) variability is not uniform around the optic nerve head, 2) testing involving different operators and visits tends to be more variable, and 3) reference planes differ in their patterns of variability.

The nature of variability in image acquisition and analysis has been studied extensively (Dreher et al, 1991; Cioffi et al, 1993; Brigatti et al, 1995; Chauhan et al, 1994; Garway-Heath et al, 1999; Orgul et al, 1995a, 1997; Rohrschneider et al, 1994; Hosking and Flanagan, 1996; Junescu-Cuypers et al, 1998; Chauhan and MacDonald, 1995; Zangwill et al, 1997, 1999; Tomita et al, 1994; Janchknecht and Funk, 1995; Chauhan and McCormick, 1995) but little is known of the nature of variability in longitudinal data. The few studies that have evaluated longitudinal data (Junescu-Cuypers et al, 1998; Chauhan and MacDonald, 1995) have not sought out reasons for variability; knowing this could help in developing strategies to optimise reproducibility. The present study assessed the relevance to rim area variability of variability in three-dimensional features of topography and studied the influence of different reference planes. A large enough sample (72 subjects)(Altman, 1991) was studied to meaningfully explore six independent variables over a range of morphologies. Additionally, variability in longitudinal image series was analysed as it is pertinent to evaluating progression.

Adjusted R^2 was higher for mean than single topography images indicating that variability in the former was better explained. It is possible that some random fluctuation is eliminated in mean topography images. However, variability was calculated differently in mean topography images (differences) and single topography images (SD) and might have influenced analysis. Variability was even better explained in longitudinal data, where it was almost totally explained in some

eyes (≥90% variability explained in 25-35% of eyes; Table 8.3). This is probably because the analysis of image series was specific to the morphology of each optic nerve head. By contrast, a broad cross-section of optic nerve head morphologies had to be accounted for in analysing test-retest data. Both cross-sectional and longitudinal models indicate that the independent variables explained a large proportion of rim area variability.

REF and *Z* were almost universally significant in explaining rim area variability, irrespective of the reference plane used. This is not surprising given that rim area is measured where the reference plane intersects the optic nerve head on the z-axis. Any change in the height positions of the optic nerve head and reference plane relative to each other—due to variation in optic nerve head and peripapillary retinal topography, reference plane position, or both—could affect rim area measurement. Reference planes differed in their explanatory models, amount of *REF*, and patterns of regional variability. *REF* was significantly higher in standard than 320μm reference plane analysis ($p<0.05$), indicating that the former shifted more relative to the optic nerve head and may explain its higher variability, as is seen in Figures 7.2, 7.3 and 7.4. Garway-Heath et al (1999) also found variability to differ between reference planes.

Shifting in the centre of gravity of the optic nerve head relative to that of the contour line reflects geometrical variation along separate vectors, as depicted in **Figure 8.2.** Shifts along the z-axis (*Z*) significantly explained rim area variability in 80% (320μm reference plane) and 95% (standard reference plane) of image series. *Z* was not inconsiderable, having a median of 78μm and range of 285μm, and there may be several reasons for this. Firstly, centring of the optic nerve head in images may vary. HRT software centres the reference ring on the image frame and not the optic nerve head, and so the location of the optic nerve head relative to the ring may vary between images to influence the referencing of pixels. **Figure 8.3** shows slight differences between images in the optic nerve head's position relative to the reference ring. Secondly, the surface of the optic nerve head may be orientated differently between images. Rim area variability in some eyes could be explained by variation in image tilt, indicating its compensation by software was mostly but not always adequate. Adequacy of compensation probably depends on the centring of the optic nerve head in each image and differences in nerve morphology.

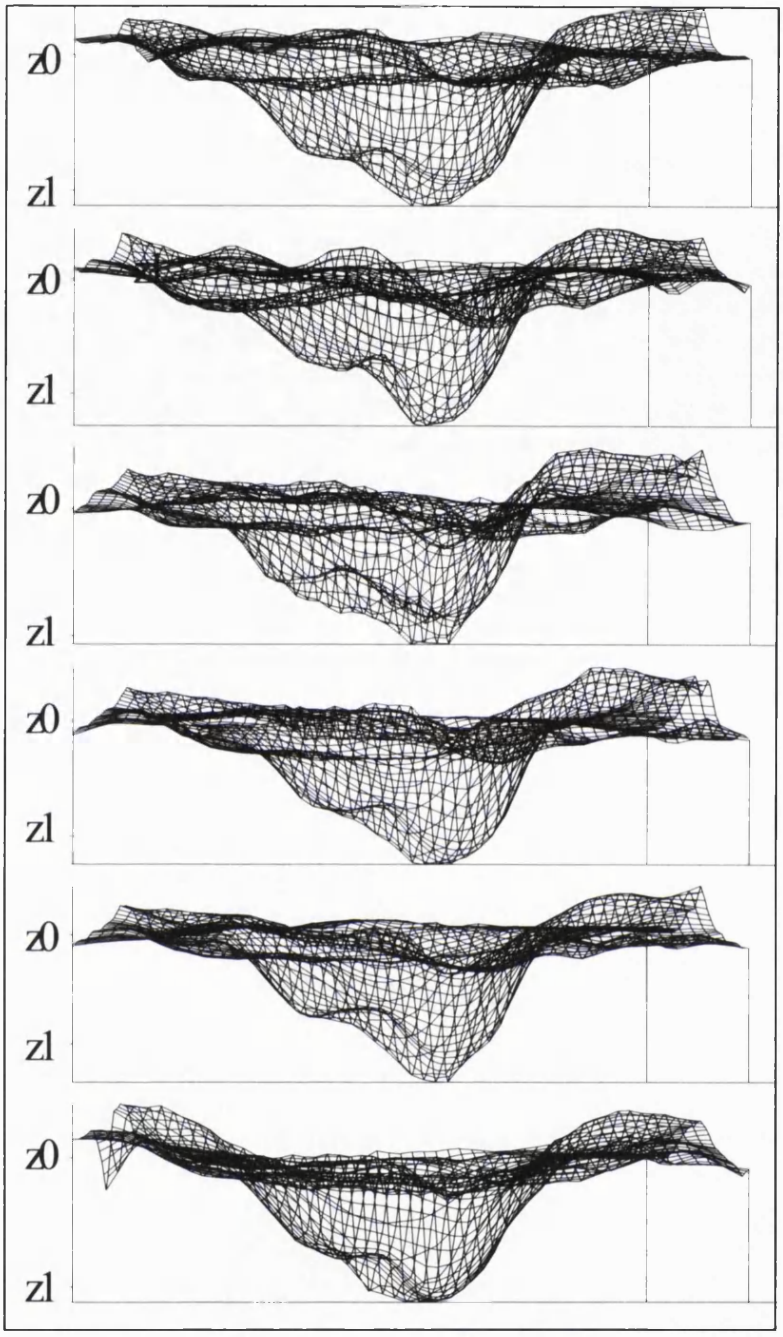

FIGURE 8.2. Image-to-image variation in the surface geometry of the imaged optic nerve head and peripapillary retina. Surface plots of six topographies from the same emmetropic eye imaged on the same day, all shown sharing a common aspect. *Central concavity* is the cup (*left*=temporal, *right*=nasal) and the *flatter periphery* is peripapillary retina. *Y-axis*=depth values relative to the mean reference ring height (z0=0μm z1=-500.00μm), *x-axis*= transverse distance (all same scale). There is variation in the: 1) shape of the cup, 2) depth of the cup (seen relative to the z1 mark), and 3) contour of peripapillary retina where the reference ring is located.

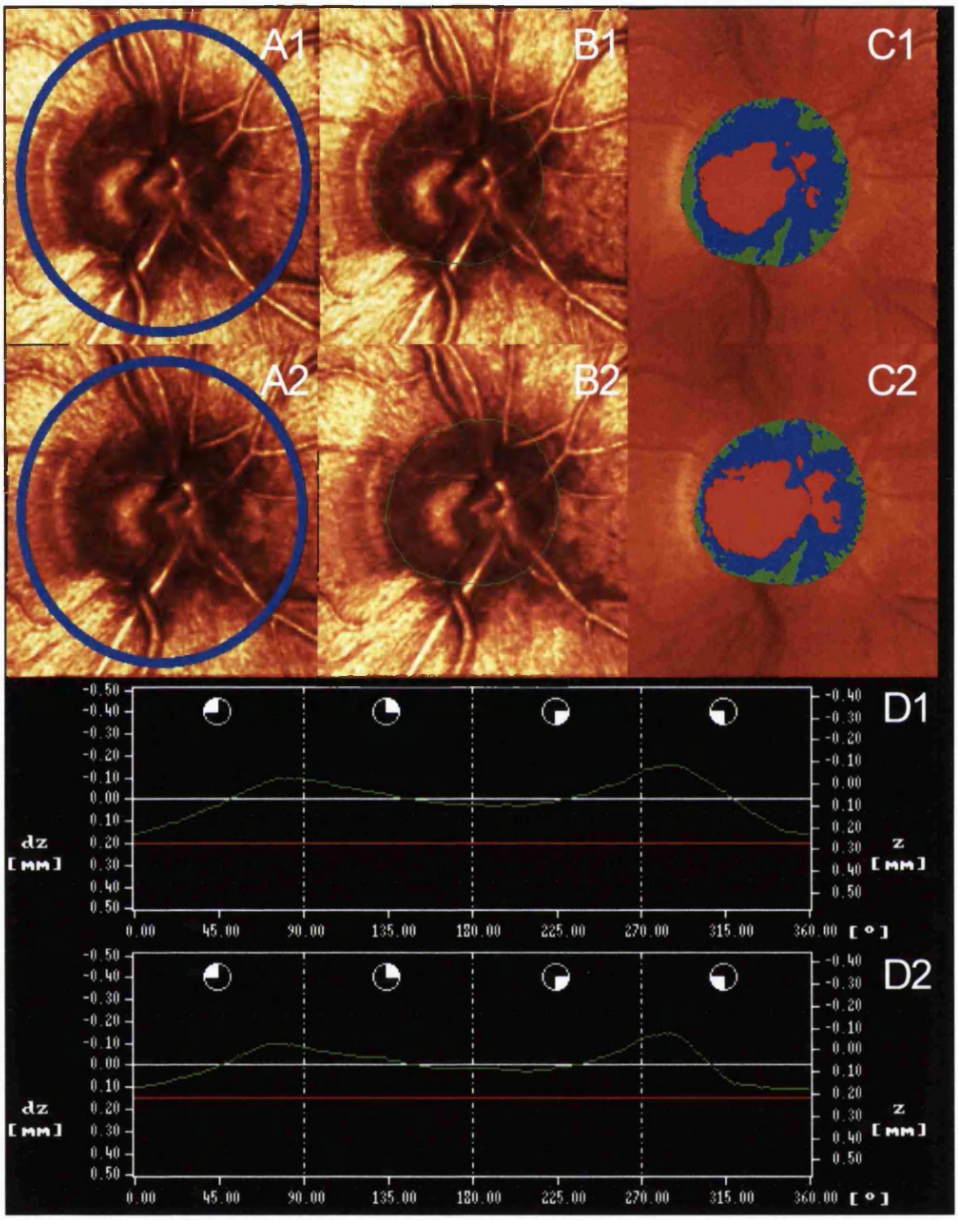

FIGURE 8.3. Sources of rim area variability. Two images of the same normal right optic nerve head from the same test visit (subject #17 in Table 3, standard reference plane). (*1*)=first image, (*2*)=second image. (*A*)=optic nerve head centring within the *reference ring*, (*B*)=contour line, (*C*)=rim area and cup area, (*D*)=height profile of contour line. *Horizontal lines*: *upper*=MHC, *lower*=reference plane.

Optic nerve head centring and orientation changes slightly from 1 to 2 in panel *A*. *RIMVARdiff* =0.152 mm^2 (17%) is associated with *Xdiff*=10µm, *Ydiff*=8µm, *Zdiff*=2µm, *HTILTdiff*=2.4° and *VTILTdiff*=1.2°. *REFdiff*= 54µm reflects a shift of the reference plane upwards towards the reference ring (D1 to D2) where it comes to lie more superficially in the optic nerve head to increase the cup and reduce rim (C1 to C2). Rim area variability is not uniform around the ONH but most marked temporally and nasally.

Incompletely compensated tilting could cause the geometry of the imaged surface to vary asymmetrically and unpredictably. Thirdly, scanning misalignment is reported to cause variable depth estimation (Orgul et al, 1995a), and could have contributed to *Z* in the eyes studied.

Considerable variability in optic nerve head image analysis is caused by fluctuation in the z-axis distances between the scanned optic nerve head, reference plane and reference ring. These fluctuations significantly affect the reproducibility of rim area. The finding that *REF* is an important contributor to *RIMVAR* suggests that reproducibility is better preserved if the distance between MHC and HRef is kept constant. Studies on measuring macular volume support this (Menezes et al, 1995; Ang et al, 2000). Maintaining a constant distance between the position of the reference plane and optic nerve head margin in image series —thereby keeping *REF* as zero—may thus help minimise variability. Although variability is unlikely to be eliminated, the models suggest that it should be reduced substantially.

Chapter 9
A NOVEL REFERENCE PLANE

9.1 DESIGN OF AN EXPERIMENTAL REFERENCE PLANE

The topographical parameter of rim area, if ascertained reliably and accurately, could be useful as a marker of progression in longitudinal analysis. For this to be possible, the reference plane needs to be positioned at an appropriate height in the optic nerve head and this positional relationship with the nerve needs to be maintained in subsequent images. Alteration in this positional relationship may cause apparent changes that reflect artifact rather than true glaucomatous change.

9.1.1 Description and rationale of an experimental reference plane

The position of the reference plane in topography is calculated in a selected mean topography image from within an eye's image series. This image is designated as the *baseline image*. The positioning of the experimental reference plane is illustrated in **Figure 9.1** and is as follows:

1. ***MHC*** (mean height of the contour line) is the mean of height locations on the contour line, measured relative to the mean height of the reference ring. MHC is used as a marker of the optic nerve head's position on the topographical z-axis.

2. ***$LOW_{5\%}$***. The lowest region ($LOW_{5\%}$) of the contour line is calculated. Height values 1° apart (360 values) on the contour lines of single topography images, from which the baseline mean topography image is derived, are read off HRT

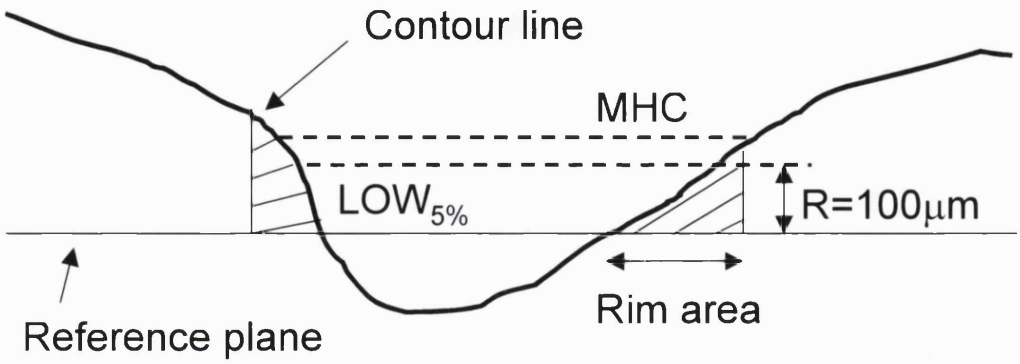

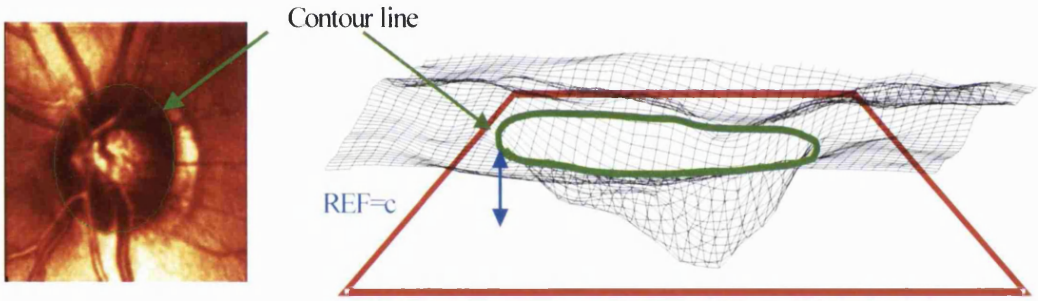

FIGURE 9.1 Positioning of the experimental reference plane. *Top*=cross-sectional profile of the optic nerve head's surface, *shaded region*=rim area. *Bottom*=three-dimensional surface plot illustrating *REFdis* [shown as REF (blue arrow)=z-axis distance between MHC (mean height of the contour line) and the reference plane] which is kept constant (c) in all images of an eye's image series.

software. Height values are ranked in each single topography image, from which the mean of the lowest 5% of values is calculated. Finally, the means of the 5% lowest values of each of the three single topography images are averaged to give $LOW_{5\%}$.

3. ***R*:** distance of the reference plane beneath $LOW_{5\%}$ where rim area variability is least. The reference plane is positioned to ensure it lies wholly beneath the circumference of the contour line. A reference plane lying above part of the contour line underestimates adjacent rim tissue, giving artifactual measurements. To determine *R*, rim area variability in longitudinal image series of normal control eyes was assessed for different reference plane levels below $LOW_{5\%}$. Once known, *R* was held constant.

4. ***REFdis.*** Once positioned at *R*, the distance of the reference plane below *MHC* is calculated; this distance is called *REFdis*. *REFdis* is unique to each optic nerve head and once calculated in the baseline image is kept ***constant*** in all the images of an eye. Keeping *REFdis* constant in all images of an eye means that the z-axis distance between the optic nerve head and reference plane is maintained across the same eye's image series. *REFdis* is expressed as:

$$REFdis = LOW_{5\%} + R \qquad \text{[equation 9.1]}$$

5. ***REFpos.*** Position of the reference plane *(REFpos)* on the z-axis can thus be expressed as:

$$REFpos = MHC + REFdis \qquad \text{[equation 9.2]}$$

$$= MHC + LOW_{5\%} + R \qquad \text{[equation 9.3]}$$

9.1.2 Emprically deriving a value for R

Image series of 19 normal subjects who had been imaged on six separate visits over three years were analysed. Demographic data of the normal subjects is shown in **Table 9.1** of Section 9.2 and their criteria for selection is described in Section 5.1. Standard deviation (SD) for the group, representing variability, was assessed at sequential 20μm levels between 0-180μm beneath $LOW_{5\%}$. **Figure 9.2** shows a trend toward decreasing rim area variability as the reference plane descends from

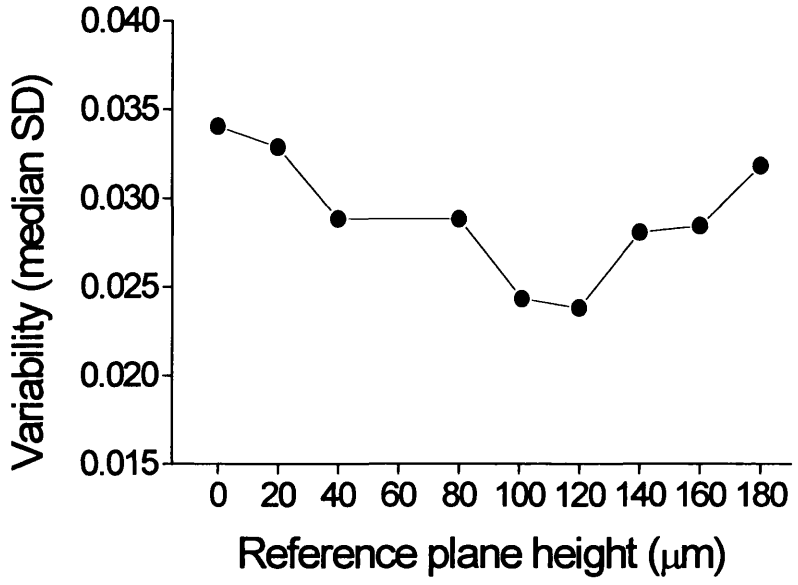

Figure 9.2. Rim area variability as the reference plane descends to different z-axis levels (reference plane height in graph) below $LOW_{5\%}$

0 to 100μm below $LOW_{5\%}$. A minimum was reached between 100-120μm but variability tended to increase when the reference plane was more than 120μm below $LOW_{5\%}$. R=100μm was chosen for subsequent analysis.

9.2 RIM AREA VARIABILITY IN ANALYSIS BY THE EXPERIMENTAL REFERENCE PLANE

Reproducibility of the experimental reference plane was evaluated in 1) *test-retest* image data, and 2) *longitudinal* image series, and compared with analysis by the standard reference plane and 320μm reference plane.

9.2.1 Investigations

9.2.1.1 Reference plane analysis

Rim area was analysed by three different reference planes, as illustrated in **Figure 9.3**. The reference planes were:

1) ***Experimental reference plane.*** The position of the reference plane (*REFpos*) relative to the optic nerve head is kept constant throughout the image series of an eye, as described in Section 9.1, and defined as follows:

$$REFpos = MHC + LOW_{5\%} + R$$

Where, MHC=mean height of the contour line, $LOW_{5\%}$=average of the optic nerve head contour line's 5% lowest height values calculated from the constituent topographies of a baseline mean image; R=level of the reference plane below $LOW_{5\%}$ where variability is least, determined as R=100μm.

2) ***Standard reference plane.*** Set 50μm posterior to the mean of contour line heights between 350-356° on the circumference of the ONH, and is default in HRT software (HRT v1.11 to 2.01, and HRT II software) (Heidelberg Engineering, 1993; Burk et al, 2000), as described in Section 5.2.

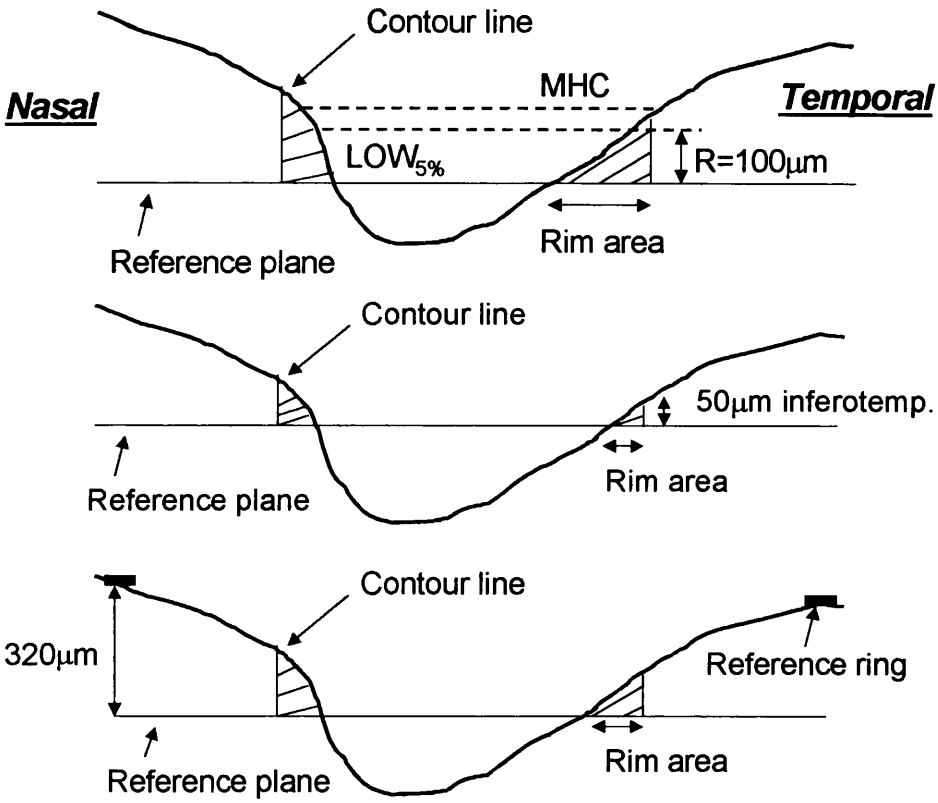

FIGURE 9.3. Diagrams comparing the positioning of the experimental reference plane and standard and 320μm reference planes. *Top*=experimental reference plane, *middle*=standard reference plane, *bottom*=320μm reference plane.

3) ***320μm reference plane***. Fixed at an offset 320μm posterior to the mean height of the "reference ring" (HRT software v1.09 to 1.10), as described in Section 5.2. The reference ring is centred on the image frame and located in its periphery, and has an outer diameter 94% and width 3% of image size (Heidelberg Engineering, 1993).

9.2.1.2 Subjects

Twenty normal subjects and 20 age-matched glaucoma (POAG) subjects underwent test-retest imaging. Subjects' selection criteria are described in Section 5.1. Nineteen of the normal subjects had images from six separate visits over three years. **Table 9.1** shows their demographics.

9.2.1.3 Reproducibility

Imaging and image analysis. Experienced operators conducted test-retest imaging of both eyes of normal and glaucoma subjects. Three well-centred 10° single topography images were acquired at each session. Corneal curvature, scan depth and focus settings were kept constant and pupils were not dilated. Normal subjects attended *two test visits* separated by six to eight months. Each visit comprised *two imaging sessions* separated by at least an hour. The same operator scanned in both imaging sessions on the first visit and one session of the second visit. A second operator scanned in the other imaging session of the second visit. Glaucoma subjects only underwent test-retest imaging in one visit; this was by the same operator. Imaging sessions were conducted in random order.

Mean topography images from one randomly selected eye of glaucoma and normal subjects were analysed, as described in Section 5.2. Contour lines were exported from the baseline image to other images of the same eye. Rim area was evaluated globally and regionally. Regional patterns of variability were examined by assessing 30° rim area sectors around the optic nerve head (0-360°).

Mean±SD	Normal	Glaucoma	P value
N=	20	20	-
Age (years)	66.5±9.2	68.8±11.5	P=0.70
Male gender	12	10	-
Right eyes	13	10	-
Visual field MD (dB)	+0.11±1.2	-4.6±1.9	P=0.0000
Visual field CPSD(dB)	0.89±0.75	3.3±1.8	P=0.0000
Mean SD (μm) of mean images*	22.6±8.1	25.9±9.65	P=0.17
Mean SD (μm) of mean images†	22.9±10.2	27.2±10.5	P=0.16

TABLE 9.1. Subjects' demographics. Subjects with glaucoma had POAG. Image reliability data from the first sessions of the first test visit* and second visit† is shown.

9.2.1.4 Statistical analysis

Global and regional variability was assessed by analysing agreement as described by Bland and Altman (1986). The degree of agreement between pairs of measurements reflects reproducibility, expressed as the width of agreement intervals (95% confidence intervals of differences) in graphs. For regional variability, analysis was modified so that agreement intervals for 30° sectors of rim area were presented in bar graphs by angular location (0-360°).

Standard deviation (SD) representing the dispersion of data was used to estimate variability in longitudinal data. The width of the intervals for the 5^{th} to 95^{th} percentiles and median values of SD for each sector were plotted in bar graphs. Significance testing was conducted using the Wilcoxon matched pairs test (signed rank sum test) for comparing paired non-parametric data.

Test-retest variability. Variability was analysed for test-retest imaging by: (1) the same operator in the same visit (same operator/same visit), and 2) different operators in separate visits (different operator/different visit). This design is relevant to longitudinal imaging in chronic glaucoma as such investigation requires testing in many different visits over time, likely involving different operators.

Variability in longitudinal image series. Longitudinal image series from normal eyes were analysed. Each image series had six sequential mean topography images from over at least three years. Individuals' series were analysed separately. Different operators with varying levels of experience had acquired these images, reflecting the turnover of technicians in the research clinic.

9.2.2 Results

9.2.2.1 Rim area variability in test-retest data

Figure 9.4 shows that 95% confidence intervals of rim area differences (agreement intervals) for global variability in normal eyes were narrower in experimental

reference plane data than standard and 320μm reference plane data. With all reference planes, there was a trend toward agreement intervals widening with different operator/different visit testing compared with same operator/same visit testing. This trend was less, however, in experimental reference plane data compared with data from other reference planes: standard reference plane (95%ci: 0.14 to 0.22) and 320μm reference plane (95%ci: 0.082 to 0.128) agreement intervals widened by about 25% more than did experimental reference plane intervals (95%ci: 0.065 to 0.086).

Figure 9.5 shows agreement intervals for regional rim area variability for normal (A and B) and glaucoma (C) eyes. The same information is shown as polar plots in **Figure 9.6.** In normal controls, agreement intervals tended to be wider in the temporal (0-90° and 270-360°) than nasal optic nerve head. In glaucoma eyes, agreement intervals tended to be widest temporally in experimental reference plane and 320μm reference plane data, but widest nasally in standard reference plane data. The profiles for experimental reference plane regional variability were ostensibly flatter, more uniform around the optic nerve head, and quite similar between groups compared with data by the other reference planes (1 vs 2 and 3 in Figure 9.5). In Figure 9.6 it is evident that, unlike other reference planes, the variability profiles for experimental reference plane data did not change appreciably with different-operator/different-visit testing or in glaucoma eyes, and were uniform around the nerve.

9.2.2.2 Rim area variability in longitudinal image series

Figure 9.7 shows that the amount and pattern of regional variability differed between reference planes. The same information is shown as polar plots in **Figure 9.8**. The intervals for the 5^{th}-95^{th} percentiles of sector variability were generally wider for the standard (A) and 320μm (B) reference planes compared with the experimental reference plane (C). Agreement intervals for the standard and 320μm reference planes were widest temporally and nasally. Intervals for the standard reference plane were particularly wide nasally, in keeping with findings in test-retest data, especially for glaucoma as shown in Figure 7.3 and Figure 9.5. Again, the variability profile for experimental reference plane data was much flatter

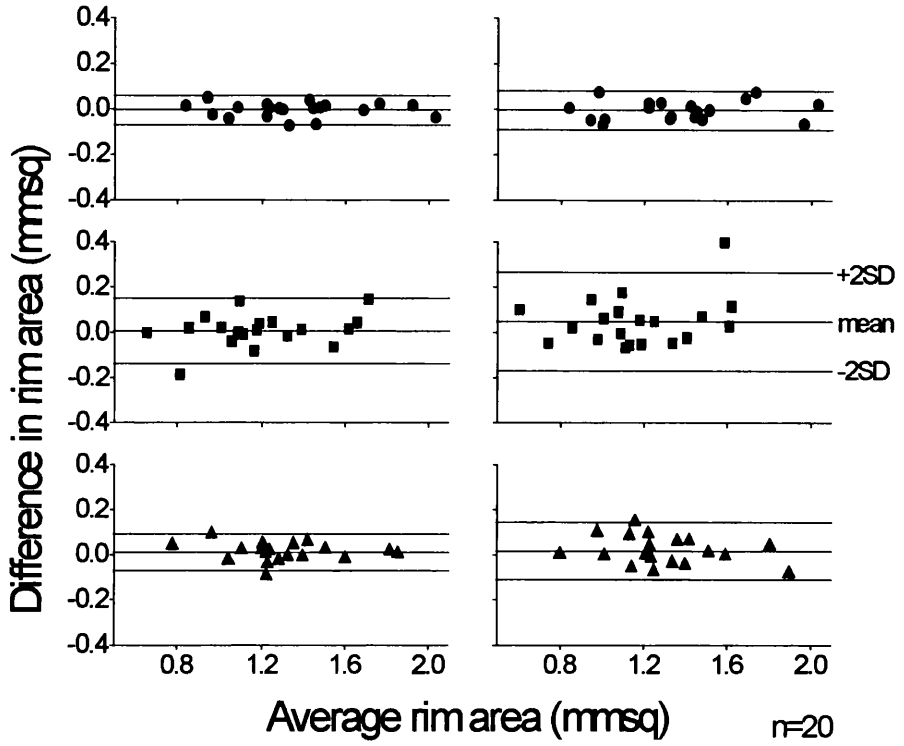

FIGURE 9.4. Global rim area variability in normal eyes as analysed by three different reference planes. *Circles*=experimental reference plane, *squares*=standard reference plane, *triangles*=320μm reference plane. *Left column*=same operator/same visit testing, *right column*=different operator/different visit testing. *Horizontal lines through data: middle*=mean difference, *flanking lines*=95% confidence intervals of differences.

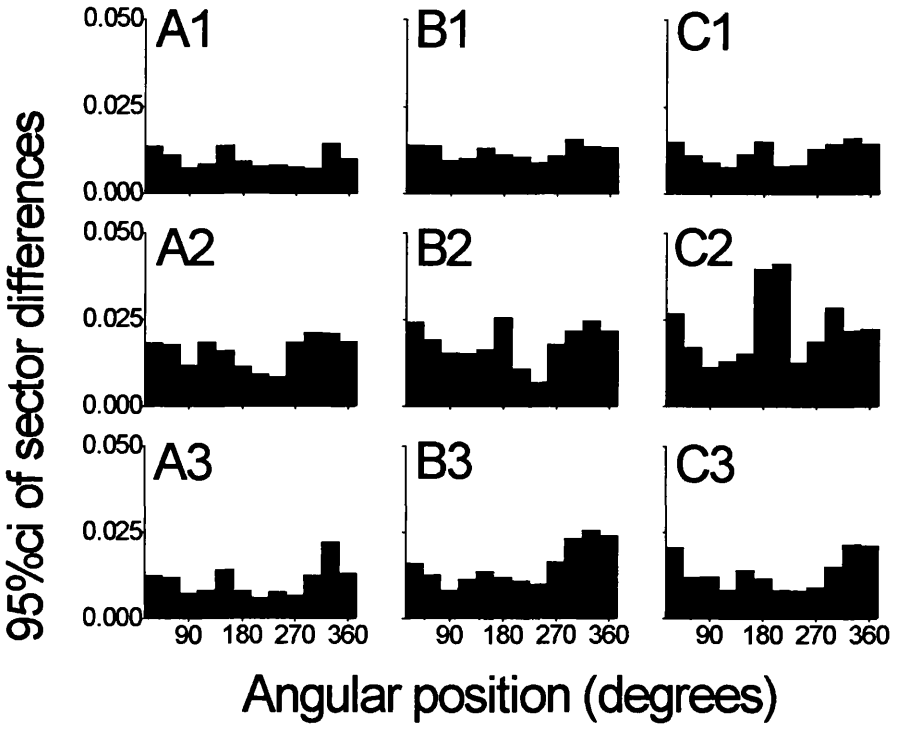

FIGURE 9.5. Regional rim area variability of different reference planes. Thirty degree sectors are located round the optic nerve head: *0°=temporal, 90°=superior, 180°=nasal, 270°=inferior*. *1*=experimental reference plane, *2*=standard reference plane, *3*=320μm reference plane. *A*=same operator/same visit testing in normal eyes, *B*=different operator/different visit testing in normal eyes, *C*=same operator/same visit testing in glaucoma eyes.

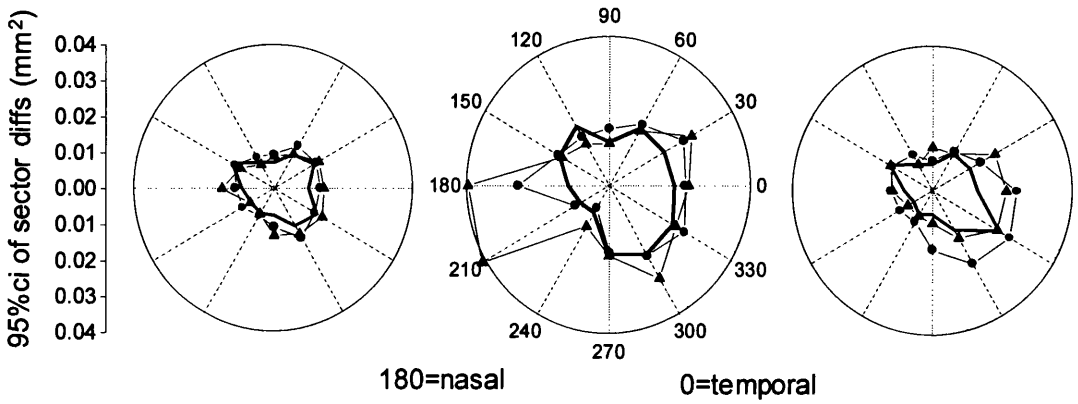

FIGURE 9.6. Polar plots for sector rim area variability. *Y-axis*= 95% confidence intervals of differences; *circumference*=angular location of 30° sectors around the optic nerve head with *0°=temporal, 90°=superior, 180°=nasal, 270°=inferior*; *centre point*: variability=0. *Left*=experimental reference plane, *middle*=standard reference plane, *right*=320μm reference plane. *Plots: Bold line*=same operator/same visit testing in normal eyes, *circles*=different operator/different visit testing in normal eyes, *triangles*=same operator/same visit testing in glaucoma eyes.

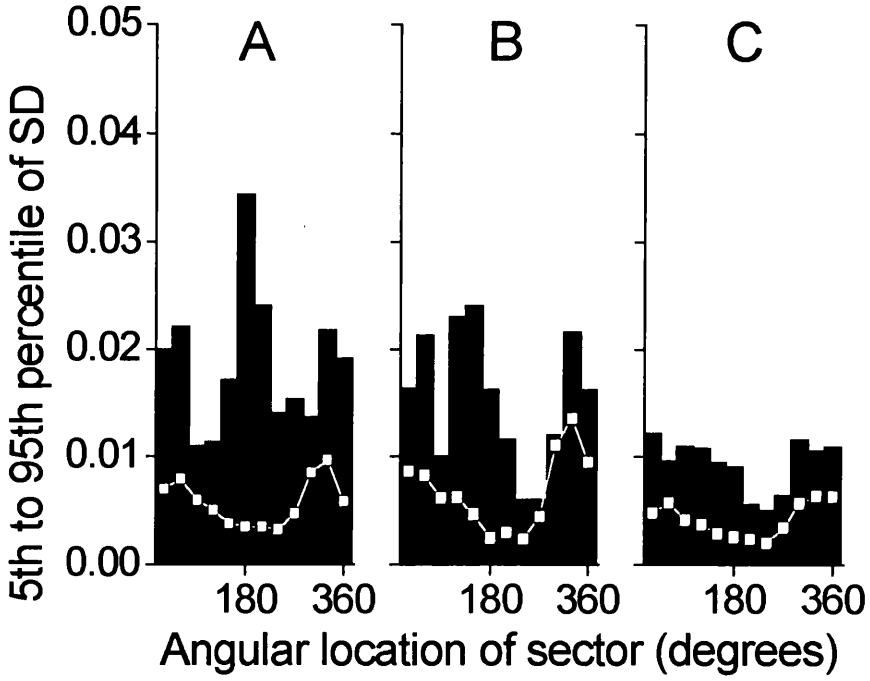

FIGURE 9.7. Regional rim area variability in longitudinal image series of normal eyes. *Y-axis*=variability expressed as the width of 5^{th}-95^{th} percentiles for SD for each sector, *x-axis*=angular location of 30° sectors: *0°=temporal, 90°=superior, 180°=nasal, 270°=inferior. Plots: Squares*=median values; *connecting line* depicts variability profile. *A*=standard reference plane, *B*=320μm reference plane and *C*=experimental reference plane.

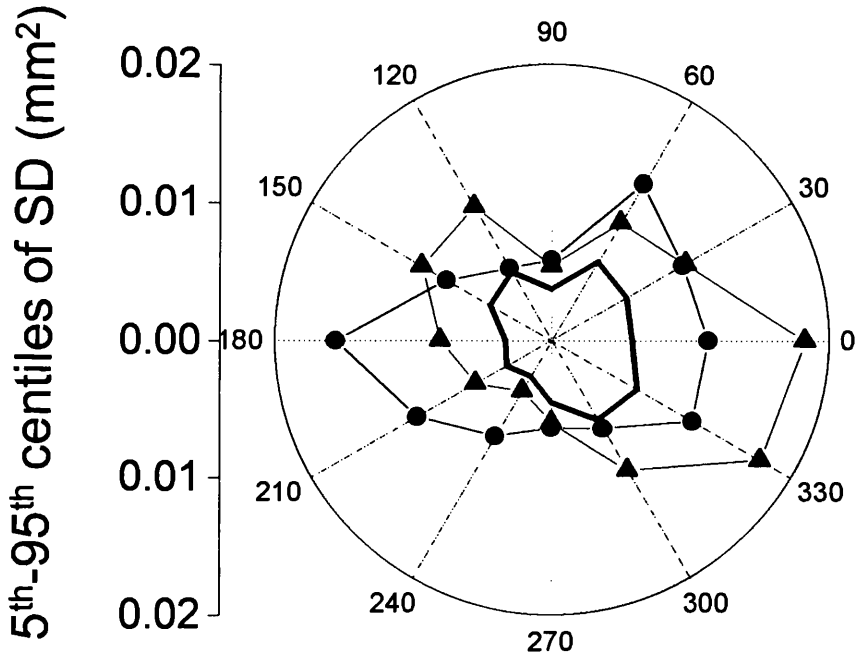

FIGURE 9.8. Sector rim area variability in the longitudinal data of normal eyes. *Polar plot y-axis*=variability expressed as the width of 5th-95th percentiles for SD in each sector, *circumference*=angular location of 30° sectors: *0°=temporal, 90°=superior, 180°=nasal, 270°=inferior*; *centre point*: variability=0. *Plots: bold line*=experimental reference plane, *circles*=standard reference plane, *triangles*=320μm reference plane.

(Figure 9.7C) and uniform around the nerve (Figure 9.8) than the profiles for standard and 320μm reference plane data.

Figure 9.9 shows rim sectors in longitudinal image series that were significantly less variable ($p<0.05$) in experimental reference plane analysis compared with analysis by the standard (A) and 320μm (B) reference planes. The pattern of sector variability differed between standard and 320μm reference plane data. **Figure 9.10** illustrates the way in which rim area variability can differ in the same normal eye because of analysis by different reference planes.

9.2.3 Discussion

Increased rim area variability can be expected if the positions of the optic nerve head and reference plane change with respect to each other from image to image (see Chapter 8). The experimental reference plane was used to keep this positional relationship constant: the mean height of the contour line (*MHC*) marked the position of the optic nerve head on the z-axis, and the experimental reference plane was positioned to remain at a constant distance below MHC in all images of an eye's image series. By this arrangement, analysis of rim area tended to be less variable than in analysis by other reference planes. Variability was also more uniform around the optic nerve head, not appreciably affected by different test conditions or glaucomatous morphology, and in longitudinal analysis, significantly less compared with other reference planes ($p<0.05$) .

No two optic nerve heads are identical and so analysis by a reference plane should ideally adapt to suit variations in morphology. The experimental reference plane was devised to lie entirely beneath the margin of the optic nerve head by factoring the height profile of each contour line into its calculations. **Figure 9.11** illustrates why this is necessary. $LOW_{5\%}$ was the level in each optic nerve head above which the reference plane should not rise. The value for $LOW_{5\%}$ was not pre-selected but derived from the lowest 5% of contour line heights and averaged from multiple topographies to minimise the effect of randomly outlying values. R=100μm (100μm below $LOW_{5\%}$) was compatible with least variability; here, the reference plane is more likely to remain entirely below the optic nerve head margin despite topographical variability. Also, the cup is probably steeper here: rim area is affected

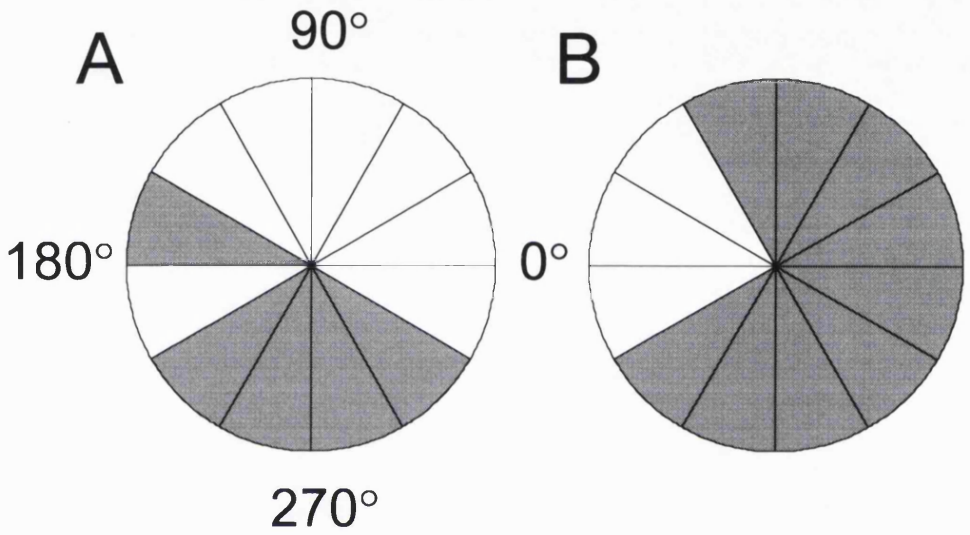

FIGURE 9.9. Schematic diagrams showing sectors where rim area variability was significantly less in experimental reference plane data compared with standard (A) and 320μm reference plane (B) data. *Gray sectors*=$p<0.05$, *white*=$p>0.05$. *Sector location*: 0°=temporal, 90°=superior, 180°=nasal, 270°=inferior.

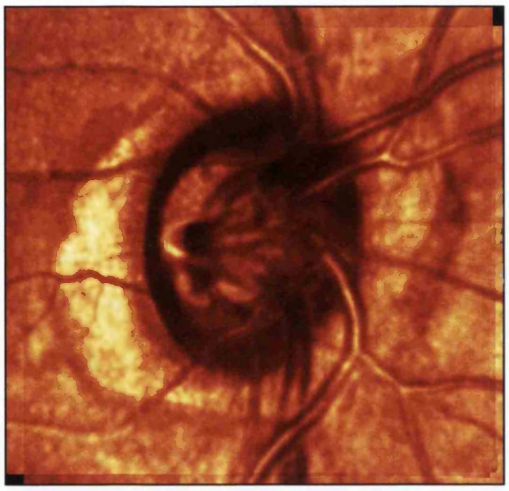

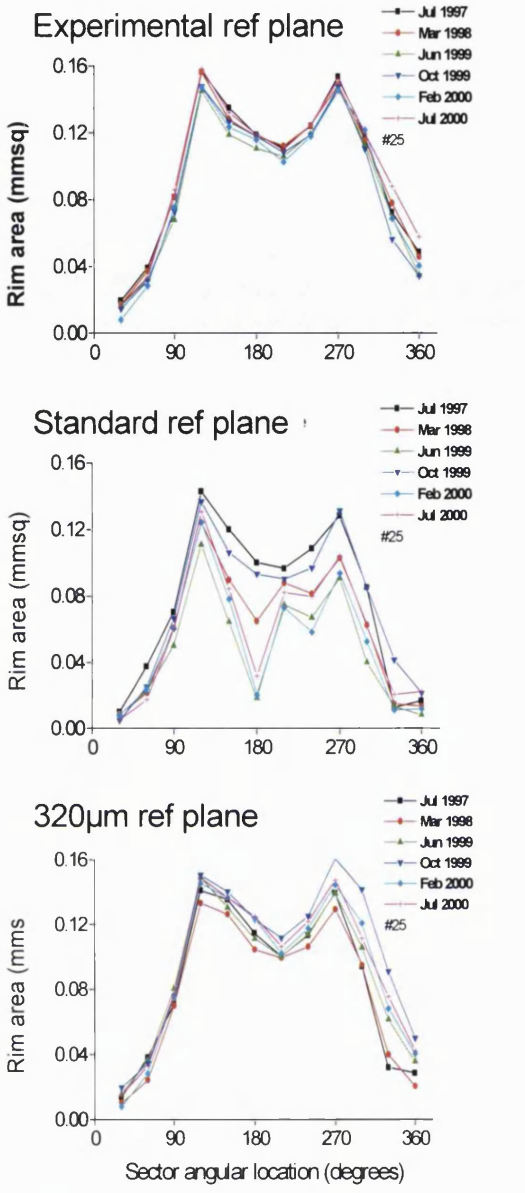

FIGURE 9.10. Examples of rim area variability in the same normal eye's longitudinal data as analysed by different reference planes. *Above image*: HRT intensity image. *Right graphs*: Rim area profiles for 30° rim sectors with each colour representing a different time-point. *X-axis*: 0=temporal, 90=superior, 180=nasal, 270=inferior. *Top graph*=experimental reference plane, *middle graph*=standard reference plane, *bottom graph*=320µm reference plane. Rim area profiles for the experimental reference plane are closely overlapping as may be expected in a normal, unchanging nerve. Profiles for other reference planes are more dispersed, indicating greater variability. Note pronounced nasal variability in standard reference plane data. *Below*: images corresponding to rim area profiles: *top row*=experimental reference plane, *middle row*=standard reference plane, *bottom row*=320µm reference plane.

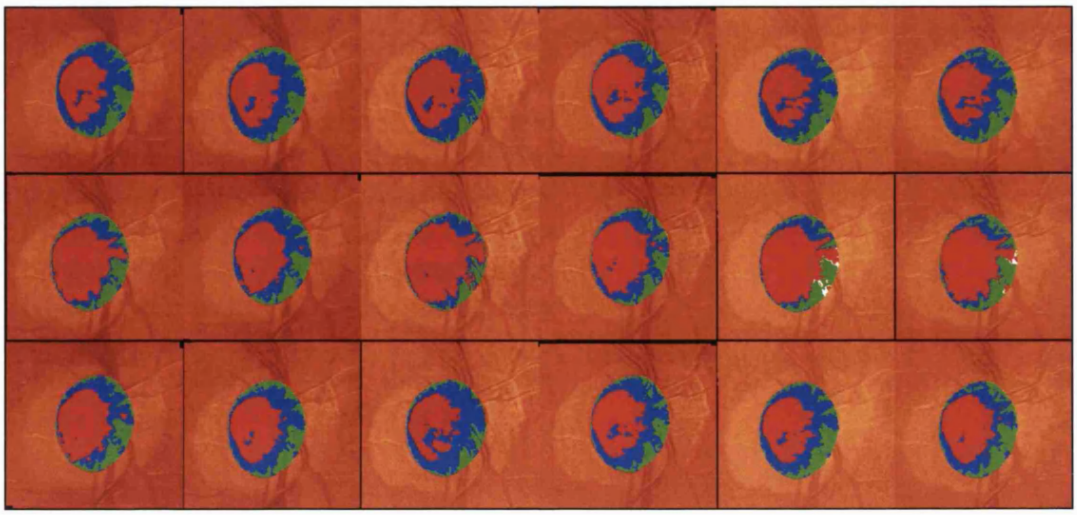

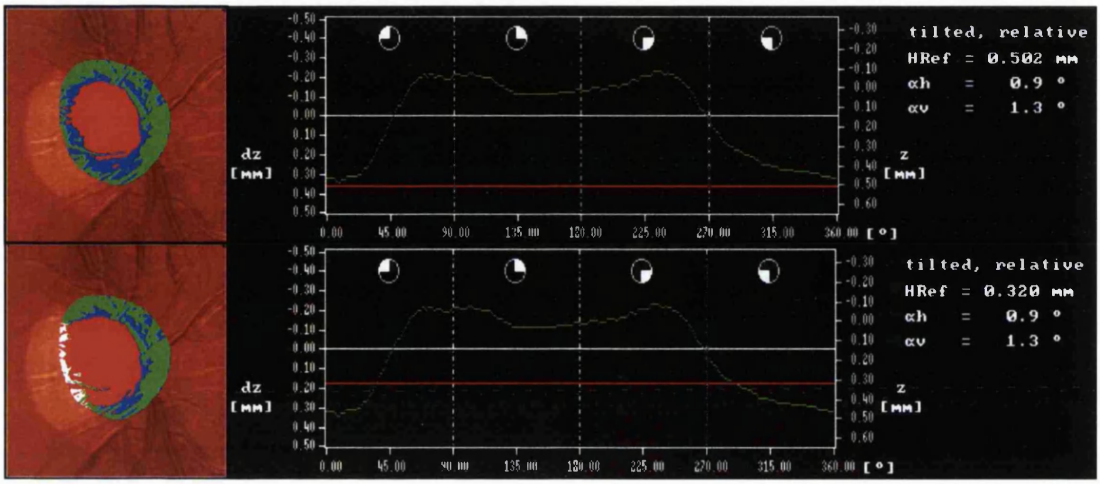

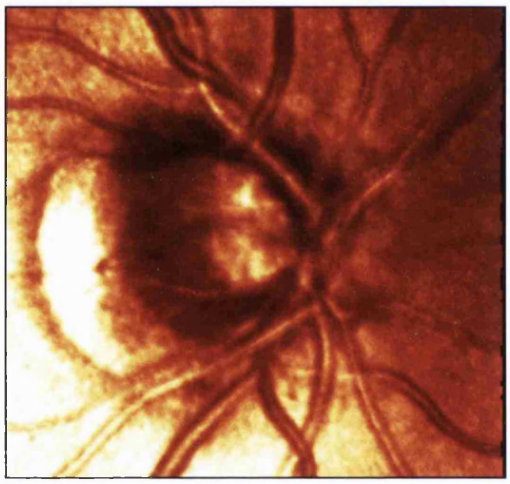

FIGURE 9.11. Description of rim area in the same optic nerve head image (*right*) by the standard reference plane (*above: upper*) and 320µm reference plane (*above: lower*). The optic nerve head is slightly tilted inferotemporally. The contour line of each analysed image of the optic nerve head is rendered in cross section by profiles, in which the: *upper white horizontal line*=MHC, *lower red horizontal line*=reference plane. In the upper image: rim area is represented as expected. In the lower image, the 320µm reference plane is situated above the temporal margin of the optic nerve head, causing rim area to be grossly underestimated, and is not well suited to this nerve. Variation in the description of the neuroretinal rim due to reference plane positioning in the two images of the same nerve is not uniform around the optic nerve head but more pronounced temporally than nasally. This is probably because the surface of nasal rim (profiles between 90° and 270°) is higher and its adjacent cup walls steeper compared with temporal rim, making the latter more prone to variability when the reference plane is positioned differently or shifts.

more when the reference plane shifts on a low-lying, gradually sloping cup than a steep cup, as suggested by Figure 9.11. Deeper than R=120μm, variability tended to increase, possibly because of proximity to the base of the major vascular trunks and the lamina cribrosa, especially in shallow cups. *REFpos* was derived from all height values on the contour line so that the position of the reference plane would not rely on localised regions nor presume selectivity in the pattern of change.

Unlike other definitions, the experimental reference plane compensates for positional changes between the reference plane and optic nerve head; this is the main reason for its reduced variability. These positional changes are probably exaggerated in testing involving different operators and visits. The standard reference plane is superficial in the temporal optic nerve head (50μm below the surface), where cup slope is gradual and susceptible to variation due to topographical variability or reference plane shifting. The 320μm reference plane does not cater well for morphological variations and may sometimes lie above parts of the optic nerve head edge (Burk et al, 2000), as illustrated by Figure 9.11. In glaucoma, the nasal optic nerve head surface may become so depressed that the reference plane comes to lie superficially in or even above this region, also making it prone to variability; such a situation is illustrated in Figure 7.6. Additionally, because the standard reference plane is fixed by a small section of the inferotemporal optic nerve head edge, image tilting or reference plane shifts may cause exaggerated variability nasally, opposite this point of fixation.

Researchers have traditionally sought to position reference planes by landmarks presumed to be relatively unchanged by glaucoma, although whether such landmarks remain truly unchanged by disease has been debated (Chen et al, 2001). The experimental reference plane, however, is linked to a landmark that is *expected* to change in glaucoma. But there are reasons why such a landmark is useful for positioning a reference plane. Firstly, experimental reference plane data was more reproducible than that of other reference planes, and was not appreciably influenced by varied test conditions or glaucomatous morphology. Variability that changes with repeat testing and advancing damage can confound analysis. Secondly, the experimental reference plane compensates for shifts of the optic nerve head. Measurement artifact results if the reference plane does not shift in tandem with the optic nerve head, as illustrated in **Figure 9.12**, and it is important that change

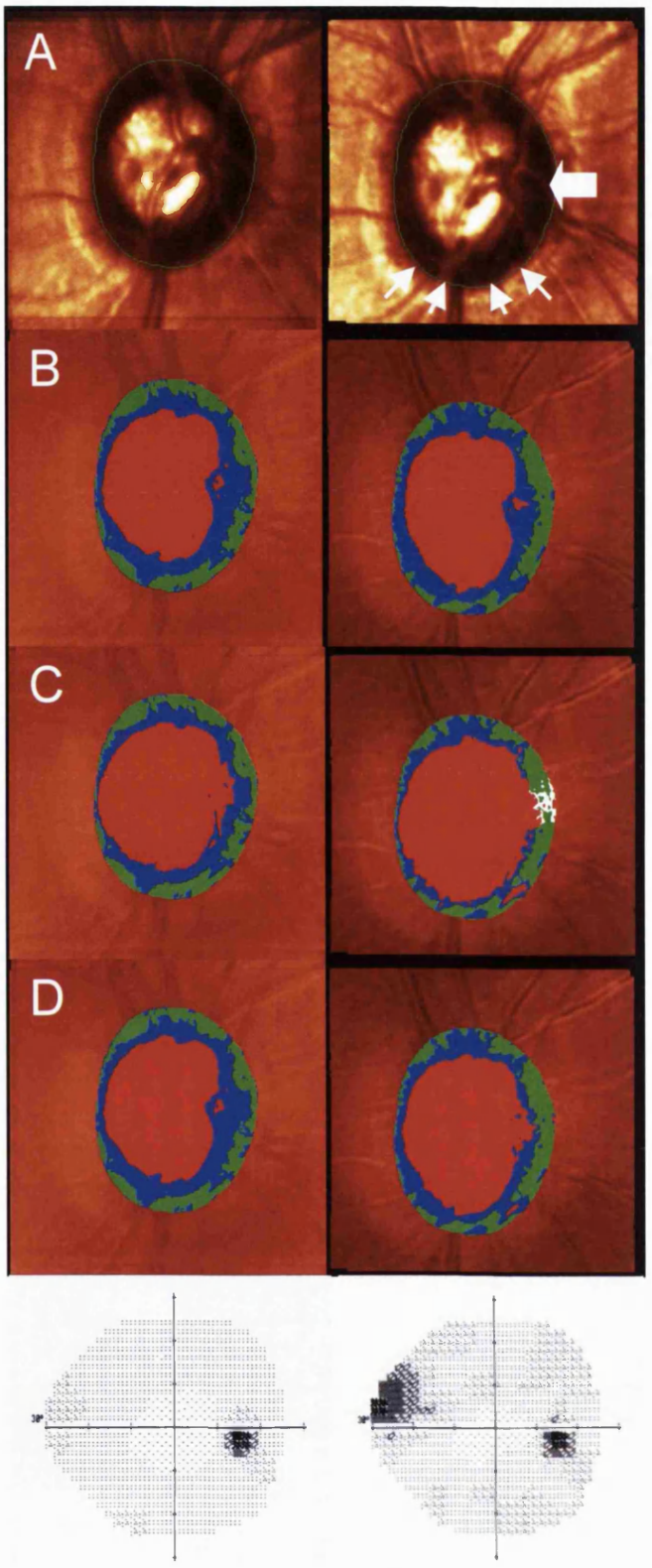

FIGURE 9.12. 'Stability' of the reference plane when there is progressive nerve damage. Optic nerve head images (row A) were acquired during the period over which a subject with ocular hypertension developed a reproducible visual field defect and 'converted' (row E). Rim area is analysed by: row B=experimental reference plane, row C=standard reference plane, row D=320μm reference plane; *Columns: left:* t=0, *right*: t=3 years. In A, there is subtle vertical extension of the cup in the inferior disc pole over 3 years (thin arrows). The fat arrow indicates prominence of the vessel trunk, which serves here as a marker for the z-axis position of the reference plane. *MHC* is: *left*=3μm, *right*=139μm, representing a height reduction of 136μm (the nerve head is shifted posteriorly); this may be caused by glaucoma, although the effect of variability cannot be excluded. In B, the rendering of rim area closely resembles the appearance of the rim in *A*. Despite markedly reduced MHC, inferior extension of the cup is evident from left to right, with the reference plane retaining a similar z-axis level in the optic nerve head (vascular trunk prominence represented similarly). This suggests the optic nerve head and reference plane have not shifted relative to each other. In C (*left*), the reference plane is superficial to the vascular trunk (not seen) and the cup is wider. The reference plane in the right image lies even more superficially in the nerve head, and to the vessel prominence, and the cup is even wider. Rim appearance does not closely resemble rim appearance in *A*. In D (*left*), level of the reference plane relative to the vessel prominence is similar to that of *B*. In the *right* image, however, the reference plane has shifted to lie more superficially in the nerve, and above the vessel trunk, rendering the cup diffusely larger and different from *A*.

identified in rim area reflects the disease process rather than such positional shifts. Menezes et al (1995) and Ang et al (2000) have reported that applying a similar concept to evaluating the macula can improve reproducibility. Thirdly, positioning the reference plane at the same distance below the optic nerve head's surface allowed standardised measurement of rim area in image series. The optic nerve head may shift relative to external landmarks such as the reference ring, which if used to anchor the reference plane can result in aberrations, as illustrated by Figure 9.12D. Bias in measuring height and volume can be expected when using the experimental reference plane, but less so rim area which is estimated perpendicular to the z-axis. Fourthly, detecting progression depends on the system's signal-to-noise ratio. It was found that the z-axis position of the optic nerve head fluctuated considerably in normal image series: 50% had a range of MHC exceeding 120μm, with this range greater than 200μm in some; possibly reflecting factors such as the cardiac cycle (Chauhan and McCormick, 1995), parallax in imaging (Orgul et al, 1995a) and variable centring of the optic nerve head in its image frame. Hence, relatively large shifts of the optic nerve head's z-axis position relative to peripapillary retina, where the reference ring is located, are not uncommon. Normal human RNFL at the optic nerve head margin is 316-406μm thick (Varma et al, 1996), and so MHC variability is considerable relative to normal RNFL thickness. MHC variability may even exceed RNFL thickness in glaucoma if significant axons are already lost by the time visual field defects appear. Empirical data from the present study suggests that the benefit of significantly reduced variability should outweigh the possibility that MHC is affected by glaucoma to bias the reference plane's position. Figure 9.12 shows that despite markedly reduced MHC, experimental reference plane analysis is sensitive to subtle loss of neuroretinal rim.

Experimental reference plane rim area variability was less, more uniform around the optic nerve head, and not appreciably affected by different operators, different visits and glaucomatous morphology compared with analysis by other reference planes. This difference was particularly marked and significant in longitudinal data. Variability that is less and more uniform around the optic nerve head should be simpler to account for and will help limit bias in detecting localised progression.

9.3 VALIDITY OF RIM AREA MEASUREMENTS BY DIFFERENT REFERENCE PLANES

Many methods have been proposed for positioning reference planes but it is unclear whether or how closely reference plane description of the neuroretinal rim corresponds to the rim's actual appearance. An ideal reference plane should be positioned so that topographical measurements are not only reproducible but also accurately represent the morphology of each optic nerve head.

Rim area as seen ophthalmoscopically or in disc images represents ganglion cell axons exiting the eye and has been extensively studied as a marker of glaucoma: it is characteristically altered in glaucoma (Kirsch and Anderson, 1973a; 1973b; Jonas et al, 1988a; 1988b; 1993a) and progressively reduced as disease worsens (Pederson and Anderson, 1980; Sommer et al, 1980; Tuulonen and Airaksinen, 1991). Conventionally, the area of the rim as seen in stereoscopic disc photographs has been taken to reflect the state of glaucoma (Tuulonen and Airaksinen, 1991; Jonas et al, 1988a; 1988b; 1993a) and has become a standard for describing normal and glaucomatous optic nerve morphology (Hitchings et al, 1993; Airaksinen et al, 1996; Bron et al, 1997). However, evaluating the rim in stereoscopic photographs requires the perceiving of subtle variations in disc contour (Jonas et al, 1988a; 1988b) and image contrast (Tuulonen et al, 1992) which can make measurements variable (Lichter, 1977; Varma et al, 1992; Kahn et al, 1975) and progression difficult to identify. While scanning laser tomography measurements of the optic nerve head are known to be reproducible to be clinically meaningful, such measurement also needs to accurately represent the state of the neuroretinal rim and not be biased by changes caused by glaucoma.

Here, we study the agreement between rim area, as analysed by the experimental, standard and 320m reference planes, and the appearance of the rim in optic nerve head images.

9.3.1 Investigations

9.3.1.1 Subjects

Optic nerve head images of 50 glaucoma (POAG) eyes and 50 normal control eyes were evaluated. Subjects' selection criteria are described in Section 5.1. **Table 9.2** shows subjects' demographics.

9.3.1.2 Objective analysis of rim area by reference planes

Mean topography images from one randomly selected eye of each subject were generated from triplets of single topography images using HRT software version 2.01, as described in Section 5.2. Images had pixel SD<50μm. A contour line corresponding to the inner margin of the scleral ring of Elschnig was outlined in each image by the same observer (JT). Stereoscopic optic disc photographs were referred to if needed. Three sets of data for rim area, each derived by different reference planes, were analysed:

1) ***Experimental reference plane.*** Position of the reference plane (*REFpos*) relative to the optic nerve head margin is kept constant in all of any eye's images and defined, as in Section 9.1, as follows:

$$REFpos = MHC + LOW_{5\%} + R$$

Where, *MHC*=mean height of the contour line, $LOW_{5\%}$=average of the optic nerve head contour line's 5% lowest height values calculated from the constituent topographies of a baseline mean image; *R*=level of the reference plane below $LOW_{5\%}$ where variability is least, previously determined as *R*=100μm.

2) ***Standard reference plane.*** Set 50μm posterior to the mean of contour line heights between 350 to 356° on the ONH's circumference and is default in HRT software (HRT v1.11 to 2.01, and HRT II software) (Heidelberg Engineering, 1993; Burk et al, 2000), as described in Section 5.2.

Mean ± SD	**Normal**	**Glaucoma**
N=	50	50
Age (years)	67.5±9.6	69.7±9.9
Visual field MD (dB)	+0.15±1.5	-4.3±1.6
Visual field CPSD(dB)	0.83±0.68	4.0±2.2
Rim area by experimental reference plane	1.40±0.24	1.21±0.31

Table 9.2 Demographic data for study subjects. Glaucoma eyes had POAG.

3) ***320μm reference plane.*** Fixed at an offset 320μm posterior to the mean height of the "reference ring" (HRT software v1.09 to 1.10), as described in Section 5.2. The reference ring is centred on the image frame and located in its periphery, and has an outer diameter of 94% and width 3% of image size (Heidelberg Engineering, 1993).

9.3.1 3 Subjective analysis of rim area as it appears in disc images

Three expert observers subjectively analysed rim area in scanning laser tomography images; results of this analysis was taken to represent rim appearance. Contour lines were drawn to outline the *cup edge* in mean topography images. The cup edge was defined where the inflection of the slope changes at the inner part of the neuroretinal rim. Pixel height in *topography images* is colour-coded and changing contour is recognised as regional variations in colour. Intensity of reflected light from tomographic imaging is also colour-coded in the pixels of *intensity images.* Both topography and intensity image displays (examples shown in Figures 4.3 and 4.4) were viewed to locate the cup edge. Blood vessels lying nasally were included as rim area if the vessels were at a similar topographical height as adjacent rim. Because such vessels may lie on the neuroretinal rim or over the rim-cup interface to obscure the rim-cup border, including these vessels as part of the rim helped standardise analysis. Similarly, objective HRT analysis by a reference plane defines any tissue lying above the reference plane and within the optic nerve head margin, either rim or blood vessel, as part of the neuroretinal rim (Heidelberg Engineering, 1993).

All observers agreed on how the cup edge should be defined and marked. Each observer drew the contour line around the cup edge of every optic nerve head thrice, doing this once each time the group of images was assessed. The first group assessment was a trial run to allow observers to familiarise themselves with the method and was discarded. Eventual analysis was only based on the second and third runs, conducted a week apart. Observers were not told diagnoses and their assessment was independent and in the absence of other observers. Each observer thus produced two sets of results for cup area. HRT software denotes this 'cup area' as 'disc area' as contour lines conventionally mark the disc edge not cup edge in HRT analysis; this data was thus adapted accordingly. Rim area was calculated by

subtracting cup area from the same disc area measurement as measured by the original contour line (by JT).

9.3.1.4 Statistical analysis

Intraobserver agreement for each of the expert observers was analysed using the statistical approach by Bland and Altman (1986), and based on experimental reference plane measurements. Rim area difference was plotted by average rim area. 95% confidence intervals for differences (agreement intervals) were graphed. To assess *interobserver agreement*, each observer's two sets of measurements were averaged to give a single mean rim area value for each eye; agreement between this value and that of other observers was analysed.

To derive a *subjective* estimate of rim area, the mean rim area values of the three observers were averaged to give a single rim area estimate for each optic nerve head. Different reference planes – experimental reference plane, standard reference plane and 320μm reference plane – determined rim area *objectively*. Agreement between subjective and objective analyses was assessed, giving three comparisons: *experimental-subjective, standard-subjective* and *320μm-subjective*. In calculations, subjective rim area was always subtracted from objective rim area. Agreement between analysis by different reference planes was also assessed. Trends in the agreement data were noted. *Global rim area* and *regional rim area* were analysed; in the latter, rim area was subdivided into 30° sectors by angle around the optic nerve head (0-360°). Significance testing for parametric data was by paired student t-tests. Agreement intervals for each sector were plotted by angular location of the sector (0-360°) in bar graphs. Previously published data by Jonas et al (1998) comparing planimetry and standard reference plane analysis was re-graphed to evaluate agreement. Differences between subjective and objective analyses were plotted by cup/disc area ratio to tell if agreement varied with the degree of cupping; here, subjectively-determined cup area was measured as described above.

9.3.2 Results

9.3.2.1 Intra- and interobserver agreement

Figures 9.13 A(1-3) show that intraobserver agreement intervals for global rim area differed between observers, with the intervals narrowest for observer 1 and widest for observer 2. **Figures 9.13 B(1-3)** show that the interobserver agreement intervals tended to be wider than intraobserver agreement intervals, indicating better agreement in the repeat measurements of a single observer than between different observers. Agreement was similar for all the interobserver comparisons, indicating that interpretation of the cup edge was consistent between observers. Interobserver agreement intervals were slightly wider than the intraobserver agreement intervals for observer 2 (Figure 9.13 A2).

9.3.2.2 Agreement between subjective analysis and analysis by different reference planes

Figures 9.13 C(x-z) show that *objective* analysis by the experimental reference plane agreed most closely with *subjective* analysis. Agreement intervals for the experimental-subjective comparison (x: 95%ci=0.28) were appreciably narrower than in the standard-subjective (y: 95%ci=0.43) and 320μm-subjective (z: 95%ci=0.40) comparisons. Standard and 320μm reference plane rim area measurements tended to be less than in subjective analysis or experimental reference plane analysis, especially in glaucoma eyes: while the mean of differences for the experimental-subjective comparison was nearly zero (overall mean=0.047; normal=0.039, glaucoma=0.067), the mean of differences was much more negative for standard-subjective (overall mean=-0.19; normal=-0.14, glaucoma=-0.25) and 320μm-subjective (overall mean=-0.15; normal=-0.081, glaucoma=-0.23) comparisons. The mean estimate of average rim area values was less in standard-subjective (mean=0.25) and 320μm-subjective (mean=0.27) comparisons than the experimental-expected comparison (mean=0.32; data further to the right on the x-axis).

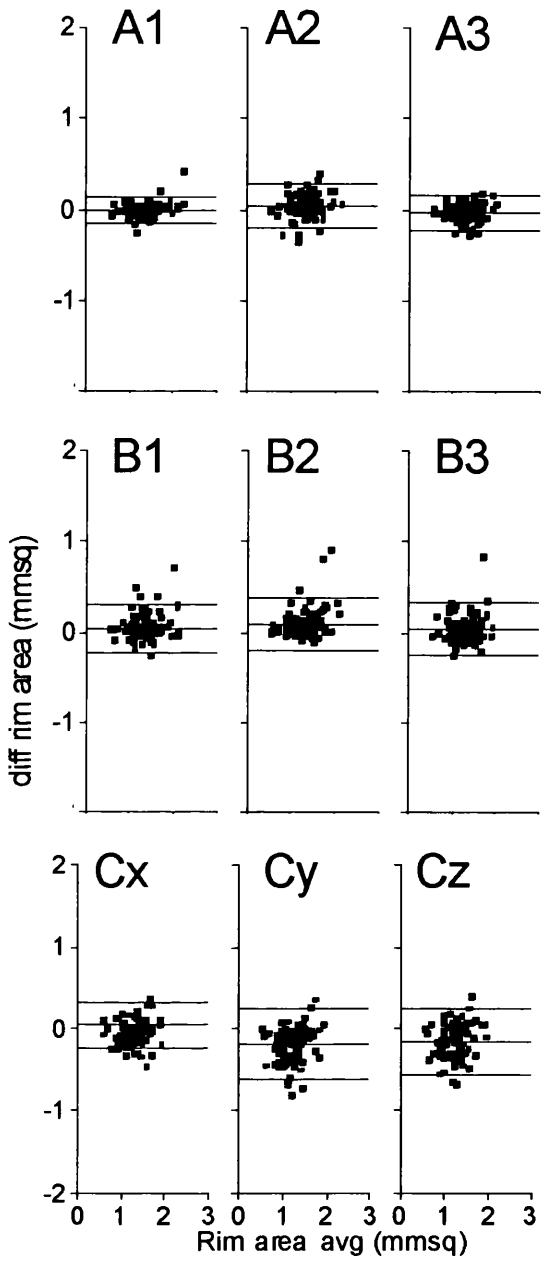

FIGURES 9.13. Analysis of agreement in global rim area measurements. *A=intraobserver agreement*: A1=observer 1, A2=observer 2, A3=observer 3. *B=interobserver agreement*: B1=between observer 1 and 2, B2=between observer 1 and 3, B3=between observer 2 and 3. *C=agreement between subjective analysis and analysis by reference planes*: x=experimental reference plane, y=standard reference plane, z=320μm reference plane. Correlation between differences and means were: Cx: r=0.16, p=0.12; Cy: r=0.28, p=0.0055; Cz: r=0.27, p=0.0089. In each graph, *middle horizontal line*=mean of differences, *flanking horizontal lines*=95% confidence limits for differences.

Difference and average estimates were weakly but significantly correlated in standard-subjective and 320μm-subjective comparisons (r=0.28, p=0.0055 and r=0.27, p=0.0089 respectively), but not in the experimental-subjective comparison (p=0.12). In **Figure 9.14**, the replotted data of Jonas *et al* (1998) also shows a very weak but significant correlation between standard reference plane analysis and planimetry (r=0.11, p=0.021, n=432).

In **Figure 9.15,** which compares the reference planes, experimental reference plane measurements tended to be higher than in analysis by the standard and 320μm reference planes: mean of differences was: +0.14 (95%ci=0.27) and +0.10 (95%ci=0.35) respectively. Mean difference of the standard-320μm comparison was –0.034 (95%ci=0.38).

Figures 9.16 A 2 and 3 show that rim area difference was negatively correlated with cup/disc area ratio in the standard-subjective and 320μm-subjective comparisons (r=0.26, p=0.0099 and r=0.29, p=0.0055 respectively), with their linear regression plots having similar slopes (-0.35 and -0.37 respectively). The experimental-subjective comparison did not show significant correlation (Figure 9.16 A1; r=0.17, p=0.11).

Figures 9.16 B(1-3) show that sector rim area agreement intervals for objective-subjective comparisons for all reference planes were widest temporally between 0-60° and 270-360°. Sector agreement intervals tended to be narrower in the experimental-subjective comparison compared with the standard-subjective and 320μm-subjective comparisons. The magnitude of differences in the former was also significantly less (all sectors p=0.000, Students t-test for normally distributed data).

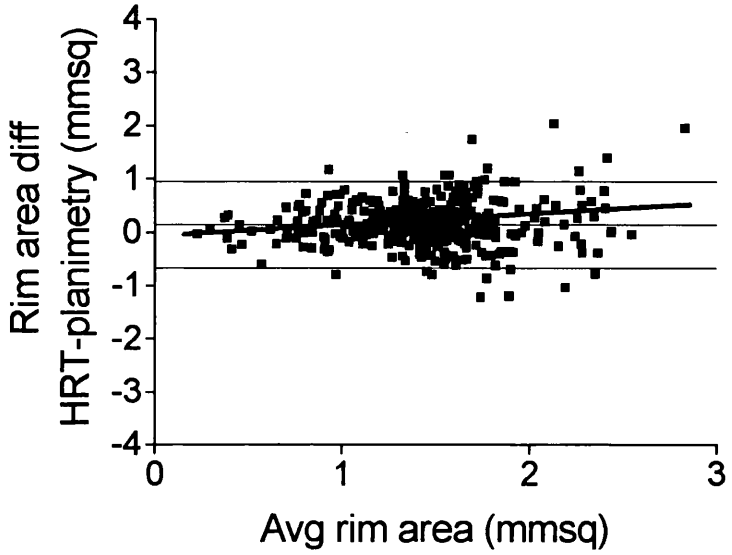

FIGURE 9.14. Rim area agreement between planimetry and HRT analysis by the standard reference plane, replotted from Jonas et al (1998c). *Middle horizontal line*=mean of differences, *flanking horizontal lines*=95% confidence limits for differences, *oblique line*=linear regression line with equation: y=0.11x-0.021; r=0.11, p=0.021; n=432.

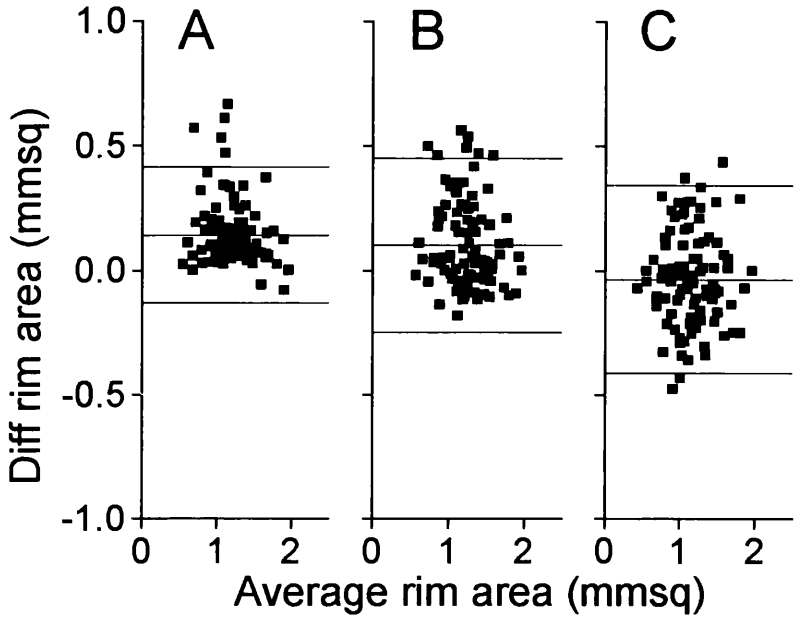

FIGURE 9.15. Global rim area: agreement between different reference planes. *A=experimental-standard, B=experimental-320μm, C=standard-320μm*. Standard and 320μm reference plane data was subtracted from experimental reference plane data respectively in A and B, and 320μm from standard reference plane data in C. In each graph, *middle horizontal line*=mean of differences, *flanking horizontal lines*=95% confidence intervals of differences.

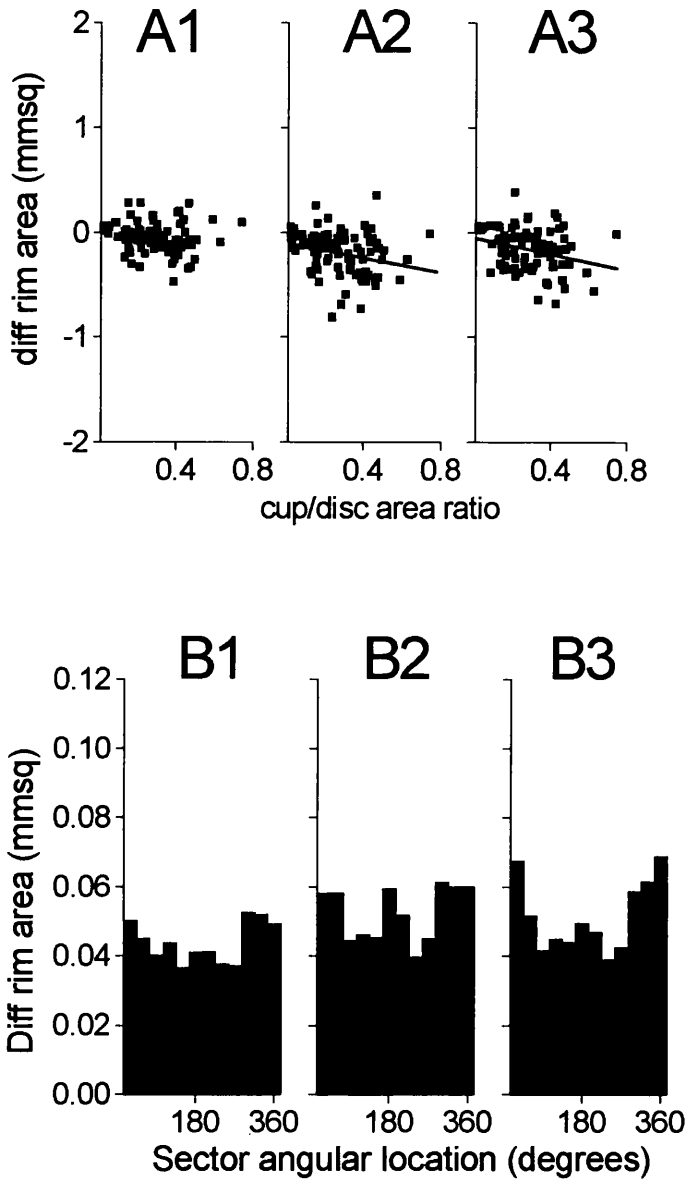

FIGURE 9.16. ***Scatter plots (A)*** show the relationship between the difference in rim area and cup/disc area ratio. Rim area differences are between subjective analysis and reference plane measurement. *1*=experimental subjective, *2*=standard-subjective, *3*=320μm-subjective. *Correlation in:* A1 was not significant (r=0.17, p=0.11) but there was a significant linear relationship in A2 (y=-0.35x-0.096, r=-0.26, p=0.0099) and A3 (y=-0.37x-0.053, r=-0.29, p=0.0050).

Bar graphs (B) show sector rim area agreement between subjective analysis and reference plane analysis. *Each bar* represents the width of the 95% agreement interval for each 30° sector, where *0°=temporal, 90°=superior, 180°=nasal, 270°=inferior*. Agreement was significantly closer in B1 than in B2 and B3 for every sector (p=0.000).

9.3.3 Discussion

This study aimed to quantify how closely rim area, as defined by different reference planes, corresponded to the appearance of the neuroretinal rim in the same images. A reference plane by its position in three-dimensional anatomy defines the inner edge of the neuroretinal rim. But the level at which the reference plane lies in topography is arbitrary, being influenced by its own method of positioning and the morphology of each measured nerve head. This level is crucial and directly affects the description of the rim: too high and rim area is underestimated, too low and overestimation is likely. At extremes, the reference plane may come to lie above the rim surface to falsely indicate that neural tissue in that region is absent (see Figure 9.11), or below the base of a shallow cup to suggest that the optic nerve head has no cup. It is unlikely, however, that there is a universal and standard absolute level at which a reference plane should be positioned in the three-dimensional architecture of nerves to 'correctly' define the rim. Instead, this position probably varies with each nerve head and should be borne in mind when positioning reference planes. The present findings indicate that the experimental reference plane more faithfully describes the neuroretinal rim of a wider spectrum of nerve morphologies than the standard and 320μm reference planes.

Scanning laser tomography images were used for subjective analysis instead of stereoscopic disc photographs because of the following. Firstly, information about surface contour in scanning laser tomography images is quantitative whereas stereoscopic information in photographs is qualitative and requires stereopsis for evaluation. Quality of stereopsis achieved varies with observers and stereophotographic quality. Secondly, it was simpler to compare subjective and objective methods in common images so that probable differences between imaging systems, such as in image magnification, would not need accounting for. Correcting for image magnification relies on modelled estimates of human ocular dioptrics which may be inaccurate in eyes not meeting standard assumptions (Arnold et al, 1993; Garway-Heath et al, 1998). Thirdly, evaluation of the cup edge in topography images in this study was consistent between observers, indicating that surface contour could be reliably interpreted in scanning laser tomography images. Contour interpretation was aided by cues from both topography and intensity images. Also,

the data for subjective analysis was obtained as rigorously as feasible, being based on the repeat analyses of three expert observers, giving six estimates of rim area per optic nerve head. Agreement between subjective and standard reference plane analysis in our study was at least as good as that reported between planimetry and standard reference plane analysis (Jonas et al, 1998c).

Subjectively analysed global rim area – representing rim appearance – agreed most closely with analysis by the experimental reference plane. Subjective analysis also agreed significantly better with the experimental reference plane than with standard and 320μm reference planes in every 30° sector of the optic nerve head (magnitude of differences: all p=0.000). That the mean of differences between subjective analysis and experimental reference plane analysis was roughly zero also indicates that the two methods tended to agree in their estimates of rim area. Hence, experimental reference plane analysis corresponded more closely with rim appearance than analysis by other reference planes; this held for both global and regional measurements.

For a reference plane to accurately describe rim appearance, the reference plane should theoretically be located at the z-axis level of the cup edge where the surface of neuroretinal rim most abruptly steepens into the cup. Findings in this study suggest that the experimental reference plane tends to be positioned at or near the level of the cup edge. The experimental reference plane's estimation of rim area also tended to be higher compared with other reference planes, as seen in Figure 9.15, indicating that the experimental reference plane lies deeper in the optic nerve head. Reproducibility is probably better here: at this depth, the reference plane is more likely to lie well below the superficial rim, where shifts in the reference plane should cause less rim area variability. Also, unlike other definitions, the experimental reference plane is designed so that its position suits the morphology of each optic nerve head.

Standard-subjective and 320μm-subjective differences were positively correlated with point estimates of rim area and negatively correlated with cup/disc area ratio. This suggests that a small (7-8% in our dataset comprising early glaucoma and normal eyes) but significant degree of bias may affect standard and 320μm reference plane analysis of rim area; this degree of bias though small may be

enough to confound the appraisal of gradual progression. Significant correlation was not seen in experimental-subjective data. Other studies seem to have similar findings: data from Jonas et al (1998c) shows that differences between subjective and standard reference plane analyses were significantly correlated with rim area, though to a lesser extent (about 1%). Similarly, Sung et al (2002) reported that rim area differences between digital planimetry and HRT standard reference plane analysis were correlated with vertical cup/disc area ratio (r^2=42%; r=0.65, p<0.0001), while Ikram et al (2002) found in a population-based sample that HRT standard reference plane analysis tended to overestimate vertical cup-disc ratio relative to direct ophthalmoscopy and stereoscopic disc photographs. It is possible that the reference plane shifts with altered morphology, becoming more superficial in the optic nerve head when rim area is smaller and cupping is larger. It is postulated that the standard and 320μm reference planes are positioned relative to regions that are relatively unchanged in glaucoma, namely the papillomacular nerve fibre layer bundle and far peripapillary retina respectively (Heidelberg Engineering, 1993; Burk et al, 2000). This has been challenged, however (Chen et al, 2001), and it is possible that changes in these regions could cause the reference plane to shift unpredictably relative to the optic nerve head. Alternatively, the deteriorating optic nerve head could itself shift relative to regions by which the reference plane is fixed so that the reference plane becomes more superficial in the optic nerve head with advancing damage, as illustrated by Figure 9.12. The relatively small bias in our data may well reflect the susceptibility of only certain discs to this effect, such as those with large cupping. In practice, it would be easy to check images to ensure that reference plane-derived neuroretinal rim reasonably approximates what is seen clinically before proceeding further with analysis. Were the experimental reference plane's position found to be inappropriate, the value of R for calculating the reference plane's position could easily be changed to suit the particular nerve head. This new value of R would then be held constant for other images of the same eye.

In summary, it was found that the subjective analysis of rim area in scanning laser tomography images was consistent between our expert observers. The pooled analysis of these observers agreed more closely with analysis by the experimental reference plane than with analysis by the standard or 320μm reference planes across a range of normal and glaucoma eyes. Agreement in the former comparison was

closer for both global and regional aspects of the optic nerve head compared with the standard and 320μm reference planes.

Chapter 10

ANALYTICAL APPROACH FOR IDENTIFYING GLAUCOMATOUS OPTIC NERVE CHANGE

10.1 DESCRIPTION OF AN ANALYTICAL APPROACH AND ITS INITIAL EVALUATION

While scanning laser tomography appears to be reproducible, analysing and interpreting the vast information in each image is complex, and consensus remains to be reached on how best to approach this data. This is evident, for example, in the variety of reference planes proposed to describe anatomical parameters such as the neuroretinal rim and cup in the nerve's three-dimensional architecture (Burk et al, 1990; 2000; Maier et al, 1990; Frohn et al, 1990; Tuulonen et al, 1993; Miller and Caprioli, 1992). Identifying change requires topography to be assessed in the extra dimension of time; to do this some advocate directly analysing surface height for change (Chauhan et al, 2000; 2001), while others have analysed summary parameters such as rim area (Kamal et al, 1999b; 2000; Burgoyne et al, 2002, Ervin et al, 2002). Paramount to such assessment is the need to rule out measurement variability as a confounder before glaucomatous change can be judged to truly have occurred.

The parameter rim area has been suggested to be useful as a marker of progression in disc photographs (Pederson and Anderson, 1980; Sommer et al, 1980; Odberg and Riise, 1985; Airaksinen et al, 1992) and Heidelberg Retina Tomograph (HRT) images (Kamal et al, 1999b). In HRT image analysis, we have found that rim area is reproducible compared with other parameters. Relating rim area loss to disease behaviour is also a familiar task to clinicians.

Here, an approach for evaluating progressive rim area loss is described that incorporates the experimental reference plane. How measurement variability can be

estimated and accounted for in small regions of the neuroretinal rim in a way that is individualised to each optic nerve head is outlined. The approach requires that any detected change should be confirmed as repeatable in 2 of 3 consecutive tests before being attributed to progression; the usefulness of this scheme is demonstrated in distinguishing eyes with progressive glaucoma from the unchanging eyes of normal controls. Finally, how the technique may be applied clinically is illustrated.

10.1.1 Overview: key elements

An analytical approach for identifying progression: (1) an experimental reference plane, as devised and tested in Chapter 9, was used to (2) analyse rim area in 30° sectors. (3) Measurement variability was estimated and accounted for in each sector so that true regional change due to glaucoma could be distinguished from variability. (4) Any apparent change had to be repeatable before being attributed to progression. (5) The approach was applied clinically.

10.1.2 Experimental reference plane

This reference plane is customised to the morphology of each optic nerve head as described in Section 9.1. The position of the reference plane (*REFpos*) relative to each optic nerve head is kept constant in any image series and defined as follows:

$$REFpos = MHC + LOW_{5\%} + R$$

Where, *MHC*=mean height of the contour line, $LOW_{5\%}$=average of the optic nerve head contour line's 5% lowest height values calculated from the constituent topographies of a baseline mean image; *R*=level of the reference plane below $LOW_{5\%}$ where variability is least, previously determined in longitudinal data as *R*=100μm.

10.1.3 Analysis of sector rim area

Thirty-degree (30°) rim area sectors were evaluated for change. The parameter of rim area was calculated within longitudinal image series using the experimental reference plane to define the inner edge of the rim. The outer extent of the rim coincided with the contour line marking the inner margin of the scleral ring of Elschnig, outlined by the same observer in each subject's baseline mean topography images (JT). Contour lines were exported to other mean and single topography images in each series. Mean topography images were derived from triplets of single topography images using HRT software version 2.01. Pixel topographical height was measured by the reference ring. Only images with mean pixel SD<50μm were used. Grainy images having a honeycombed appearance were excluded. These steps are described in more detail in Section 5.2.

Data from the mean topography image of a test visit was used as the point-estimate of rim area for that visit. Single topography images from within a visit provided the data with which to: 1) derive mean topography images by HRT software as instructed by the manufacturers, and 2) estimate variability (see below).

10.1.4 Estimating and accounting for sector rim area variability

10.1.4.1 Intra-visit difference estimates (δ) for calculating limits of variability.

Measurement variability in each sector of an image series was estimated and accounted for by way of *limits of variability.* The limits were modeled from *intra-visit difference estimates (denoted 'δ')*, calculated as the area difference in each rim sector between a pair of same-visit single topography images, as shown in **Figure 10.1**. By this method, three single topography images per visit yield three δ per sector. But the more images acquired per visit, the greater the number of δ: hence, four intra-visit images yield six δ per visit, five images per visit yield 10 δ, six images per visit yield 15 δ and so on. The number of δ per visit can be calculated by:

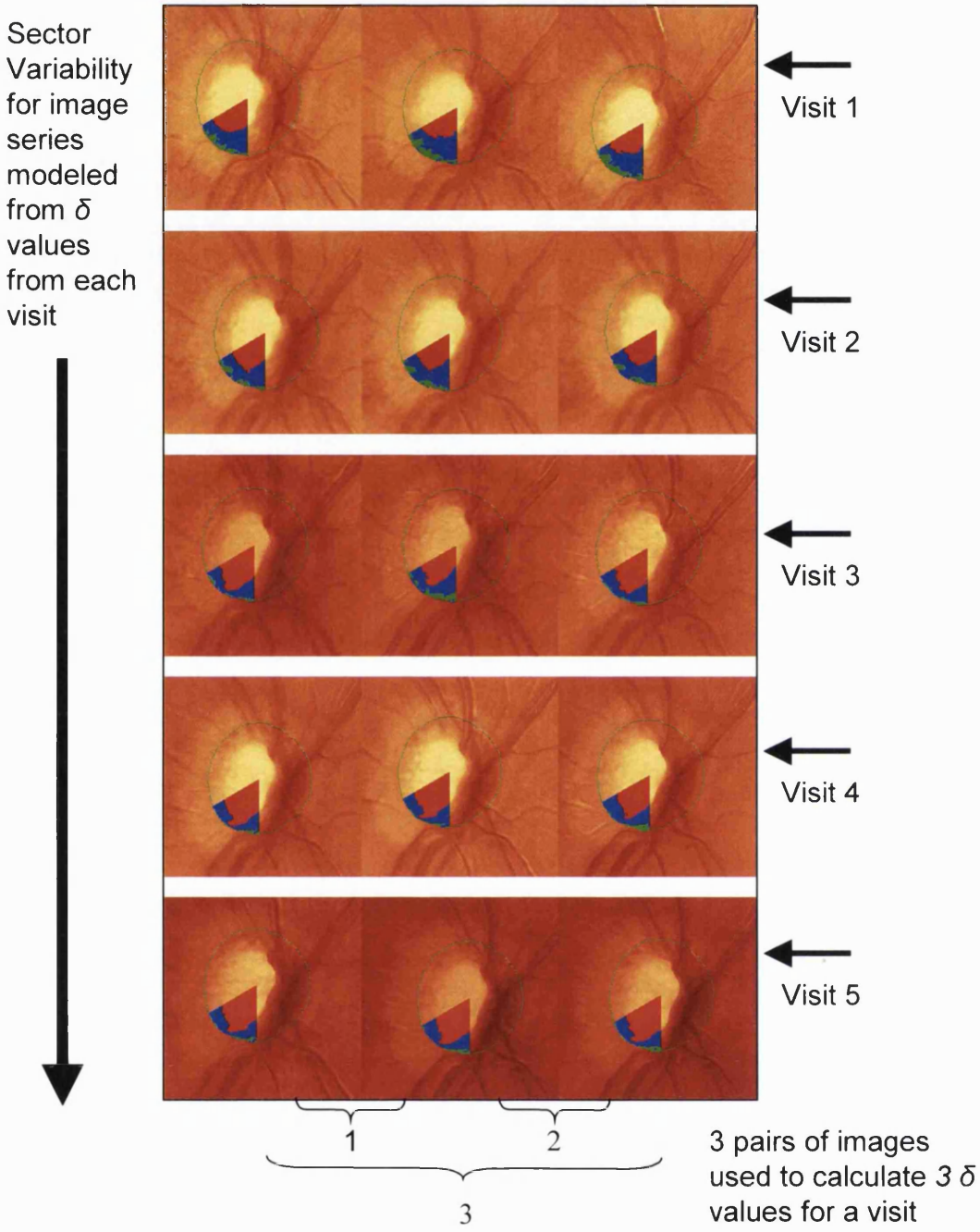

FIGURE 10.1. Illustration of how sector rim area variability is estimated in longitudinal image series. Intra-visit variability for each 30° rim area sector is estimated in each test visit's image triplets, with analysis by the experimental reference plane. *Images: rows*=images acquired in different test sessions over time. In this example, two adjacent inferotemporal 30° sectors having progressive rim area loss are highlighted (developing notch from top to bottom). *Variability in each of these sectors is analysed separately*: firstly, estimates of intra-visit variability (δ) are calculated; secondly, estimates of intravisit variability from all visits are used to model variability for the sector in longitudinal data.

$$^{m}C_r = \frac{m!}{(m-r)!r!}$$ [equation 10.1]

This gives the number of ways in which m single topography images from a visit can be combined to calculate δ, with r the number of images used in each combination (r=2). The number of δ in any image series equates the total of all δ from all visits; all are used to calculate limits of variability. δ is taken to be free from glaucomatous change, being derived from data from within a visit not between visits. Using experimental reference plane analysis, it is expected that δ will not be appreciably affected by glaucoma or testing involving different operators and visits.

10.1.4.2 Limits of variability to account for sector variability in image series.

Limits of variability were the confidence limits for each sector's range of δ values, calculated by multiplying the SD of δ by the appropriate point of the t-distribution for n-1 degrees of freedom. This allowed for better estimates of the limits of variability when dealing with relatively small samples (say of less than 60) (Altman, 1991). Limits of variability can be considered a measure of agreement between repeat measures of the same sector, and derived as described by Bland and Altman (1986) and Altman (1991). Here, the limits of variability define the extent to which measurements vary with respect to baseline rim area. For an image series, limits of variability for each sector (*VARLIM*) can be calculated by:

$$VARLIM_a = Y * \sqrt{\Sigma(\delta_i - X)^2/(n-1)}$$ [equation 10.2]

Where, a=sector number (corresponding to the order of a sector's location on the optic nerve head circumference between 0-360°), δ=sector rim area difference between pairs of intra-visit single topography images, i=ith value of δ, X=mean of observations of δ, and n=number of observations of δ. Y=value of the t-statistic for degrees of freedom for δ, corresponding to a chosen two-tailed probability value such as p=0.05. The distribution of δ in sectors was examined using histograms, normal plots and Shappiro-Wilk W significance testing (SPSS v9 for Windows by SPSS Inc; Chicago, IL, USA, 1998), and found to approximate normality in over

95% of sectors tested. It is expected that the distribution of differences will tend to be normal (Bland and Altman, 1986), but any departures from normality were transformed using: $\ln(X^2)$. Following transformation where needed, 99.6% (478/480) of all tested sectors had normal distributions. Limits of variability can be expected to narrow with increasing degrees of freedom for L. For this study, limits of variability were defined by a probability level of p=0.05, compatible with a 95% confidence limit.

10.1.5 Criterion for confirming change

The limits of variability defined the smallest expected amount of change that can be detected above test variability. Additionally, a criterion was established to further ensure that identified change is consistent with glaucomatous progression and not variability. This criterion took the form of a system of duplicate testing as espoused by Schulzer et al (1991b, 1994) for assessing visual fields in the Collaborative Normal Tension Glaucoma Study (1998a; 1998b). Sequential rim area data for each sector was assessed for change exceeding limits of variability; however, a single observation of change was not accepted as progression but only regarded as tentative. To be attributed to progression, a criterion was adopted in which tentative change had to be verified as repeatable in at least two of three consecutive tests. Hence, following an initially positive result, there are three possible outcomes: (a) the subsequent second test is positive, (confirmed), (b) the second test is negative but the third test is positive, (confirmed), and (c) both subsequent tests are negative (not confirmed).

Sensitivity and the false positive rate for identifying change by this 'two-of-three' criterion was assessed empirically in the reference dataset described in Section 5.4. The dataset comprised longitudinal image series of 1) eyes with glaucoma progression: ocular hypertension "converters" to glaucoma that had developed reproducible visual field defects, and 2) unchanging eyes of normal controls. These results were compared with other plausible criteria for confirming change: a) 'two-of-two', requiring two consecutive positive tests; b) 'three-of-three', requiring three consecutive positive tests; c) two adjacent sectors on a single test; d) two adjacent sectors on two consecutive tests.

10.1.6 Clinical application of approach

10.1.6.1 Identifying and confirming progression

Collation of data. Sequential rim area data was plotted as *rim area profiles;* spatial and temporal information could thus be integrated simply. Profiles were plots of rim area by angular location round the optic nerve head (0-360°, with 0°=temporal, 90°=superior, 180°=nasal, 270°=inferior) from the same image series; this represented rim area at different points in time in a common graph. Limits of variability for each sector were plotted relative to the baseline profile, with the region beneath the lower limits termed the *zone of change*. Rim area in a sector that diminished, exceeded its lower limit of variability and entered the zone of change was taken to have changed more than measurement variability alone. A *single positive test* occurred if at least one sector exceeded its limit of variability on a single test. The repeated exceeding of a limit of variability meant that change was no longer regarded as tentative but to represent disease progression.

10.1.6.2 Evaluation in progressing and unchanging eyes

Testing. The approach for detecting progressive rim area loss was tested in the longitudinal image series of 40 eyes of 40 subjects – 20 *normal controls* and 20 age-matched *ocular hypertension converters*. Their demographic data is shown in **Table 10.1**. Each subject contributed only one eye to analysis: a randomly selected eye in controls and the eye that had converted in converters. Ocular hypertension converters and controls regularly attended the Ocular hypertension and early glaucoma research clinic at Moorfields Eye Hospital and had received imaging on at least six separate occasions over a minimum of three years.

Criteria for selecting subjects are described in Section 5.1 and are briefly as follows:

Eyes of ***normal controls*** were taken to be unchanging. Normal subjects were volunteers comprising spouses or friends of hospital patients, hospital staff, or members of external non-medical social organisations. They had 1) intraocular pressures (IOP) repeatedly<22 mmHg, 2) serially normal and reliable Humphrey 24-2 visual fields (Humphrey Instruments Inc, Palo Alto, CA, USA) with AGIS

	Converters	Normal controls	p-value
N=	20	20	—
Age (mean±SD) years	66.2±10.8	63.6±4.79	p>0.05
Visual field MD dB (mean±SD)	-2.82±1.88	+0.35±1.18	p=0.001
Visual Field CPSD dB (mean±SD)	4.02±1.27	0.96±0.51	p=0.000

TABLE 10.1. Subjects' demographics. Visual field indices pertain to measurement at final follow up.

visual field scores=0, 3) no concurrent ocular disease or previous intraocular surgery, 4) no family history of glaucoma, 5) refractive errors< ±6D, and were 6) aged>40 years. Optic nerve head appearance was not taken into account for entry into the study.

Ocular hypertension converters were assumed to have glaucoma progression in the eye that 'converted'. They initially had a diagnosis of ocular hypertension with: 1) IOP consistently≥22mmHg in one or both eyes without IOP lowering treatment, 2) open angles on gonioscopy, 3) initially normal Humphrey 24-2 visual fields with AGIS scores=0, determined following a learning period of 3 consecutive tests, 4) refractive errors<±6D, 5) no concurrent ocular disease or previous intraocular surgery, 6) were aged>40 years. They had over the course of monitoring 7) developed visual field abnormality according to AGIS criteria (score>0) that was reproducible on 3 consecutive tests, as described in Sections 5.3 and 5.4. A glaucoma expert independently confirmed this. Other possible causes of visual field defects were excluded. Those on topical IOP lowering treatment did not receive intervention that altered IOP during the period of monitoring reported in this study. Optic nerve head appearance was not part of the criteria for inclusion.

Excluding images with changed magnification. Longitudinal image series were checked for magnification changes by examining how well exported contour lines from baseline images fitted the margins of the optic nerve head in follow up images. Changed magnification was suspected if the fit was poor. To verify that magnification was indeed changed, distances between fixed landmarks (eg, vessel bifurcations) in the baseline and follow up images were measured and compared after contour lines were exported/imported using the software's 'interactive measures' function. Seven repeat measurements were made in each image and the median value for each image determined. Percentage size change was the ratio of the median value of measurements for baseline to follow up images. Measurement change exceeding an arbitrary cutoff of 5% above baseline was tantamount to changed size. Series having these changes were excluded from analysis for progression. The same person did all this checking (JT).

10.1.7 Findings on applying the approach clinically

Figure 10.2 shows the rim area profiles of two different normal control eyes. Regional or global depression in profiles relative to their respective baselines appears to suggest localised or diffuse rim area loss respectively. However, apparent change here (especially in Figure 10.2 A) appears random and does not exceed limits of variability; this is consistent with measurement variability in eyes without progression. Widely-dispersed profiles in Figure 10.2 A are associated with wider limits of variability representing variable data compared with the less variable, tightly-bound profiles of Figure 10.2 B which have narrower limits of variability. Width of the limits of variability differs between sectors, demonstrating the specific accounting of variability in each sector.

Figure 10.3 shows localised rim area loss in an ocular hypertension converter eye that developed a focal field defect. **Figure 10.4** shows diffuse rim area loss in a different converter eye. In progressing eyes, extent of sector change between time-points and with respect to variability reflects the relative rate of loss. Width of the limits of variability did not significantly differ between normal controls and converters when the groups were compared sector for sector (all $p>0.06$; Mann-Whitney-U test).

Eighteen of 20 converters (90%) had single positive tests in which at least one sector of rim area was reduced and exceeded its limit of variability once. Seven of 20 (35%) normal controls had single positive tests. Hence, for the single test strategy, sensitivity was 90% and the false positive rate was 35%, corresponding to a specificity of 65%. When assessed by the 'two of three' criterion of duplicate testing, repeatable change was found in 17/20 (85%) of converters and 1/20 (5%) of normal controls, giving a sensitivity of 85% and false positive rate of 5%. **Table 10.2** compares the two-of-three criterion with other criteria for confirming change.

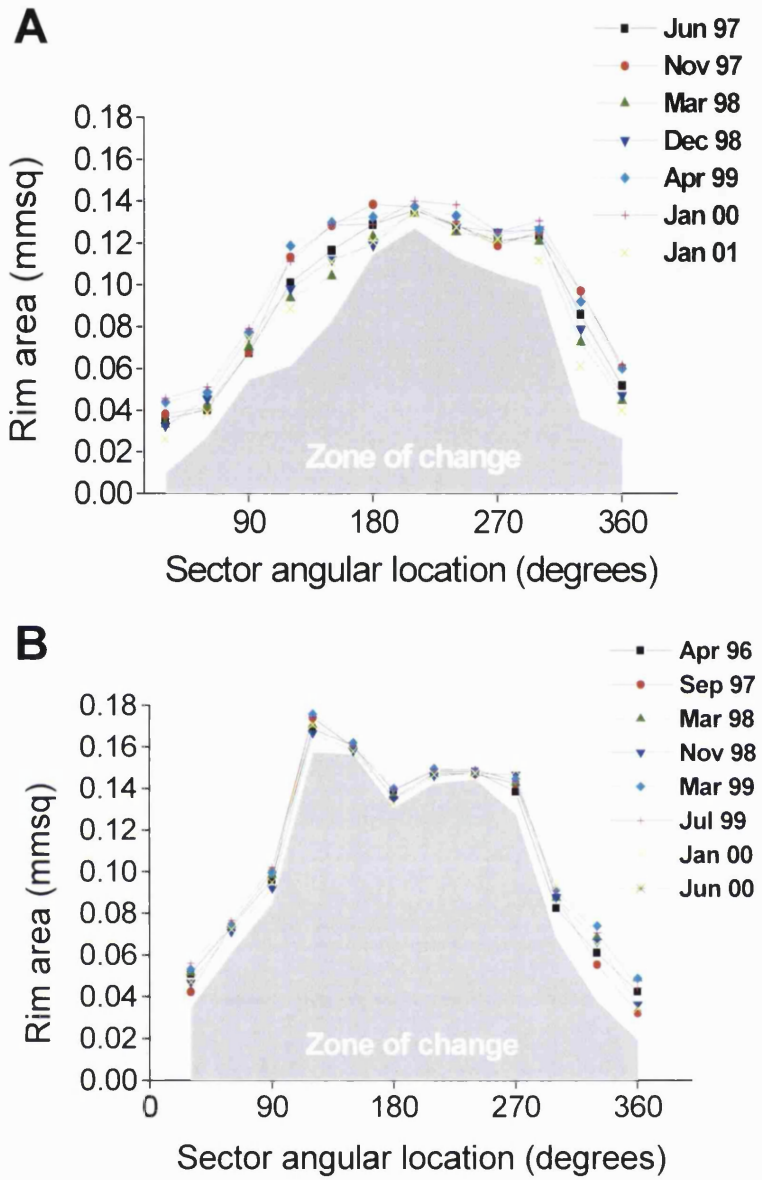

FIGURE 10.2. *Rim area profiles* from two different normal subjects' eyes, *A* and *B*. Lower *limits of variability* are represented by the superior extent of the grey *zone of change*. As expected in normal eyes, no rim area sectors have exceeded their limits of variability. *Limits of variability are 1) specific to each eye:* in *A*, sequential rim area profiles are more dispersed and associated with wider limits of variability than in *B* where data is more reproducible; 2) *specific to each region within each eye:* in *A*, limits of variability are wider where data is variable (example at 120-150°) and narrower where data is more reproducible (example at 180-210°).

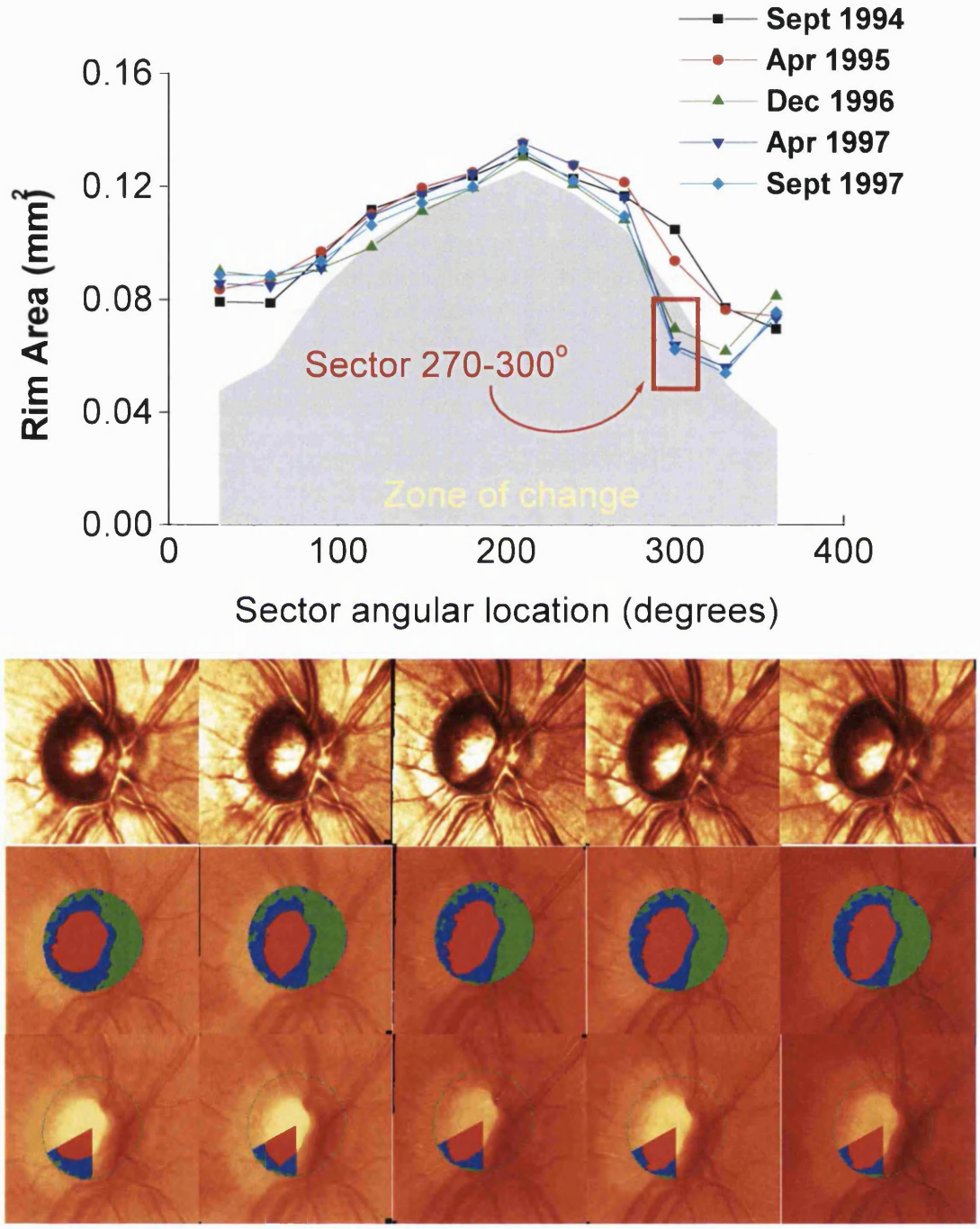

FIGURE 10.3. Confirmed localised change. *Rim area profiles* from a converter's eye, with corresponding 95% *limits of variability* forming the upper border of the 'zone of change'. *Graph:* there is localised rim area change infero-temporally at 270-300° where a single sector has exceeded its limit of variability. This change is repeatable on three consecutive tests. Sequential reduction at 300-330° (black arrow) is very suggestive of progression although its limit of variability has not been exceeded. *Upper series of images*: sequential intensity images of the same optic nerve head. *Middle series of images*: sequential global rim area as described by the experimental reference plane. *Lower series of images*: sectors 270-300° and 300-330° are highlighted.

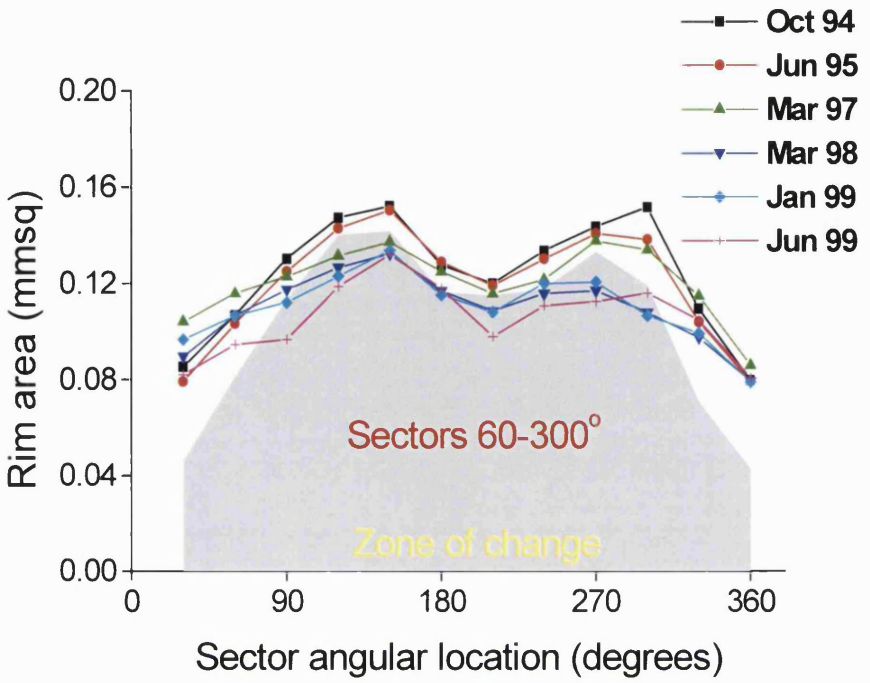

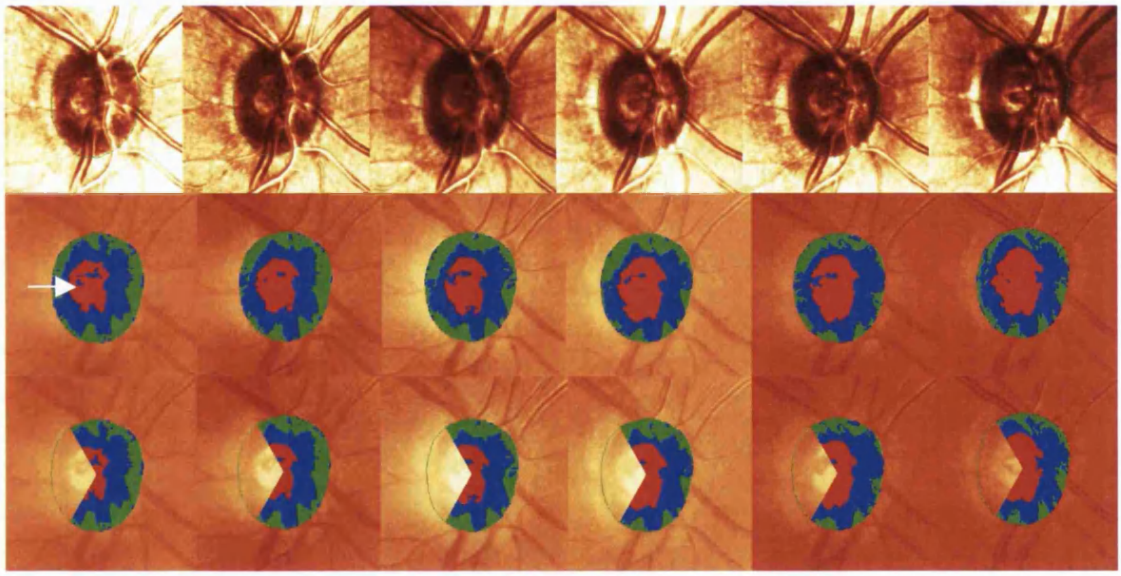

FIGURE 10.4. Confirmed diffuse change. *Rim area profiles* from a converter's eye with corresponding 95% *limits of variability*. *Graph*: gradual, diffuse and repeatable change is seen between 60-300°. *Upper series of images*: sequential intensity images of the same optic nerve head in which change appears subtle. *Middle series of images*: sequential global rim area as described by the experimental reference plane. The reference plane appears to transect a blood vessel over the cup at roughly the same level throughout (*arrow*). *Lower series of images*: sectors identified as changed are highlighted.

Criteria for duplicate testing	1 of 1	2 of 3	2 of 2	3 of 3	Two adjacent sectors on a single test	Two adjacent sectors on two consecu-tive tests.
Sensitivity	90% (18/20)	85% (17/20)	75% (15/20)	55% (11/20)	80% (16/20)	50% (10/20)
False-positive rate	35% (7/20)	5% (1/20)	5% (1/20)	0% (0/20)	20% (4/20)	0% (0/20)

Table 10.2. Sensitivity and false positive rates for various criteria used for confirming change.

10.1.8 Discussion of findings

Various innovative methods of analysing topography for change have been proposed. Chauhan et al (2000; 2001) described a technique for detecting statistical change in clusters of HRT image pixels ('superpixels") so that triplets of images from between pairs of visits – a baseline and a follow up visit – could be compared. The probability that change in superpixels exceeded variability was evaluated by analysis of variance and expressed as probability maps, analogous to the probability maps initially decribed by Yamada et al (1997; 1998) and Quigley and Pease (1996) for the Glaucoma-scope system. Criteria were introduced requiring repeatable significant change in clusters of at least 20 superpixels on three consecutive tests. The technique has been tested against computer simulations and against Statpac II visual field change analysis of normal and glaucomatous eyes and reported as useful. The empirical false positive rate of this technique is not known, however.

Burgoyne et al (2002) reported a method for detecting change in optic nerve head parameters defined by a reference plane fixed 150μm below zero of the z-axis. Parameters were analysed singly and in groups using univariate and multivariate analysis of variance respectively, to tell if change had occurred between baseline and follow up visits. Analysis was based on six single topography images per visit. The method was tested in image series of 12 monkey eyes. Using a criterion requiring two positive tests in a row, multivariate analysis showed confirmed change in 11 eyes having experimental glaucoma (sensitivity=92%) and one to two contralateral normal eyes. The method has been reported to be at least as good as expert subjective assessment of stereoscopic disc photographs (Ervin et al, 2002).

The approach described herein tests discrete rim area sectors for change and allows the discerning of patterns of loss. A new experimental reference plane is used that facilitates reproducible analysis of rim area. Variability is accounted for in each sector of each optic nerve head by way of limits of variability, calculated from intra-visit image data from across all test visits. The estimation of variability is dynamic and changes as an image series grows. Mean topography images, each from one visit in time, provide the point estimates of rim area; in judging progression, data from any number of visits can be simultaneously assessed and

weighed against variability. Only change repeatedly exceeding variability in two of three tests is attributed to progression. By this approach it was found that eyes having unambiguous glaucoma progression could be distinguished from unchanging normal control eyes.

Measurement variability had to be rigorously accounted for and this was dealt with in several ways. Firstly, a novel reference plane was introduced that allows rim area to be analysed reproducibly. By this, variability is expected to be significantly less and not appreciably affected by glaucoma or testing involving different operators and visits, compared with other reference planes. Variability was thus simpler to account for. Secondly, it was not presumed that variability is uniform across the optic nerve head and so variability was estimated in each sector separately. Thirdly, estimation of variability was unique to each eye; necessary because apart from optic nerve head morphology, individual factors such as media opacity (Zangwill et al, 1997) and ability to maintain fixation (Orgul et al, 1995a) may affect variability differently in each eye. Fourthly, only change that was repeatable in two of three tests was attributed to progression. This confirmation test strategy had fewer false positives than the single test strategy, while sensitivity in confirming change was not appreciably compromised. Hence, confirming change resulted in fewer eyes being misidentified as progressing. Sensitivity and the false positive rate were also favourably balanced in the two-of-three criterion compared with other criteria. Fifthly, variability was estimated using *all* image data from each series, with limits of variability updateable to factor in data from subsequently acquired images. This is desirable as the estimation of variability can be expected to improve with more δ values. Higher degrees of freedom of δ would result in narrower limits of variability, with the t-statistic decreasing as degrees of freedom increase (equation 10.2). The methods of Chauhan et al (2000) and Burgoyne et al (2002) account for variability on the basis of pairs of visits only. Sixthly, while obtaining three single topographies per visit is advised, more images could be acquired per visit if the number of δ needs to be quickly increased; this is possible as the number of δ increases exponentially according to ${}^{n}C_{r}$ (equation 10.1). For example, three images per visit yields three δ, but six images will yield 15 δ (five-fold increase) and nine images will yield 36 δ (12-fold increase). Thus, robust estimates of variability can be obtained rapidly, giving flexibility in clinical situations where indicated.

However, patient fatigue and its consequences on variability need to be considered when acquiring many images at a single sitting.

To verify progression, a rigorously defined reference dataset was contructed based on 'converters' with unambiguous visual field progression and normal controls. Ascertaining progression in converters – defined as the development of persistent defects in previously normal fields – is simpler than doing so in established glaucomatous fields with defects. The latter can be an uncertain measure for external validation because perimetric variability (Schulzer, 1994; Werner, 1994; The AGIS Investigators, 1994a; Flammer et al, 1984a; 1994b) and inconsistency in interpreting change (Werner et al, 1988; Katz, 1999) make ascertaining true change difficult. Also, perimetric variability in ocular hypertension is expected to be less than in glaucomatous fields (Werner et al, 1982; Flammer et al, 1984a). Visual field conversion was assessed by objective criteria using a rational and accepted visual field template (AGIS), defects were required to be repeatable in exactly the same locations in three consecutive tests, and independent verification was sought. It was reasonable to assume that eyes which developed visual field conversion had glaucomatous progression and coexisting morphological change (Pederson and Anderson, 1980; Sommer et al, 1980; Odberg and Riise, 1985; Airaksinen et al, 1992). Age-matched normal eyes with similar follow-up acted as controls.

Described here is an analytical approach for identifying rim loss in sequential scanning laser tomography images. Measurement variability was arbitrarily defined by 95% confidence limits and the approach was tested in two suitable groups of subjects and found to be able to distinguish eyes having progression from the unchanging eyes of normal controls.

10.2 FURTHER EVALUATION OF THE LIMITS OF VARIABILITY AND CRITERIA FOR CONFIRMING CHANGE

Next, how different limits of variability affect the discrimination of change from no change was tested. How this is influenced by different criteria for confirming change was also assessed. Then the correspondence between rim loss, as identified by the analytical approach, and the findings of serial perimetry was evaluated.

10.2.1 Investigations

10.2.1.1 Testing the identification of change by different limits of variability

Measurement variability in an image series was estimated by way of *limits of variability*. For an image series, limits of variability for each sector (*VARLIM*) can be expressed as:

$$VARLIM_a = Y * \sqrt{\Sigma(\delta_i - X)^2/(N-1)}$$

Where, a=sector number (corresponding to the order of angular location around the ONH, between 0-360°), δ=sector rim area difference between pairs of intra-session single topography images, δ_i=ith value of δ, X=mean of observations of δ, and N=number of observations of δ. Y=value of the t-statistic for degrees of freedom for δ, corresponding to a chosen two-tailed probability value, such as p=0.05 that represents a 95% confidence limit.

What effect different probability levels for Y have on the identification of change and distinguishing between progressing and unchanging eyes was studied. To do this, probability was varied according to p=0.2, 0.1, 0.05, 0.02, 0.01, 0.001, corresponding to limits of variability ranging from 80%-99.9%. Y was previously arbitrarily defined by p=0.05 in Section 10.1.

10.2.1.2 Further testing of criteria for determining change

The previous section showed that duplicate testing to confirm tentative change reduces false positives but does not appreciably compromise sensitivity. The chosen criterion requires at least one sector to change and exceed variability in any two of three consecutive tests before an eye is said to have glaucomatous progression.

This criterion (*'2-of-3' criterion*) was compared with a strategy not requiring confirmation (*single strategy*) at different limits of variability. Sectors were called *'progressed sectors'* for a strategy if they met that strategy's criterion for change. The number of progressed sectors arising by different limits of variability in the 2-of-3 criterion and single strategy were calculated and plotted in bar graphs. The 2-of-3 criterion was then compared with other plausible criteria: 2) 2-of-2 consecutive tests, 3) 3-of-3 consecutive tests, 4) two adjacent sectors in a single test, and 5) two adjacent sectors in 2-of-3 consecutive tests. Receiver operating characteristic curves (ROC curves) were plotted to evaluate how well each criterion distinguished eyes with glaucomatous change from the unchanging eyes of normal controls. Any progressed sectors in control eyes were considered false positives. The spatial relationship between rim loss and visual field change was then examined. This was done by associating an optic nerve head hemisphere (superior or inferior) having confirmed rim loss with the presence or absence of confirmed perimetric change (conversion) in the opposite visual field hemisphere.

10.2.1.3 Analysis of rim area by an experimental reference plane

Rim area was assessed for change in 30° sectors in longitudinal series of mean topography images. The experimental reference plane defined the inner extent of the neuroretinal rim as outlined in Section 9.1 and 10.1.3, while the drawing of the contour line, as described in Section 5.2, marked the rim's outer extent. Sectors were identified by their location on the optic nerve head circumference (0-360°). Data for single topography images from each visit were used to estimate intra-visit sector variability so that sector variability could be accounted for, as described in Section 10.1.4. Rim area was analysed using the experimental reference plane, as described in Section 9.1, and images series were checked to ensure they were free from magnification changes over time as previously described in Section 10.1.6.2.

Sequential rim area data was plotted as *rim area profiles*, as outlined in Section 10.1.6.1. Profiles were plots of rim area by angular location round the optic nerve head (0-360°, with 0°=temporal, 90°=superior, 180°=nasal, 270°=inferior) from the same image series, representing rim area at different points in time in a common graph. Limits of variability for each sector was plotted relative to the baseline profile, with the region beneath the lower limits termed the *zone of change*. Rim area in a sector that diminished, exceeded its limit of variability and entered the zone of change once was taken to represent tentative change. Only change meeting set criteria for confirmation was attributed to glaucoma. The testing of various limits of variability led the author to modify the defining of the zone of change to reflect a more graded definition of variability; in this way, the possibility of change could be evaluated by several different limits of variability simultaneously.

10.2.1.4 Subjects

Sixty-three longitudinal image series from 30 ocular hypertension converter and 32 normal control eyes were analysed. Subjects' selection criteria are outlined in Section 5.1. All had received imaging on at least four separate occasions over a minimum of three years.

10.2.2 Results

Longitudinal image series of 30 ocular hypertension converters and 32 normal controls were included in this study. Thirty-three converters initially met the inclusion criteria but three were excluded because image size changes were identified in their series. No normal controls were excluded from the study. **Table 10.3** shows study subjects' demographic information. For converters, there was a significant difference ($p<0.05$) between final and initial visual field indices and global rim area.

Figure 10.5 shows that many more converter rim sectors exceeded their limits of variability to be counted as *progressed sectors* compared with normal controls. This was true at each limit of variability and whether (A) or not (B) confirmation was

	Normal controls (median (Q1, Q3))			Converters (median (Q1, Q3))		
	Initial	Final	p-value*	Initial	Final	p-value*
N=		32			30	
Age (years)		65.0(59.0,71.0)			66.1(55.0,69.8)	
Intraocular pressure (mm Hg)	14.5 (12.0,18.5)	15.0 (13.5, 17.0)	p=0.76	26.0 (24.0, 28.0)	26.0 (23.0,29.0)	p=0.465
Visual field mean deviation (MD, dB)	0.58 (-0.26,1.00)	0.24 (0.39, 0.390)	p=0.77	-0.58 (0.08, -1.46)	-2.54 (-3.86,-0.77)	p=0.008
Visual field corrected pattern standard deviation (CPSD, dB)	1.06 (0.11,1.42)	1.07 (0.52, 1.38)	p=0.56	1.63 (1.01, 2.14)	3.22 (2.30,4.34)	p=0.000
Rim area (mm^2)	1.46 (1.27,1.70)	1.48 (1.32 1.70)	p=0.10	1.28 (1.06, 1.48)	1.24 (0.99,1.42)	p=0.002

TABLE 10.3 Subjects' demographics. *Significance testing by the Wilcoxon test. Rim area was analysed by the experimental reference plane.

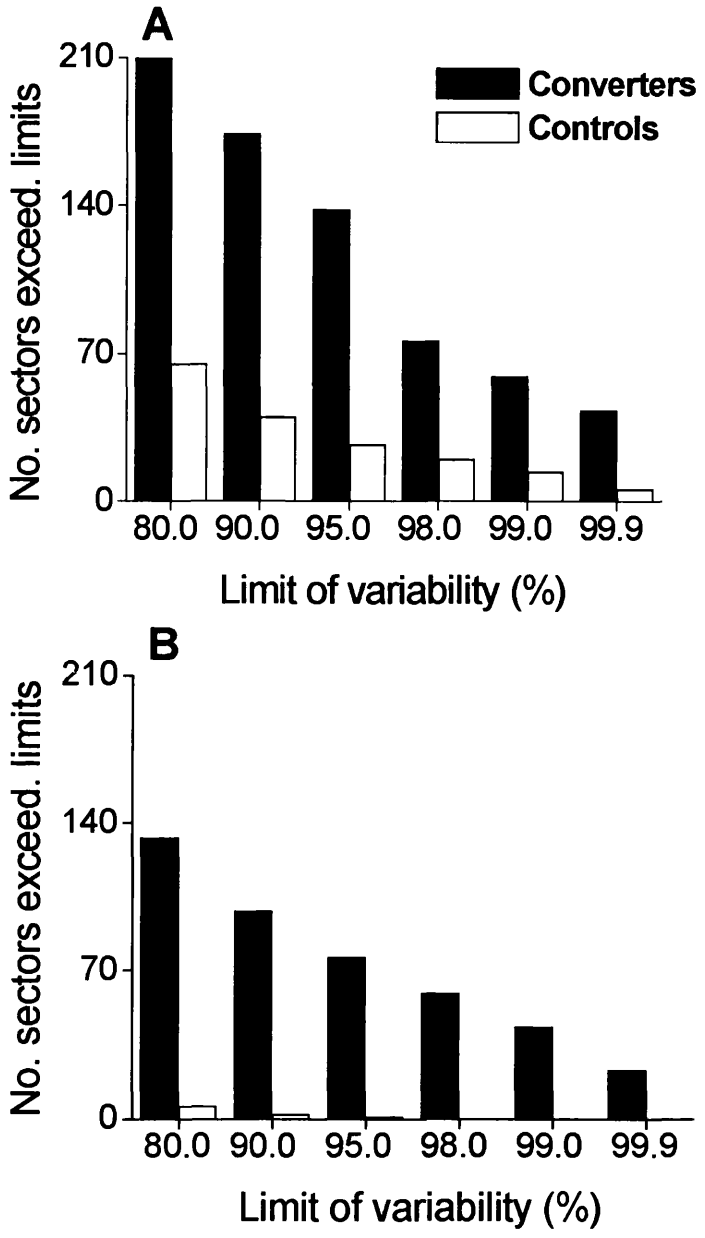

FIGURE 10.5. Number of sectors exceeding different limits of variability to be counted as progressed sectors in converter and control groups for the *single test strategy* (A) and *2-of-3 criterion* (B).

necessary. Increasingly stringent limits of variability resulted in fewer progressed sectors in either strategy. Judged by the number of progressed sectors, converter and control groups were more widely separated at more stringent limits of variability, and in the confirmation strategy than single strategy.

With the *single strategy*, converters had 216 and 52 progressed sectors with the 80% and 99.9% limits of variability respectively; controls had 65 and 6 progressed sectors with 80% and 99.9% limits of variability respectively. Ratio of converters to controls for the number of progressed sectors was 3:1 for 80% limits of variability rising to 9:1 for 99.9% limits.

With the *2-of-3 criterion*, converters had 137 and 24 progressed sectors with 80% and 99.9% limits respectively; controls had 6 and 1 progressed sector with 80% and 95% limits of variability respectively. No progressed sectors were found in normal eyes for limits of variability between 98% and 99.9%. Ratio of converters to controls for the number of progressed sectors was 23:1 for the 80% limits of variability and 76:1 for the 95% limits of variability.

Figure 10.6 shows that the ROC curve for the 2-of-3 criterion lies almost horizontally to the left of the curve for the single strategy; the former criterion had fewer false positives but its sensitivity was roughly similar to that of the single strategy for limits of variability between 80% and 95%. Compared with the other criteria, sensitivity of the 2-of-3 criterion was higher at every confidence limit tested. The 3-of-3 criterion and 2 adjacent sectors in 2-of-3 tests criterion did not have any false positives whatsoever but this occurred at the expense of sensitivity; each achieved best sensitivity at the 80% limit of variability: 76.7% in the former and 60.0% in the latter, as shown in Figure 10.6. For the 2-of-3 strategy, the 95% limit of variability had a sensitivity of 83.3% (25/30) and false positive rate of 3.1% (1/32), corresponding to a specificity of 96.9%; the 90% limit of variability yielded a sensitivity of 90.0% (27/30) and false positive rate of 6.2% (2/32), corresponding to specificity of 93.8%.

Figures 10.7, 10.8 and 10.9 are examples of converter eyes evaluated by different limits of variability simultaneously and the 2-of-3 criterion. In **Figure 10.7**, two inferior sectors are confirmed to have repeatedly exceeded their 90% but not 95%

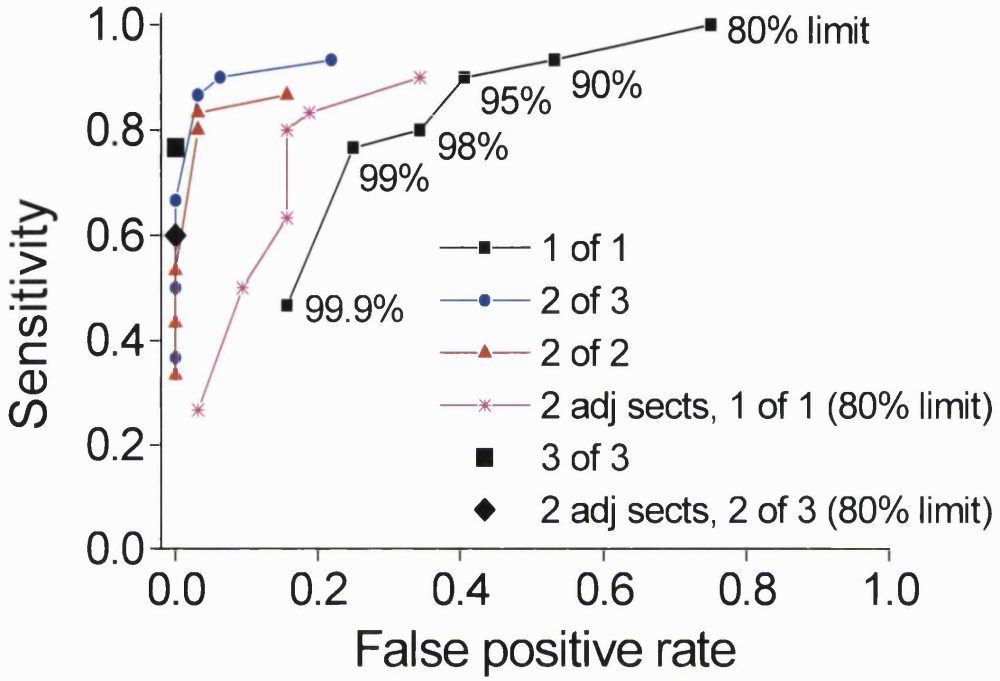

Figure 10.6. Receiver operating characteristic (ROC) curves for the single test strategy (*black squares*), '2-of-3' confirmation test strategy (*blue circles*), '2-of-2' criterion (*red triangles*) and '2 adjacent sectors in a single test' criterion (magenta stars) plotted for limits of variability between 80% and 99.9%. ROC curves for the '3-of-3' criterion (*single black square*) and '2 adjacent sectors in 2-of-3 consecutive tests' criterion (*single black diamond*) were vertical along x=0, indicating no false positives; only their highest sensitivity is plotted, corresponding to their respective 80% limits of variability.

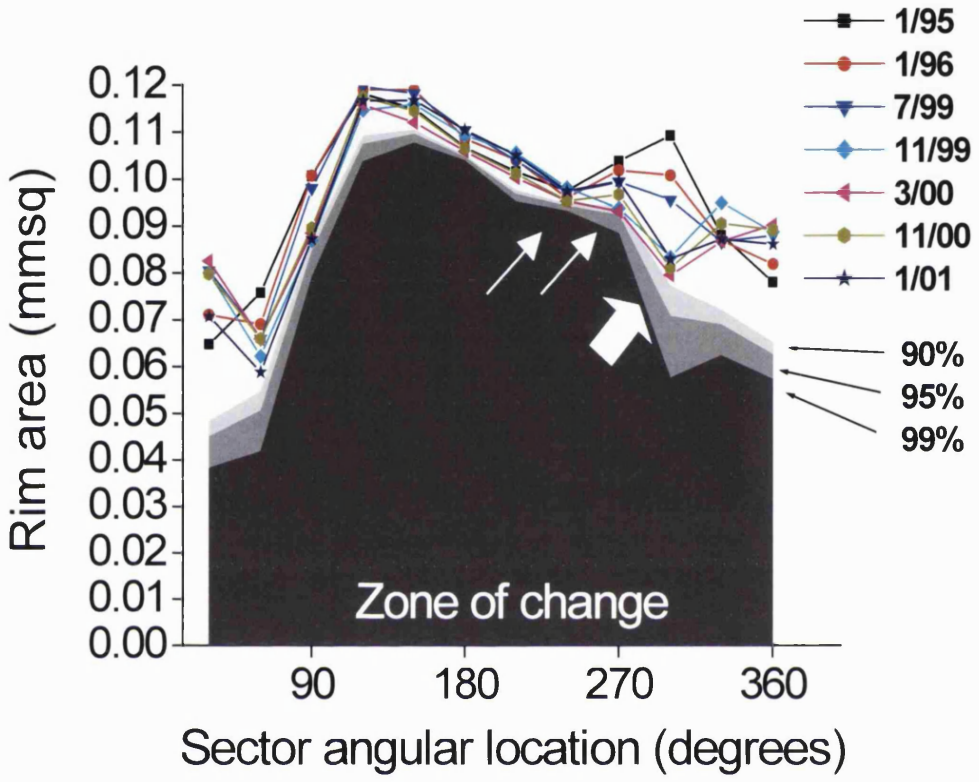

FIGURE 10.7. Applying different limits of variability to identifying progression. *Rim area profiles* of a converter with 90%, 95% and 99% limits of variability. Two inferior sectors (210-240° and 240-270°, *thin arrows*) have exceeded the 90% but not 95% limits of variability. A third sector (270-300°, *fat arrow*) has not exceeded its relatively wide 90% limit of variability but the sector's pattern of sequential change strongly suggests progression.

CORRESPONDING IMAGES shown on next page. *Left series of images*=global measurement of rim area, *Right series of images*=sectors identified as changing are highlighted.

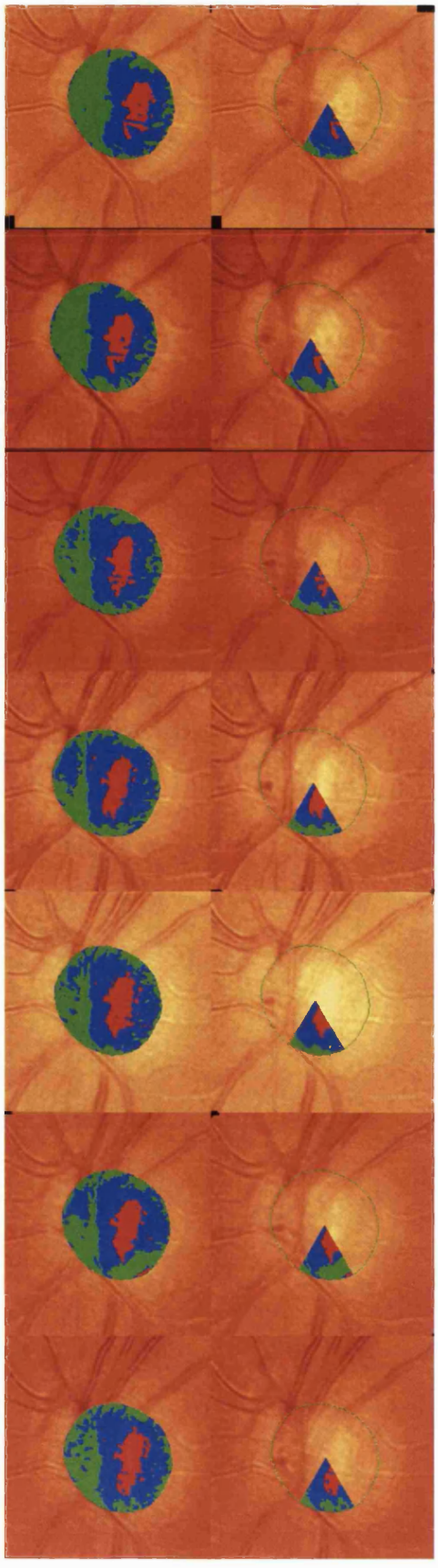

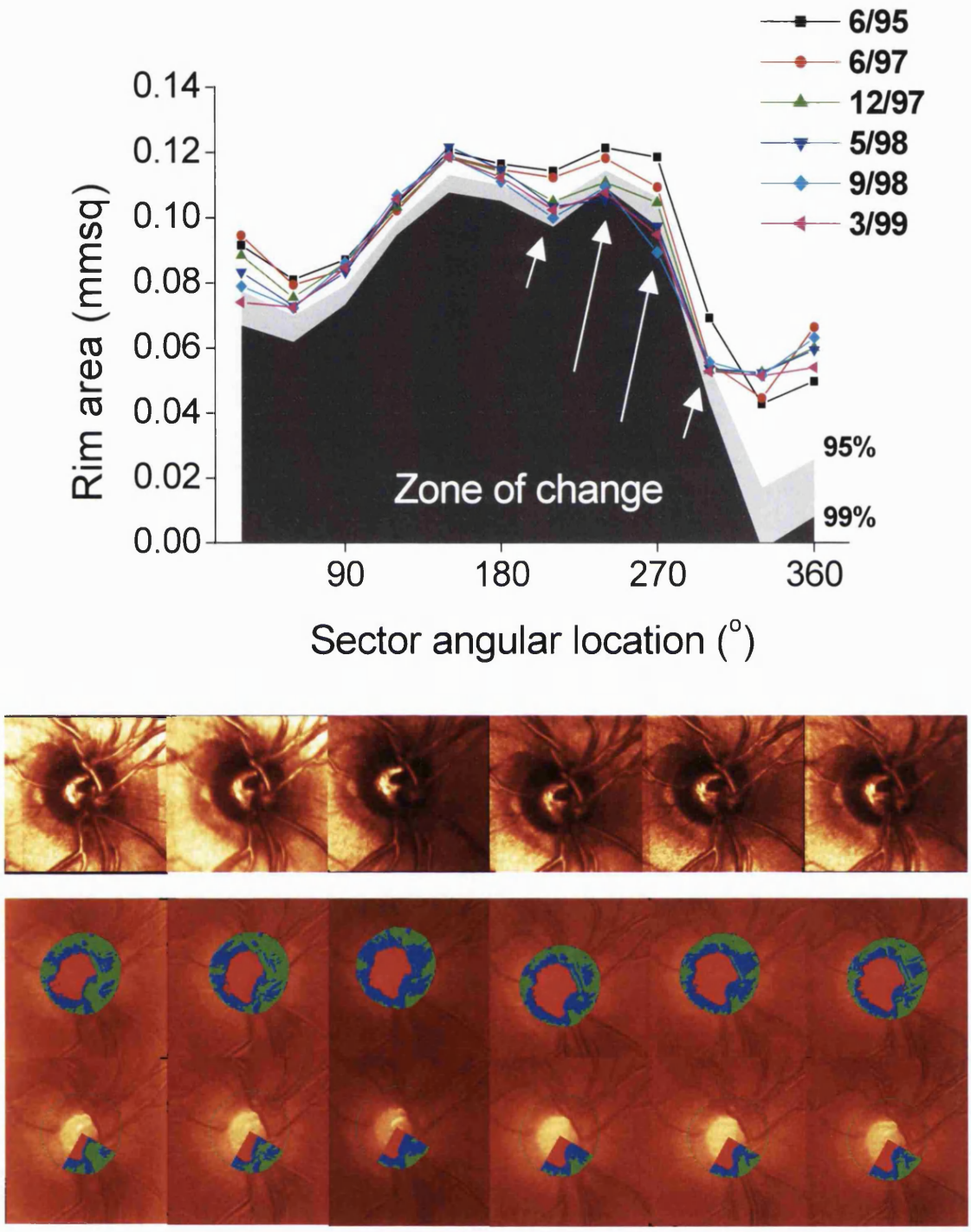

FIGURE 10.8. Illustration of different rates of change within the same nerve. Change in sectors 210-240° and 240-270° (*long arrows*) have exceeded stricter limits of variability than sectors 180-210° and 270-300° (*short arrows*) within the same timeframe, indicating a higher rate of change in the former sectors. This is consistent with a notch developing inferiorly.

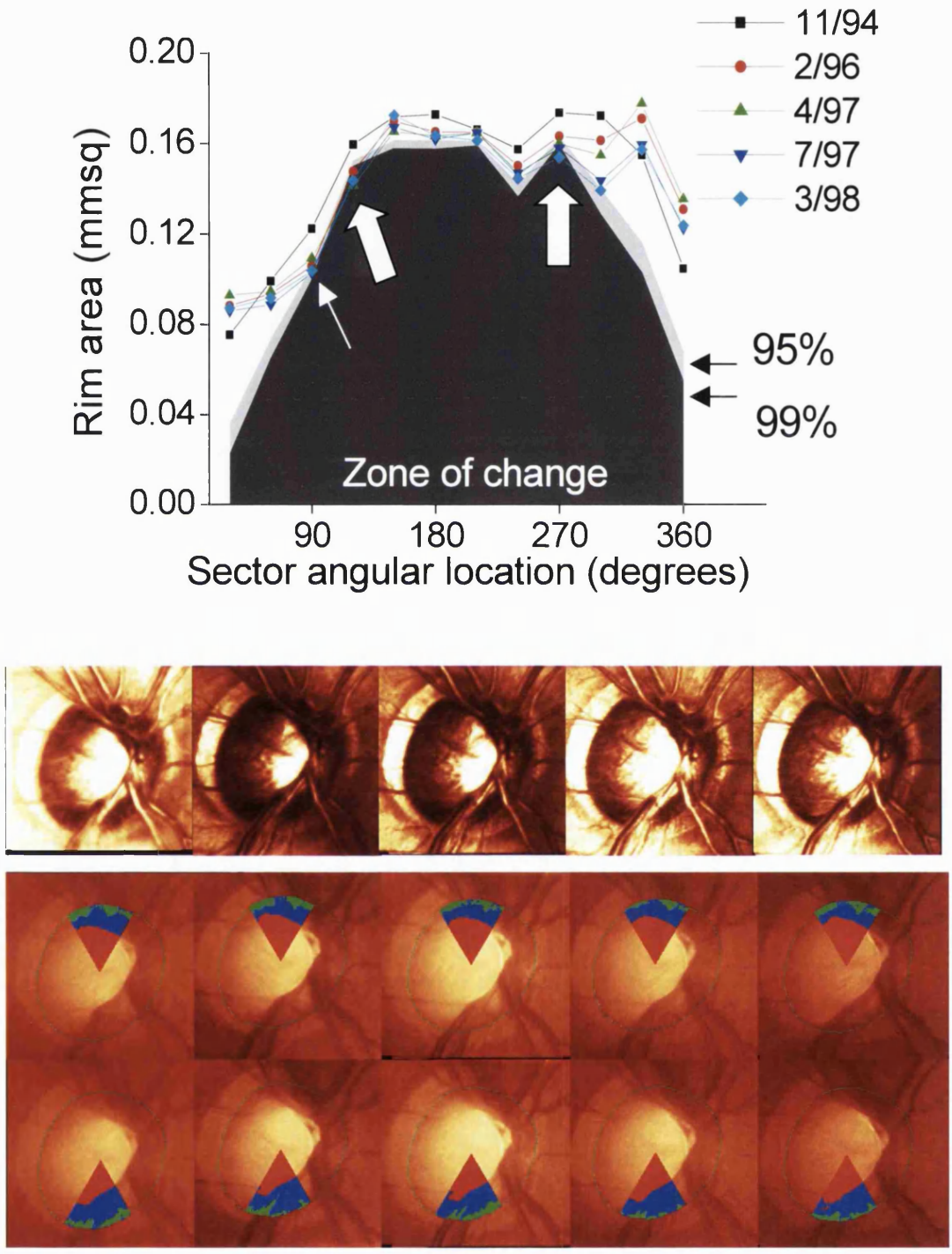

FIGURE 10.9. Rim area profiles of a converter with 95% and 99% limits of variability. Change at sectors 90-120° and 240-270° are repeatable, exceeding both the 95% and 99% limits of variability (*fat arrows*). Sector change at 60-90° (*thin arrow*) exceeds the 95% but not the 99% limits of variability. The *two lower series of images* highlight the different sectors identified as having confirmed change. This same optic nerve is also shown in Figure 11.10.

limits of variability. Suspicion of change is raised by the sequentially depressed profile of a third adjacent sector, although its limit of variability is not exceeded and change cannot be verified statistically. **Figure 10.8** shows a different eye, also with inferior rim loss, but in which change has exceeded the more stringent 95% and 99% limits of variability. In **Figure 10.9,** there is superior and inferior rim change exceeding the 95% and 99% limits of variability.

Figure 10.10 shows that rim loss, as identified by 90% limits of variability and confirmed by the 2-of-3 criterion, was most frequent in the inferior hemisphere of the optic nerve head, especially between 240-300°. In the superior hemisphere of the optic nerve head, rim loss was most common supero-temporally between 60-90°. Change in the nasal rim was not uncommon. 81.5% (22/27) of converter eyes had confirmed field abnormality that was matched by confirmed rim loss in the opposite hemisphere of the optic nerve head. Half of converter eyes (14/27) had confirmed rim loss in both optic nerve head hemispheres but in 10/14 of these eyes, confirmed perimetric abnormality developed in only one field hemisphere.

10.2.3 Discussion

This approach for identifying change has previously been tested and found to be sensitive and specific; the present findings in a larger group of subjects support this. Fine-tuning of various parameters of the analytical approach by the testing of various limits of variability and criteria for confirming change showed the following. Firstly, the 2-of-3 criterion had fewer false positives but reasonably preserved sensitivity compared with the single strategy. The 2-of-3 criterion was more sensitive and specific than the other criteria we tested; only the criteria requiring change in two adjacent sectors in 2-of-3 tests and 3-of-3 consecutive tests had better specificity, but their sensitivity of 60% and 77% respectively was not optimal. Secondly, stricter limits of variability within each criterion reduced the number of progressed sectors in both converter and normal eyes. But normal eyes were affected proportionately more, indicating a selective reduction in false positives. Thirdly, as with stricter limits of variability, the 2-of-3 criterion also reduced the number of progressed sectors in normal eyes relative to the single test strategy, resulting in false positives being eliminated for confidence limits

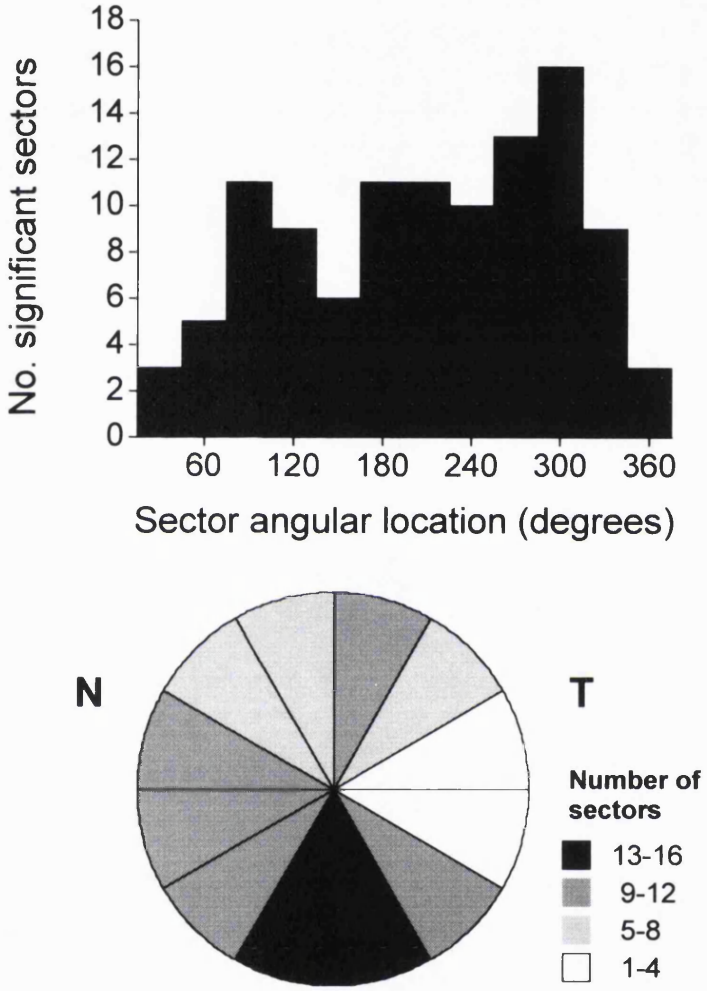

FIGURE 10.10. Distribution of sectors identified as progressing in converter eyes as assessed by 90% limits of variability and the 2-of-3 criterion. *Graph A*=bar graph showing the frequency distribution of progressed sectors in the optic nerve head. *Graph B*=schematic diagram of the optic nerve head showing the frequency distribution of progressed sectors, where *N*=nasal, *T*=temporal.

of 98% and above. Sensitivity for the 98% limit of variability, however, was only 67%. ROC curve analysis of the 2-of-3 criterion indicated that the optimal balance of sensitivity and specificity was achieved at either the 90% or 95% limits of variability. The 90% limit of variability had a sensitivity of 90.0% and false positive rate of 6.2%; the 95% limit of variability had a sensitivity of 83.3% and false positive rate of 3.1%. While the identification of change in converters was not markedly different between the two limits of variability, the 95% limits of variability had marginally fewer false negatives. Separation between converters and controls for testing by the 95% limits of variability and verification by the 2-of-3 criterion was high: converters had 76 times as many progressed sectors as normal controls.

The author has shown how sequential data can be evaluated by graded limits of variability to give extra information on the nature of progression. The stricter the limit of variability, the greater the magnitude of change needed to exceed it, and the more likely it is that measured change is not due to variability alone. Thus, the exceeding of stricter limits of variability reflects a greater probability of change than when less strict limits are exceeded; this is illustrated by Figures 10.8 and 10.9. Conversely, that glaucomatous change could be small and not exceed test variability can also be subjectively judged based on the quantitative analysis, as is illustrated in Figure 10.7. Thus, the approach's method of objective analysis combined with the option of qualitative appraisal provides a potentially useful composite framework for guiding clinical decisions.

Having an empirical basis for duplicate testing is important for knowing the usefulness of a test, but also because duplicate testing affects clinical resource allocation. A 3-of-3 criterion for confirming change (as used by Chauhan et al (2001)) requires 50% more testing than a 2-of-2 criterion (as used by Burgoyne et al (2002)). It was found that most tentative change could be confirmed by two consecutive tests, as evident in the relative positions of the ROC curves for the 2-of-2 and 2-of-3 criteria in Figure 10.6. But allowing a third test in the event of a second test's failing to confirm tentative change increased sensitivity but did not compromise specificity.

The trade-off of introducing criteria to improve test specificity is that the severity of minimally detected change is not the same at all points along an ROC curve, nor for different criteria of duplicate testing. This should be noted when interpreting the ROC curve analysis presented here. Stricter limits of variability within an ROC curve can be expected to detect change that is more severe, possibly when underlying disease is also worse, compared with less strict limits. Likewise, each ROC curve probably represents a different degree of change corresponding to a different stage of disease, especially when compared with the single strategy. Subjects reported here did not prospectively undergo duplicate testing, instead their pre-existing longitudinal measurements were examined for repeatable change. The degree to which these results had 'bias' depends on the underlying rates of progression and how quickly duplicate testing for confirmation was completed in each series. Other comparable studies having criteria for repeatable change have also used retrospective assessment and their findings should be interpreted accordingly. Still, findings on testing by the confirmation strategy are in line with what is predicted by theoretical modelling; namely that the 2-of-3 criterion markedly improves specificity but does not appreciably compromise sensitivity (Schulzer et al, 1991b; 1994).

The reference dataset used for validation may not fully represent the whole spectrum of disease severity. Only converters were tested because unequivocally telling that they had progression – converter visual fields simply had to change from normal to abnormal – was simple and unambiguous compared with judging progression in eyes with pre-existing glaucomatous field defects. While converters might be considered to have 'early' glaucoma, it was found that some already had extensive cupping at conversion; nevertheless rim loss could be identified in these eyes; Figure 10.9 shows an example, and more examples of change in nerves already having large cupping are shown in Chapter 11. Because variability is accounted for separately in each part of each optic disc, and because the experimental reference plane is customised to suit the morphology of each optic nerve head, variations in nerve morphology are not expected to pose problems in seeking to identify change.

Most converters (four-fifths) had detectable rim loss that matched the field hemisphere in which conversion occurred. Why the remainder did not have

matching rim loss is unclear. The concepts underlying field conversion and our method of detecting rim loss are different: for conversion, visual sensitivity loss had simply to reach threshold, whereas for significant rim loss to be identified, a specified amount of change exceeding test variability was needed. Their measurements are also scaled differently, with change in rim area measured on a linear scale but the decibel scale of visual sensitivity being logarithmic. Thus, it could be that visual sensitivity thresholds were reached before corresponding neuroretinal rim loss exceeded the statistical limits of variability. Some eyes had statistical rim loss that did not have matching confirmed field loss, and it is possible that morphological change predated white-on-white field defects in these eyes, as has been reported by several investigators (Pederson and Anderson, 1980; Sommer et al, 1980; Odberg and Riise, 1985). In eyes with ocular hypertension, Kamal et al (1999b; 2000) have reported detecting rim changes by scanning laser tomography before visual field conversion. In glaucoma eyes, Chauhan et al (2001) have identified topographical changes by scanning laser tomography before the detection of field progression by Humphrey Statpac-2 analysis. The finding herein that converters had more frequent rim loss in the disc poles, especially inferiorly, agrees with the observations in optic disc photographs of Tuulonen and Airaksinen (1991), Sommer et al (1980), Kirsch and Anderson (1973a) and Jonas et al (1993a).

This study sought to empirically determine optimal criteria for longitudinal analysis and further validate the analytical approach. It was found that the limits of variability of 90% or 95% provided a reasonable cut-off for identifying progression when the 2-of-3 criterion was used to verify change. The assessing of change by a range of statistically graded limits of variability can give extra information on the nature of change and is potentially useful clinically. Further study of this analytical approach in patients with diverse manifestations of glaucoma and severity should help determine the approach's broader clinical significance and applicability.

Chapter 11

IDENTIFICATION AND DESCRIPTION OF OPTIC NERVE CHANGE IN DIVERSE PRESENTATIONS OF GLAUCOMA

11.1 PROGRESSION IN GLAUCOMA SUSPECTS, POAG AND NPG

It is not known whether and in what form progression in different clinical presentations of glaucoma is identifiable by scanning laser tomography. Previous longitudinal studies documenting rim loss have mostly been in ocular hypertension eyes progressing to develop field abnormalities (Pederson and Anderson, 1980; Sommer et al, 1980; Odberg and Riise, 1985; Tuulonen and Airaksinen, 1991). At this stage of disease, the observed pattern of cupping is predominantly that of generalized expansion or vertical elongation. In the latter, inferior and superior rim loss exceeds change nasally and temporally so that the optic nerve head is considered preferentially affected in its poles. Cross-sectional studies (Read and Spaeth, 1974; Kirsch and Anderson, 1973; Jonas et al, 1993) agree that the cup commonly becomes vertically oval in 'early' glaucoma. The nature of neuroretinal rim loss at more advanced stages of glaucoma is understood largely by cross-sectional studies (Read and Spaeth, 1974; Hitchings and Spaeth, 1976; 1977; Kirsch and Anderson, 1973a; Jonas et al, 1993a). Jonas et al (1993a) have suggested that rim loss at a given stage of glaucoma may involve any region of the optic nerve head, although the location of most pronounced loss varies with the severity of disease.

Concerning the pattern of glaucomatous optic nerve head change seen in scanning laser tomography, two longitudinal studies are notable. The findings of Kamal et al (1999b; 2000) on analysing images of eyes with ocular hypertension or ocular hypertension conversion suggested a preponderance of change in the superior and

inferior regions of the rim and cup. Burgoyne et al (2002) in their testing of primates with experimental glaucoma identified vertical cup-disc ratio and temporal and superior peripapillary retinal height as regional parameters that might be useful for modelling and detecting change.

The author's approach for identifying change was tested in the longitudinal image series of normal control eyes and eyes with ocular hypertension, primary high-pressure glaucoma (POAG), suspected normal pressure glaucoma (NPG) and established NPG. Groups were also compared cross-sectionally at the start and end of follow up. Patterns of rim change, and the association between rim loss and serial perimetry in these groups were then described.

11.1.1 Investigations

11.1.1.1 Criteria for selecting subjects

The analytical approach for identifying rim area change described in Chapter 10 was tested in 372 longitudinal image series of 219 subjects: 1) both eyes of 120 subjects with ocular hypertension, 2) both eyes of 33 subjects with asymmetric NPG, 3) the eye that converted in 34 ocular hypertension converters to POAG, and 4) one eye each of 32 normal controls. Subjects attended either the ocular hypertension and early glaucoma, or normal pressure glaucoma research clinics at Moorfields Eye Hospital. All had received imaging on at least four separate occasions over a minimum of three years. Except for NPG eyes, disc appearance was not part of the criteria for recruitment to the study. This study adhered to the tenets of the Declaration of Helsinki, having appropriate institutional review board approval and subjects' informed consent.

Criteria for selecting subjects are described in Section 5.1. This is briefly as follows:

Subjects with ocular hypertension had 1) IOP consistently≥22mmHg in one or both eyes without IOP lowering treatment, 2) open angles on gonioscopy, 3) initially normal Humphrey 24-2 visual fields with AGIS scores=0, determined following a

learning period of 3 consecutive tests, 4) refractive errors<±6D, 5) no concurrent ocular disease or previous intraocular surgery, 6) were aged>40 years.

Eyes of *ocular hypertension converters* had developed reproducible visual field defects, as defined by AGIS criteria (score>0), in the same location on 3 consecutive tests. An independent glaucoma expert confirmed this. Converters had POAG and were assumed to have glaucomatous progression.

To have *asymmetric NPG*, both eyes of subjects had 1) untreated mean IOP on phasing of less than 22 mmHg with no single reading exceeding 23 mmHg, 2) open drainage angles on gonioscopy, 3) no concurrent ocular disease, previous intraocular surgery or any secondary cause for raised IOP. 4) Only one eye had reproducible visual field abnormality at baseline (*established NPG*) with other causes of the abnormality excluded, while 5) the contralateral eye had no field defects (*suspected NPG*). Over the follow-up, some eyes with suspected NPG developed reproducible defects (defined as for ocular hypertension converters) and were considered *NPG converters.*

Eyes of *normal controls* were taken to be unchanging. Normal subjects were volunteers comprising spouses or friends of hospital patients, hospital staff, or members of external non-medical social organisations. They had 1) intraocular pressures (IOP) repeatedly<22 mmHg, 2) serially normal and reliable Humphrey 24-2 visual fields with AGIS visual field scores=0, 3) no concurrent ocular disease or previous intraocular surgery, 4) no family history of glaucoma, 5) refractive errors< ±6D, and were 6) aged>40 years.

11.1.1.2 Approach for longitudinally analysing rim area for change

This approach has already been described in detail in Chapter 10. Briefly, thirty-degree (30°) rim area sectors were evaluated for change. The parameter of rim area was evaluated within longitudinal image series using a new experimental reference plane to define the inner edge of the rim. The outer extent of the rim coincided with the contour line marking the inner margin of the scleral ring of Elschnig. The same observer drew the contour line in each subject's baseline mean topography image (JT). Mean images were derived from triplets of single topography images using HRT software version 2.01. Contour lines were exported from a baseline mean topography image to other mean and single topography images in each series. Only images with mean pixel SD<50μm were used, and grainy images having a honeycombed appearance were excluded.

For an image series, limits of variability for each sector (*VARLIM*) were calculated according to:

$$VARLIM_a = Y * \sqrt{\Sigma(\delta_i - X)^2/(n-1)} \qquad \text{[equation 10.2]}$$

Where, a=sector number (corresponding to the order of a sector's location on the ONH circumference between 0-360°), δ=sector rim area difference between pairs of intra-visit single topography images, i=ith value of δ, X=mean of observations of δ, and n=number of observations of δ. Y=value of the t-statistic for degrees of freedom for δ, corresponding to a chosen two-tailed probability value. A probability level of p=0.10, corresponding to a 90% limit of variability, was used based on the findings in Section 10.2.

Sequential rim area data, as measured in mean topography images, was plotted as *rim area profiles*. Profiles were plots of rim area by angular location round the optic nerve head (0-360°, with 0°=temporal, 90°=superior, 180°=nasal, 270°=inferior) from the same image series. This represented rim area at different points in time in a common graph. Limits of variability for each sector were plotted relative to the baseline profile, with the region beneath the lower limits termed the *zone of change*. Rim area in a sector that diminished, exceeded its limit of variability and entered the zone of change was taken to represent tentative change. Only sector change

repeatedly exceeding variability in two of three tests was attributed to progression. In judging progression, rim data from any number of visits over time can be simultaneously assessed and weighed against variability. An eye was considered to have progression if at least one rim sector was confirmed as changed. Image series were checked to ensure they were free from magnification changes over time as previously described in Section 10.1.6.2. Any subjects having image series with magnification changes were excluded from analysis.

11.1.1.3 Statistical analysis

Analysis was first of individuals' longitudinal image series, then cross-sectionally of group data at baseline and final follow up.

Analysing longitudinal image series by the analytical approach. In analysing individuals, each image series was analysed for change using the said analytical approach. The frequency distribution of change in 30° sectors in each diagnostic category was plotted in schematic diagrams of the optic nerve head. In schematic diagrams, sectors straddling the superior (60-120°) and inferior vertical (240-300°) were taken to represent the *superior and inferior disc poles* respectively; the sectors straddling the horizontal meridian temporally (330-360, 0-30°) and nasally (150-210°) were termed *temporal-horizontal* and *nasal-horizontal sectors* respectively. In eyes with reproducible field defects, the location of abnormality in the Humphrey field grid was described as nasal or temporal, or superior or inferior as defined by the AGIS field template and described in Section 5.3. Paracentral abnormality affecting any of the four field locations next to fixation was noted.

Cross-sectional analysis of diagnostic groups at baseline and final follow up. In the analysis of groups, the median of rim area values was calculated for each sector in each diagnostic group. Each group's sectors' median values were then subtracted from the normal control group's median values sector for sector. This gave each diagnostic group a value for *rim area deviation from normal* (subsequently referred to simply as "deviation") for each sector. The magnitude of deviations was plotted in schematic diagrams of the optic nerve head for two time-points: at baseline and at final follow up. The probability of accepting the null hypothesis that a particular deviation was significantly different from normal was calculated by the Mann-

Whitney-U test; this was expressed as p-values per sector in schematic diagrams of the optic nerve head. P≤0.05 was considered statistically significant and to reflect true deviation from normal. Smaller p-values for a sector indicated that it was more probable that rim area truly deviated from normal. Statistical analysis was conducted in the software package SPSS v9 for Windows (SPSS Inc; Chicago, IL, USA, 1998).

11.1.2 Results

11.1.2.1 Demographics of subjects

Ninety-seven of 110 ocular hypertension subjects, 26/33 subjects with asymmetric NPG, 30/33 ocular hypertension converters, and 32/32 normal control eyes had longitudinal image series meeting the inclusion criteria; this amounted to 288 longitudinal image series in all. Their demographics are shown in **Table 11.1**. Excluded images were of poor quality as described, or had magnification problems. Disc area was found to not be significantly different between groups (p>0.05), although there was a trend toward NPG discs being bigger than in other groups. Only eyes with established NPG had field defects at baseline. At final follow up, visual field mean deviation (MD) in established NPG was worse than in ocular hypertension converters (p=0.003, Mann-Whitney-U test). Other between group comparisons showed no differences (p>0.05). There were five NPG converters; their visual field indices were not significantly different from those of ocular hypertension converters (p>0.05, Mann-Whitney-U test).

11.1.2.2 Longitudinal analysis of individual eyes

Two of 32 *normal control* eyes (6.2%) had repeatable change in at least one rim sector.

Of 97 *ocular hypertension subjects*, repeatable rim change was identified in one eye each of 11 (11%) subjects. By definition, all had no field defects at baseline and final follow up. **Figures 11.1 and 11.2** respectively show localised superior change and diffuse change in eyes with ocular hypertension. **Figure 11.3 A** shows that changed sectors were most frequently identified in the inferior pole (240-300°), followed by superiorly (60-90°) and nasally (150-210°). 3/11 (27%) had rim change

Mean (SD)	Normal	OHT	OHT Convert.	NPG better	NPG worse
N=	32	11	30	26	26
Age	66.2 (10.8)	65.5 (5.54)	63.6 (4.79)	64.4 (8.0)	64.4 (8.0)
Follow up	5.7 (0.85)	6.0 (0.56)	6.2 (0.52)	5.8 (0.73)	5.8 (0.73)
MD start	+0.35 (1.18)	-0.73 (2.12)	-0.75 (1.09)	-0.12 (1.23)	-6.16 (5.09)
MD end	+0.30 (1.64)	+0.25 (2.03)	-2.82 (1.88)	-0.37 (1.63)	-6.54 (9.02)
CPSD start	0.88 (0.72)	1.39 (1.43)	1.64 (0.86)	1.33 (1.21)	7.27 (4.56)
CPSD end	0.96 (0.51)	1.90 (1.92)	4.02 (1.27)	1.82 (1.07)	9.93 (3.51)
Rim area start	1.48 (0.30)	1.26 (0.30)	1.30 (0.35)	1.21 (0.35)	1.10 (0.37)
Rim area end	1.49 (0.30)	1.22 (0.34)	1.24 (0.26)	1.17 (0.33)	1.10 (0.38)
Disc area	1.92 (0.39)	1.90 (0.35)	1.83 (0.43)	1.99 (0.34)	2.01 (0.42)

TABLE 11.1 Subjects' demographics. OHT=ocular hypertension, OHT convert=ocular hypertension converters, NPG better=suspected NPG, NPG worse=established NPG. Values in the table are for mean and standard deviation (SD). Units for visual field indices (MD and CPSD) are dB, and for optic disc parameters (rim area and disc area) are mm^2.

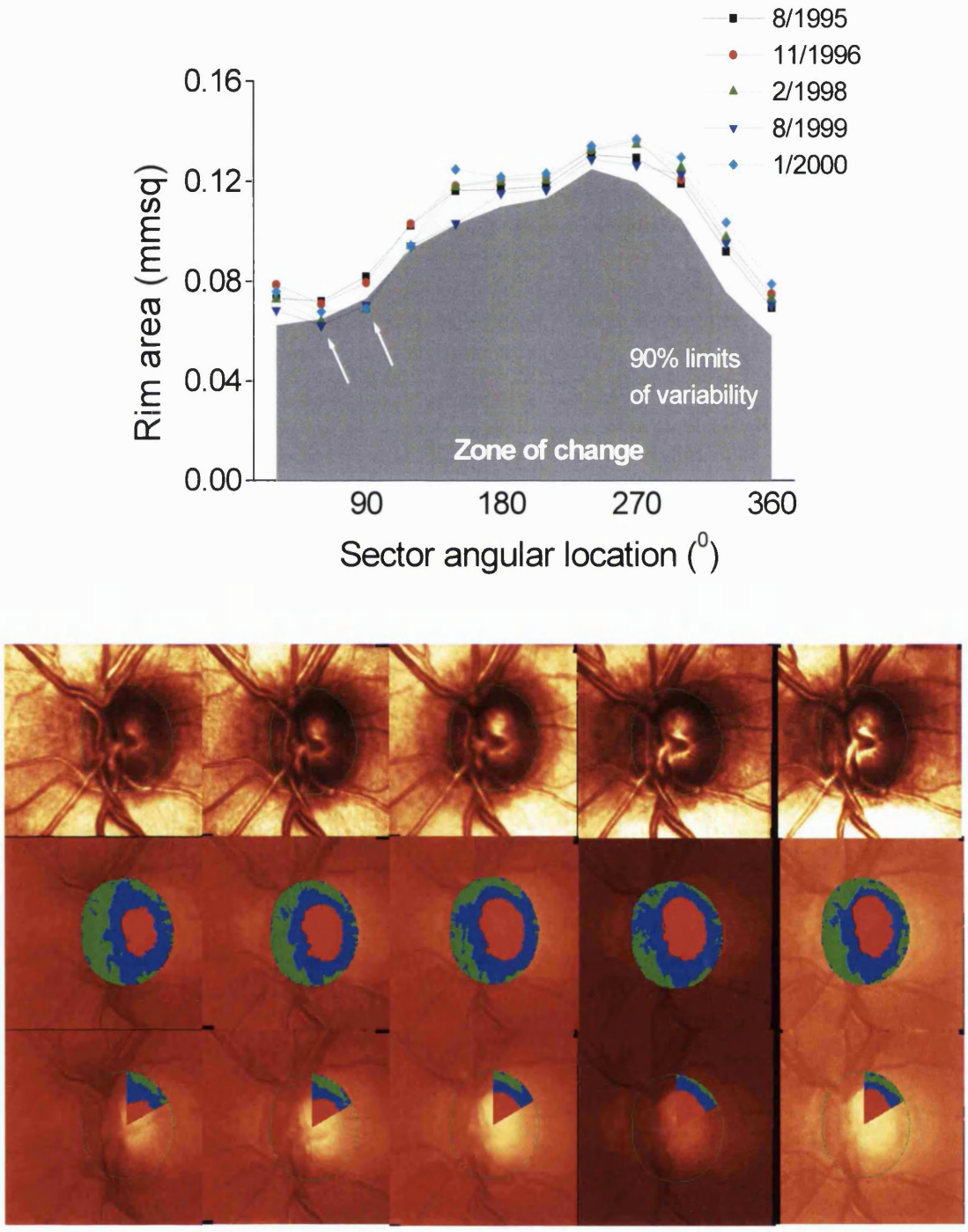

FIGURE 11.1. Progressive rim loss in ocular hypertension. Two superior-temporal sectors, 30-60 and 90-120° have exceeded their 90% limits of variability repeatedly (*arrows in graph*), and the cup has enlarged to become more vertically elongated. 90% limits of variability form the upper extent of the zone of change.

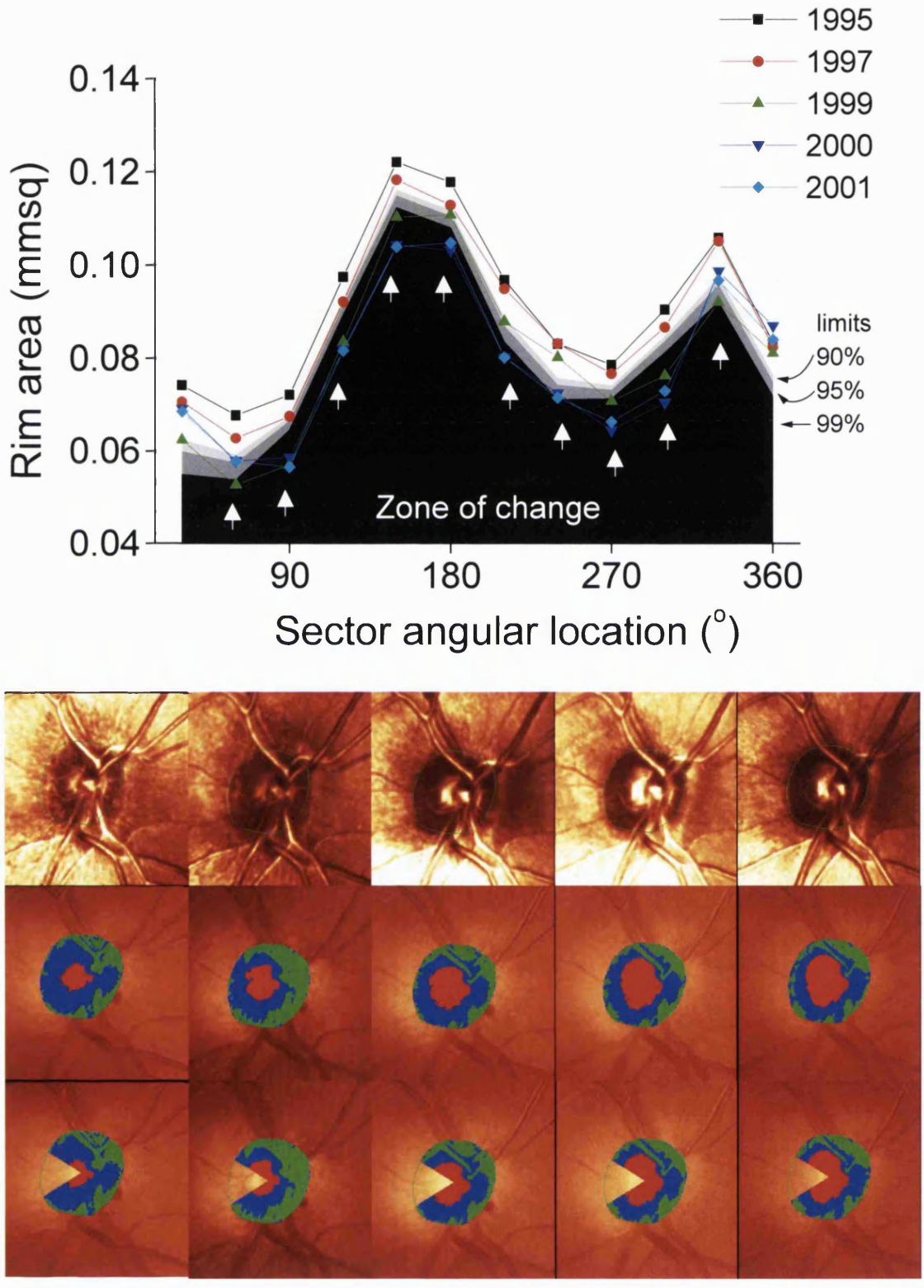

FIGURE 11.2. This optic nerve of an eye with ocular hypertension had diffuse rim loss over time repeatably exceeding the 90% limits of variability (*arrows*), with only two temporal-horizontal sectors remaining without confirmed change. Many sectors have met the criterion for change by the stricter 99% limits of variability. The cup is seen to enlarge concentrically.

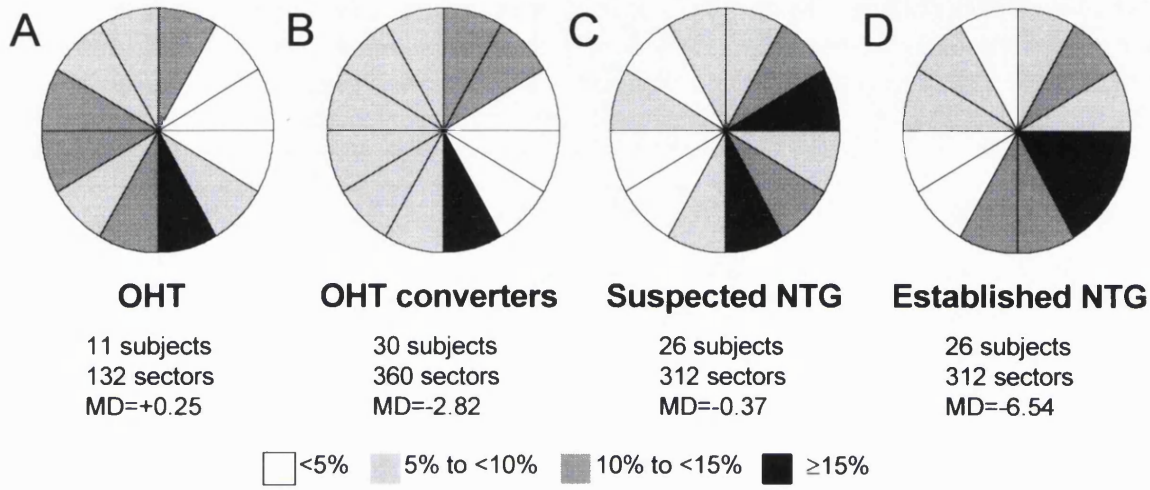

FIGURE 11.3. Frequency distribution of rim area sectors having change exceeding the 90% limits of variability and meeting the 2-of-3 criterion. *A*) Ocular hypertension, *B*) ocular hypertension converters, *C*) suspected NPG, *D*) established NPG. Each sector is greyscale-coded to indicate the frequency with which confirmed change was detected in the sector as a proportion of all tested sectors (r): *white*: r<5%, *light grey*: 5%≤r<10%, *dark grey*: 10%≤r<15%, *black*: 15%≤r. *For each schematic: left*=nasal, *right*=temporal. Mean visual field MD at final follow up for each group is shown as 'MD'. Number of sectors for each group is the total number of sectors identified as changed among all of each group's subjects' eyes.

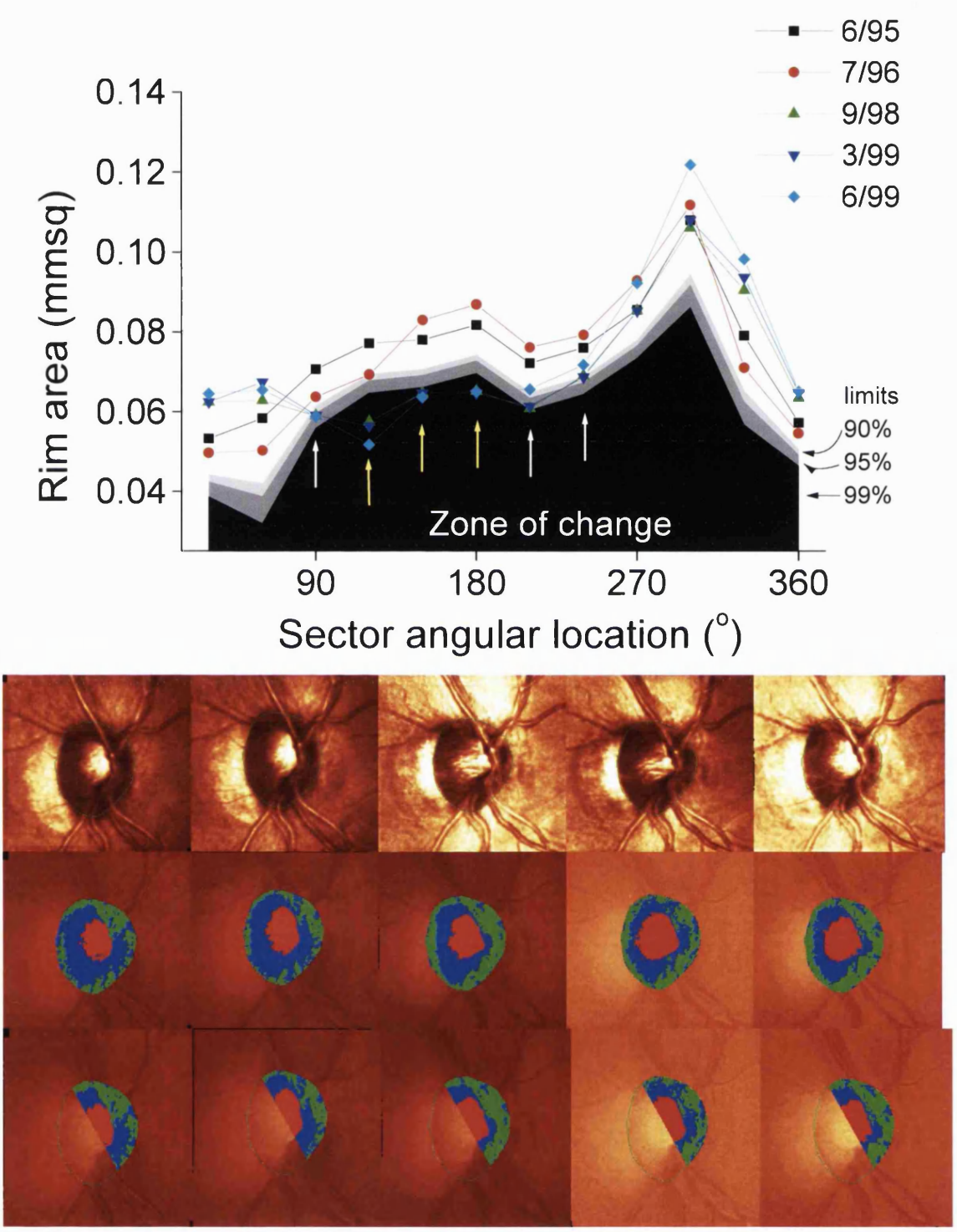

FIGURE 11.4. Predominantly nasal rim loss identified in an ocular hypertension converter. Six sectors (*arrows*) have repeatedly exceeded the 90% limits of variability. A sector at 210-240° has exceeded only the 90% limit of variability (*last arrow*) to meet the 2-of-3 criterion, while sectors at 60-90° and 180-210° have met the criterion for the 95% limits of variability. Other sectors have met the criterion for the stricter 99% limits of variability (*yellow arrows*). The cup, which is initially vertically oval, becomes rounder over time, reflecting change that is greater in the disc's horizontal axis than vertically. Such change may conceivably be mistaken as being concentric when judged subjectively.

nasal-horizontally (150-210°), but temporal-horizontal change was rare.

Repeatable rim change was identified in 27/30 *ocular hypertension converters*. **Figure 11.4** is an example of a converter eye. **Figure 11.3 B** shows that rim change was most frequently in the inferior pole (270-300°), followed by superotemporally between 30-90°. 42% (13/31) had change nasal-horizontally (150-210°), but change temporal-horizontally (330-360°, 0-30°) was rare. 23/30 (77%) of converters had nasal visual field defects, while 2/30 (6.7%) had paracentral field defects.

In *suspected NPG*, rim change was identified in 15/26 (58%) of eyes. 5/26 eyes (19%) developed reproducible field abnormality over follow-up and were considered NPG converters; visual fields of the other 21/26 eyes remained normal throughout. **Figure 11.5** shows widespread temporal progression, and also inferior and inferonasal change in a subject who retained normal visual fields. **Figure 11.3 C** shows that change in suspected NPG was most frequently in the inferior pole (270-300°) and temporal-horizontally (0-30)°. Nasal change was relatively uncommon.

Of *NPG converters*, repeatable rim change was detected in 3/5 eyes; **Figure 11.6** shows one of the NPG converters who had tentative change but insufficient follow up data for confirmation. 3/5 (60%) NPG converters developed paracentral defects at conversion. **Figure 11.7** and **Figure 11.8** are other examples of NPG converter eyes.

In established NPG, 14/26 (54%) of eyes had repeatable rim change. **Figure 11.3 D** shows that change was most frequent inferotemporally (300-330°) and temporal-horizontally (330-360°), followed by superotemporally (30-60°) and in the inferior pole (240-300°). **Figures 11.9 and 11.10** show examples of change in eyes with established NPG that were identified as having changed. As in suspected NPG, but unlike ocular hypertension and ocular hypertension converter eyes, nasal change was relatively infrequent.

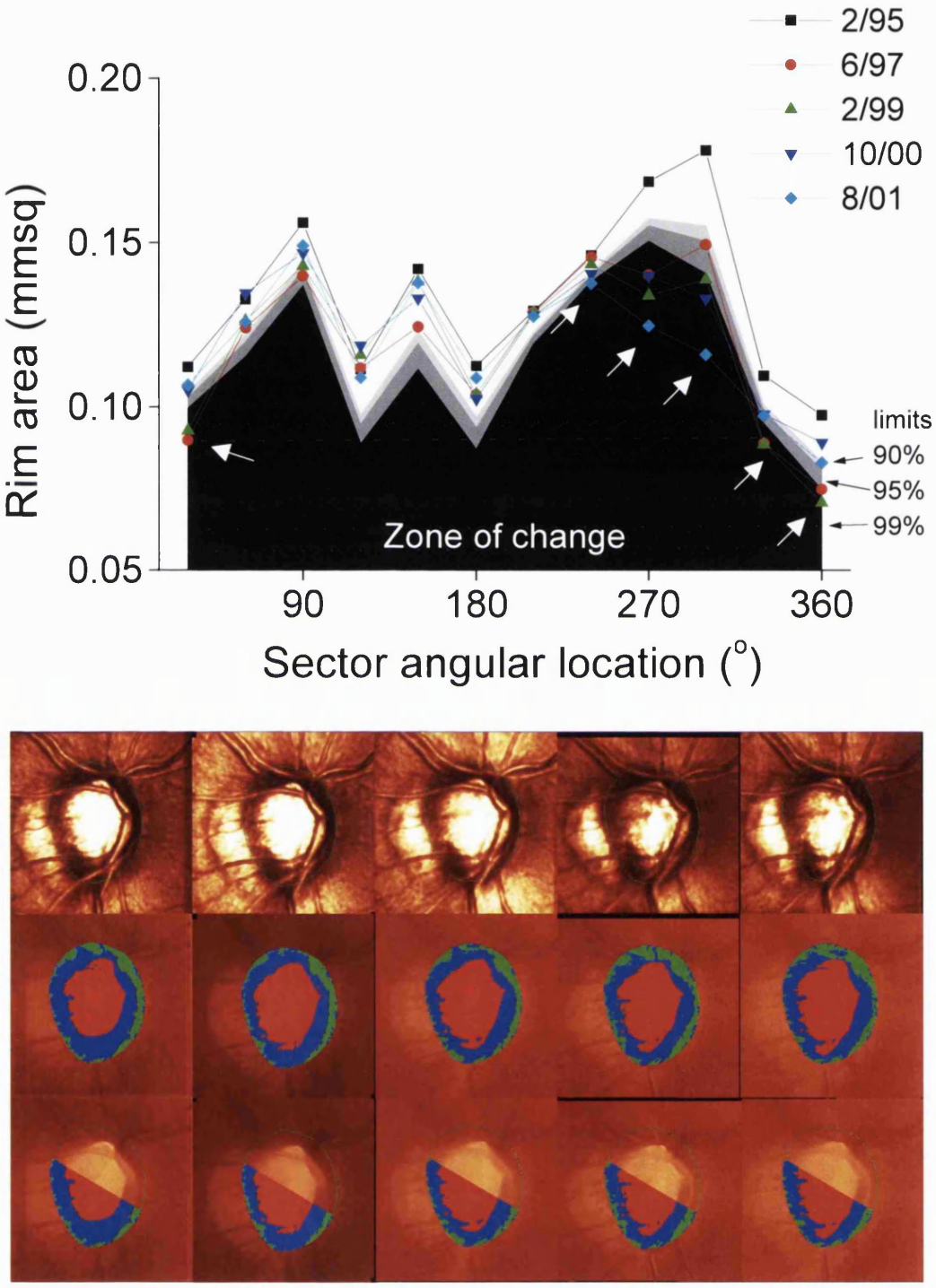

FIGURE 11.5. This suspect NPG eye has reproducible rim area loss exceeding the 95% limits of variability in seven inferior and temporal sectors (*arrows*); six of these sectors have also repeatedly exceeded the 99% limits of variability.

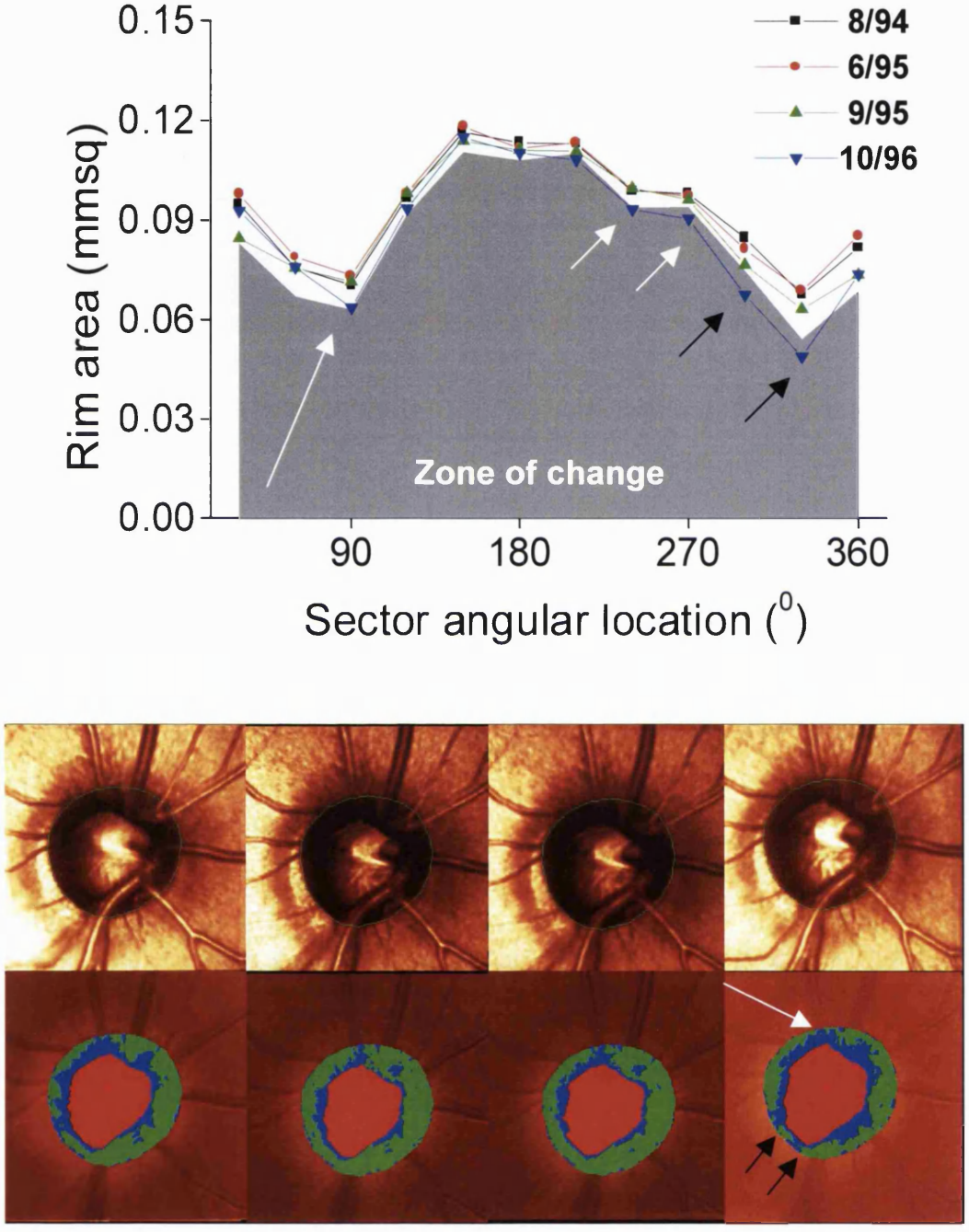

FIGURE 11.6. Analysis of an NPG converter whose tentative rim loss could not be confirmed because of insufficient follow-up data. Suspicious rim change inferiorly between 210-330° (*short arrows in graph*) was suggested by the final (1996) rim area profile exceeding its 90% limit of variability. Change between 270-330° (*short black arrows in graph and image*) is sequential and also most marked, and is especially apparent in the upper row of topography images. One superior sector at 90° also shows tentative change (*long arrows in graph and image*). 90% limits of variability mark the upper limit of the zone of change.

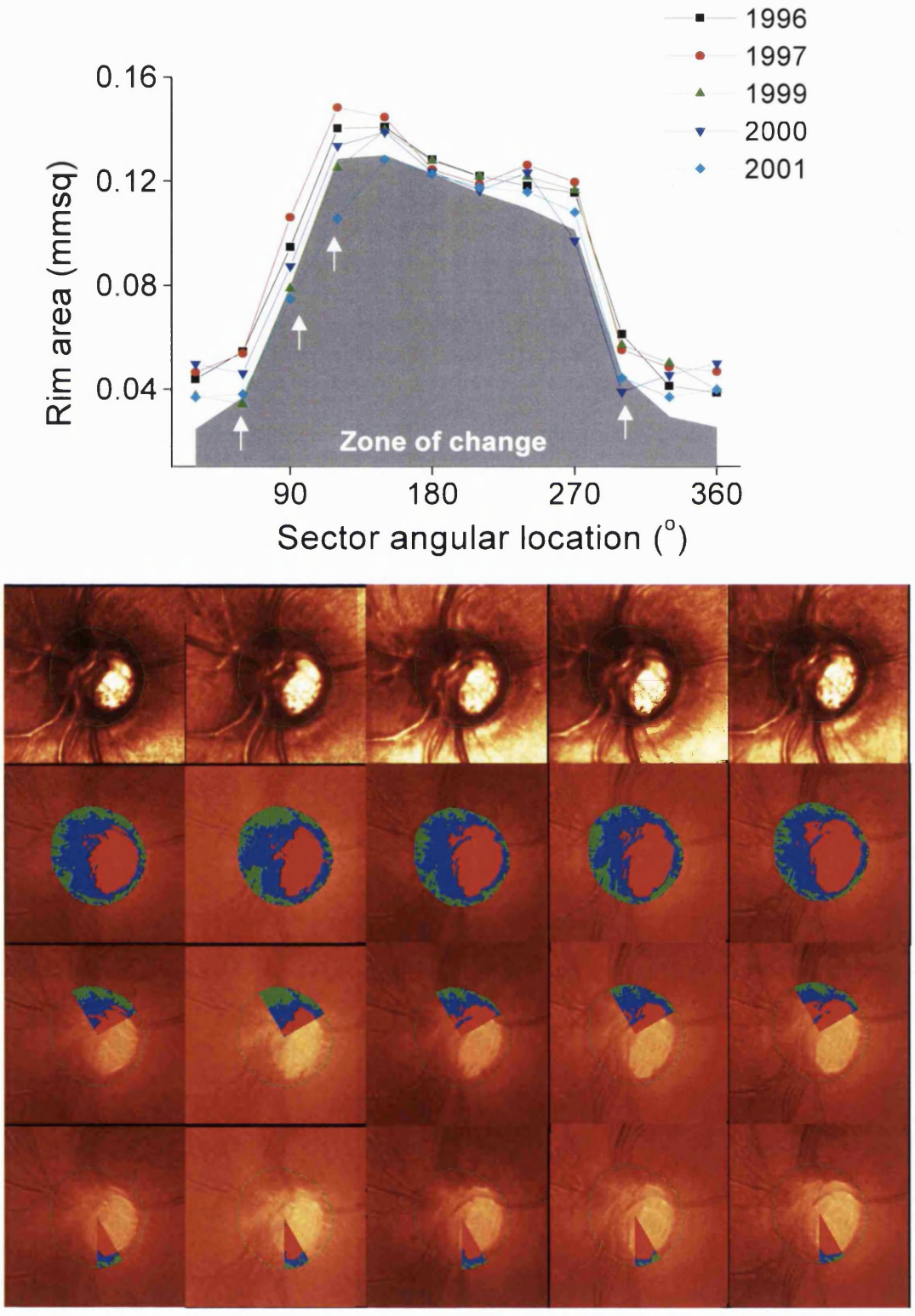

FIGURE 11.7. This NPG converter eye has confirmed rim change (*arrows*) superotemporally (30-90°) and supranasally (90-120°), and in one inferotemporal sector (270-300°). 90% limits of variability form the upper extent of the zone of change.

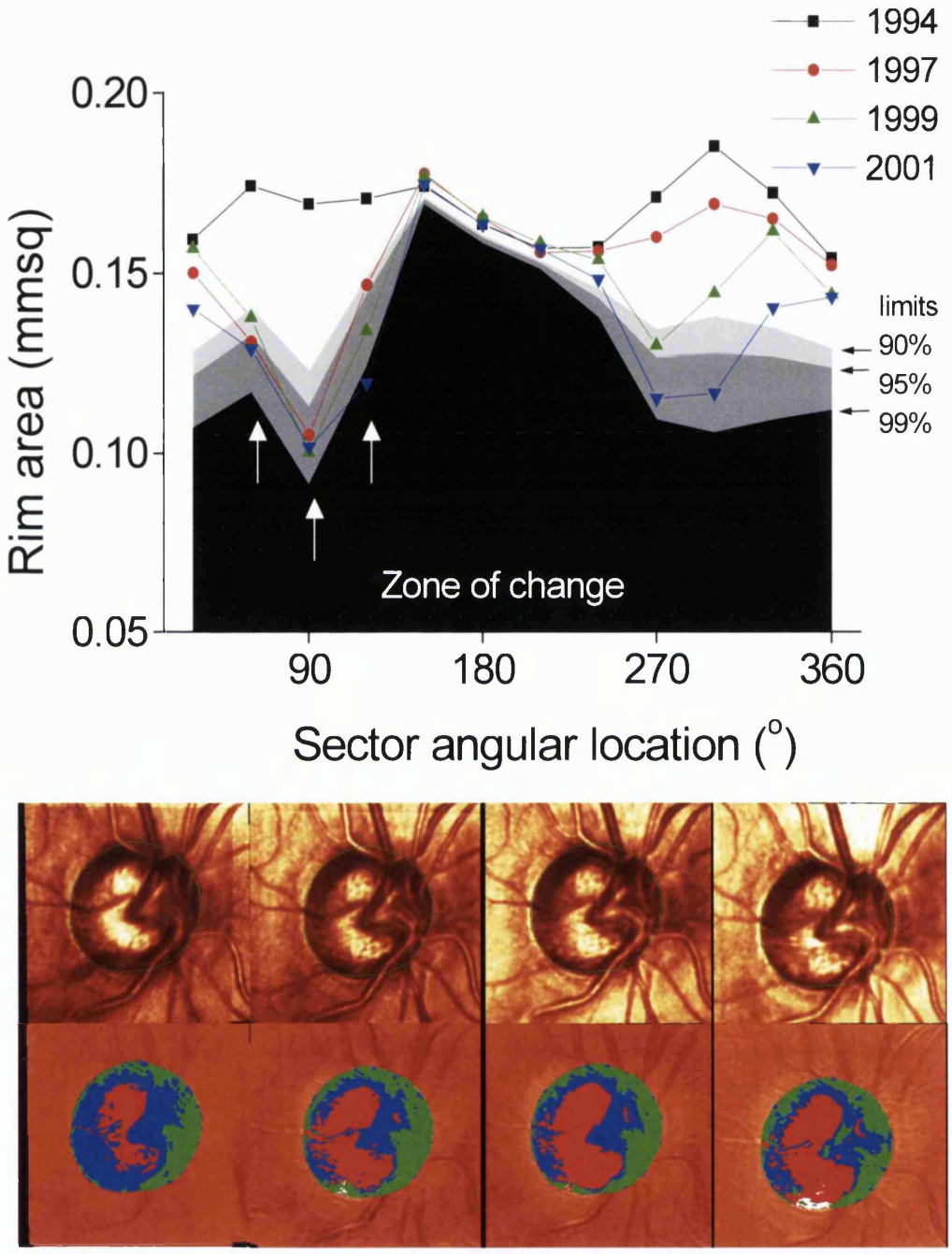

FIGURE 11.8. This NPG converter eye with high image variability has reproducibly decreased rim area exceeding the 90% limits of variability in four sectors in the superior (30-120°) and inferior (240-270°) disc poles. Limits of variability are wide in the temporal half of the disc, especially in the poles, as is also suggested by the images. The apparently large change in rim profiles should be interpreted relative to variability: although the profiles are markedly reduced, the wide limits of variability mean that only three superior sectors meet the 2-of-3 criterion for the 95% limits of variability (*white arrows in graph and image*) and no sectors are confirmed as changed for the more stringent 99% limits of variability.

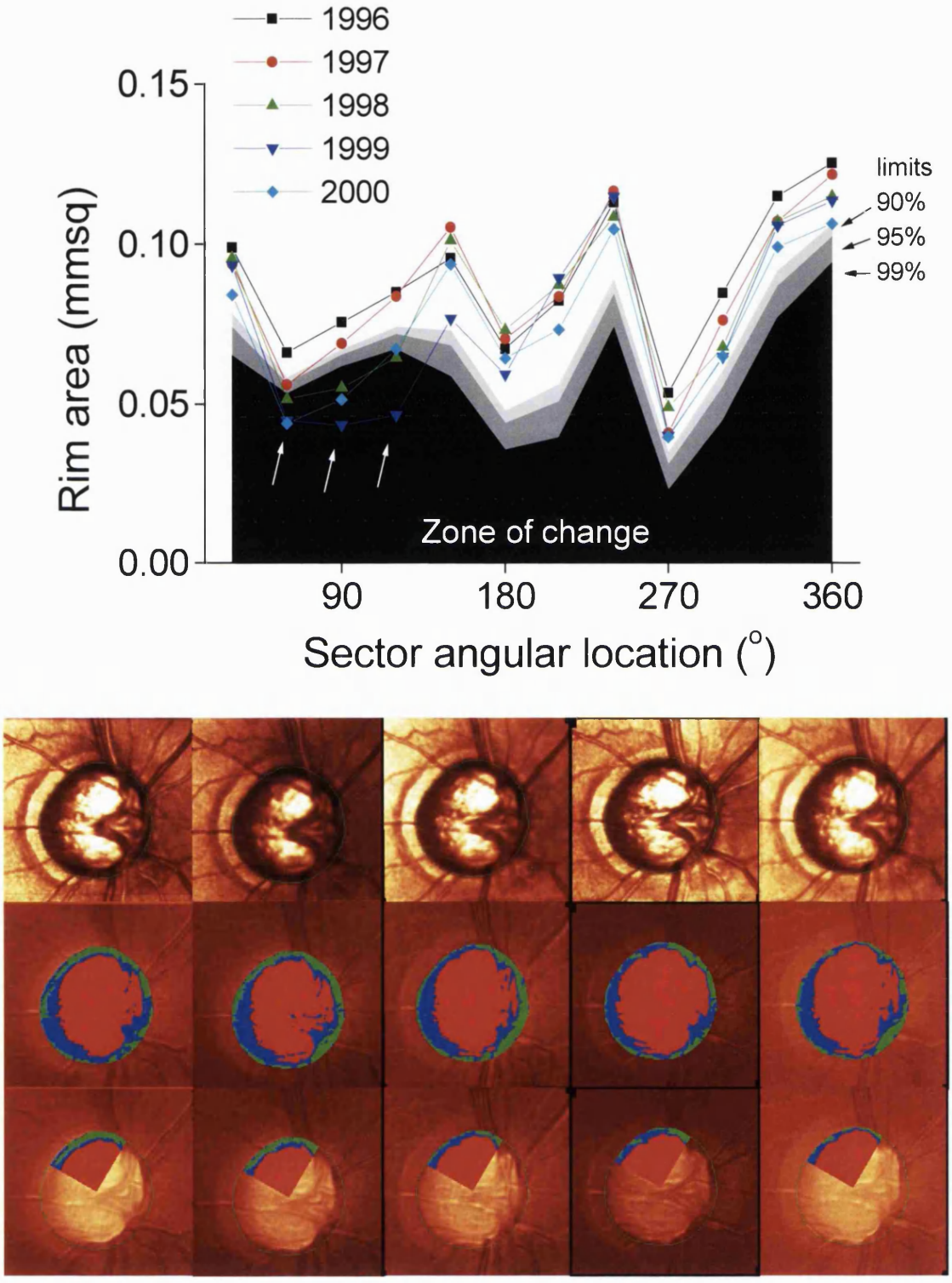

FIGURE 11.9. Three superior rim sectors (*arrows*) in this eye with established NPG and large disc cupping have exceeded the 99% limits of variability and met the 2-of-3 criterion. Several sectors elsewhere are sequentially reduced over time (especially inferiorly and nasally) but have not exceeded the 90% limits of variability. In the images, rim area variability is seen nasally and inferiorly as tufts of blue representing blood vessels cut by the reference plane at slightly different levels, which may be affecting the statistical detection of change here.

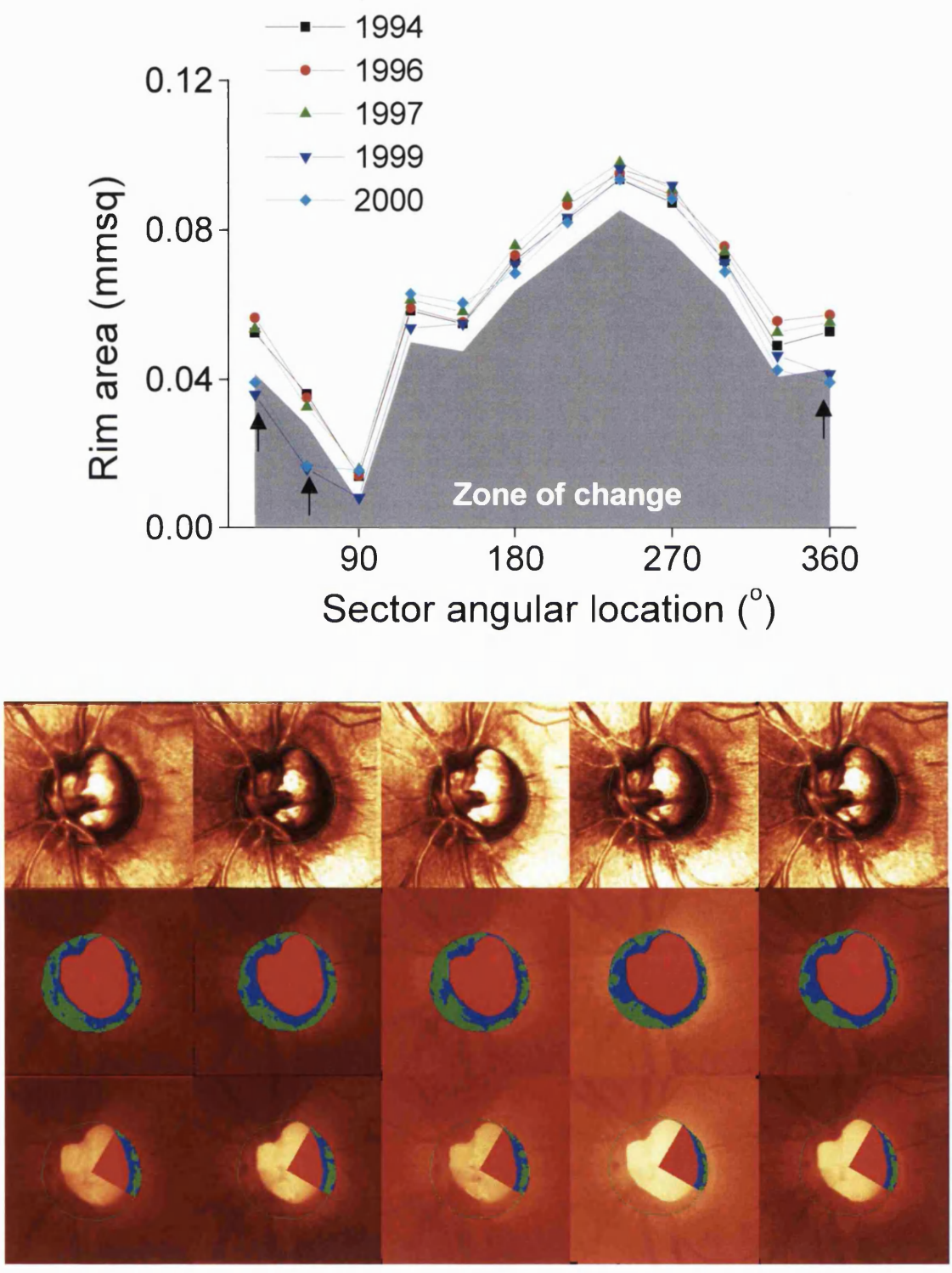

FIGURE 11.10. This eye with established NPG and large disc cupping has reproducible change temporally (*arrows*). 90% limits of variability mark the upper limit of the zone of change.

11.1.2.3 Cross-sectional analysis of groups at baseline and final follow up

Figures 11.11 A-D show the magnitude of *rim area deviation from normal* per sector for diagnostic groups at baseline (**1**) and at final follow up (**2**). **Figures 11.12 A-D** show the probability of rejecting the null hypothesis of true deviation for each sector.

In Figure 11.11, all groups had more sectors with large (black sectors) or moderate (dark gray) deviations at final follow up than at baseline. This was most marked in ocular hypertension converters (B), suspected NPG (C) and established NPG (D). There was a propensity for the disc poles to have large and also significant deviations in all diagnostic groups (Figure 11.12: sectors with $p \leq 0.05$). At final follow up, all groups had larger deviations and more sectors with significant deviations than at baseline.

In **Figures 11.11 and 11.12**, eyes with established NPG (D) had more sectors with large and significant deviations compared with other groups (A-C). Visual fields of established NPG eyes were also more damaged (Table 11.1: mean MD= -6.5 dB, mean CPSD=9.9dB). Sectors with large and significant deviations tended to be clustered around the superior and inferior poles (Figures 11.11D and 11.12D), but sectors clustered around the temporal-horizontal also showed large and significant deviations. 17/26 (65.3%) of eyes with established NPG had paracentral field defects; these defects were superior only in 11/17 (64.7%), inferior only in 5/17 (29.4%) and concurrently in both hemispheres in 2/17 (11.8%). In suspected NPG, rim sector deviations were smaller, and fewer were significant compared with established NPG.

All ocular hypertension (A), ocular hypertension converter (B) and suspected NPG (C) eyes had normal fields at baseline. However, suspected NPG eyes had more rim sectors with large or moderate deviations and significant deviations, especially in the disc poles, compared with ocular hypertension or ocular hypertension converters at baseline (1) and at final follow up (2) (Figures 11.11 and 11.12). This suggests that suspect NPG discs were more cupped than ocular hypertension or ocular hypertension converter discs despite their fields being similar. At final follow up, suspect NPG discs still appeared more cupped than ocular hypertension

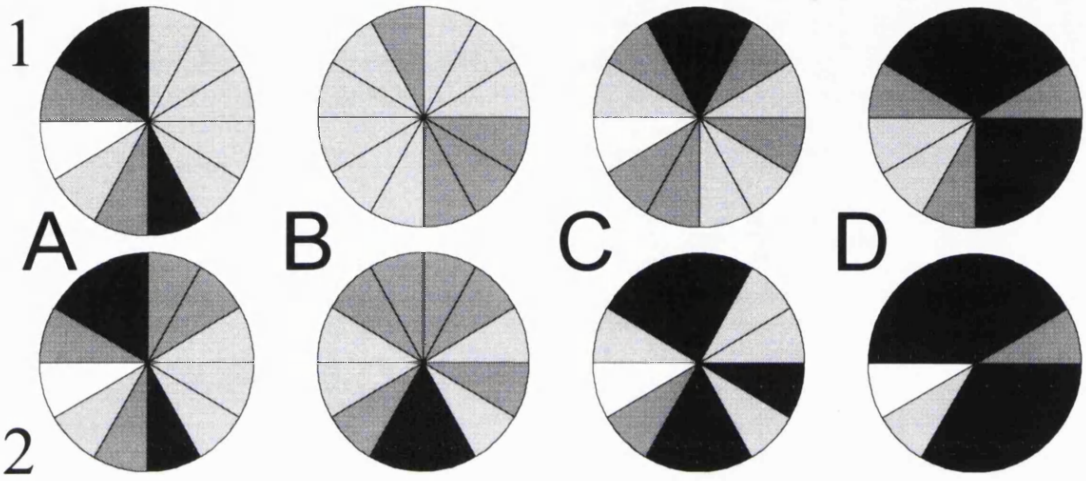

FIGURE 11.11. Schematics of the optic nerve head showing the magnitude of sector rim deviation from normal at baseline and at final follow up for each sector. *A to D:* comparison between normal eyes and A) ocular hypertension, B) ocular hypertension converters, C) suspected NPG, D) established NPG. *Rim area (negative) deviation from normal: white*: $0<D<0.0075$ mm^2, *light grey* (small): $0.0075\leq D<0.0150$ mm^2, *dark grey* (moderate): $0.0150\leq D<0.0225$ mm^2, *black* (large): $D\geq 0.0225$ mm^2. Each schematic's aspect is as for the left eye, with *left*=nasal, *right*=temporal; *1*=baseline comparison, *2*=final follow up comparison.

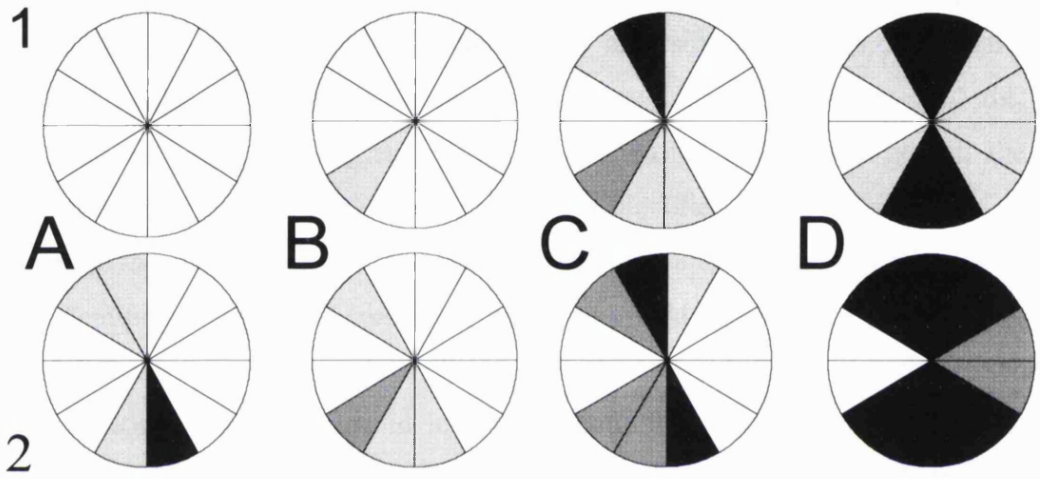

FIGURE 11.12. Schematics of the optic nerve head showing statistically significant deviations in rim area point-estimates at final follow up compared with baseline for each sector in ocular hypertension, ocular hypertension converters, NPG suspects and established NPG. *A to D:* comparison between normal eyes and A) ocular hypertension, B) ocular hypertension converters, C) suspected NPG, D) established NPG. *Probability of rejecting the null hypothesis for significant deviation: white*: $p>0.05$, *light grey*: $0.01<p\leq0.05$, *dark grey*: $0.005<p\leq0.01$, *black*: $p\leq0.005$. Each schematic's aspect is as for the left eye, with *left*=nasal, *right*=temporal; *1*=baseline comparison, *2*=final follow up comparison.

converters; this was despite all ocular hypertension converters having developed field defects but most suspected NPG eyes (21/25 or 81%) having retained normal fields. Reanalysis after removing the 5/26 NPG converter eyes yielded a similar result.

11.1.3 Discussion

The approach for identifying progressive rim loss has been tested in eyes with different clinical presentations of glaucoma, as defined by intraocular pressure and visual field status. Based on longitudinally analysing the images of normal controls and ocular hypertension converters by 90% limits of variability and the 2-of-3 criterion, and assuming no change in the former and progression in the latter, repeatable rim loss could be considered as identified with a sensitivity of 90% and false positive rate of 6.2%. By the same analytical approach, rim change was identified in 3/5 NPG converters developing field defects. In eyes with established NPG and moderately severe disease, rim change was identified in 54%. Repeatable rim loss was also detected in eyes without field abnormalities: 11% (11/97) of ocular hypertension eyes and 57% (12/21) of suspect NPG eyes that retained normal fields. Patterns of change were then documented in the various diagnostic categories.

The longitudinal and cross-sectional analyses agreed that similar patterns of rim change were seen in ocular hypertension and ocular hypertension converters having 'early' glaucoma. Rim change was frequently detected in the disc poles, especially inferiorly, and is consistent with a pattern of the cup elongating vertically. These findings concur with longitudinal (Sommer et al, 1980; Airaksinen et al, 1992) and cross-sectional (Read and Spaeth, 1974; Kirsch and Anderson, 1973a; Jonas et al, 1993a) photographic studies of the disc in ocular hypertension and conversion. Preferential rim loss at or near the disc poles has been associated clinically with the common location of disc haemorrhages (Airaksinen et al, 1981a; Jonas and Xu, 1994), localised nerve fibre layer atrophy (Airaksinen et al, 1981b) and early field defects (Heijl and Lundqvist, 1983), and histologically with the configuration of lamina cribrosa pores (Quigley et al, 1983; Pederson and Gaasterland, 1984).

That concentric cupping may be relatively common in ocular hypertension converters (Pederson and Anderson, 1980; Tuulonen and Airaksinen, 1991) was reflected in our findings too. The not uncommon pattern of nasal rim loss seen in ocular hypertension and ocular hypertension converters suggests that cupping did not occur solely vertically. Still, the overall pattern of change would have been strongly influenced by the preponderance of rim loss in the disc poles. Also, as the normal cup tends to be horizontally oval, more vertical than horizontal rim tissue would have to be lost for cupping to appear concentric in 'early' disease (Spaeth, 1993; Airaksinen et al, 1996). Thus, initially, cupping that appears concentric may actually be due to vertical rim loss exceeding horizontal loss. Such loss may not be easy to detect by subjective assessment, however (Airaksinen et al, 1996), as illustrated in Figure 11.1 and 11.7. Likewise, in Figure 11.4, localised superior and nasal rim loss may be perceived as concentric cupping.

Some patterns were common to all groups. As with high-pressure presentations (ocular hypertension and ocular hypertension converters with IOP>21mmHg), both NPG groups (suspected and established) had relatively frequent rim change that was moderate to large and also significant in the disc poles, especially inferiorly. Patterns of change were similar within high-pressure groups, whether or not field defects were present, and the same was true within normal-pressure presentations. Repeatable rim loss was identified in similar proportions of eyes with suspected NPG and established NPG (between 50-60% of eyes). But there were some differences. Unlike high-pressure presentations, NPG rim loss was common in the temporal disc but not nasally. This was seen both in the individual and group analyses. It could be that the relatively large and frequent temporal rim change in established NPG was due to disease being more severe (mean MD= -6.5 dB, mean CPSD=9.9dB), as Jonas et al (1993a) suggest. NPG suspects, however, had baseline fields that were normal and equivalent to those of ocular hypertension and ocular hypertension converter eyes, and yet they still had relatively frequent temporal rim loss. The temporal rim changes in NPG seemed to correlate with what was observed of their visual fields: paracentral field defects were found at conversion in 3/5 NPG converters, but only 2/30 (6.7%) ocular hypertension converters. Ocular hypertension converters had predominantly nasal field defects (77%). 65% of eyes with established NPG had paracentral field defects. Several investigators have found that field defects tend to be closer to fixation in NPG than in POAG (Levene,

1980; Gramer et al, 1986; Hitchings and Anderton, 1983; Caprioli and Spaeth, 1984), and even in suspected NPG compared with ocular hypertension (Poinoosawmy et al, 1995). Also, the present study found that sector rim area deviations from normal were larger and more often significant in suspected NPG than in ocular hypertension or ocular hypertension converters, suggesting that suspected NPG discs were more cupped despite the groups having similar baseline fields. Other investigators have reported more cupping in NPG than POAG for the same amount of field damage (Levene, 1980; Gramer et al, 1986; Caprioli and Spaeth, 1985; Fazio et al, 1990).

Using an objective analytical approach for detecting progressive rim loss, common patterns of change were observed within high-pressure and normal-pressure presentations of glaucoma. In comparing groups, there were apparent similarities but also differences that seemed to correlate with previously published findings. The approach identified progression in glaucoma suspect eyes without visual field defects, eyes that progressed to develop field defects, and eyes with established and more severe glaucoma.

11.2 REVERSAL OF OPTIC DISC CUPPING AFTER IOP REDUCTION

Disc photography and scanning laser tomography have been used to study 'reversal of cupping' across groups of people after therapeutically-lowered IOP, but what happens in individual eyes over time is not as well characterised. It is also not clear whether or how long such reversal persists when measured by scanning laser tomography. Irak et al (1996) found that the reversal of disc topographic parameters persisted till at least three months after filtration surgery. Kotecha et al (2001) reported that rim area and rim volume were not significantly raised above baseline at three months and one year post-operatively but they were at two years post-operatively. Topouzis et al (1999) found that initial reversal in cup volume, mean cup depth and cup shape measure was not significantly different from baseline at four and eight months after surgery. Greenidge et al (1985) photographically documented reversal that persisted beyond two years.

Most patients are treated medically and so it would be useful to know what happens to reversal of cupping over time after IOP is lowered by topical medication. Subjects with ocular hypertension and glaucoma in whom IOP was lowered medically and sustained at at least 25% below baseline for at least a year were evaluated for reversal of cupping.

11.2.1 Investigations

11.2.1.1 Subjects

Serial images of one eye each of 40 subjects – 10 with ocular hypertension, 10 with POAG and 20 normal controls – were evaluated. IOP had been lowered by topical medication (levobunolol or latanaprost) and sustained at at least 25% below baseline for one year. Subjects had been imaged at least three times over this period. Twenty normal controls were similarly imaged over a period equivalent to that of the treated subjects. Subjects' criteria for selection are decribed in Section 5.1. Only one eye of each subject was analysed. Optic disc appearance was not considered for entry into this study. **Table 11.2** shows their demographics.

11.2.1.2 Analysis of rim area to detect change

The analytical approach described in Chapter 10 was used to analyse the area of rim sectors for change. However, to identify progressive enlargement of the neuroretinal rim rather than progressive rim loss, the approach was modified so that analysis to detect change was by the upper instead of lower limits of variability. Variability was defined by 90% confidence limits. Upper limits of variability were plotted relative to the baseline rim area profile so that changes in sector rim area exceeding variability could be identified. Elevation of part or all of a follow up profile to exceed upper 90% limits of variability was tentatively taken to represent increased regional or global rim area respectively. But to be attributed to true reversal of cupping, measured change in a sector had to repeatably exceed the upper limits of variability in two of three consecutive tests.

Mean (SD)	Ocular hypertension	Glaucoma	Normal controls
Age (years)	65.7 (5.3)	63.3 (4.6)	67.0 (9.5)
Rim area before treatment (mm^2)	1.39 (0.33)	1.31 (0.33)	1.50 (0.30)
Visual field MD (dB)	+0.21 (2.12)	-3.22 (1.98)	+0.12 (0.88)
Visual field CPSD (dB)	1.80 (1.72)	4.23 (1.34)	0.88 (0.47)
Initial IOP reduction (mmHg)	13.5 (4.7)	11.0 (4.3)	-
Initial %IOP reduction	38.2 (9.5)	33.2 (7.3)	-

Table 11.2. Subjects' demographics. *Number of subjects*: ocular hypertension=10, glaucoma (POAG)=10, normal controls=20. Values in the table are for mean and standard deviation (SD).

11.2.2 Results

All treated subjects were imaged within six months of medical treatment to lower IOP, with most having been imaged within four months. Change in global rim area in the first post-treatment image was not correlated with absolute ($r=0.24$, $p=0.32$) or percentage ($r=0.088$, $p=0.71$) IOP reduction.

Thirteen of 20 (65%) treated eyes (POAG or ocular hypertension) had at least one sector exceed their upper 90% limits of variability following IOP lowering; 7/13 of these eyes had a diagnosis of ocular hypertension. Six of 20 (30%) normal control subjects had at least one sector exceed their upper 90% limits of variability over the equivalent period of follow up.

A total of fifty sectors from across all treated eyes (21% of tested sectors) had change exceeding their upper limits of variability at least once, compared with nine sectors across all normal control eyes (4% of tested sectors). **Figure 11.13** shows the frequency distribution of sectors that exceeded their upper limits of variability at least once following IOP reduction. In treated eyes, the majority of such sectors were located in the nasal half of the optic disc (between 90-270°).

Of the treated eyes, 6/20 (30%) had at least one sector exceed its limit of variability repeatedly to meet the 2-of-3 criterion; a total of 18 sectors met this criterion. This reproducible change persisted at one year in 14 sectors of four treated eyes, of which three eyes had a diagnosis of POAG. All sectors with persistent change were identified to be in the nasal half of the disc. **Figure 11.14** shows an example of an eye in which rim area increased after IOP reduction and persisted at one year. No sectors in normal controls exceeded their upper 90% limits of variability repeatedly to meet the 2-of-3 criterion. No sectors were seen to decrease to repeatably exceed their lower 90% limits of variability in either the treated or control eyes.

11.2.3 Discussion

This study identified and characterised reversal of cupping following IOP reduction longitudinally in individual eyes rather than cross-sectionally across groups of eyes. Following IOP reduction that was sustained at at least 25% below baseline, rim area increased and exceeded measurement variability on single tests in twice as many

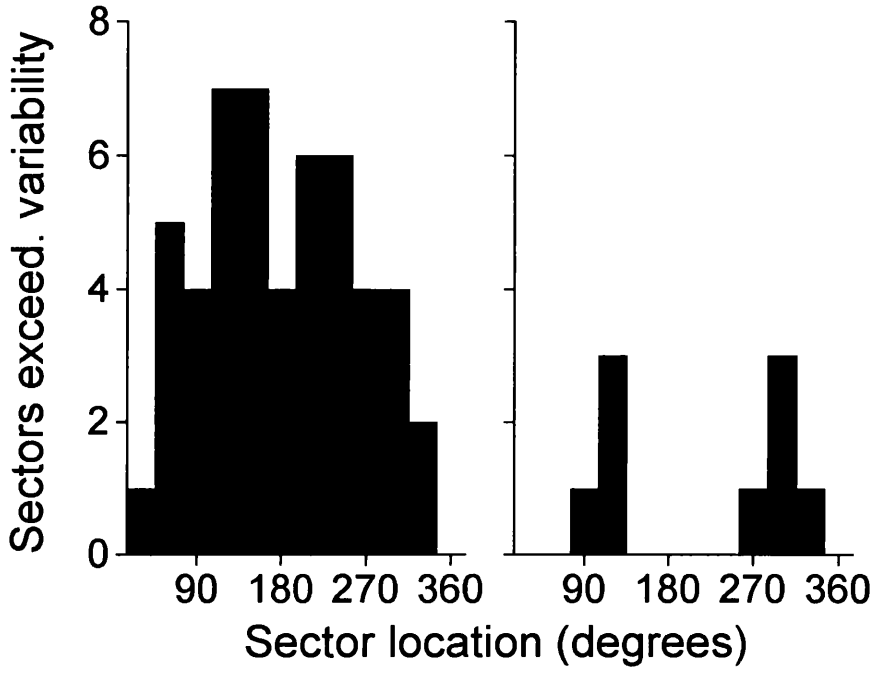

FIGURE 11.13. Frequency distribution of rim area sectors that exceeded their upper limits of variability at least once after IOP was reduced compared with control data. *Bar graphs*: *Left*=treated eyes, *right*=normal controls. *Sectors: 0°=temporal, 90°=superior, 180°=nasal, 270°=inferior*

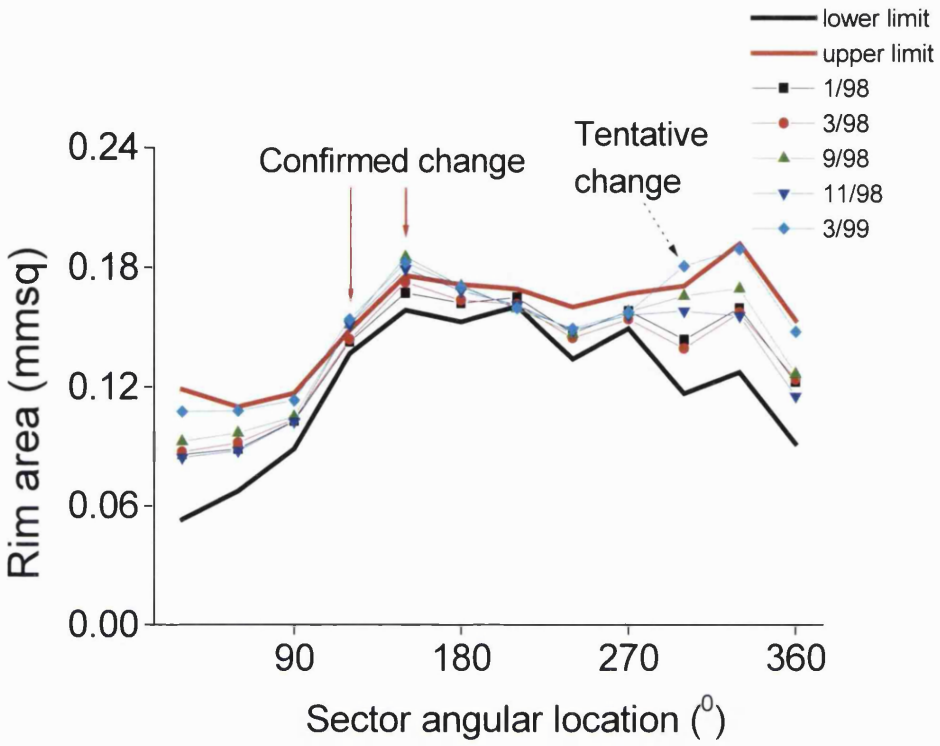

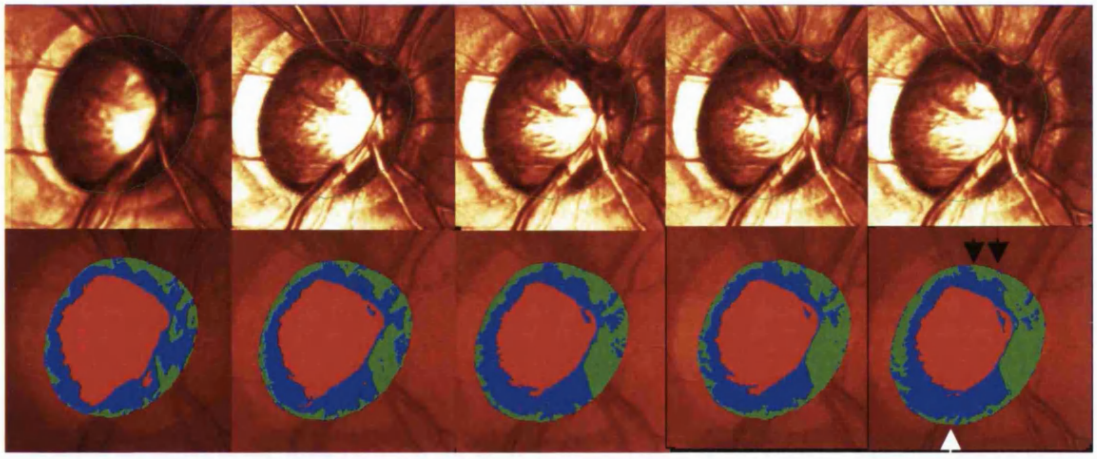

FIGURE 11.14. Increased rim area persisting beyond one year in an ocular hypertension eye treated after 'conversion' to POAG. This converter's nerve is the same as that illustrated as having progression in Figure 10.10. The converter was classified as POAG in the present study of reversal of cupping. Reproducibly increased rim area is seen superonasally (*black arrows in image*). Change seen inferiorly (270-300°, *white arrow*) is only tentative, mainly because of higher variability here and inadequate follow up data for verification. Height of the 'rim' surrounding the cup appears to have increased over time so that more tissue is defined as neuroretinal rim by the reference plane.

treated eyes (POAG or ocular hypertension) as normal control eyes. The number of sectors exceeding their limits of variability was five times more frequent in treated eyes compared with controls. Fewer false positives can be expected if change can be demonstrated to be repeatable: the '2-of-3' criterion was used to confirm change and it was found that 30% of treated eyes (six eyes) had at least one rim sector increased in area following IOP lowering. Change persisted beyond one year in 20% of treated eyes (four eyes). By contrast, no control eyes had reproducibly increased rim area following IOP reduction.

It is possible that more eyes would have been detected as having increased rim area following IOP reduction if imaging had been more frequent. Image series comprised images taken three to six months apart, and so it is possible that a proportion of eyes having initially increased rim area may have had this increase regress in the interval between imaging. Reproducibly increased rim area was seen in 6/20 (30%) treated eyes, but change in 2/6 of these eyes subsequently regressed over follow up so that even if any change lingered, it was indistinguishable from measurement variability. Likewise, some immediate reversal of cupping might well have regressed unnoticed in the time between starting treatment and the first post-treatment image in this study.

Previous studies using scanning laser tomography to assess reversal of cupping have defined topographic parameters such as rim area or rim volume by the standard reference plane (Irak et al, 1996; Topouzis et al, 1999; Lesk et al, 1999; Bowd et al, 2000; Kotecha et al, 2001). Kotecha et al (2001) reported that rim area and rim volume were significantly increased above baseline at two years post-operatively, but not at three months and one year postoperatively. But Topouzis et al (1999) found that initial enlargement and deepening of the cup after filtration surgery did not persist beyond four to eight months. It could be that persisting or slowly evolving nerve changes in response to reduced IOP reflect underlying gradual micro-structural or cellular changes, as has been suggested by Minckler et al (1976b), Anderson and Hendrickson (1974) and Shaffer (1969). However, that IOP reduction could have affected topography and shifted the reference plane to influence HRT measurement of the rim and cup should be considered. For instance, IOP is suggested to affect the compliance and position of the optic nerve head and lamina cribrosa (Burgoyne et al, 1995a; 1995b; Zeimer and Ogura, 1989; Quigley,

1977; Azuara-Blanco et al, 1998), and its effect on topography could unpredictably influence the reference plane's position in three-dimensional space and relative to the optic nerve head. Chen et al (2001) have suggested that the standard reference plane may shift with topographical change due to glaucoma; the author's own studies show that fluctuation from test to test in the position of the optic nerve head, reference plane or both can itself affect measurement (Chapters 7, 8 and 9). Analysis of reversal of cupping in the present study was by the experimental reference plane, which is positioned and customised to each eye to maintain an unchanging height relationship with the optic nerve head. The foregoing data in Chapter 9 suggests that this arrangement should help minimise possible measurement artifact caused by IOP variation.

Kotecha et al (2001) reported that initially increased rim volume following reduced IOP tended to persist superotemporally and in the nasal half of the optic nerve head, and suggested that persistent reversal occurred in regions of the optic nerve head that were least damaged. The present study found increased rim area most often in the nasal half of the optic nerve head too, and sectors that still remained enlarged one year after IOP reduction were also all located nasally. It has been postulated that reversal of cupping due to IOP lowering could be caused by increased intravascular volume (Greendige et al, 1985; Shin et al, 1989; Katz et al, 1989; Schwartz et al, 1985; Hayreh, 1976), and could well explain in part our observation of increased rim in the nasal disc following IOP reduction. Main branches of the central vessel trunk tend to lie in the nasal disc region, often adjacent to or on nasal neuroretinal rim. As HRT analysis includes vessels lying above the topographical z-axis level of the reference plane as part of neuroretinal rim, it is possible that rim area or rim volume may appear larger, especially nasally, if intravascular volume is increased.

About a third of treated eyes in this study had confirmed reversal of cupping following IOP reduction. In a fifth of eyes, reversal of cupping persisted at one year. Overall, the number of sectors in which increased rim area persisted at a year was small, however (less than 6% of all sectors tested in treated eyes). Nevertheless, the effects of IOP reduction on topography, especially in the short term, should be considered when longitudinally assessing rim area for progression by scanning laser tomography.

Chapter 12
CONCLUSIONS

Summary of findings

To study the possibility that magnification may change in HRT longitudinal image series, imaging was conducted of the optic disc of a model eye in which lens power, axial length, and the eye-scanner distance were varied. It was found that the disc's imaged size varied with lens power and axial length, wherein the effect of lens power increasing by +1D was equivalent to a third the effect of an axial length increase of 1 mm. Magnification increased with myopia, especially for longer eye-scanner distances. Short eye-scanner distances tended to have the most stable magnification despite changing lens and axial length conditions. Increasing hyperopia resulted in minification. This suggests that changed lens power or axial length, such as with developing cataract or following the surgical lowering of IOP respectively can affect image magnification. The HRT software's image-to-image scaling procedure could correct some changes in magnification but this only seemed effective within a fixed range of induced ametropia. Hence, it is advisable in the present HRT setup to re-establish baseline images after intraocular surgery, note changes in patients' refraction over time, and try to maintain a standard and relatively short eye-scanner distance throughout imaging. It seemed prudent in the rest of the investigation to scale all images within series by exporting the contour line, and check image series to exclude altered magnification.

Measurement variability in scanning laser tomography of the optic nerve head was characterised to provide a framework for analysing and interpreting longitudinal measurements. The topographic parameter of rim area was found to be reproducible among other parameters, making it suitable as a marker for evaluating progression. Regional rim area variability, however, was not uniform around the optic nerve head but was often highest temporally, with this pattern differing between normal and glaucoma eyes and by reference plane definition, and influenced by testing involving different operators and visits.

Possible sources of rim area variability were evaluated in image analysis. Across a range of nerve morphologies, 40-60% of rim area variability could be explained by image-to-image variation in the three-dimensional features of topography studied. In individual image series, these features explained a median 85% of variability, exceeding 90% in at least a quarter of eyes. Of these features, fluctuation in the z-axis distance between the reference plane and surface height at the optic nerve head margin contributed most often to rim area variability; this was significant in over 95% of eyes. Next most important, significant in over 80%, was variability in the optic nerve head's centre of gravity along the z-axis. Both these factors also explained more variability than other factors in the explanatory models. Standard and 320μm reference planes differed in their explanatory models of rim area variability. These findings indicate that significant rim area variability is caused by fluctuation in the z-axis distance (height) between the optic nerve head surface and the reference ring and conventional reference planes.

A novel experimental reference plane was designed to try to nullify major sources of variability to improve reproducibility while ensuring measurements were clinically valid. Central to this design is the maintaining of the z-axis distance between the optic nerve head and reference plane in all images of any image series. A second important feature of the experimental reference plane is that its position is customised to suit each optic nerve head's morphology. On testing the experimental reference plane, rim area variability was less in test-retest and longitudinal data, more uniform around the optic nerve head, and not appreciably affected by different test visits, operators or glaucomatous morphology compared with standard and 320μm reference plane analysis.

Experimental reference plane analysis also corresponded more closely with rim appearance compared with standard and 320μm reference plane analysis in every part of the nerve. Analysis by the standard and 320μm reference planes showed a small (7-8%) but significant measurement bias in that they tended to estimate rim area as less than by subjective analysis when discs were more cupped. This suggests that analysis by the standard and 320μm reference planes can be influenced by optic

nerve head morphology. No such bias was seen in experimental reference plane analysis.

An analytical approach based on the experimental reference plane was devised for identifying progression and patterns of change in the optic nerve head. Variability is accounted for in 30° sectors of each optic nerve head by way of limits of variability, calculated in intra-visit image data from across all test visits for any image series. Mean topography images, one from each visit in time, provide the point estimates of rim area. In judging progression, data from any number of visits can be simultaneously assessed and weighed against variability and only change repeatedly exceeding variability in two of three tests is attributed to progression. By this approach, it was found that ocular hypertension converter eyes having unambiguous glaucoma progression could be distinguished from unchanging normal control eyes.

Next, the influence of different statistical limits of variability and criteria for verifying change on distinguishing between ocular hypertension converter nerves and the unchanging nerves of controls was assessed. More sectors were identified as progressing in converters than control eyes at every limit of variability. Stricter limits of variability resulted in fewer progressing sectors, especially in controls. Verifying that apparent change was repeatable in two of three tests resulted in fewer false positives compared with the single test strategy, but with the former's sensitivity not appreciably compromised. When compared with four other criteria for confirming change, the 2-of-3 criterion had the most favourable combination of sensitivity and specificity; by this criterion, sensitivity and the false positive rate for the 90% limits of variability was 90.0% and 6.2% respectively, and for the 95% limits of variability was 83.3% and 3.1% respectively. That eyes presumed to have progression could be distinguished from control eyes suggests that variability was well accounted for by these limits of variability when the 2-of-3 criterion was met. The pattern of confirmed rim area loss seen in ocular hypertension converters corresponded with the findings of previously published photographic studies of similar eyes. The observed pattern of rim loss also broadly corresponded with the visual field hemisphere in which conversion was identified.

The analytical approach was tested in various presentations of glaucoma. By the 90% limits of variability and 2-of-3 criterion, confirmed rim loss was detected in

2/32 (6.2%) of normal controls, 11/97 (11%) of ocular hypertension subjects, 27/30 (90%) of ocular hypertension converters, 15/26 (58%) suspect NPG eyes without visual field defects, and 14/26 (54%) of established NPG eyes with moderately damaged fields. Visual field conversion was found in 5/26 (19%) of suspect NPG eyes, of which reproducible rim loss was identified in 3/5. Of the two eyes without confirmed change, rim loss was evident in one but not enough data was available to verify this. Within high-pressure and normal-pressure presentations of glaucoma, common patterns of change were observed. Rim progression was frequently seen in the inferior and superior poles in all groups. Patterns of change were similar within high-pressure groups whether or not field defects were present, and the same was true within normal-pressure presentations. Between high-pressure and normal-pressure groups, there were apparent similarities but also differences that correlated with previously published observations of disc photographs. Confirmed rim change was more common temporally than nasally in normal-pressure groups but the converse was seen in high-pressure groups. Suspect NPG optic nerves had more frequent rim change temporally and tended to be more cupped than ocular hypertension and ocular hypertension converter nerves despite all the groups being perimetrically equivalent. There was a preponderance of paracentral visual field defects in both NPG converter and established NPG eyes.

The analytical approach was used to longitudinally study optic disc 'reversal of cupping' in eyes in which IOP had been lowered by topical medication and sustained at at least 25% below baseline. Normal eyes with equivalent follow up were tested as controls. Many treated eyes were suggested to have at least some reversal of cupping based on single readings: rim area increased and exceeded the upper 90% limits of variability in twice as many treated eyes (POAG or ocular hypertension) as control eyes; five times as many sectors exceeded their upper limits of variability in treated eyes as in controls. Judged by the 2-of-3 criterion, about a third of treated eyes had confirmed reversal of cupping following IOP reduction but no control eyes had confirmed change. In a fifth of treated eyes, change persisted at one year. Overall, however, the number of sectors with persistently increased rim area at one year was small (less than 6% of all sectors tested in treated eyes).

The empirically based approach the author has devised for identifying progressive rim loss incorporates a series of novel strategies to optimise reproducibility and deal with any residual variability; this is its key feature. Variability that is unaccounted for can seriously confound the interpretation of change in longitudinal data. In the absence of a well-accepted external gold standard for glaucoma progression, it was necessary to rigorously define and construct a reference dataset to test and refine the approach, and to determine if it is good enough for clinical use. Testing showed that the method ably distinguished eyes having glaucomatous progression from the unchanging eyes of normal controls. In wider testing, change was identified in glaucoma suspect eyes without field defects, eyes that deteriorated to develop visual field abnormality, and eyes with established and more advanced glaucoma.

Future directions

The analysis reported herein was mostly done manually, but the large number of calculations needed in any series and the recalculation needed as a series grows is most efficiently automated in software. This could help with further refinements to improve reproduciblity. For example, the level of the reference plane in the optic nerve head compatible with least variability (R) could be individualised to each nerve. In the present investigation, R was determined in group-data and then applied universally. However, R is likely to vary between eyes and it would be useful if it were determined individually to better customise the position of the reference plane to each optic nerve.

Imaging by the newer HRT-II has some theoretical advantages over the HRT, although this needs to be verified empirically. Variation in the tilting of the imaged nerve and in its compensation by HRT software, a source of rim area variability, is likely to be less in HRT-II imaging, in which the position of the scanner relative to the eye is now fixed. The eye-scanner distance in HRT-II imaging is also fixed and relatively short and can be expected to help minimise magnification changes. The duration of fixation needed for HRT II imaging is much longer than for the HRT, however, and how this influences reproducibility needs addressing. HRT-II software uses a different and easier method of drawing the contour line but the reproducibility in exporting this contour line remains untested. Image-to-image

scaling when exporting the contour line appears to be useful for standardising magnification within image series and the manufacturers might consider refining it further. Presently, HRT-II software only allows analysis by the standard reference plane so that alternative positioning of the reference plane is not possible.

Detailed studies need to be conducted into the evolving of 'reversal of cupping' due to lowered IOP; reversal should be characterised in individual nerves, by region within each nerve, during the immediate period after treatment, and over the longer term. Such data would be useful in trying to account for the possible confounding effect of reversal of cupping in longitudinal evaluation. Finally, it would be worthwhile to devise a way of measuring the time-pattern and rate of progression in each nerve and within each of its regions. Sequential rim area data derived by the new experimental reference plane should provide a suitable basis for this. Being able to quantify trends in glaucomatous progression should complement the analytical approach described herein.

References

Agar, A., Yip, S. S., Hill, M. A., and Coroneo, M. T. 2000 Pressure related apoptosis in neuronal cell lines, *J Neurosci Res*, 60, 495-503

Agar, A., Agarwal, N. J., Hill, M. and Coroneo, M. T. 2001 Retinal ganglion cell line apoptosis in a hydrostatic pressure model for chronic glaucoma. *Invest Ophthalmol Vis Sci* [ARVO abstract], 42, S25

Airaksinen, P. J., Mustonen, E., and Alanko, H. I. 1981a Optic disc hemorrhages. Analysis of stereophotographs and clinical data of 112 patients, *Arch Ophthalmol*, 99, 1795-801.

Airaksinen, P. J., Mustonen, E., and Alanko, H. I. 1981b Optic disc haemorrhages precede retinal nerve fibre layer defects in ocular hypertension, *Acta Ophthalmol (Copenh)*, 59, 627-41.

Airaksinen, P. J. and Heijl, A. 1983 Visual field and retinal nerve fibre layer in early glaucoma after optic disc haemorrhage, *Acta Ophthalmol (Copenh)*,61, 186-94.

Airaksinen, P. J. and Tuulonen, A. 1984 Early glaucoma changes in patients with and without an optic disc haemorrhage, *Acta Ophthalmol (Copenh)*, 62, 197-202.

Airaksinen, P. J., Drance, S. M., and Schulzer, M. 1985 Neuroretinal rim area in early glaucoma, *Am J Ophthalmol*, 99, 1-4.

Airaksinen, P. J., Juvala, P. A., Tuulonen, A., et al. 1987 Change of peripapillary atrophy in glaucoma, In: Krieglstein, G. K., ed. Glaucoma Update III, New York: Springer-Verlag, 97-102

Airaksinen, P. J., Tuulonen, A., and Alanko, H. I. 1992 Rate and pattern of neuroretinal rim area decrease in ocular hypertension and glaucoma, *Arch Ophthalmol*, 110, 206-10.

Airaksinen, P. J., and Tuulonen, A. 1993 Retinal nerve fibre layer examination, In: Varma, R., and Spaeth, G. L., eds: The optic nerve in glaucoma, Philadelphia: JB Lippincott.

Airaksinen, P. J., Tuulonen, A., and Werner, E. B. 1996 Clinical evaluation of the optic disc and retinal nerve fiber layer, In: Ritch, R., Shields, M.B., and Krupin, T., eds: The Glaucomas, St Louis: Mosby.

Ally, F, Garway-Heath, D. F., Mardin, C. Y., Burk, R. O., Greaney, M. J., Caprioli, J., Swindale, N. V., Stjepanovic, G., and Chin, A. 2001 Comparison of algorithms used to classify eyes by means of Heidelberg Retina Tomograph measurement data [ARVO abstract], *Invest Ophthalmol Vis Sci,* 42, S118.

Altman, D. G. 1991 Practical statistics for medical research, London: Chapman and Hall, 336-51.

Anderson, D. R., Hoyt, W. F., and Hogan, M. J. 1967 The fine structure of the astroglia in the human optic nerve and optic nerve head, *Trans Am Ophthalmol Soc,* 65, 275-305.

Anderson, D. R. 1969 Ultrastructure of human and monkey lamina cribrosa and optic nerve head, *Arch Ophthalmol,* 82, 800.

Anderson, D. R. and Hendrickson, A. 1974 Effect of intraocular pressure on rapid axoplasmic transport in monkey optic nerve, *Invest Ophthalmol,* 13, 771-83.

Anderson, R. S., and O'Brien, C. 1997 Psychophysical evidence for a selective loss of M ganglion cells in glaucoma, *Vision Res*, 37, 1079-1083.

Anderson, D. R., Chauhan, B. C., Johnson, C., Katz, J., Patella, M., and Drance, S. M. 2000 Criteria for progression of glaucoma in clinical management and in outcome studies (Editorial), Am J Ophthalmol, 130, 827-829.

Ang, A., Tong, L., and Vernon, S. A. 2000 Improvement of reproducibility of macular volume measurements using the Heidelberg retinal tomograph. *Br J Ophthalmol*, 84, 1194-7

Armaly, M. F. and Sayegh, R. E. 1969 The cup-disc ratio. The findings of tonometry and tonography in the normal eye, *Arch Ophthalmol,* 82, 191-6.

Armaly, M. F., Krueger, D. E., Maunder, L., Becker, B., Hetherington, J. J., Kolker, A. E., Levene, R. Z., Maumenee, A. E., Pollack, I. P., and Shaffer, R. N. 1980 Biostatistical analysis of the collaborative glaucoma study. I. Summary report of the risk factors for glaucomatous visual-field defects, *Arch Ophthalmol,* 98, 2163-71.

Arnold, J. V., Gates, J. W., and Taylor, K. M. 1993 Possible errors in the measurement of retinal lesions, *Invest Ophthalmol Vis Sci,* 34, 2576-80.

Asawaphureekorn, S., Zangwill, L., and Weinreb, R. N. 1996 Ranked-segment distribution curve for interpretation of optic nerve topography, *J Glaucoma,* 5, 79-90.

Asrani, S., Zeimer, R., Wilensky, J., Gieser, D., Vitale, S., and Lindenmuth, K. 2000 Large diurnal fluctuations in intraocular pressure are an independent risk factor in patients with glaucoma, *J Glaucoma,* 9, 134-42.

Assad, A., and Caprioli, J. 1992 Digital image analysis of optic nerve head pallor as a diagnostic test for early glaucoma, *Graefes Arch Clin Exp Ophthalmol,* 230, 432-6.

Aulhorn, E., and Harms, H. 1967 Early visual field defects in glaucoma, In: Glaucoma Symposium, Tutzing Castle, Basel, Switzerland: S Karger, 151-86.

Aulhorn, E , and Karmeyer, H. 1977 Frequency distribution in early glaucomatous visual field defects, *Doc Ophthalmol Proc Ser*, 14, 75-83.

Azuara-Blanco, A., Harris, A., Cantor, L. B., Abreu, M. M., and Weinland, M. 1998 Effects of short term increase of intraocular pressure on optic disc cupping, *Br J Ophthalmol,* 82, 880-3.

Balazsi, A. G., Rootman, J., Drance, S. M., Schulzer, M., and Douglas, G. R. 1984 The effect of age on the nerve fiber population of the human optic nerve, *Am J Ophthalmol,* 97, 760-6.

Bartsch, D. U. and Freeman, W. R. 1993 Laser-tissue interaction and artifacts in confocal scanning laser ophthalmoscopy and tomography, *Neurosci Biobehav Rev,* 17, 459-67.

Bartsch, D. U. and Freeman, W. R. 1994 Axial intensity distribution analysis of the human retina with a confocal scanning laser tomograph, *Exp Eye Res,* 58, 161-73.

Bartz-Schmidt, K. U., Weber, J., and Heimann, K. 1994 Validity of two-dimensional data obtained with the Heidelberg Retina Tomograph as verified by direct measurements in normal optic nerve heads, *Ger J Ophthalmol,* 3, 400-5.

Bartz-Schmidt, K. U., Sengersdorf, A., Esser, P., Walter, P., Hilgers, R. D., and Krieglstein, G. K. 1996 The cumulative normalised rim/disc area ratio curve, *Graefes Arch Clin Exp Ophthalmol,* 234, 227-31.

Bathija, R., Zangwill, L., Berry, C. C., Sample, P. A., and Weinreb, R. N. 1998 Detection of early glaucomatous structural damage with confocal scanning laser tomography, *J Glaucoma,* 7, 121-7.

Bebie, H., Fankhauser, F., and Spahr, J. 1976 Static perimetry: accuracy and fluctuations, *Acta Ophthalmol,* 54, 339-48.

Bebie, H., and Frankhauser, F. 1982 Delta manual, Interzeag AG: Schlieren.

Begg, I. S., Drance, S. M., and Sweeney, V. P. 1970 Haemorrhage on the disc – a sign of acute ischaemic optic neuropathy in chronic simple glaucoma, *Can J Ophthalmol,* 5, 321-330

Bengtsson, B. and Krakau, C. E. 1977 Some essential optical features of the Zeiss fundus camera, *Acta Ophthalmol (Copenh),* 55, 123-31.

Bengtsson, B. 1981 The prevalence of glaucoma, *Br J Ophthalmol,* 65, 46-9.

Bengtsson, B, Holmin, C, Krakau, C.E.T. 1981 Disc haemorrhages and glaucoma. *Acta Ophthalmol (Copenhagen),* 59, 1-14

Bengtsson, B. and Krakau, C. E. 1992 Correction of optic disc measurements on fundus photographs, *Graefes Arch Clin Exp Ophthalmol,* 230, 24-8.

Bengtsson, B., Lindgren, A., Heijl, A., Lindgren, G., Asman, P., and Patella, M. 1997a Perimetric probability maps to separate change caused by glaucoma from that caused by cataract, *Acta Ophthalmol Scand,* 75, 184-8.

Bengtsson, B., Olsson, J., Heijl, A., and Rootzen, H. 1997b A new generation of algorithms for computerized threshold perimetry, SITA, *Acta Ophthalmol Scand,* 75, 368-75.

Bengtsson, B., Heijl, A., and Olsson, J. 1998 Evaluation of a new threshold visual field strategy, SITA, in normal subjects. Swedish Interactive Thresholding Algorithm, *Acta Ophthalmol Scand,* 76, 165-9.

Bengtsson, B., and Heijl, A. 1998a Evaluation of a new perimetric threshold strategy, SITA, in patients with manifest and suspect glaucoma, *Acta Ophthalmol Scand,* 76, 268-72.

Bengtsson, B., and Heijl, A. 1998b SITA Fast, a new rapid perimetric threshold test. Description of methods and evaluation in patients with manifest and suspect glaucoma, *Acta Ophthalmol Scand,* 76, 431-7.

Bennett, A. G., Rudnicka, A. R., and Edgar, D. F. 1994 Improvements on Littmann's method of determining the size of retinal features by fundus photography, *Graefes Arch Clin Exp Ophthalmol,* 232, 361-7.

Bergea, B., Bodin, L., and Svedbergh, B. 1999 Impact of intraocular pressure regulation on visual fields in open-angle glaucoma, *Ophthalmology,* 106, 997-1004.

Bhandari, A., Fontana, L., Fitzke, F. W., and Hitchings, R. A. 1997 Quantitative analysis of the lamina cribrosa in vivo using a scanning laser opthalmoscope, *Curr Eye Res,* 16, 1-8.

Birch, M. K., Wishart, P. K., and O' Donnell, N. P. 1995 Determining progressive visual field loss in serial Humphrey visual fields, *Ophthalmology,* 102, 1227-5.

Bland, J. M., and Altman, D. G. 1986 Statistical methods for assessing agreement between two methods of clinical measurement, *Lancet*, 1, 307-310

Blomdahl, S., Calissendorff, B. M., Tengroth, B., and Wallin, O. 1997 Blindness in glaucoma patients, *Acta Ophthalmol Scand*, 75, 589-591

Bowd, C., Weinreb, R. N., Lee, B., Emdadi, A., and Zangwill, L. M. 2000 Optic disk topography after medical treatment to reduce intraocular pressure, *Am J Ophthalmol*, 130, 280-6.

Brigatti, L., Weitzman, M., and Caprioli, J. 1995 Regional test-retest variability of confocal scanning laser tomography, *Am J Ophthalmol*, 120, 433-40.

Brigatti, L., Hoffman, D., and Caprioli, J. 1996 Neural networks to identify glaucoma with structural and functional measurements, *Am J Ophthalmol*, 121, 511-21.

Britton, R. J., Drance, S. M., Schulzer, M., Douglas, G. R., and Mawson, D. 1987 The area of the neuroretinal rim of the optic nerve in normal eyes, *Am J Ophthalmol*, 103, 497-504.

Broadway, D. C., Nicolela, M. T., and Drance, S. M. 1999 Optic disk appearances in primary open-angle glaucoma, *Surv Ophthalmol*, 43, S223-243.

Bron, A. J., Tripathy, R. C, Tripathy, B. J. 1997 The visual pathway. In: Bron, A., Tripathi, R. C., and Tripathi, B.J., eds: Wolff's anatomy of the eye and orbit, Oxford: Oxford University Press

Burgoyne, C. F., Quigley, H. A., Thompson, H. W., Vitale, S., and Varma, R. 1995a Early changes in optic disc compliance and surface position in experimental glaucoma, *Ophthalmology*, 102, 1800-9.

Burgoyne, C. F., Quigley, H. A., Thompson, H. W., Vitale, S., and Varma, R. 1995b Measurement of optic disc compliance by digitized image analysis in the normal monkey eye, *Ophthalmology*, 102, 1790-9.

Burgoyne, C. F., Mercante, D. E., and Thompson, H. W. 2002 Change detection in regional and volumetric disc parameters using longitudinal confocal scanning laser tomography, *Ophthalmology*, 109, 455-66.

Burk, R. O. W., Rohrschnider, K., Volcker, H. E., and Zinser, G. 1990 Analysis of three-dimensional optic disc topography by scanning laser tomography, In: Nasemann, J. E., and Burk, R. O. W., eds: Laser scanning ophthalmoscopy and tomography, Munich: Quintessenz, 161-171.

Burk, R. O., Vihanninjoki, K., Bartke, T., Tuulonen, A., Airaksinen, P. J., Volcker, H. E., and Konig, J. M. 2000 Development of the standard reference plane for the Heidelberg retina tomograph, *Graefes Arch Clin Exp Ophthalmol,* 238, 375-84.

Caprioli, J., and Spaeth, G.L. 1984 Comparison of visual field defects in low tension glaucoma with those in the high tension glaucomas, *Am J Ophthalmol*, 102, 730-737

Caprioli, J., and Spaeth, G.L. 1985 Comparison of the optic nerve in high and low tension glaucoma, *Am J Ophthalmol*, 103, 1145-1149

Caprioli, J., and Miller, J. M. 1987 Optic disc rim area is related to disc size in normal subjects, *Arch Ophthalmol,* 105, 1683-5.

Caprioli, J., Park, H. J., Ugurlu, S., and Hoffman, D. 1998 Slope of the peripapillary nerve fiber layer surface in glaucoma, *Invest Ophthalmol Vis Sci,* 39, 2321-8.

Cashwell, L. F., and Martin, C. A. 1999 Axial length decrease accompanying successful glaucoma filtration surgery, *Ophthalmology,* 106, 2307-11.

Chatuverdi, N., Hedley-White, E. T., and Dreyer, E. B. 1993 Lateral geniculate nucleus in glaucoma, *Am J Ophthalmol,* 116, 182-8.

Chauhan, B. C., Le Blanc, R. P., McCormick, T. A., and Rogers, J. B. 1994 Test-retest variability of topographic measurements with confocal scanning laser tomography in patients with glaucoma and control subjects, *Am J Ophthalmol,* 118, 9-15.

Chauhan, B. C., and MacDonald CA 1995 Influence of time separation on variability estimates of topographic measurements with confocal scanning laser tomography, *J Glaucoma,* 4, 189-93.

Chauhan, B. C., and McCormick, T. A. 1995 Effect of the cardiac cycle on topographic measurements using confocal scanning laser tomography, *Graefes Arch Clin Exp Ophthalmol,* 233, 568-72.

Chauhan, B. C., House, P. H., McCormick, T. A., and LeBlanc, R. P. 1999 Comparison of conventional and high-pass resolution perimetry in a prospective study of patients with glaucoma and healthy controls, *Arch Ophthalmol,* 117, 24-33.

Chauhan, B. C., Blanchard, J. W., Hamilton, D. C., and LeBlanc, R. P. 2000 Technique for detecting serial topographic changes in the optic disc and peripapillary retina using scanning laaser tomography, *Invest Ophthalmol Vis Sci,* 41, 775-82.

Chauhan, B. C., McCormick, T. A., Nicolela, M. T., and Le Blanc, R. P. 2001 Optic disc and visual field changes in a prospective longitudinal study of patients with glaucoma. Comparison of scanning laser tomography with conventional perimetry and optic disc photography, *Arch Ophthalmol,* 119, 1492-9.

Chen, E., Gedda, U., and Landau, I. 2001 Thinning of the papillomacular bundle in the glaucomatous eye and its influence on the reference plane of the Heidelberg retinal tomography, *J Glaucoma,* 10, 386-9.

Chen, P. P., and Bhandari, A. 2000 Fellow eye prognosis in patients with severe visual field loss in 1 eye from chronic open-angle glaucoma, *Arch Ophthalmol,* 118, 473-8.

Chi, T., Ritch, R., Stickler, D., Pitman, B., Tsai, C., and Hsieh, F. Y. 1989 Racial differences in optic nerve head parameters, *Arch Ophthalmol,* 107, 836-9.

Chumbley, L. C. and Brubaker, R. F. 1976 Low-tension glaucoma, *Am J Ophthalmol,* 81, 761-7.

Cioffi, G. A., Robin, A. L., Eastman, R. D., Perell, H. F., Sarfarazi, F. A., and Kelman, S. E. 1993 Confocal laser scanning ophthalmoscope. Reproducibility of optic nerve head topographic measurements with the confocal laser scanning ophthalmoscope, *Ophthalmology,* 100, 57-62.

Coffey, M., Reidy, A., Wormald, R., Xian, W. X., Wright, L., and Courtney, P. 1993 Prevalence of glaucoma in the west of Ireland, *Br J Ophthalmol,* 77, 17-21.

Coleman, A. L., Quigley, H. A., Vitale, S., and Dunkelberger, G. 1991 Displacement of the optic nerve head by acute changes in intraocular pressure in monkey eyes, *Ophthalmology,* 98, 35-40.

Collaborative Normal-Tension Glaucoma Study Group 1998a Comparison of glaucomatous progression between untreated patients with normal-tension glaucoma and patients with therapeutically reduced intraocular pressures. [see comments] [published erratum appears in Am J Ophthalmol 1999 Jan;127(1):120], *Am J Ophthalmol,* 126, 487-97.

Collaborative Normal-Tension Glaucoma Study Group 1998b The effectiveness of intraocular pressure reduction in the treatment of normal-tension glaucoma. [see comments], *Am J Ophthalmol,* 126, 498-505.

Congdon, N. G., Quigley, H. A., Hung, P. T., Wang, T. H., and Ho, T. C. 1996 Screening techniques for angle-closure glaucoma in rural Taiwan, *Acta Ophthalmol Scand,* 74, 113-9.

Cooper, R.L., Alder, V. A., and Constable, I. J. 1982 Measurement vs judgment of cuo-disc ratios: statistical evaluation of intraobserver and interobserver error, *Glaucoma,* 4, 169-76.

Dandona, L., Quigley, H. A., Brown, A. E., and Enger, C. 1990 Quantitative regional structure of the normal human lamina cribrosa. A racial comparison, *Arch Ophthalmol,* 108, 393-8.

Dandona, L., Hendrickson, A., and Quigley, H. A. 1991 Selective effects of experimental glaucoma on axonal transport by retinal ganglion cells to the lateral geniculate nucleus, *Invest Ophthalmol Vis Sci,* 32, 1593-1599

David, R., Livingstone, D. G., Luntz, M. H. 1977 Ocular hypertension: a long-term follow-up of treated and untreated patients, *Br J Ophthalmol,* 61, 668

Dichtl, A., Jonas, J. B., and Mardin, C. Y. 1996 Comparison between tomographic scanning evaluation and photographic measurement of the neuroretinal rim, *Am J Ophthalmol,* 121, 494-501.

Diehl, D. L., Quigley, H. A., Miller, N. R., Sommer, A., and Burney, E. N. 1990 Prevalence and significance of optic disc hemorrhage in a longitudinal study of glaucoma, *Arch Ophthalmol,* 108, 545-50.

Dielemans, I., Vingerling, J. R., and Wolfs, R. C. 1994 The prevalence of primary open angle glaucoma in a population-based study in the Netherlands, *Ophthalmology,* 101, 1851-5.

Dielemans, I., Vingerling, J. R., Algra, D., Hofman, A., Grobbee, D. E., and de Jong, P. T. 1995 Primary open-angle glaucoma, intraocular pressure, and systemic blood pressure in the general elderly population. The Rotterdam Study, *Ophthalmology,* 102, 54-60.

Douglas, G. R. 1993 Planimetry, In: Varma R, Spaeth GL, eds: The optic nerve in glaucoma, Philadelphia: JB Lippincott.

Drance, S. M. 1969 The early field defects in glaucoma, *Invest Ophthalmol,* 8, 84-91.

Drance, S. M., Fairclough, M., Butler, D. M., and Kottler, M. S. 1977 The importance of disc hemorrhage in the prognosis of chronic open angle glaucoma, *Arch Ophthalmol,* 95, 226-8.

Dreher, A. W., Tso, P. C., and Weinreb, R. N. 1991 Reproducibility of topographic measurements of the normal and glaucomatous optic nerve head with the laser tomographic scanner, *Am J Ophthalmol,* 111, 221-9.

Dreher, A. W. and Weinreb, R. N. 1991 Accuracy of topographic measurements in a model eye with the laser tomographic scanner, *Invest Ophthalmol Vis Sci,* 32, 2992-6.

Dreyer, E. B., Zurakowski, D., Schumer, R. A., Podos, S. M., and Lipton, S. A. 1996 Elevated glutamate levels in the vitreous body of humans and monkeys with glaucoma, *Arch Ophthalmol,* 114, 299-305.

Epstein, D. L., Krug, J. H. J., Hertzmark, E., Remis, L. L., and Edelstein, D. J. 1989 A long-term clinical trial of timolol therapy versus no treatment in the management of glaucoma suspects, *Ophthalmology,* 96, 1460-7.

Ervin, J. C., Lemij, H. G., Mills, R. P., Quigley, H. A., Thompson, H. W., and Burgoyne, C. F. 2002 Clinician change detection viewing longitudinal stereophotographs compared to confocal scanning laser tomography in the LSU Experimental Glaucoma (LEG) Study, *Ophthalmology,* 10, 467-81.

Esterman B 1982 Functional scoring of the binocular field, *Ophthalmology,* 89, 1226-34.

Falcao-Reis, F., O' Donoghue, E., Buceti, R., Hitchings, R. A., and Arden, G. B. 1990 Peripheral contrast sensitivity in glaucoma and ocular hypertension, *Br J Ophthalmol,* 74, 712-6.

Fazio, P., Krupin, T., Feitl, M. E., Werner, E. B., and Carre, D. A. 1990 Optic disc topography in patients with low tension and primary open angle glaucoma, *Arch Ophthalmol,*108, 705-708

Fishbein, S. L. and Schwartz, B. 1977 Optic disc in glaucoma: Topography and extent of fluorescein filling defects, *Arch Ophthalmol,* 95, 1975-9.

Fitzke, F. W., Crabb, D. P., McNaught, A. I., Edgar, D. F., and Hitchings, R. A. 1995 Image processing of computerised visual field data [see comments], *Br J Ophthalmol,* 79, 207-12.

Fitzke, F. W., Hitchings, R. A., Poinoosawmy, D., McNaught, A. I., and Crabb, D. P. 1996 Analysis of visual field progression in glaucoma, *Br J Ophthalmol,* 80, 40-8.

Flammer, J., Drance, S. M., and Zulauf, M. 1984a Differential light threshold. Short- and long-term fluctuation in patients with glaucoma, normal controls, and patients with suspected glaucoma, *Arch Ophthalmol,* 102, 704-6.

Flammer, J., Drance, S.M., Frankhauser, F., and Augustiny, L. 1984b Differential light threshold in automated static perimetry. Factors influencing short-term fluctuation, *Arch Ophthalmol,* 102, 876-879

Flammer, J., Drance, S.M., and Schulzer, M. 1984c Covariates of long term fluctuation of the differential light threshold, *Arch Ophthalmol,* 102, 880-882

Foster, P. J., Baasanhu, J., Alsbirk, P. H., Munkhbayar, D., Uranchimeg, D., and Johnson, G. J. 1996 Glaucoma in Mongolia. A population-based survey in Hovsgol province, northern Mongolia, *Arch Ophthalmol,* 114, 1235-41.

Foster, P. J., Wong, J. S., Wong, E., Chen, F. G., Machin, D., and Chew, P. T. 2000 Accuracy of clinical estimates of intraocular pressure in Chinese eyes, *Ophthalmology* 107, 1816-21.

Frohn A, Jean B, Zinser G, Thiel HJ. 1990 The problem of reference plane definition for cup volume measurements, In: Nasemann, J.E., Burk, R.O.W., eds: Laser scanning ophthalmoscopy and tomography, Munich: Quintessenz, 197-206.

Funk, J., Dieringer, T., and Grehn, F. 1989 Correlation between neuroretinal rim area and age in normal subjects, *Graefes Arch Clin Exp Ophthalmol,* 227, 544-8.

Funk, J. 1991a Early detection of glaucoma by longitudinal monitoring of the optic disc structure, *Graefes Arch Clin Exp Ophthalmol,* 229, 57-61.

Funk, J. 1991b [Detection of progressive glaucomatous papilla changes before onset of visual field defects], *Klin Monatsbl Augenheilkd,* 198, 271-6.

Garway-Heath, D. F., Rudnicka, A. R., Lowe, T., Foster, P. J., Fitzke, F. W., and Hitchings, R. A. 1998 Measurement of optic disc size: equivalence of methods to correct for ocular magnification, *Br J Ophthalmol,* 82, 643-9.

Garway-Heath, D. F., Poinoosawmy, D., Wollstein, G., Viswanathan, A., Kamal, D., Fontana, L., and Hitchings, R. A. 1999 Intraobserver variation in the analysis of optic disc images: comparison of the Heidelberg Retina Tomograph and computer assisted perimetry, *Br J Ophthalmol,* 83, 664-669

Garway-Heath, D. F., Caprioli, J., Fitzke, F. W., and Hitchings, R. A. 2000 Scaling the hill of vision: the physiological relaionship between light sensitivity and ganglion cell numbers, *Invest Ophthalmol Vis Sci,* 41, 1774-82.

Geijssen, H. C. and Greve, E. L. 1987 The spectrum of primary open angle glaucoma. I: Senile sclerotic glaucoma versus high tension glaucoma, *Ophthalmic Surg,* 18, 207-13.

Gloster, J. 1981 Incidence of optic disc haemorrhages in chronic simple glaucoma and ocular hypertension, *Br J Ophthalmol,* 65, 452-6.

Glovinsky, Y., Quigley, H. A., and Dunkelberger, G. R. 1991 Retinal ganglion cell loss is size dependent in experimental glaucoma, *Invest Ophthalmol Vis Sci,* 32, 484-91.

Gordon, M. O. and Kass, M. A. 1999 The Ocular Hypertension Treatment Study: design and baseline description of the participants, *Arch Ophthalmol,* 117, 573-83.

Gramer, E., Althaus, G., and Leydhecker, W. 1986 [Site and depth of glaucomatous visual field defects in relation to the size of the neuroretinal rim edge zone of the optic disc in glaucoma without ocular hypertension, simple glaucoma and pigmentary glaucoma. A clinical study with the Octopus perimeter 201 and the optic nerve head analyzer.], *Klin Monatsbl Augenheilkd,* 189, 190-198

Greenidge, K. C., Spaeth, G. L., and Traverso, C. E. 1985 Change in appearance of the optic disc associated with lowering of intraocular pressure, *Ophthalmology,* 92, 897-903.

Gundersen, K. G., Heijl, A., and Bengtsson, B. 2000 Comparability of three-dimensional optic disc imaging with different techniques. A study with confocal scanning laser tomography and raster tomography, *Acta Ophthalmol Scand,* 78, 9-13.

Guthauser, U. and Flammer, J. 1988 Quantifying visual field damage caused by cataract, *Am J Ophthalmol,* 106, 480-4.

Hart, W. M. J. and Becker, B. 1982 The onset and evolution of glaucomatous visual field defects, *Ophthalmology,* 89, 268-79.

Harweth, R. S., Carter-Dawson, L., Shen, F., Smith, E. L., and Crawford, M. L. J. 1999 Ganglion cell losses underlying visual field defects from experimental glaucoma, *Invest Ophthalmol Vis Sci,* 40, 2250.

Hatch, W. V., Trope, G. E., Buys, Y. M., Macken, P., Etchells, E. E., and Flanagan, J. G. 1999 Agreement in assessing glaucomatous discs in a clinical teaching setting with stereoscopic disc photographs, planimetry, and laser scanning tomography, *J Glaucoma,* 8, 99-104.

Hattenhauer, M. G., Johnson, D. H., Ing, H. H., Herman, D. C., Hodge, D. O., Yawn, B. P., Butterfield, L. C., and Gray, D. T. 1998 The probability of blindness from open-angle glaucoma, *Ophthalmology,* 105, 2099-104.

Hayreh, S. S. 1976 The pathogenesis of optic nerve lesions in glaucoma, *Trans Am Acad Ophthalmol Otolaryngol,* 81, 197-213.

Hayreh, S. S., Jonas, J. B., and Zimmerman, M. B. 1998 Parapapillary chorioretinal atrophy in chronic high-pressure experimental glaucoma in rhesus monkeys, *Invest Ophthalmol Vis Sci,* 39, 2296-303.

Hayreh, S. S., Pe'er, J., and Zimmerman, B. 1999 Morphologic changes in chronic high-pressure experimental glaucoma in rhesus monkeys, *J Glaucoma,* 8, 56-71.

Healey, P. R., Mitchell, P., Smith, W., and Wang, J. J. 1998 Optic disc haemorrhages in a population with and without signs of glaucoma, *Ophthalmology,* 105, 216-23.

Heidelberg Enginnering. 1993 Operation manual for the Heidelberg Retina Tomograph software versions 1.09-2.01 (1993-99); Heidelberg, Germany.

Heijl, A., and Lundqvist, L. 1983 The location of earliest glaucomatous visual field defects documented by automatic perimetry, In: Greve, E.L., Heijl, E.L., eds: Fifth International Visual Field Symposium, The Hague: Dr W Junk, 153-8.

Heijl, A. 1986 Frequent disc photography and computerized perimetry in eyes with optic disc haemorrhage. A pilot study, *Acta Ophthalmol (Copenh)*, 64, 274-81.

Heijl, A., Lindgren, G., and Olsson, J. 1987 Normal variability of static perimetric threshold values across the central visual field, *Arch Ophthalmol*, 105, 1544-9.

Heijl, A., Lindgren, A., and Lindgren, G. 1989a Test-retest variability in glaucomatous visual fields, *Am J Ophthalmol*, 108, 130-5.

Heijl, A., Lindgren, G., and Olsson, J. 1989b The effect of perimetric experience in normal subjects, *Arch Ophthalmol*, 107, 81-6.

Heijl, A., Lindgren, G., Lindgren, A., et al. 1991 Extended empirical statistical package for evaluation of single and multiple fields in glaucoma: Statpac 2, In: Mills, R., and Heijl, A., eds: Perimetry Update 1990/1, Amsterdam: Kugler Publications, pp303-315

Heijl, A. 1993 Flicker analysis, In: Varma, R., and Spaeth, G. L., eds: The optic nerve in glaucoma, Philadelphia: JB Lippincott.

Heijl, A. and Bengtsson, B. 1996 The effect of perimetric experience in patients with glaucoma, *Arch Ophthalmol*, 114, 19-22.

Hendrickx, K. H., van den Enden, A., Rasker, M. T., and Hoyng, P. F. 1994 Cumulative incidence of patients with disc hemorrhages in glaucoma and the effect of therapy, *Ophthalmology*, 101, 1165-72.

Hernandez, M. R., Luo, X. X., Igoe, F., and Neufeld, A. H. 1987 Extracellular matrix of the human lamina cribrosa, *Am J Ophthalmol*, 104, 567-76.

Hernandez, M. R., Luo, X. X., Andrzejewska, W., and Neufeld, A. H. 1989 Age-related changes in the extracellular matrix of the human optic nerve head, *Am J Ophthalmol*, 107, 476-84.

Hernandez, M. R., Andrzejewska, W. M., and Neufeld, A. H. 1990 Changes in the extracellular matrix of the human optic nerve head in primary open-angle glaucoma, *Am J Ophthalmol*, 109, 180-8.

Hernandez, M. R., Wang, N., Hanley, N. M., and Neufeld, A. H. 1991 Localization of collagen types I and IV mRNAs in human optic nerve head by in situ hybridization, *Invest Ophthalmol Vis Sci,* 32, 2169-77.

Hernandez, M. R. 1992 Ultrastructural immunocytochemical analysis of elastin in the human lamina cribrosa. Changes in elastic fibers in primary open-angle glaucoma, *Invest Ophthalmol Vis Sci,* 33, 2891-903.

Hernandez, M. R., Ye, H., and Roy, S. 1994 Collagen type IV gene expression in human optic nerve heads with primary open angle glaucoma, *Exp Eye Res,* 59, 41-51.

Heuer, D. K., Anderson, D. R., Knighton, R. W., Feuer, W. J., and Gressel, M. G. 1988 The influence of simulated light scattering on automated perimetric threshold measurements, *Arch Ophthalmol,* 106, 1247-51.

Hitchings, R. A. and Spaeth, G. L. 1976 The optic disc in glaucoma. I: Classification, *Br J Ophthalmol,* 60, 778-85.

Hitchings, R. A. and Spaeth, G. L. 1977 The optic disc in glaucoma II: correlation of the appearance of the optic disc with the visual field, *Br J Ophthalmol,* 61, 107-13.

Hitchings, R. A., and Anderton, S. A. 1983 A comparative study of visual field defects seen in patients with low tension glaucoma and chronic simple glaucoma, *Br J Ophthalmol,* 67, 8181-821

Hitchings, R. A., Varma, R., and Poinoosawmy, D. 1993 Optic disc photographs, In: Varma, R., and Spaeth, G. L. eds: The optic nerve in glaucoma, Philadelphia: JB Lippincott.

Hitchings, R. A. 1994 Perimetry--back to the future? [editorial], *Br J Ophthalmol,* 78, 805-6.

Hitchings, R. A. 2000 Chronic glaucoma: definition of the phenotype, *Eye,* 14, 419-21.

Hitchings, R., and Tan, J. 2001 Target pressure, *J Glaucoma,* 10, S68-70.

Holden, A. L. and Fitzke, F. W. 1988 Image size in the fundus: structural evidence for wide-field retinal magnification factor, *Br J Ophthalmol,* 72, 228-30.

Hollows, F. C. and Graham, P. A. 1966 Intraocular pressure, glaucoma, and glaucoma suspects in a defined population, *Br J Ophthalmol,* 50, 570-86.

Holmin, C. and Krakau, C. E. 1982 Regression analysis of the central visual field in chronic glaucoma cases. A follow-up study using automatic perimetry, *Acta Ophthalmol (Copenh),* 60, 267-74.

Hosking, S. L. and Flanagan, J. G. 1996 Prospective study design for the Heidelberg Retina Tomograph: the effect of change in focus setting, *Graefes Arch Clin Exp Ophthalmol,* 234, 306-10.

Hovding, G., and Aased, H. 1986 Prognostic factors in the development of manifest open-angle glaucoma: a long-term follow-up study of hypertensive and normotensive eyes, *Ophthalmologica,* 64, 601.

Hoyt, W. F. and Newman, N. M. 1972 The earliest observable defect in glaucoma?, *Lancet,* 25 March, 692-3.

Iester, M., Mikelberg, F. S., Courtright, P., and Drance, S. M. 1997a Correlation between the visual field indices and Heidelberg retina tomograph parameters, *J Glaucoma,* 6, 78-82.

Iester, M., Swindale, N. V., and Mikelberg, F. S. 1997b Sector-based analysis of optic nerve head shape parameters and visual field indices in healthy and glaucomatous eyes, *J Glaucoma,* 6, 370-6.

Iester, M., Mikelberg, F. S., Courtright, P., Burk, R. O., Caprioli, J., Jonas, J. B., Weinreb, R. N., and Zangwill, L. 2001 Interobserver variability of optic disk variables measured by confocal scanning laser tomography, *Am J Ophthalmol,* 132, 57-62.

Ikram, M. K., Bolger, P. H., Assink, J. J., Jonas, J. B., Hofman, A., and de Jong, P. T. 2002 Comparing ophthalmosciopy, slide viewing and semiautomated systems in optic disc morphometry, *Ophthalmology,* 109, 485-493

Irak, I., Zangwill, L., Garden, V., Shakiba, S., and Weinreb, R. N. 1996 Change in optic disk topography after trabeculectomy, *Am J Ophthalmol,* 122, 690-5.

Janknecht, P. and Funk, J. 1994 Optic nerve head analyser and Heidelberg retina tomograph: accuracy and reproducibility of topographic measurements in a model eye and in volunteers, *Br J Ophthalmol,* 78, 760-8.

Janknecht, P. and Funk, J. 1995 Optic nerve head analyzer and Heidelberg retina tomograph: relative error and reproducibility of topographic measurements in a model eye with simulated cataract, *Graefes Arch Clin Exp Ophthalmol,* 233, 523-9.

Jay, J. L., and Murray, S. B. 1988 Early trabeculectomy versus conventional management in primary open angle glaucoma, *Br J Ophthalmol,* 72:881-889

Jay, J. L. and Murdoch, J. R. 1993 The rate of visual field loss in untreated primary open angle glaucoma, *Br J Ophthalmol,* 77, 176-8.

Johnson, C. A. and Keltner, J. L. 1983 Incidence of visual field loss in 20,000 eyes and its relationship to driving performance, *Arch Ophthalmol,* 101, 371-5.

Johnson, C. A., Adams, A. J., Casson, E. J., and Brandt, J. D. 1993 Blue-on-yellow perimetry can predict the development of glaucomatous visual field loss, *Arch Ophthalmol,* 111, 645-50.

Johnson, C. A. 1994 Selective versus nonselective losses in glaucoma, *J Glaucoma,* 3, S32.

Johnson, C. A., Brandt, J. D., Khong, A. M., and Adams, A. J. 1995 Short-wavelength automated perimetry in low-, medium-, and high-risk ocular hypertensive eyes. Initial baseline results, *Arch Ophthalmol,* 113, 70-6.

Jonas, J. B., Gusek, G. C., and Naumann, G. O. 1988a Optic disc, cup and neuroretinal rim size, configuration and correlations in normal eyes [published errata appear in *Invest Ophthalmol Vis Sci*, 1991, 32, 1893 and 1992, 32, 474-5], *Invest Ophthalmol Vis Sci,* 29, 1151-8.

Jonas, J. B., Gusek, G. C., and Naumann, G. O. 1988b Optic disc morphometry in chronic primary open-angle glaucoma. I. Morphometric intrapapillary characteristics, *Graefes Arch Clin Exp Ophthalmol,* 226, 522-30.

Jonas, J. B., Gusek, G. C., and Naumann, G. O. 1988c Optic disk morphometry in high myopia, *Graefes Arch Clin Exp Ophthalmol,* 226, 587-90.

Jonas, J. B., Gusek, G. C., Guggenmoos-Holzmann, I., and Naumann, G. O. 1988d Size of the optic nerve scleral canal and comparison with intravital determination of optic disc dimensions, *Graefes Arch Clin Exp Ophthalmol,* 226, 213-5.

Jonas, J. B., Gusek, G. C., Guggenmoos-Holzmann, I., and Naumann, G. O. 1988e Correlations of the neuroretinal rim area with ocular and general parameters in normal eyes, *Ophthalmic Res,* 20, 298-303.

Jonas, J. B. and Naumann, G. O. 1989a Parapapillary chorioretinal atrophy in normal and glaucoma eyes. II. Correlations, *Invest Ophthalmol Vis Sci,* 30, 919-26.

Jonas, J. B., Nguyen, X. N., Gusek, G. C., and Naumann, G. O. 1989b Parapapillary chorioretinal atrophy in normal and glaucoma eyes. I. Morphometric data, *Invest Ophthalmol Vis Sci,* 30, 908-18.

Jonas, J. B., Schmidt, A. M., Muller-Bergh, J. A., Schlotzer-Schrehardt, U. M., and Naumann, G. O. 1992a Human optic nerve fiber count and optic disc size, *Invest Ophthalmol Vis Sci,* 33, 2012-8.

Jonas, J. B., Fernandez, M. C., and Naumann, G. O. 1992b Glaucomatous parapapillary atrophy. Occurrence and correlations, *Arch Ophthalmol,* 110, 214-22.

Jonas, J. B., Fernandez, M. C., and Sturmer, J. 1993a Pattern of glaucomatous neuroretinal rim loss, *Ophthalmology,* 100, 63-8.

Jonas, J. B., and Schiro, D. 1993b Visibility of the normal retinal nerve fiber layer correlated with rim width and vessel caliber, *Graefes Arch Clin Exp Ophthalmol,* 231, 207-11.

Jonas, J. B., and Xu, L. 1994 Optic disk hemorrhages in glaucoma, *Am J Ophthalmol,* 118, 1-8.

Jonas, J. B., and Konigsreuther, K. A. 1994 Optic disk appearance in ocular hypertensive eyes, *Am J Ophthalmol,* 117, 732-40.

Jonas, J. B., and Schiro, D. 1994 Localised wedge shaped defects of the retinal nerve fibre layer in glaucoma, *Br J Ophthalmol,* 78, 285-90.

Jonas, J. B., Dichtl, A., Budde, W. M., and Lang, P. 1998a Optic disc morphology in pigmentary glaucoma, *Br J Ophthalmol,* 82, 875-9.

Jonas, J. B., Grundler, A. E., and Gonzales-Cortes, J. 1998b Pressure-dependent neuroretinal rim loss in normal-pressure glaucoma, *Am J Ophthalmol,* 125, 137-44.

Jonas, J. B., Mardin, C.Y., and Grundler, A. E. 1998c Comparison of measurements of neuroretinal rim area between confocal laser scanning tomography and planimetry of photographs, *Br J Ophthalmol,* 82, 362-366

Jonas, J. B., Budde, W. M., and Panda-Jonas, S. 1999 Ophthalmoscopic evaluation of the optic nerve head, *Surv Ophthalmol,* 43, 293-320.

Jonescu-Cuypers, C. P., Thumann, G., Hilgers, R. D., Bartz-Schmidt, K. U., Krott, R., and Krieglstein, G. K. 1998 Long-term fluctuations of the normalised rim/disc area ratio quotient in normal eyes, *Graefes Arch Clin Exp Ophthalmol,* 237, 181-6.

Kahn, H. A., Moorhead, H. B. 1973 Statistics on blindness in the model reporting area 1969-1970, *US department of Health, Education and Welfare Publication,* 73, 427

Kahn, H. A., Leibowitz, H., Ganley, J. P., Kini, M., Colton, T., Nickerson, R., and Dawber, T. R. 1975 Randomized controlled clinical trial. National Eye Institute workshop for ophthalmologists. Standardizing diagnostic procedures, *Am J Ophthalmol,* 79, 768-75.

Kalloniatis, M., Harweth, D. S., Smith, E. L., and DeSantis, L. 1993 Colour vision anomalies following experimental glaucoma in monkeys, *Ophthalmic Physiol Opt*, 13, 56-67

Kamal, D. S., Garway-Heath, D. F., Hitchings, R. A., Ruben, S., and O'Sullivan, F. 1999a Preliminary results of the betoptic treatment vs placebo randomised controlled trial in ocular hypertension: survival time to conversion to early glaucoma [ARVO abstract], *Invest Ophthalmol Vis Sci*, 40, S185.

Kamal, D. S., Viswanathan, A. C., Garway-Heath, D. F., Hitchings, R. A., Poinoosawmy, D., and Bunce, C. 1999b Detection of optic disc change with the Heidelberg retina tomograph before confirmed visual field change in ocular hypertensives converting to early glaucoma, *Br J Ophthalmol*, 83, 290-4.

Kamal, D., Garway-Heath, D. F., Hitchings, R. A., and Fitzke, F. W. 2000 Use of sequential Heidelberg retina tomograph images to identify changes at the optic disc in ocular hypertensive patients at risk of developing glaucoma, *Br J Ophthalmol*, 84, 993-8.

Kaplan, E., Lee, B. B., and Shapley, R. M. 1990 New views of primate retinal function, *Prog Retinal Res*, 7, 273-336.

Kasner, O., Feuer, W. J., and Anderson, D. R. 1989 Possibly reduced prevalence of peripapillary crescents in ocular hypertension, *Can J Ophthalmol*, 24, 211-5.

Kass, M. A., Gordon, M. O., Hoff, M. R., Parkinson, J. M., Kolker, A. E., Hart, W. M. J., and Becker, B. 1989 Topical timolol administration reduces the incidence of glaucomatous damage in ocular hypertensive individuals. A randomized, double-masked, long-term clinical trial, *Arch Ophthalmol*, 107, 1590-8.

Katz, J., and Sommer, A. 1986 Asymmetry and variation in the normal hill of vision, *Arch Ophthalmol*, 104, 65-8.

Katz, L. J., Spaeth, G. L., Cantor, L. B., Poryzees, E. M., and Steinmann, W. C. 1989 Reversible optic disk cupping and visual field improvement in adults with glaucoma, *Am J Ophthalmol*, 107, 485-92.

Katz, J., Gilbert, D., Quigley, H. A., and Sommer, A. 1997 Estimating progression of visual field loss in glaucoma, *Ophthalmology,* 104, 1017-25.

Katz, J. 1999 Scoring systems for measuring progression of visual field loss in clinical trials of glaucoma treatment, *Ophthalmology,* 106, 391-5.

Katz, J., Congdon, N., and Friedman, D. S. 1999 Methodological variations in estimating apparent progressive visual field loss in clinical trials of glaucoma treatment, *Arch Ophthalmol,* 117, 1137-42.

Katz, J. 2000 A comparison of the pattern- and total deviation-based Glaucoma Change Probability programs, *Invest Ophthalmol Vis Sci,* 41, 1012-6.

Keltner, J. L., Johnson, C. A., Quigg, J. M., Cello, K. E., Kass, M. A., and Gordon, M. O. 2000 Confirmation of visual field abnormalities in the Ocular Hypertension Treatment Study. Ocular Hypertension Treatment Study Group, *Arch Ophthalmol,* 118, 1187-94.

Kerrigan, L. A., Zack, D. J., Quigley, H. A., Smith, S. D., and Pease, M. E. 1997 TUNEL-positive ganglion cells in human primary open-angle glaucoma, *Arch Ophthalmol,* 115, 1031-5.

Kerrigan-Baumrind, L. A., Quigley, H. A., Pease, M. M., Kerrigan, D., and Mitchell, R. S. 2000 Number of ganglion cells in glaucoma eyes compared with threshold visual field tests in the same persons, *Invest Ophthalmol Vis Sci,* 41, 741-8.

Kirsch, R. E. and Anderson, D. R. 1973a Clinical recognition of glaucomatous cupping, *Am J Ophthalmol,* 75, 442-54.

Kirsch, R. E. and Anderson, D. R. 1973b Identification of the glaucomatous disc, *Trans Am Acad Ophthalmol Otolaryngol,* 77, 143-156.

Kitazawa, Y., Horie, T., Aoki, S., Suzuki, M., and Nishioka, K. 1977 Untreated ocular hypertension. A long-term prospective study, *Arch Ophthalmol,* 95, 1180-4.

Kitazawa, Y., Shirato, S., and Yamamoto, T. 1986 Optic disc hemorrhage in low-tension glaucoma, *Ophthalmology,* 93, 853-7.

Klein, B. E., Magli, Y. L., Richie, K. A., Moss, S. E., Meuer, S. M., and Klein, R. 1985 Quantitation of optic disc cupping, *Ophthalmology,* 92, 1654-6.

Klein, B. E., Klein, R., Sponsel, W.E., Franke, T., Cantor. L.B., Martone, J., Menage, M.J. Meuer, S. M., and Goetz, L. A. 1992 Prevalence of glaucoma. The Beaver dam eye study, *Ophthalmology,* 99, 1499-1504

Klein, B. E., Klein, R., Meuer, S. M., and Goetz, L. A. 1993 Migraine headache and its association with open-angle glaucoma: the Beaver Dam Eye Study, *Invest Ophthalmol Vis Sci,* 34, 3024-7.

Klein, B. E., Klein, R., and Jensen, S. C. 1994 Open-angle glaucoma and older-onset diabetes. The Beaver Dam Eye Study, *Ophthalmology,* 101, 1173-7.

Knighton, R. W. 1995 Quantitative Reflectometry of the Ocular Fundus, *IEEE Engineering in Medicine & Biology,* 43-51.

Kook, M. S., Kim, H. B., and Lee, S. U. 2001 Short-term effect of mitomycin-C augmented trabeculectomy on axial length and corneal astigmatism, *J Cataract Refract Surg,* 27, 518-23.

Kotecha, A., Siriwardena, D., Fitzke, F. W., Hitchings, R. A., and Khaw, P. T. 2001 Optic disc changes following trabeculectomy: longitudinal and localisation of change, *Br J Ophthalmol,* 85, 956-61.

Krakau, C. E., Bengtsson, B., and Holmin, C. 1983 The glaucoma theory updated, *Acta Ophthalmol (Copenh),* 61, 737-41.

Kronfield, P.C. 1974 Glaucoma and the optic nerve: a historical review, *Surv Ophthalmol,* 19, 154-165

Kwon, Y. H., Kim, C. S., Zimmerman, M. B., Alward, W. L., and Hayreh, S. S. 2001 Rate of visual field loss and long-term visual outcome in primary open-angle glaucoma, *Am J Ophthalmol,* 132, 47-56.

Lachenmayr, B. J., Kiermeir U, and Kojetinsky S 1995 Points of a normal visual field are not statistically independent, *Ger J Ophthalmol,* 4, 175-81.

Lam, B. L., Alward, W. L., and Kolder, H. E. 1991 Effect of cataract on automated perimetry, *Ophthalmology,* 98, 1066-70.

Lesk, M. R., Spaeth, G. L., Azuara-Blanco, A., Araujo, S. V., Katz, L. J., Terebuh, A. K., Wilson, R. P., Moster, M. R., and Schmidt, C. M. 1999 Reversal of optic disc cupping after glaucoma surgery analyzed with a scanning laser tomograph, *Ophthalmology,* 106, 1013-8.

Leske, M. C., Connell, A. M., Wu, S. Y., Hyman, L. G., and Schachat, A. P. 1995 Risk factors for open-angle glaucoma. The Barbados Eye Study, *Arch Ophthalmol,* 113, 918-24.

Leske, M. C., Heijl, A., Hyman, L., and Bengtsson, B. 1999a Early Manifest Glaucoma Trial: design and baseline data, *Ophthalmology,* 106, 2144-53.

Leske, M. C., Hyman, L., Hussein, M., Heijl, A., and Bengtsson, B. 1999b The effectiveness of intraocular pressure reduction in the treatment of normal tension glaucoma (letter), *Am J Ophthalmol,* 127, 625-6.

Leske, M. C., Nemesure, B., He, Q., Wu, S. Y., Fielding, H. J., and Hennis, A. 2001a Patterns of open-angle glaucoma in the Barbados Family Study, *Ophthalmology,* 108, 1015-22.

Leske, M. C., Connell, A. M., Wu, S. Y., Nemesure, B., Li, X., Schachat, A., and Hennis, A. 2001b Incidence of open-angle glaucoma: the Barbados Eye Studies. The Barbados Eye Studies Group, *Arch Ophthalmol,* 119, 89-95.

Levene, R.Z. 1980 Low tension glaucoma: a critical review and new material, *Surv Ophthalmol,* 24, 621-664

Lewis, R.A., Hayreh, S.S., and Phillips, C.D. 1983 Optic disc and visual field correlations in primary open angle and low tension glaucoma, *Am J Ophthalmol,* 96, 148-152

Leydhecker W, Al-Hamad, A., and Neuringer, M. 1958 Der intraokulare Drucke gesunder menschicher Augen, *Klin Monatsbl Augenheilkd,* 133, 662.

Lichter, P. R. 1977 Variability of expert observers in evaluating the optic disc, *Trans Am Ophthalmol Soc,* 74, 532-72.

Lichter, P. R. and Henderson, J. W. 1978 Optic nerve infarction, *Am J Ophthalmol,* 85, 302-10.

Lipton, S. A. and Rosenberg, P. A. 1994 Excitatory amino acids as a final common pathway for neurologic disorders, *N Engl J Med,* 330, 613-22.

Littmann, H. 1982 [Determination of the real size of an object on the fundus of the living eye], *Klin Monatsbl Augenheilkd,* 180, 286-9.

Littmann, H. 1988 [Determining the true size of an object on the fundus of the living eye], *Klin Monatsbl Augenheilkd,* 192, 66-7.

Liu, J. H., Kripke, D. F., Twa, M. D., Hoffman, R. E., Mansberger, S. L., Rex, K. M., Girkin, C. A., and Weinreb, R. N. 1999 Twenty-four-hour pattern of intraocular pressure in the aging population, *Invest Ophthalmol Vis Sci,* 40, 2912-7.

Lotmar, W. 1984 Dependence of magnification upon the camera-to-eye distance in the Zeiss fundus camera, *Acta Ophthalmol (Copenh),* 62, 131-4.

Lusky, M., Bosem, M., and Weinreb, R. N. 1993 Reproducibility of optic nerve head topography measurements in eyes with undilated pupils, *J Glaucoma,* 2, 104-9.

Maddess, T., and Henry, G.H. 1992 Performance of nonlinear visual units in ocular hypertension and glaucoma, *Clin Vis Sc,* 7, 371-83.

Maier, H., Siebert, M., Gramer, E., and Kampik, A. 1990 Eine Mebßzahl für die nervenfaserschichtdicke – Messungen mit dem laser tomographic scanner (LTS). In: Gramer E, ed: Glaukom – diagnostic und therapie, Stuttgart: Enke, 120-145

Mansour, A. M. 1990 Measuring fundus landmarks, *Invest Ophthalmol Vis Sci,* 31, 41-2.

Mardin, C. Y., Horn, F. K., Jonas, J. B., and Budde, W. M. 1999 Preperimetric glaucoma diagnosis by confocal scanning laser tomography of the optic disc, *Br J Ophthalmol,* 83, 299-304.

Mardin, C. Y., Horn, F., Budde, W. M., and Jonas, J. B. 2000 [Monitoring of morphometric changes of optic discs with morphologic progression of glaucomatous optic atrophy by means of laser scanner tomography], *Klin Monatsbl Augenheilkd,* 217, 82-7.

Martin, P. R., White, A. J., Goodchild, A. K., Wilder, H. D., and Sefton, A. E. 1997 Evidence that blue-on cells are part of the third geniculocortical pathway in primates, *Eur J Neurosci*, 9, 1536-41

McNaught, A. I., Crabb, D. P., Fitzke, F. W., and Hitchings, R. A. 1995 Modelling series of visual fields to detect progression in normal-tension glaucoma, *Graefes Arch Clin Exp Ophthalmol,* 233, 750-5.

McNaught, A. I., Crabb, D. P., Fitzke, F. W., and Hitchings, R. A. 1996 Visual field progression: comparison of Humphrey Statpac2 and pointwise linear regression analysis, *Graefes Arch Clin Exp Ophthalmol,* 234, 411-8.

Membrey, W.L., Viswanathan, A.C., Hitchings, R.A., Khaw, P.T., and Fitzke, F.W. 2001 Predicting the effect of cataract progression on visual fields using linear regression analysis [ARVO abstract]. *Invest Ophthalmol Vis Sci,* 42, S816

Menezes, A. V., Giunta, M., Chisholm, L., Harvey, P. T., Tuli, R., and Devenyi, R. G. 1995 Reproducibility of topographic measurements of the macula with a scanning laser ophthalmoscope, *Ophthalmology,* 102, 230-5.

Migdal, C., Gregory, W., and Hitchings, R. 1994 Long-term functional outcome after early surgery compared with laser and medicine in open-angle glaucoma, *Ophthalmology*, 101:1651-1657.

Miglior, S., Casula, M., Guareschi, M., Marchetti, I., Iester, M., and Orzalesi, N. 2001 Clinical ability of Heidelberg retinal tomograph examination to detect glaucomatous visual field changes, *Ophthalmology,* 108, 1621-7.

Mikelberg, F. S. and Drance, S. M. 1984 The mode of progression of visual field defects in glaucoma, *Am J Ophthalmol,* 98, 443-5.

Mikelberg, F. S., Schulzer, M., Drance, S. M., and Lau, W. 1986 The rate of progression of scotomas in glaucoma, *Am J Ophthalmol,* 101, 1-6.

Mikelberg, F. S., Drance, S. M., Schulzer, M., Yidegiligne, H. M., and Weis, M. M. 1989 The normal human optic nerve. Axon count and axon diameter distribution, *Ophthalmology,* 96, 1325-8.

Mikelberg, F., Wijsman, K., and Schulzer, M. 1993 Reproducibility of topographic parameters obtained with the Heidelberg Retina Tomograph, *J Glaucoma,* 2, 101-3.

Mikelberg, F., Parfitt, C. M., Swindale, N. V., Graham, S., Drance, S. M., and Gosine, R. 1995a Ability of the Heidelberg Retina Tomograph to detect early glaucomatous visual field loss, *J Glaucoma,* 4, 242-7.

Mikelberg, F. S., Yidegiligne, H. M., and Schulzer, M. 1995b Optic nerve axon count and axon diameter in patients with ocular hypertension and normal visual fields, *Ophthalmology,* 102, 342-8.

Miller, J. M. and Caprioli, J. 1992 An optimal reference plane to detect glaucomatous nerve fiber layer abnormalities with computerized image analysis, *Graefes Arch Clin Exp Ophthalmol,* 230, 124-8.

Miller, K. M. and Quigley, H. A. 1988 The clinical appearance of the lamina cribrosa as a function of the extent of glaucomatous optic nerve damage, *Ophthalmology,* 95, 135-8.

Mills, R. P. and Drance, S. M. 1986 Esterman disability rating in severe glaucoma, *Ophthalmology,* 93, 371-8.

Minckler, D. S. and Tso, M. O. 1976 A light microscopic, autoradiographic study of axoplasmic transport in the normal rhesus optic nerve head, *Am J Ophthalmol,* 82, 1-15.

Minckler, D. S., McLean, I. W., and Tso, M. O. 1976a Distribution of axonal and glial elements in the rhesus optic nerve head studied by electron microscopy, *Am J Ophthalmol,* 82, 179-87.

Minckler, D. S., Tso, M. O., and Zimmerman, L. E. 1976b A light microscopic, autoradiographic study of axoplasmic transport in the optic nerve head during ocular hypotony, increased intraocular pressure, and papilledema, *Am J Ophthalmol,* 82, 741-57.

Minckler, D. S., Bunt, A. H., and Johanson, G. W. 1977 Orthograde and retrograde axoplasmic transport during acute ocular hypertension in the monkey, Invest Ophthalmol Vis Sci, 16, 426-441

Mitchell, P., Smith, W., Attebo, K., and Healey, P. R. 1996 Prevalence of open-angle glaucoma in Australia. The Blue Mountains Eye Study, *Ophthalmology,* 103, 1661-9.

Mitchell, P., Smith, W., Chey, T., and Healey, P. R. 1997 Open-angle glaucoma and diabetes: the Blue Mountains eye study, Australia, *Ophthalmology,* 104, 712-8.

Mitchell, P., Hourihan, F., Sandbach, J., and Wang, J. J. 1999 The relationship between glaucoma and myopia: the Blue Mountains Eye Study, *Ophthalmology,* 106, 2010-5.

Molteno AC, Bosma NJ and Kittleson JM 1999 Otago glaucoma surgery outcome study: lon-term results of trabeculectomy-1976 to 1995, *Ophthalmology,* 106, 1742-50.

Morgan, J. E., Jeffery, G., and Foss, A. J. 1998 Axon deviation in the human lamina cribrosa, *Br J Ophthalmol,* 82, 680-683

Morgan, J. E., Uchida, H., and Caprioli, J. 2000 Retinal ganglion cell death in experimental glaucoma, *Br J Ophthalmol,* 84, 303-10.

Morrison, J. C., Dorman-Pease, M. E., Dunkelberger, G. R., and Quigley, H. A. 1990 Optic nerve head extracellular matrix in primary optic atrophy and experimental glaucoma, *Arch Ophthalmol,* 108, 1020-4.

Moss, I. D., Wild, J. M., and Whitaker, D. J. 1995 The influence of age-related cataract on blue-on-yellow perimetry, *Invest Ophthalmol Vis Sci,* 36, 764-73.

Motolko, M. and Drance, S. M. 1981 Features of the optic disc in preglaucomatous eyes, *Arch Ophthalmol,* 99, 1992-4.

Nanba, K. and Schwartz, B. 1988 Nerve fiber layer and optic disc fluorescein defects in glaucoma and ocular hypertension, *Ophthalmology,* 95, 1227-33.

Nemeth, J. and Horoczi, Z. 1992 Changes in the ocular dimensions after trabeculectomy, *Int Ophthalmol,* 16, 355-7.

Neufeld, A.H. 1999 Nitric oxide: a potential mediator of retinal ganglion cell damage in glaucoma, *Surv Ophthamol,* 43, S129-135

O' Brien, C. and Schwartz, B. 1990 The visual field in chronic open angle glaucoma: the rate of change in different regions of the field, *Eye,* 4, 557-62.

Odberg, T., and Riise, D. 1985 Early diagnosis of glaucoma: the value of successive stereophotography of the optic disc, *Acta Ophthalmol (Copenh),* 63, 257-63.

Ogden, T. E., Duggan, J., Danley, K.,' Wilcox, M., and Minckler, D. S. 1988 Morphometry of nerve fiber bundle pores in the optic nerve head of the human, *Exp Eye Res,* 46, 559-68.

Okisaka, S., Murakami, A., Mizukawa, A., and Ito, J. 1997 Apoptosis in retinal ganglion cell decrease in human glaucomatous eyes, *Jpn J Ophthalmol,* 41, 84-8.

Orgul, S., Cioffi, G. A., Bacon, D. R., and van Buskirk, M. 1995a Sources of variability of topometric data with a scanning laser ophthalmoscope, *Arch Ophthalmol,* 114, 161-4.

Orgul, S., Cioffi, G. A., Bacon, D. R., and van Buskirk, E. M. 1995b Reproducibility of topometric data with a scanning laser ophthalmoscope in rabbits, *Jpn J Ophthalmol,* 39, 438-42.

Orgul, S., Cioffi, G. A., and van Buskirk, E. M. 1997 Variability of contour line alignement on sequential images with the Heidelberg Retina Tomograph, *Graefes Arch Clin Exp Ophthalmol,* 235, 86.

Pach, J., Pennell, D. O., and Romano, P. E. 1989 Optic disc photogrammetry: magnification factors for eye position, centration, and ametropias, refractive and axial; and their application in the diagnosis of optic nerve hypoplasia, *Ann Ophthalmol,* 21, 454-62.

Pease, M. E., McKinnon, S. J., Quigley, H. A., Kerrigan-Baumrind, L. A., and Zack, D. J. 2000 Obstructed axonal transport of BDNF and its receptor TrkB in experimental glaucoma, *Invest Ophthalmol Vis Sci,* 41, 764-74.

Pederson, J. E. and Anderson, D. R. 1980 The mode of progressive disc cupping in ocular hypertension and glaucoma, *Arch Ophthalmol,* 98, 490-5.

Pederson, J. E. and Gaasterland, D. E. 1984 Laser-induced primate glaucoma. I. Progression of cupping, *Arch Ophthalmol,* 102, 1689-92.

Poinoosawmy, D., Bunce, C., Membrey, W.L., Fitzke, F.W., and Hitchings, R.A. 1999 The rate of visual field progression during long-term follow-up of normal tension glaucoma patients, In: Wall M, Wild JM, eds: Perimetry Update. The Hague: Kugler, 147-53.

Poinoosawmy, D., McNaught, A.I., Fitzke, F.W., and Hitchings, R.A. 1995 Location of early field deterioration in glaucoma suspects, In: Mills RP, Wall M, eds: Perimetry Update. Amsterdam/New York: Kugler, 289-297.

Polansky, J. R., Fauss, D. J., Chen, P., Chen, H., Lutjen-Drecoll, E., Johnson, D., Kurtz, R. M., Ma, Z. D., Bloom, E., and Nguyen, T. D. 1997 Cellular pharmacology and molecular biology of the trabecular meshwork inducible glucocorticoid response gene product, *Ophthalmologica,* 211, 126-39.

Polyak SL, 1941, The Retina, Chicago: University of Chicago Press

Provis, J. M., van Driel, D., Billson, F. A., and Russell, P. 1985 Human fetal optic nerve: overproduction and elimination of retinal axons during development, *J Comp Neurol,* 238, 92-100.

Quigley, H. A. 1977 The pathogenesis of reversible cupping in congenital glaucoma, *Am J Ophthalmol,* 84, 358-70.

Quigley, H. A. and Anderson, D. R. 1977 Distribution of axonal transport blockade by acute intraocular pressure elevation in the primate optic nerve head, *Invest Ophthalmol Vis Sci,* 16, 640-4.

Quigley, H. A., Davis, E. B., and Anderson, D. R. 1977a Descending optic nerve degeneration in primates, *Invest Ophthalmol Vis Sci,* 16, 841-9.

Quigley, H. A., and Green, W. R. 1979 The histology of human glaucoma cupping and optic nerve damage: clinicopathologic correlation in 21 eyes, *Ophthalmology,* 86, 1803-30.

Quigley, H. A., and Addicks, E. M. 1981 Regional differences in the structure of the lamina cribrosa and their relation to glaucomatous optic nerve damage, *Arch Ophthalmol,* 99, 137-43.

Quigley, H. A., Addicks, E. M., Green, W. R., and Maumenee, A. E. 1981 Optic nerve damage in human glaucoma. II. The site of injury and susceptibility to damage, *Arch Ophthalmol,* 99, 635-49.

Quigley, H. A. and Addicks, E. M. 1982 Quantitative studies of retinal nerve fiber layer defects, *Arch Ophthalmol,* 100, 807-14.

Quigley, H. A., Addicks, E. M., and Green, W. R. 1982a Optic nerve damage in human glaucoma. III. Quantitative correlation of nerve fiber loss and visual field defect in glaucoma, ischemic neuropathy, papilledema, and toxic neuropathy, *Arch Ophthalmol,* 100, 135-46.

Quigley, H. A., Hohman, R. M., and Addicks, E. M. 1982b Quantitative study of optic nerve head capillaries in experimental optic disk pallor, *Am J Ophthalmol,* 93, 689-99.

Quigley, H. A., Hohman, R. M., Addicks, E. M., Massof, R. W., and Green, W. R. 1983 Morphologic changes in the lamina cribrosa correlated with neural loss in open-angle glaucoma, *Am J Ophthalmol,* 95, 673-91.

Quigley, H. A., Hohman, R. M., Addicks, E. M., and Green, W. R. 1984 Blood vessels of the glaucomatous optic disc in experimental primate and human eyes, *Invest Ophthalmol Vis Sci,* 25, 918-31.

Quigley, H. A., Sanchez, R. M., Dunkelberger, G. R., L'Hernault, N. L., and Baginski, T. A. 1987 Chronic glaucoma selectively damages large optic nerve fibers, *Invest Ophthalmol Vis Sci,* 28, 913-20.

Quigley, H. A., Dunkelberger, G. R., and Green, W. R. 1989 Retinal ganglion cell atrophy correlated with automated perimetry in human eyes with glaucoma, *Am J Ophthalmol,* 107, 453-64.

Quigley, H. A., Brown, A. E., Morrison, J. D., and Drance, S. M. 1990 The size and shape of the optic disc in normal human eyes, *Arch Ophthalmol,* 108, 51-7.

Quigley, H. A., Coleman, A. L., and Dorman-Pease, M. E. 1991a Larger optic nerve heads have more nerve fibers in normal monkey eyes [see comments], *Arch Ophthalmol,* 109, 1441-3.

Quigley, H. A., Dorman-Pease, M. E., and Brown, A. E. 1991b Quantitative study of collagen and elastin of the optic nerve head and sclera in human and experimental monkey glaucoma, *Curr Eye Res,* 10, 877-88.

Quigley, H. A., Brown, A., and Dorman-Pease, M. E. 1991c Alterations in elastin of the optic nerve head in human and experimental glaucoma, *Br J Ophthalmol,* 75, 552-7.

Quigley, H. A., Katz, J., Derick, R. J., Gilbert, D., and Sommer, A. 1992 An evaluation of optic disc and nerve fiber layer examinations in monitoring progression of early glaucoma damage, *Ophthalmology,* 99, 19-28.

Quigley, H. A., Enger, C., Katz, J., Sommer, A., Scott, R., and Gilbert, D. 1994 Risk factors for the development of glaucomatous visual field loss in ocular hypertension, *Arch Ophthalmol,* 112, 644-9.

Quigley, H. A. 1995 Ganglion cell death in glaucoma: pathology recapitulates ontogeny, *Aust N Z J Ophthalmol,* 23, 85-91.

Quigley, H. A., Nickells, R. W., Kerrigan, L. A., Pease, M. E., Thibault, D. J., and Zack, D. J. 1995 Retinal ganglion cell death in experimental glaucoma and after axotomy occurs by apoptosis, *Invest Ophthalmol Vis Sci,* 36, 774-86.

Quigley, H. A. and Pease, M. E. 1996 Change in the optic disc and nerve fiber layer estimated with the glaucoma-scope in monkey eyes, *J Glaucoma,* 5, 106-16.

Quigley, H. A. 1996 The number of persons with glaucoma worldwide, *Br J Ophthalmol,* 80, 389-393

Quigley, H. A. 1999 Neuronal death in glaucoma, *Prog Retin Eye Res,* 18, 39-57.

Radius, R. L. 1980 Thickness of the retinal nerve fibre layer in primate eyes, *Arch Ophthalmol,* 98, 1625.

Radius, R. L. and Gonzales, M. 1981 Anatomy of the lamina cribrosa in human eyes, *Arch Ophthalmol,* 99, 2159-62.

Radius, R. L. and Pederson, J. E. 1984 Laser-induced primate glaucoma. II. Histopathology, *Arch Ophthalmol,* 102, 1693-8.

Rakic, P. and Riley, K. P. 1983 Overproduction and elimination of retinal axons in the fetal rhesus monkey, *Science,* 219, 1441-4.

Ramrattan, R. S., Wolfs, R. C., Jonas, J. B., Hofman, A., and de Jong, P. T. 1999 Determinants of optic disc characteristics in a general population: The Rotterdam Study, *Ophthalmology,* 106, 1588-96.

Rasker, M. T., van den Enden, A., Bakker, D., and Hoyng, P. F. 1997 Deterioration of visual fields in patients with glaucoma with and without optic disc hemorrhages, *Arch Ophthalmol,* 115, 1257-62.

Rasker, M. T., van den Enden, A., Bakker, D., and Hoyng, P. F. 2000 Rate of visual field loss in progressive glaucoma, *Arch Ophthalmol,* 118, 481-8.

Read, R. M. and Spaeth, G. L. 1974 The practical clinical appraisal of the optic disc in glaucoma: the natural history of cup progression and some specific disc-field correlations, *Trans Am Acad Ophthalmol Otolaryngol,* 78, OP255-OP274.

Repka, M. X. and Quigley, H. A. 1989 The effect of age on normal human optic nerve fiber number and diameter, *Ophthalmology,* 96, 26-32.

Rockwood, E. J. and Anderson, D. R. 1988 Acquired peripapillary changes and progression in glaucoma, *Graefes Arch Clin Exp Ophthalmol,* 226, 510-5.

Rodieck RW, Binmoeller KF, and Dineen 1985 Parasol and midget cells in the human retina, *J Comp Neurol,* 233, 115-32.

Rohrschneider, K., Burk, R. O., Kruse, F. E., and Volcker, H. E. 1994 Reproducibility of the optic nerve head topography with a new laser tomographic scanning device, *Ophthalmology,* 101, 1044-9.

Rudnicka, A. R., Edgar, D. F., and Bennett, A. G. 1992 Construction of a model eye and its applications, *Ophthalmic Physiol Opt,* 12, 485-90.

Rudnicka, A. R., Burk, R. O., Edgar, D. F., and Fitzke, F. W. 1998 Magnification characteristics of fundus imaging systems, *Ophthalmology,* 105, 2186-92.

Schulzer, M., Drance, S. M., and Douglas, G. R. 1991a A comparison of treated and untreated glaucoma suspects, *Ophthalmology,* 98, 301-7.

Schulzer, M., Anderson, D. R., and Drance, S. M. 1991b Sensitivity and specificity of a diagnostic test determined by repeated observations in the absence of an external standard [published erratum appears in *J Clin Epidemiol,* 1992, 45, 91], *J Clin Epidemiol,* 44, 1167-79.

Schulzer, M. 1994 Errors in the diagnosis of visual field progression in normal-tension glaucoma, *Ophthalmology,* 101, 1589-94.

Schwartz, B., Takamoto, T., and Nagin, P. 1985 Measurements of reversibility of optic disc cupping and pallor in ocular hypertension and glaucoma, *Ophthalmology,* 92, 1396-407.

Schwartz, M. and Yoles, E. 2000 Self-destructive and self-protective processes in the damaged optic nerve: implications for glaucoma, *Invest Ophthalmol Vis Sci,* 41, 349-51.

Shaffer, R. N. 1969 The role of the astroglial cells in glaucomatous disc cupping, *Doc Ophthalmol,* 26:516-25, 516-25.

Shah, S., Chatterjee, A., Mathai, M., Kelly, S. P., Kwartz, J., Henson, D., and McLeod, D. 1999 Relationship between corneal thickness and measured intraocular pressure in a general ophthalmology clinic, *Ophthalmology,* 106, 2154-60.

Shapley R and Perry VH 1986 Cat and monkey retinal ganglion cells and their visual functional role, *Trends Neurosci,* 9, 229-35.

Shihab, Z. M., Lee, P. F., and Hay, P. 1982 The significance of disc hemorrhage in open-angle glaucoma, *Ophthalmology,* 89, 211-3.

Shin, D. H., Bielik, M., Hong, Y. J., Briggs, K. S., and Shi, D. X. 1989 Reversal of glaucomatous optic disc cupping in adult patients, *Arch Ophthalmol,* 107, 1599-603.

Siegner, S. W. and Netland, P. A. 1996 Optic disc hemorrhages and progression of glaucoma, *Ophthalmology,* 103, 1014-24.

Silverman, S. E., Trick, G. L., and Hart, W. M. J. 1990 Motion perception is abnormal in primary open-angle glaucoma and ocular hypertension, *Invest Ophthalmol Vis Sci,* 31, 722-9.

Singh, K., Spaeth, G., Zimmerman, T., and Minckler, D. 2000 Target pressure: glaucomatologists' holey grail, *Ophthalmology,* 107, 629-30.

Smith, S. D., Katz, J., and Quigley, H. A. 1996 Analysis of progressive change in automated visual fields in glaucoma, *Invest Ophthalmol Vis Sci,* 37, 1419-28.

Smith, S. D., Katz, J., and Quigley, H. A. 1997 Effect of cataract extraction on the results of automated perimetry in glaucoma, *Arch Ophthalmol,* 115, 1515-9.

Sommer, A., Pollack, I., and Maumenee, A. E. 1980 Optic disc parameters and onset of glaucomatous field loss. 1: methods and progressive changes in disc morphology, *Arch Ophthalmol,* 9, 1444-8.

Sommer, A. 1989 Intraocular pressure and glaucoma, *Am J Ophthalmol,* 107, 186-8.

Sommer, A., Tielsch, J. M., Katz, J., Quigley, H. A., Gottsch, J. D., Javitt, J., and Singh, K. 1991a Relationship between intraocular pressure and primary open angle glaucoma among white and black Americans. The Baltimore Eye Survey, *Arch Ophthalmol,* 109, 1090-5.

Sommer, A., Tielsch, J. M., Katz, J., Quigley, H. A., Gottsch, J. D., Javitt, J. C., Martone, J. F., Royall, R. M., Witt, K. A., and Ezrine, S. 1991b Racial differences in the cause-specific prevalence of blindness in east Baltimore [see comments], *N Engl J Med,* 325, 1412-7.

Sommer, A., Katz, J., Quigley, H. A., Miller, N. R., Robin, A. L., Richter, R. C., and Witt, K. A. 1991c Clinically detectable nerve fiber atrophy precedes the onset of glaucomatous field loss, *Arch Ophthalmol,* 109, 77-83.

Sommer, A. 1996 Glaucoma risk factors observed in the Baltimore Eye Survey, *Curr Opin Ophthalmol,* 7, 93-8.

Sonnsjo, B., Krakau, C. E., and Bengtsson, B. 1988 Disc haemorrhages and glaucoma in a general ophthalmic practice, *Acta Ophthalmol (Copenh),* 66, 174-9.

Spaeth, G. L., Hitchings, R. A., and Sivalingam, E. 1976 The optic disc in glaucoma: pathogenetic correlation of five patterns of cupping in chronic open-angle glaucoma, *Trans Am Acad Ophthalmol Otolaryngol,* 81, 217-23.

Spaeth, G. L. 1993 Development of glaucomatous changes of the optic nerve. In: Varma R, Spaeth GL, eds: The optic nerve in glaucoma, Philadelphia: JB Lippincott.

Spencer, A. F., Sadiq, S. A., Pawson, P., and Vernon, S. A. 1995 Vertical optic disk diameter: discrepancy between planimetric and SLO measurements, *Invest Ophthalmol Vis Sci,* 36, 796-803.

Spry, P. G., Bates, A. B., Johnson, C. A., and Chauhan, B. C. 2000 Simulation of longitudinal threshold visual field data, *Invest Ophthalmol Vis Sci,* 41, 2192-200.

Stone, E. M., Fingert, J. H., Alward, W. L., Nguyen, T. D., Polansky, J. R., Sunden, S. L., Nishimura, D., Clark, A. F., Nystuen, A., Nichols, B. E., Mackey, D. A., Ritch, R., Kalenak, J. W., Craven, E. R., and Sheffield, V. C. 1997 Identification of a gene that causes primary open angle glaucoma, *Science,* 275, 668-70.

Sung, V.C., Bhan, A., Vernon, S.A. 2002 Agreement in assessing optic discs with a digital stereoscopic optic disc camera (DISCAM) and Heidelberg Retina Tomograph, *Br J Ophthalmol,* 86, 196-202

Susanna, R., Drance, S. M., and Douglas, G. R. 1978 The visual prognosis of the fellow eye in uniocular chronic open-angle glaucoma, *Br J Ophthalmol,* 62, 327-9.

Susanna, R. J. 1983 The lamina cribrosa and visual field defects in open-angle glaucoma, *Can J Ophthalmol,* 18, 124-6.

Swindale, N. V., Stepanovic G, Chin A, and Mikelberg, F. S. 2000 Automated analysis of normal and glaucomatous optic nerve head topography images, *Invest Ophthalmol Vis Sci,* 41, 1730-42.

Takamoto, T., and Schwartz, B. 1993 Stereophotogrammetry. In: Varma R, Spaeth GL, eds: The optic nerve in glaucoma, Philadelphia: JB Lippincott.

Teesalu, P., Vihanninjoki, K., Airaksinen, P. J., Tuulonen, A., and Laara, E. 1997 Correlation of blue-on-yellow visual fields with scanning confocal laser optic disc measurements, *Invest Ophthalmol Vis Sci,* 38, 2452-9.

Teesalu, P., Vihanninjoki, K., Airaksinen, P. J., and Tuulonen, A. 1998 Hemifield association between blue-on-yellow visual field and optic nerve head topographic measurements, *Graefes Arch Clin Exp Ophthalmol,* 236, 339-45.

Tezel, G., Kolker, A. E., Kass, M. A., Wax, M. B., Gordon, M., and Siegmund, K. D. 1997a Parapapillary chorioretinal atrophy in patients with ocular hypertension. I. An evaluation as a predictive factor for the development of glaucomatous damage, *Arch Ophthalmol,* 115, 1503-8.

Tezel, G., Kolker, A. E., Wax, M. B., Kass, M. A., Gordon, M., and Siegmund, K. D. 1997b Parapapillary chorioretinal atrophy in patients with ocular hypertension. II. An evaluation of progressive changes, *Arch Ophthalmol,* 115, 1509-14.

Tezel, G. and Wax, M. B. 2000 Increased production of tumor necrosis factor-alpha by glial cells exposed to simulated ischemia or elevated hydrostatic pressure induces apoptosis in cocultured retinal ganglion cells, *J Neurosci,* 20, 8693-700.

The AGIS investigators 1994a Advanced Glaucoma Intervention Study. 2. Visual field test scoring and reliability [see comments], *Ophthalmology,* 101, 1445-55.

The AGIS investigators 1994b The Advanced Glaucoma Intervention Study (AGIS): 1. Study design and methods, and baseline characteristics of study patients, *Control Clin Trials,* 15, 299-325.

AGIS Investigators 2000 AGIS 7: The relationship between control of intraocular pressure and visual field deterioration, *Am J Ophthalmol,* 130, 429-40

The World Bank/The International Bank for Reconstruction and Development 1993 World development report 1993: investing in health, New York: Oxford University Press.

Thylefors, B., Negrel, A. D., Pararajasegaram, R. and Dadzie, K. Y. 1995 Global data on blindness, *Bull World Health Organ,* 73, 115-21.

Tielsch, J. M., Katz, J., Quigley, H. A., Miller, N. R., and Sommer, A. 1988 Intraobserver and interobserver agreement in measurement of optic disc characteristics, *Ophthalmology,* 95, 350-6.

Tielsch, J. M., Sommer, A., Witt, K., Katz, J., and Royall, R. M. 1990 Blindness and visual impairment in an American urban population, *Arch Ophthalmol,* 108, 286-290

Tielsch, J. M., Sommer, A., Katz, J., Royall, R. M., Quigley, H. A., and Javitt, J. 1991 Racial variations in the prevalence of primary open-angle glaucoma. The Baltimore Eye Survey [see comments], *JAMA,* 266, 369-74.

Tielsch 1993 Therapy for glaucoma: costs and consequences in glaucoma and therapy, In: Bull, S.F., and Franklin, R.M., eds: Transactions of the New Orleans Academy of Ophthalmology, Amsterdam: Kugler

Tielsch, J. M., Katz, J., Sommer, A., Quigley, H. A., and Javitt, J. C. 1994 Family history and risk of primary open angle glaucoma. The Baltimore Eye Survey, *Arch Ophthalmol,* 112, 69-73.

Tielsch, J. M., Katz, J., Quigley, H. A., Javitt, J. C., and Sommer, A. 1995a Diabetes, intraocular pressure, and primary open-angle glaucoma in the Baltimore Eye Survey, *Ophthalmology,* 102, 48-53.

Tielsch, J. M., Katz, J., Sommer, A., Quigley, H. A., and Javitt, J. C. 1995b Hypertension, perfusion pressure, and primary open-angle glaucoma. A population-based assessment, *Arch Ophthalmol,* 113, 216-21.

Tomita, G., Honbe, K., and Kitazawa, Y. 1994 Reproducibility of measurements by laser scanning tomography in eyes before and after pilocarpine treatment, *Graefes Arch Clin Exp Ophthalmol,* 232, 406-8.

Topouzis, F., Peng, F., Kotas-Neumann, R., Garcia, R., Sanguinet, J., Yu, F., and Coleman, A. L. 1999 Longitudinal changes in optic disc topography of adult patients after trabeculectomy, *Ophthalmology,* 106, 1147-51.

Tsai, C. S., Ritch, R., Shin, D. H., Wan, J. Y., and Chi, T. 1992 Age-related decline of disc rim area in visually normal subjects [see comments], *Ophthalmology,* 99, 29-35.

Tso, M. O., Shih, C. Y., and McLean, I. W. 1975 Is there a blood-brain barrier at the optic nerve head?, *Arch Ophthalmol,* 93, 815-25.

Tuulonen, A., Nagin, P., Schwartz, B., and Wu, D. C. 1987 Increase of pallor and fluorescein-filling defects of the optic disc in the follow-up of ocular

hypertensives measured by computerized image analysis, *Ophthalmology,* 94, 558-63.

Tuulonen, A. and Airaksinen, P. J. 1991 Initial glaucomatous optic disk and retinal nerve fiber layer abnormalities and their progression, *Am J Ophthalmol,* 111, 485-90.

Tuulonen, A., Airaksinen, J., Schwartz, B., Alanko, H. I., and Juvala, P. A. 1992 Neuroretinal rim area measurements by configuration and by pallor in ocular hypertension and glaucoma, *Ophthalmology,* 99, 1111-6.

Tuulonen A, Vihanninjoki K, Airaksinen PJ, Alanko H, Nieminen H. 1993 The effect of reference levels on neuroretinal rim area and rim volume measurements in the Heidelberg Retina Tomograph (HRT) [ARVO abstract]. *Invest Ophthalmol Vis Sci*, 35, S1729

Uchida, H., Brigatti, L., and Caprioli, J. 1996 Detection of structural damage from glaucoma with confocal laser image analysis, *Invest Ophthalmol Vis Sci,* 37, 2393-401.

Unoki K, Ohba N, Chan R, Viswanathan AC, Fitzke FW, Hitchings RA 2000 Pointwise linear analysis of glaucomatous visual fields: comparison between sensitivity, total and pattern deviation values [ARVO abstract]. *Invest Ophthalmol Vis Sci*, 41, S294

Varma, R., Spaeth, G. L., Hanau, C., Steinmann, W. C., and Feldman, R. M. 1987 Positional changes in the vasculature of the optic disk in glaucoma, *Am J Ophthalmol,* 104, 457-64.

Varma, R., Steinmann, W. C., and Scott, I. U. 1992 Expert agreement in evaluating the optic disc for glaucoma, *Ophthalmology,* 99, 215-21.

Varma, R., Tielsch, J. M., Quigley, H. A., Hilton, S. C., Katz, J., Spaeth, G. L., and Sommer, A. 1994 Race-, age-, gender-, and refractive error-related differences in the normal optic disc, *Arch Ophthalmol,* 112, 1068-76.

Varma, R., Skaf, M., and Barron, E. 1996 Retinal nerve fiber layer thickness in normal human eyes [published erratum appears in *Ophthalmology*, 104, 174], *Ophthalmology*, 103, 2114-9.

Vickers, J. C., Hof, P. R., Schumer, R. A., Wang, R. F., Podos, S. M., and Morrison, J. H. 1997 Magnocellular and parvocellular visual pathways are both affected in a macaque monkey model of glaucoma, *Aust N Z J Ophthalmol*, 25, 239-43.

Viswanathan, A. C., Fitzke, F. W., and Hitchings, R. A. 1997a Early detection of visual field progression in glaucoma: a comparison of PROGRESSOR and STATPAC 2 [see comments], *Br J Ophthalmol*, 81, 1037-42.

Viswanathan, A. C., Hitchings, R. A., and Fitzke, F. W. 1997b How often do patients need visual field tests? *Graefes Arch Clin Exp Ophthalmol*, 235, 563-8.

Viswanathan, A. C., McNaught, A. I., Poinoosawmy, D., Fontana, L., Crabb, D. P., Fitzke, F. W., and Hitchings, R. A. 1999 Severity and stability of glaucoma: patient perception compared with objective measurement, *Arch Ophthalmol*, 117, 450-4.

Viswanathan AC, Fitzke FW, Hitchings RA 2001 Improving the detection of focal glaucomatous visual field progression [ARVO abstract]. *Invest Ophthalmol Vis Sci*, 42, S154

Vorwerk, C. K., Naskar, R., Schuettauf, F., Quinto, K., Zurakowski, D., Gochenauer, G., Robinson, M. B., Mackler, S. A., and Dreyer, E. B. 2000 Depression of retinal glutamate transporter function leads to elevated intravitreal glutamate levels and ganglion cell death, *Invest Ophthalmol Vis Sci*, 41, 3615-21.

Wang, J. J., Mitchell, P., and Smith, W. 1997 Is there an association between migraine headache and open-angle glaucoma? Findings from the Blue Mountains Eye Study, *Ophthalmology*, 104, 1714-9.

Wang, L., Cioffi, G. A., Cull, G., Dong, J., and Fortune, B. 2002 Immunohistologic evidence for retinal glial cell changes in human glaucoma, *Invest Ophthalmol Vis Sci*, 43, 1088-94.

Weber, A.J., Kaufman, P.L., and Hubbard, W.C. 1998 Morphology of single cells in the glaucomatous primate retina. *Invest Ophthalmol Vis Sci*, 39, 2304-20.

Weber, A. J., Chen, H., Hubbard, W. C., and Kaufman, P. L. 2000 Experimental glaucoma and cell size, density, and number in the primate lateral geniculate nucleus, *Invest Ophthalmol Vis Sci,* 41, 1370-9.

Weinreb, R.N., and Dreher, A.W. 1990 Reproducibility and accuracy of topographic measurements of the optic nerve head with the Laser Tomographic Scanner. In: Nasemann, J.E., and Burk, R.O.W., eds: Laser scanning ophthalmoscopy and tomography, Munich: Quintessenz, 177-182.

Weinreb, R. N., Lusky, M., Bartsch, D. U., and Morsman, D. 1993 Effect of repetitive imaging on topographic measurements of the optic nerve head, *Arch Ophthalmol,* 111, 636-8.

Weinreb, R.N. 1998 Assessment of optic disc topography for diagnosing and monitoring glaucoma, *Arch Ophthalmol*, 116, 1229-1231

Werner, E. B. and Drance, S. M. 1977 Increased scatter of responses as a precursor of visual field changes in glaucoma, *Can J Ophthalmol,* 12, 140-2.

Werner, E. B., Saheb, N., and Thomas, D. 1982 Variability of static visual threshold responses in patients with elevated IOP's, *Arch Ophthalmol,*100, 1627-31

Werner, E. B., Bishop, K. I., Koelle, J., Douglas, G. R., LeBlanc, R. P., Mills, R. P., Schwartz, B., Whalen, W. R., and Wilensky, J. T. 1988 A comparison of experienced clinical observers and statistical tests in detection of progressive visual field loss in glaucoma using automated perimetry, *Arch Ophthalmol,* 106, 619-23.

Werner, E. B. 1994 In discussion of: Schulzer M, and the Normal Tension Glaucoma Study Group. Errors in the diagnosis of visual field progression in normal tension glaucoma, *Ophthalmology*, 101, 1595

Westcott, M. C., Hoffman, D., Gaasterland, D., Viswanathan, A., and Caprioli, J. 2001 Agreement between pointwise linear regression and AGIS score change in identifying visual field deterioration in glaucoma [ARVO abstract]. *Invest Ophthalmol Vis Sci*, 42, S560

Wild, J. M., Hutchings, N., Hussey, M. K., Flanagan, J. G., and Trope, G. E. 1997 Pointwise univariate linear regression of perimetric sensitivity against follow-up time in glaucoma [see comments], *Ophthalmology*, 104, 808-15.

Wild, J. M., Pacey, I. E., Hancock, S. A., and Cunliffe, I. A. 1999a Between-algorithm, between-individual differences in normal perimetric sensitivity: full threshold, FASTPAC, and SITA. Swedish Interactive Threshold algorithm, *Invest Ophthalmol Vis Sci*, 40, 1152-61.

Wild, J. M., Pacey, I. E., O'Neill, E. C., and Cunliffe, I. A. 1999b The SITA perimetric threshold algorithms in glaucoma, *Invest Ophthalmol Vis Sci*, 40, 1998-2009.

Wilson, R. M., and Martone, J. F. 1996 Epidemiology of Chronic Open-Angle Glaucoma, In: Ritch R, Shields MB, Krupin T, eds: The Glaucomas, St Louis: Mosby, 753-69.

Wilson, M. R., Coleman, A. L., and Yu, F. 1998 Functional status and well-being in patients with glaucoma as measured by the Medical outomces study short form-36 questionnaire, *Ophthalmology*, 105, 2112-6.

Wolfs, R. C., Klaver, C. C., Ramrattan, R. S., van Duijn, C. M., Hofman, A., and de Jong, P. T. 1998 Genetic risk of primary open-angle glaucoma. Population-based familial aggregation study, *Arch Ophthalmol*, 116, 1640-5.

Wollstein, G., Garway-Heath, D. F., and Hitchings, R. A. 1998 Identification of early glaucoma cases with the scanning laser ophthalmoscope, *Ophthalmology*, 105, 1557-63.

Wood, J. M., Wild, J. M., Smerdon, D. L., and Crews, S. J. 1989 Alterations of shape of the automated perimetric profile arising from cataract, *Graefes Arch Clin Exp Ophthalmol*, 227, 157-61.

Yablonski, M. E., Zimmerman, T. J., Kass, M. A., and Becker, B. 1980 Prognostic significance of optic disk cupping in ocular hypertensive patients, *Am J Ophthalmol,* 89, 585-92.

Yamada, N., Mills, R. P., Leen, M. M., Emond, M. J., Reynolds, A. C., and Stanford, D. C. 1997 Probability maps of sequential glaucoma-scope images help identify significant change, *J Glaucoma,* 6, 279-87.

Yamada, N., Edmond, M. J., Mills, R., Chen, P. P., and Stanford, D. C. 1998 Detection of optic disc changes with Glaucoma-scope probability maps, *J Glaucoma,* 7, 378-87.

Yamazaki, Y., Koide, C., Miyazawa, T., Kuwagaki, N., and Yamada, H. 1991 Comparison of retinal nerve-fiber layer in high- and normal-tension glaucoma, *Graefes Arch Clin Exp Ophthalmol,* 229, 517-20.

Yuan, J., and Yanker, B. A. 2000 Apoptosis in the nervous system, *Nature,* 407, 802-9.

Yucel, Y. H., Zhang, Q., Gupta, N., Kaufman, P. L., and Weinreb, R. N. 2000 Loss of neurons in magnocellular and parvocellular layers of the lateral geniculate nucleus in glaucoma, *Arch Ophthalmol,* 118, 378-84.

Yucel, Y. H., Zhang, Q., Weinreb, R. N., Kaufman, P. L., and Gupta, N. 2001 Atrophy of relay neurons in magno- and parvocellular layers in the lateral geniculate nucleus in experimental glaucoma, *Invest Ophthalmol Vis Sci,* 42, 3216-22.

Zangwill, L., Shakiba, S., Caprioli, J., and Weinreb, R. N. 1995 Agreement between clinicians and a confocal scanning laser ophthalmoscope in estimating cup/disk ratios, *Am J Ophthalmol,* 119, 415-21.

Zangwill, L., Irak, I., Berry, C. C., Garden, V., de Souza, L., and Weinreb, R. N. 1997 Effect of cataract and pupil size on image quality with confocal scanning laser ophthalmoscopy, *Arch Ophthalmol,* 115, 983-90.

Zangwill, L. M., Berry, C. C., and Weinreb, R. N. 1999 Optic disc topographic measurements after pupil dilation, *Ophthalmology,* 106, 1751-5.

Zeimer, R. C. and Ogura, Y. 1989 The relation between glaucomatous damage and optic nerve head mechanical compliance, *Arch Ophthalmol,* 107, 1232-4.

Zeimer, R. C., Wilensky, J. T., Gieser, D. K., and Viana, M. A. 1991 Association between intraocular pressure peaks and progression of visual field loss [see comments], *Ophthalmology,* 98, 64-9.

Zeyen, T. G. and Caprioli, J. 1993 Progression of disc and field damage in early glaucoma, *Arch Ophthalmol,* 111, 62-5.

Zinser, G., Wijnaendts-van-Resandt, R. W., Dreher, A. W., Weinreb, R. N., Harbarth, U., and Burk, R. O. 1989 Confocal laser tomographic scanning of the eye, *Proc SPIE,* 1161, 337-44.

Zinser, G., Harbarth, U., and Schroder, H. 1990 Formation and analysis of three-dimensional data with the Laser Tomographic Scanner. In: Nasemann, J.E., Burk, R.O.W., eds: Laser scanning ophthalmoscopy and tomography, Munich: Quintessenz, 243-252.

List of publications

Hitchings, R. A., and Tan, J. C. H. 2001Target pressure, *J Glaucoma*, 10, S68-70

Tan, J. C. H., Franks, W. A., and Hitchings, R. A. 2002 Interpreting glaucoma progression by white-on-white perimetry, *Graefes Arch Clin Exp Ophthalmol*, 240, 585-592

Tan, J. C. H., Garway-Heath, D. F., Fitzke, F. W., and Hitchings, R. A. 2003 Variability across regions of the optic nerve head in scanning laser tomography, *Br J Ophthalmol*, 87, 557-9

Tan, J. C. H., Garway-Heath, D. F., Fitzke, F. W., and Hitchings, R. A. 2003 Reasons for rim area variability in scanning laser tomography, *Invest Ophthalmol Vis Sci*, 44, 1126-31

Tan, J. C. H., and Hitchings, R. A. 2003 Reference plane definition and reproducibility in optic nerve head images *Invest Ophthalmol Vis Sci*, 44, 1132-7

Tan, J. C. H., and Hitchings, R. A. 2003 An approach for identifying glaucomatous optic nerve progression by scanning laser tomography, *Invest Ophthalmol Vis Sci*, 44, 2621-6

Tan, J. C. H., Poinoosawmy, D., and Hitchings, R. A. 2003 Magnification changes in scanning laser tomography, *J Glaucoma*, in press

In review or to be submitted

Tan, J. C. H., and Hitchings, R. A. Validation of an approach for identifying glaucomatous change in optic nerve head topography

Tan, J. C. H., Poinoosawmy, D. and Hitchings, R. A. Optic nerve progression in glaucoma suspects, high-pressure glaucoma and normal pressure glaucoma

Tan, J. C. H., Poinoosawmy, D., White, E., and Hitchings, R. A. Validity of rim area as measured by different reference planes

Tan, J. C. H., and Hitchings, R. A. Longitudinal changes following reversal of optic disc cupping from reduced intraocular pressure